

**University of Stellenbosch
Department of Civil Engineering**

**STRUCTURAL CAPACITY OF
FREESTANDING GLASS
BALUSTRADES**

By

Alberto Goosen



Thesis submitted in partial fulfilment of the requirements for the degree of
Master of Civil Engineering (Structural) to the University of Stellenbosch

Study Leader:

Prof. Jan Wium

February 2007

DECLARATION

I declare that this work is essentially my own work and is being submitted for the degree of Master of Engineering at the University of Stellenbosch. It has not been submitted before for any degree or examination in any other University.

Signature: _____

Date: _____



SUMMARY

The introduction of toughened glass into the construction industry has had several significant consequences. For the first time, glass panels can be used without continuous edge supports, and as a result can be used as load-bearing element. An excellent and very common example of the use of glass as structural element is a freestanding glass balustrade.

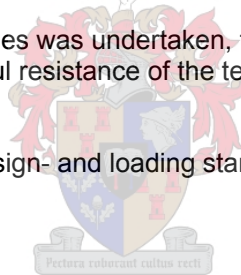
During an undergraduate investigation, a number of impact tests were performed on continuous supported freestanding glass balustrade panels at the University of Stellenbosch [6]. It was observed that none of the balustrade panels complied with the guidelines for impact loading stipulated in the SABS [7] loading standards. The failure to meet the loading requirements highlighted the need to investigate the design of glass balustrades.

This thesis describes the investigation undertaken to determine the static- and dynamic loading capacity of freestanding glass balustrades. Following a review of South African and international design standards, the static- and dynamic material properties of toughened glass was established by means of a laboratory test series. The laboratory test series consisted of both a destructive laboratory test series and finite element analysis, the outcome of which determined the static- and dynamic material properties of toughened glass. The series also included the influence of different connection types.

A second phase employed the identified material properties of toughened glass to determine the loading capacity of full-scale balustrades. Using finite elements each balustrade set-up was loaded as required by the relevant South African loading standards. The finite element analyses identified which balustrade set-ups could resist the required imposed loads.

Finally, a second laboratory test series was undertaken, the aim of which was to verify the finite element results. The successful resistance of the tested balustrade set-ups confirmed the finite element model.

Recommendation to the existing design- and loading standards are made based on the results of the thesis.



OPSOMMING

Die daarstelling van versterkte glas in die konstruksie bedryf het belangrike gevolge gehad. Vir die eerste keer kan glas panele sonder aaneenlopende rand-ondersteunings gebruik word en kan dus as las-draende element gebruik word. 'n Uitstekende en alledaagse voorbeeld van die gebruik van glas as strukturele element, is 'n vrystaande glas balustrade.

Tydens 'n voorgraadse studie, by die Universiteit van Stellenbosch, is 'n aantal impak-toetse op aaneenlopend-ondersteunde vrystaande glas balustrades uitgevoer [6]. Daar is bevind dat geen van die getoetsde balustrades aan die impak belastingsriglyne, soos uiteengesit in die SABS 0160 [7] belastingstandaarde, voldoen nie. Hierdie resultate het die noodsaaklikheid van 'n ondersoek na die ontwerp van glasbalustrades geïdentifiseer.

Hierdie verhandeling beskryf die ondersoek wat ingestel is om die statiese- en dinamiese las kapasiteit van vrystaande glas balustrades vas te stel. Na afloop van 'n literatuur studie van die Suid Afrikaanse en internasionale ontwerp kodes, is die statiese- en dinamiese material eienskappe van versterkte glas met behulp van 'n laboratorium toetsreeks bepaal. Die laboratorium toetsreeks het uit destruktiewe toets sowel as uit eindige element analyses bestaan, waarvan die uitslae die statiese- en dinamiese materiaal eienskappe van versterkte glas bepaal het. Die invloed van verskillende aanhegting tipes is ook vasgestel.

In 'n tweede fase is die geïdentifiseerde materiaal eienskappe van versterkte glas aangewend om die belastings kapasiteit van 'n vol-skaal balustrade vas te stel. Deur eindige elemente te gebruik is elke balustrade opstelling belas soos vereis deur die relevante Suid Afrikaanse belastingstandaarde. Die uitslae van die eindige element analiese het geïdentifiseer watter balustrade-opstellings die vereiste voorgeskrewe belasting kan weerstaan.

Laastens is 'n tweede reeks toetse uitgevoer, met die doel om die eindige element uitslae te verifieer. Die suksesvolle weerstand van die getoetsde balustrade-opstelling het die resultate van die eindige element model bevestig.

Gebaseer op die resultate van die tesis, word voorstelle vir die verbetering op die bestaande ontwerp-en-belasting standaarde gemaak.



ACKNOWLEDGEMENTS

Several individuals and institutions have contributed to enable the research reported in this thesis. With these acknowledgements I would like to express my sincere gratitude to everyone who, by their support, encouragement, help or remarks has contributed to this work.

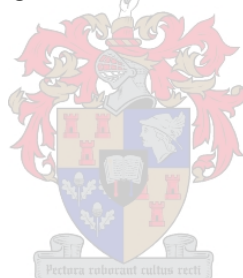
Firstly I would like to thank my study leader and mentor, Prof. Jan Wium for the central role he played in the realization of this thesis. His assistance, motivation and ability to explain concepts not only influenced the outcome of the thesis but also the way I think today.

I would also like to thank Prof. Gideon van Zijl for the assistance he provided throughout the duration of the thesis.

The experimental work could not have been conducted without the assistance of the laboratory personal. For the construction of testing equipment and installation thereof I would like to thank to Mr. Dion Viljoen and Mr. Louis Fredrick. For the proper installation and set-up of the testing equipment I would like to thank Mr. Arthur Layman and Mr. Ashley Lindor.

I would like to thank all the people involved from G.S.A (Glass South Africa) for their support and material contribution. I would also like to thank Mr. Nick Wright and Mr. Mike Pote for their involvement in the project, their assistance is gratefully acknowledged.

Special thanks to my family and friends for their support during the research period. Thanks for keeping me sane and out of work when it was necessary. Finally, thank you, Mirja, for your patience and understanding and being there when I needed you.



CONTENTS

		Page
1.	INTRODUCTION	12
	1.1 GLASS AS ENGINEERING MATERIAL	13
	1.2 BACKGROUND TO INVESTIGATION	15
	1.3 PURPOSE OF THE STUDY	16
	1.3.1 PROBLEMS WITH EXISTING DESIGN STANDARDS	
	1.3.2 OBJECTIVES	
	1.4 SCOPE OF INVESTIGATION	18
	1.5 PLAN OF STUDY	19
	1.6 LIMITATIONS OF INVESTIGATION	22
	1.7 KEY TO THE USE OF THIS REPORT	23
	1.8 LITERATURE REVIEW	24
2.	CODE DESIGN OF FREESTANDING GLASS BALUSTRADES	26
	INTRODUCTION	
	2.1 HANDRAILING AND BALUSTRADING DESIGN PHASE	28
	2.1.1 South African Handrailing and Balustrading Design Standard	
	2.1.1.1 Design requirements	
	2.1.1.2 Handrail Requirements	
	2.1.1.3 Deflection Requirements	
	2.1.2 British Handrailing and Balustrading Design Standard	
	2.1.2.1 Design requirements	
	2.1.2.2 Handrailing Requirement	
	2.1.2.3 Deflection requirement	
	2.1.3 American Handrailing and Balustrading Design Standard	
	2.1.3.1 Design requirements	
	2.1.3.2 Handrailing Requirement	
	2.1.3.3 Deflection requirement	
	2.1.4 Comparison between the international and the South African handrailing and balustrading design standards	
	2.2 MATERIAL CLASSIFICATION DESIGN PHASE	34
	2.2.1 Test Procedure	
	2.2.1.1 Test specimen	
	2.2.1.2 Test frame	
	2.2.1.3 Impactor	
	2.2.2 Impactors	
	2.2.2.1 Lead shot impactor	
	2.2.2.2 Twin tyre impactor	
	2.2.2.3 Comparison between Lead shot impactor and Twin tyre impactor	
	2.2.2.3.1 Impulse	
	2.2.2.3.2 Repeatability	
	2.2.2.3.3 Reproducibility	

2.2.3 Drop heights	
2.2.3.1 Development of human engineering data chart	
2.2.3.2 Comparison between the international and South African drop heights	
2.2.4 Breakage requirements	
2.2.4.1 Comparison between International and South African classifications	
2.3 LOADING REQUIREMENT DESIGN PHASE	45
2.3.1 Static loading requirements	
2.3.2 Impact loading requirements	
2.4 CONCLUSION	
3. CONNECTION CAPACITY OF FREESTANDING BALUSTRADES	49
INTRODUCTION	
3.1 TEST GEOMETRY	52
3.1.1 Test panel thickness	
3.1.2 Test panel hole geometries	
3.1.2.1 Residual stresses near edges and holes	
3.1.2.2 Cylindrical hole with chamfer	
3.1.3 Test panel geometry	
3.2 DESIGN OF TEST SET-UP	58
3.2.1 Test Rig	
3.2.1.1 Initial test rig	
3.2.1.2 Final test rig	
3.2.2 Test Measurements	
3.3 TEST LOADING	66
3.3.1 Loading Rate	
3.3.1.1 Determination of each loading rate	
3.3.1.1.1 Panels with holes	
3.3.1.1.2 Panel without holes	
3.4 SPECIMEN PREPERATION	71
3.4.1 Determination of level of prestress	
3.4.1.1 Procedure	
3.4.2 Examination of surface flaws surrounding holes	
3.4.3 Taping of glass panels	
3.4.4 Positioning blocks	
3.5 POST FAILURE ANALYSIS	77
3.5.1 Specimen Evaluation	
3.5.1.1 Fracture Pattern	
3.5.1.2 Fracture origin	
3.5.1.3 Loading rate fracture effect	

3.5.2	Test measurements	
3.5.2.1	Ultimate Force	
3.5.2.2	Level of prestress	
3.5.2.3	Displacement	
3.5.2.4	Elasticity modulus	
3.6	CONCLUSION	
4.	TEST PANEL FINITE ELEMENT MODEL	90
	INTRODUCTION	
4.1	MESH CALIBRATION	91
4.1.1	In-Plane Tension	
4.1.1.1	Finite-width panel with a circular hole under in plane tension	
4.1.1.1.1	2D Finite element model	
4.1.1.1.2	3D Finite element model	
4.1.2	Out-of-plane bending	
4.1.2.1	3D Finite element model	
4.2	MODEL GEOMETRY	100
4.2.1	Geometry	
4.2.1.1	Hole Geometry	
4.2.1.2	Panel Geometry	
4.2.2	Constraints	
4.2.3	Material Properties	
4.2.4	Loading	
4.3	FINITE ELEMENT RESULTS	106
4.3.1	Connection Loading Capacity	
4.3.1.1	Point supported	
4.3.1.2	Continuously supported	
4.3.1.3	Comparison between point- and continuously supported connections	
4.3.2	Calculated Fracture Stress	
4.3.3	Weibull statistical model	
4.3.3.1	Weibull parameters	
4.3.3.1.1	Scaled Panels (300x300mm)	
4.3.3.1.1.1	Weibull modulus for glass panels with holes	
4.3.3.1.1.2	Weibull modulus for glass panels without holes	
4.3.3.1.1.3	Comparison between panels with- and without holes	
4.3.3.1.2	Full scale Panels (1300 x 1000mm)	
4.3.3.1.2.1	Weibull modulus for glass panels with- and without holes	
4.4	CONCLUSION	
5.	BALUSTRADE FINITE ELEMENT MODEL	123
	INTRODUCTION	
5.1	FREESTANDING BALUSTRADE FINITE ELEMENT MODEL	125

5.1.1 BALUSTRADE GEOMETRY

5.1.1.1 Dimensions of freestanding balustrade panels

5.1.1.2 Support conditions

5.1.1.2.1 Continuous support

5.1.1.2.2 Point support

5.1.1.2.2.1 The influence of distance between hole and edge

5.1.1.2.2.2 Influence of position of holes relative to each other

5.1.1.2.2.3 Single and double horizontal rows of holes

5.1.1.3 Constraints of Finite element model

5.1.1.3.1 Single horizontal row of holes

5.1.1.3.2 Double horizontal row of holes

5.1.2 LOADING REQUIREMENTS

5.1.2.1 Static Loading

5.1.2.2 Dynamic Loading

5.1.2.2.1 Calibration of four side supported model

5.1.2.2.2 Freestanding balustrade Method

5.1.3 LOADING CAPACITY

5.1.3.1 Static loading capacity

5.1.3.1.1 Continuous support

5.1.3.1.2 Point support

5.1.3.1.3 Comparison to SABS 0160 requirements

5.1.3.1.3.1 SABS Static loading requirements

5.1.3.1.3.2 SABS Deflection requirements

5.1.3.2 Dynamic loading capacity

5.1.3.2.1 Comparison to SABS requirements

5.2 CONTINUOUS BALUSTRADES

155

5.2.1 BALUSTRADE GEOMETRY

5.2.1.1 Handrail

5.2.1.2 Support conditions

5.2.1.3 Constraints

5.2.2 LOADING REQUIREMENTS

5.2.2.1 Static loading requirements

5.2.2.2 Dynamic loading requirements

5.2.3 LOADING CAPACITY

5.2.3.1 Handrail influence

5.2.3.2 Number of connected panels

5.2.3.3 Static Capacity

5.2.3.4 Dynamic Capacity

5.2.3.4.1 Continuously supported

5.2.3.4.2 Point supported

5.2.3.4.3 Comparison to SABS 0160 requirements

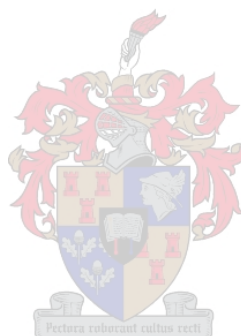
5.2.3.4.3.1 Continuously supported

5.2.3.4.3.2 Point supported

5.3 CONCLUSION

6.	VERIFICATION LABORATORY TEST SERIES	167
	INTRODUCTION	
	6.1 BALUSTRADE GEOMETRY	168
	6.1.1 Test handrail detail	
	6.1.2 Test panel supports	
	6.1.3 Test panel geometry	
	6.1.4 Test panel set-up	
	6.2 TEST SET-UP	173
	6.2.1 Test Rig	
	6.2.2 Loading rig	
	6.3 TEST LOADING	178
	6.3.1 Impact loading	
	6.4 TEST RESULTS	180
	6.4.1 Test Results	
	6.5 CONCLUSION	
7.	IMPLICATIONS OF EXPERIMENTAL AND NUMERIC ANALYSIS RESULTS	183
	7.1 SATISFYING THE SABS REQUIREMENTS	183
	7.1.1 Freestanding balustrades	
	7.1.1.1 Satisfying the SABS Deflection requirements	
	7.1.1.2 Satisfying SABS Static loading requirements	
	7.1.1.3 Satisfying SABS Dynamic loading requirements	
	7.1.2 Continuous balustrade	
	7.1.2.1 Satisfying SABS Dynamic loading requirements	
8.	CONCLUSIONS	186
	8.1 LITERATURE STUDY	187
	8.1.1 Handrail and balustrading standard [SABS: 0104]	
	8.1.2 Material classification standard [SABS: 1263]	
	8.1.3 Loading standard [SABS: 0160]	
	8.2 LABORATORY TEST SERIES 1	188
	8.2.1 Parameter test series	
	8.2.2 Finite element analysis	
	8.3 LABORATORY TEST SERIES 2	191
	8.3.1 Finite element analysis	
	8.3.2 Verification test series	

9. RECOMMENDATIONS	193
9.1 DEVELOPMENT OF SABS GUIDELINES	193
9.1.1 Standard for handrailing and balustrading	
9.1.1.1 Connection type to use with glass balustrade	
9.1.1.2 Handrail use and details	
9.1.1.3 Loading requirement	
9.1.1.4 Containment requirement	
9.1.1.5 Glass type and thickness	
9.1.2 Standard for loading requirements and material classification	
9.1.2.1 Integration of material classification and loading requirements	
9.1.2.2 Impact loading requirements	
9.1.2.2.1 Differentiation of balustrade application	
9.1.2.2.2 Inclusion of human impact engineering chart	
9.1.2.2.3 Movement space	
9.2 FURTHER RESEARCH	197
APPENDIX A	198
APPENDIX B	214
APPENDIX C	215
APPENDIX D	216
REFERENCES	217



CHAPTER 1 INTRODUCTION

Glass is a material that has always inspired architects and engineers. Designers have used it to realize the seamless transparent skin and to create clear yet load bearing walls and facades.

Glass made its first appearance in Europe as structural element in the mid 19th century, based on ingenious methods of exploiting iron and glass prefabrication, in the form of metal-glass domes and roofs of train stations [1]. In 1959, this construction technique transformed dramatically with the introduction of the float process by Pilkington. For the first time the technology required to produce affordable large panes was available. The introduction the floating process led to the discovery of toughened glass, which would eventually make structural transparent structures a reality. Toughened glass is up to five times stronger than ordinary float glass. For the first time glass, panels could be used without linear edge supports.

In the past, glass was designed with very high safety factors [2], but as structural engineers and architects began to understand its characteristics more fully, and as methods of toughening became more sophisticated, the idea of glass as structural element became more realistic.

Today, concerns to conserve natural energy and reduce the greenhouse effect in the earth's atmosphere have led to designs that combine seamless transparent skins with high performance environmental control. New responsive glass facades use self-regulating thermal protection and solar control measures to adapt in a dynamic way to changing light and weather conditions. In this way, they meet the needs of building users while reducing energy consumption levels. [3] A self-cleaning glass produced by Pilkington, originally developed for aircraft windscreens, is now available for use in external windows. The glass, coated with microscopic chemical coatings has properties that repel moisture and dirt, allowing them to be washed away during normal rainy weather.



1.1 GLASS AS ENGINEERING MATERIAL

Introduction

In contrast to certain transparent plastic materials, glass has the advantage of durability and resistance to corrosion and high temperature, and as modern architecture shows, the use of glass, especially in facades, has become very popular [4].

Traditionally, from a structural engineer's point of view, glass is a non-load bearing material. It is three times weaker than steel and has a brittle mode of fracture. For this reason, glass never formed part of the structural supporting system, and was always used in conjunction with linear edge supports. However, with the introduction of toughened- and laminated glass into the construction market, glass has evolved from a transparent room enclosure to a structural load-bearing element.

Annealed glass

Annealed- or float glass is formed by heating the ceramic material to an elevated temperature at which melting occurs, and then slowly cooling it to room temperature where the glass appears to be in a rigid state [5]. The result is a glass, which is brittle, relatively hard with a low ductibility. When broken produces shards, which are harmful. This is the most common form of glass, used for windows.

One process by which sheet glass is formed is illustrated in figure 1.1. Flatness and the surface finish is significantly improved by floating the sheet on a bath of molten tin the piece is then slowly cooled and subsequently heat treated by annealing [5].

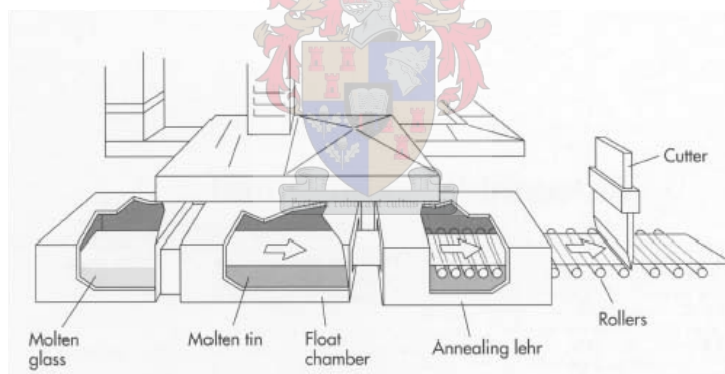


Figure 1.1 The float process [46]

Toughened glass

Toughened glass is regarded as structural glass, since it is up to five times stronger than ordinary annealed glass. The increase in strength is as a result of an induced compressive strength, which is accomplished through thermal - or chemical toughening. Thermal toughening is the most common, and ultimately produces the best results [2]. With this procedure, a glass panel is heated to the glass transition temperature, and then rapidly cooled to room temperature. Initially, the surface cools more rapidly and once having dropped to a temperature below the strain point of glass becomes rigid. Overtime, the interior contracts to a greater degree than the now rigid exterior will allow. Consequently, after the glass panel has cooled to room temperature it sustains a compressive stress on the surface with a tensile stress at the interior (figure 1.2). This parabolic stress distribution forms towards the middle of the glass panel, away from any edges or holes.

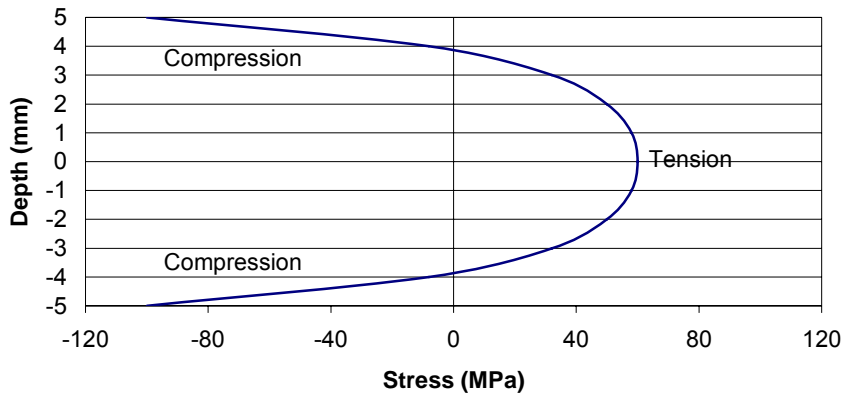
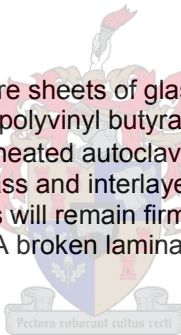


Figure 1.2 Residual stress distribution over the depth of a toughened glass panel [5]

To cause fracture of a toughened glass piece, the magnitude of the externally applied tensile stress must be great enough to first overcome the residual surface compression, and in addition, to stress the surface in tension sufficiently to initiate a crack. A panel of toughened glass breaks at once over the whole area when a crack propagates into the tensile zone in consequence of the rapid release of the strain energy built up in the glass.

Laminated glass

Laminated glass consists of two or more sheets of glass, annealed glass or tempered glass are bonded together with one or more polyvinyl butyral (PVB) interlayers in sheet form. The sheets are heated in an electronically heated autoclave to 140°C at a pressure of 12 bar for six hours removing the air between glass and interlayer. Under impact, the laminated glasses may fracture but any broken fragments will remain firmly bonded to the interlayer. Laminated glass is considered as security glass. A broken laminated glass can be left in place until replacement is convenient.



1.2 BACKGROUND TO INVESTIGATION

The introduction of toughened glass into the construction industry has had several significant consequences. For the first time, glass panels can be used without linear edge supports, and as a result can be used as load-bearing element.

An excellent and very common example of the use of glass as structural element is a freestanding glass balustrade.

What is a freestanding glass balustrade?

A freestanding glass balustrade is a barrier where there are no vertical or horizontal supporting members, or balusters. Each balustrade panel is fixed to the structure along its bottom edge, the designer determines whether it is point- or continuously supported. In this type of balustrade, the glass is designed to withstand all the design loads as required by the loading code.



Figure 1.3 Example of freestanding glass balustrade

Here, for the first time, the glass must be able to sustain static- or impact loads (as required by the loading standard) whilst the old-fashioned continuous glass balustrade could simply distribute the force to the linear edge supports.

During an undergraduate investigation, a number of impact tests were performed on continuous supported freestanding glass balustrade panels at the University of Stellenbosch [6]. The balustrade panels were constructed according to guidelines set out in supplier documentation because of the inconsistency of the existing South African design standards. These panels were subjected to the static- and impact loading requirements as set out in the loading codes. It was observed that none of the balustrade panels complied with the guidelines for impact loading stipulated in the SABS [7] loading standards. The failure to meet the loading requirements highlighted the conservative nature of the design standards, and reinforced the need for urgent attention.

Some suppliers have produced guidelines and design rules based on trial and error. The predicament herein lies that, since a balustrade is defined as a railing guarding a change in level to prevent people from falling, balustrades are often situated in places where human safety is of concern.

The inability of glass balustrades to meet actual imposed loads can result in serious injuries and, in some cases, loss of life. Therefore, the development and elaboration of the existing design- and loading design standards for structural glass is necessary.

1.3 PURPOSE OF THE STUDY

1.3.1 PROBLEMS WITH EXISTING DESIGN STANDARDS

Michael Wigginton [1] summarises the current problems surrounding designing with glass, which equally summarizes the limitations of glass balustrades.

“Glass structures are developing rather in the way that stone structures developed in the middle ages, by pragmatism and trial and error. Engineers, who invariably have to stand responsible for structural failure, have no real codes or structural data to design with, and are forced into accepting the recommendation of the glassmakers, or into a programme of testing which demonstrate that a proposal is sound. This usually means the construction of prototypes, the cost of which may deter an otherwise enthusiastic client.”- Michael Wigginton

The only way of addressing the above mentioned limitations, is by the formulation and inclusion of design guidelines, which would assist in the designing of structurally correct freestanding balustrades. An evaluation of existing design standards reveals a number of incomplete areas otherwise fundamental to the effective design and construction of the freestanding balustrades. The glass balustrade design process is controlled by three standards, each playing a vital role in the proper design and construction of the freestanding glass balustrade. The three standards are:

- Standard for handrailing and balustrading
- Standard for safety glass classification and the
- Standard for loading requirements

The limitations to the glass balustrade design process are listed below under each of the standards.

- **Insufficient handrailing and balustrading design guidelines**

Little reliable information in the South African codes exists concerning the design of freestanding glass balustrades. The information that is currently documented in the standards is incomplete in that:

- No distinction between one-, two- or three sided supported balustrade-,
- No indication of when a handrail should be installed or how it should be attached to the balustrade- or neighbouring panels-,
- No guidance to glass type or thickness- and
- No guidance how panel should be attached to the support is provided
- No requirement for containment

- **Ambiguous material classification**

Where human impact on glazing material is of risk, the South African loading standard [7] requires that a simulated impact be delivered by means of a 45 kg lead shot impactor swung from a specified height of 400 mm. The standard requires that the material when impacted to break in a “safe” manner, which is not harmful to humans. (Cutting piercing) In a freestanding balustrade, the glass may fail in a “safe” fashion meeting the requirements set out in the codes, but still allow the person to fall to his or her death. Presently, there is no containment clause in the South African [21] standard.

- **Conservative loading requirement**

The loading code requires an impact of 400 J to be performed, by means of a 250 mm diameter bag filled with dry sand to a weight of 30 kg, on a prototype of the balustrade to be installed. This simulated impact is representative of the most severe accidental human impact, which could occur during its serviceability lifetime. The requirement is conservative and as a result often not performed. The origin of this value is not revealed, and intermediate values are not provided.

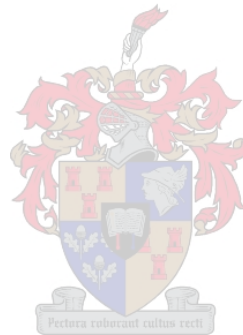
1.3.2 OBJECTIVES

Because of the apparent lack of design guidelines proposed in current design standards [7, 17, 19], the preliminary objective of the study is to:

1. Determine the static- as well as the dynamic material properties of toughened glass. This is determined by means of a laboratory test series, in which glass panels are destructively tested under varying loading rates.

Having done this the main objective of the investigation is to:

2. Determine the static- and dynamic loading capacity of freestanding glass balustrades, which includes the influence of the following parameters:
 - Connection types and sizes
 - Addition of a handrail
3. To make recommendations to the existing design standards based on the results obtained from the study.



1.4 SCOPE OF INVESTIGATION

The scope of this investigation is to firstly identify all parameters that play a major role- and secondly to determine the magnitude of their effect on the static- and dynamic loading capacity of freestanding glass balustrades. The investigated parameters can be categorized under:

- Glass balustrade design and
- Loading requirements.

1.4.1 Glass balustrade design

Due to the lack of design guidelines, the glass balustrade panels, connection type and load arrangements are chosen as to represent the practical range of possibilities that might be found in a modern building. Different connection- and balustrade geometry parameters are investigated as to their effect on the ultimate loading capacity of freestanding glass balustrades. Although not all parameters and the effect they have on the balustrade design can be investigated, it was within the scope of the investigation to determine the effect of the following geometric effects on the loading capacity of a freestanding glass balustrade;

- Hole diameters
- Glass thicknesses
- Number of connections
- Connection types
- Number of rows of connections
- Handrail dimensions
- Number of neighbouring panels

1.4.2 Loading requirements

Given the conservative nature of the South African loading requirements, it is within the scope of the investigation to determine the influence of numerous parameters on the static- and dynamic loading capacity of freestanding glass balustrades. The following parameters with respect to the loading of the balustrade panels are investigated;

- Loading rate
- Impactor stiffness



1.5 STUDY PLAN

The study can be divided into four phases, each of which is identified and described below. Figure 1.4, illustrates the different phases of the project.

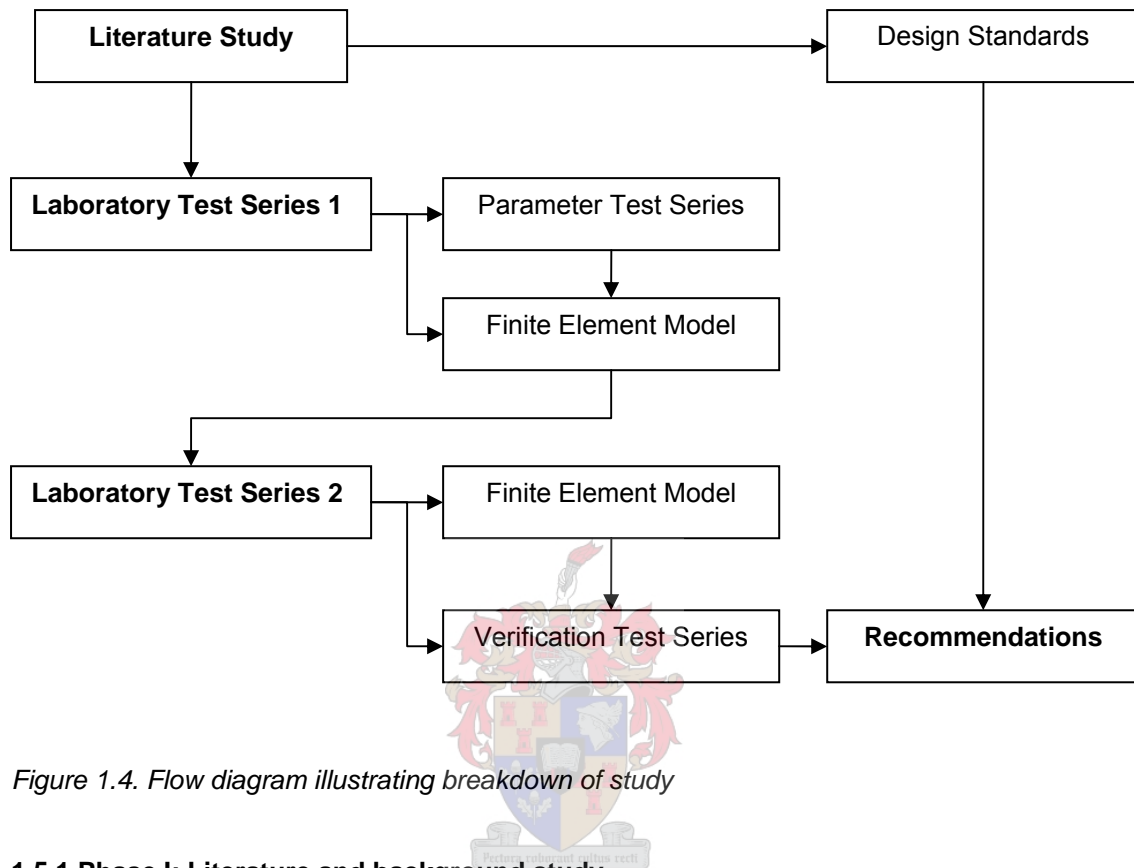


Figure 1.4. Flow diagram illustrating breakdown of study

1.5.1 Phase I: Literature and background study

The first phase consisted of a literature study. The focus of the literature study was firstly to determine the general trend in design standards, and secondly to review all available literature applicable to the investigation.

During the revision of the standards, presented in chapter 2, a comparison of the different standards (South African, American and British) took place in order to determine the general trend in:

- Balustrade and handrail design,
- Material classification and,
- Loading requirements

During the literature review, presented in chapter 1, all literature applicable to the investigation was undertaken to determine:

- Balustrade and handrail design
- Material classification
- Loading requirements

The outcome of this review identified the different loading conditions for which the identified connection- and glass types were modelled and tested.

1.5.2 Phase II: Determination of static- and dynamic material properties

Before the testing of the actual balustrade panels, the static- and dynamic material properties of toughened glass had to be established. The second phase consisted of a laboratory test series, presented in chapter 3, in which 37 scaled down toughened glass panels were tested until failure. During this laboratory test series, the effect of different connection geometry (types and sizes) on the loading capacity of toughened glass panels was investigated. In the laboratory test series, following parameters were investigated:

- Different hole diameters,
- Different glass thicknesses and
- Different connections types

Three different toughened glass thicknesses along with four different connection types were tested. For statistical reasons, three identical panels were tested for each investigated parameter. The panels were loaded until failure under three different loading rates,

- Static-,
- Quasi static and
- Dynamic loading rate.

From the laboratory test series, presented in chapter 3, the ultimate force and displacement was recorded. Due to the stress concentration and complex geometry of the holes, finite element software DIANA [44] was employed to calculate the fracture stress. Using three-dimensional quadratic elements, only half of the glass panels had to be modelled, due to symmetry. The finite element model, presented in chapter 4, was used to investigate the effect of:

- Different hole profiles,
- Determine the loading capacity of each panel.

Finally, the static and dynamic material properties of toughened glass were predicted using the Weibull statistical model.

1.5.3 Phase III: Balustrade Geometry Investigation

Having determined the static- and dynamic material properties of toughened glass, full-scale balustrades could now be analysed using finite elements. The third phase consisted of the finite element modelling of full-scale balustrade panels, presented in chapter 5. The finite element models were used to investigate the effect of different geometry on the loading capacity of the freestanding glass balustrades, and ultimately determine the static- and dynamic loading capacity of each freestanding balustrade. The following parameters were investigated:

- Number of holes
- Connection types
- Number of rows of connections
- Handrail dimensions
- Number of neighbouring panels

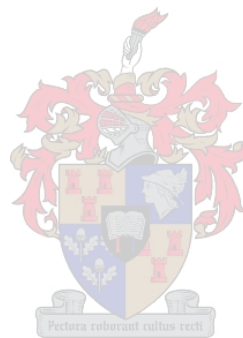
Each panel was loaded as identified in the code revision during phase I. The impact load was modelled in the finite element software, Abaqus as a soft body impact, and as result, an equivalent static force determined.

Having calculated the dynamic loading capacity of each loaded panel for each parameter, it could be determined if the given set-up would be able to sustain the SABS [7] required loading.

1.5.4 Phase IV: Verification

The fourth and final stage consisted of a second laboratory test series, the aim of which was to verify the finite element results of the previous chapter. The second laboratory test series, presented in chapter 6, consisted of three different balustrade set-ups, impact loaded according to its loading capacity as calculated in the previous stage of the study.

The successful resistance of the tested balustrade set-ups resulted in the verification of the balustrade finite element model.



1.6 LIMITATIONS OF INVESTIGATION

Several limitations influenced the results of the project. The main components are described in the following section:

1.6.1 Number of panels

Due to the variability in results in glass, primarily due to flaws and cracks, a large number of panels need to be tested to produce a statistically accurate mean strength.

During the laboratory test series different geometries were tested, which included thickness, hole diameter and panels without a hole. Although only three panels were tested per category, these values could be extrapolated and contribute to the calculation of a statistically acceptable confidence interval. In total 37 panels were tested.

1.6.2 Prediction of prestress around holes

Although the prestress was measured at a number of locations for each panel, the exact level of prestress around the holes and edges could not be determined.

1.6.3 Zwick loading speed

In order to determine the static- and dynamic loading conditions for glass, specimens were tested at three different loading rates. To simulate the dynamic impact load, a loading rate equal to the Zwick upper limit was used.

1.6.4 Extrapolation of stress around holes

Insufficient literature for chamfered holes resulted in the finite element analysis of each tested glass pane. The stress concentration around the holes were numerically computed using the finite element program DIANA. Element sizes around the holes were determined using existing literature, to produce accurate extrapolated stresses. The gradient of the stress concentration tend to infinity around the hole, which produce difficulties when predicting failure stresses numerically.



1.6.5 Prediction of glass static- and dynamic loading capacity

A high variability in the size-, orientation- and distribution of the surface flaws between glass specimens in turn, lead to a high variability of strength in glass. A statistical model is therefore required to give a true prediction of strength of glass, which results in glass strength expressed as a probability of failure.

Each balustrade panel's static- and dynamic loading capacity was determined using a 0.8% probability of failure. This percentage, although conservative, is the typical design value used in the engineering industry [43]. The predicted loading capacity of each freestanding balustrade was therefore determined, taking into account these conservative safety factors.

1.6.6 Determination of Impact load

The dynamic magnitude of the impact force was numerically simulated using a finite element model in Abaqus. In order to model this impact a number of assumptions was made, which influenced the outcome. Impulse was simulated as an elastic collision. The stiffness of the non-compressed impactor was established by a quasi-static compression test. Variability was found to exist between the compressed and uncompressed impactor, which in turn influenced the magnitude of the impact force.

1.7 KEY TO THE USE OF THIS REPORT

In the beginning of each chapter is flow diagram presenting all the major topics to be covered in the chapter. The diagram is there to provide the reader of a visual summary of the chapter and show the position of each topic (section number).

A typical flow diagram consists of different levels (i.e. top, middle and bottom). The top level is occupied by the chapter heading. The middle level is occupied by all the major topics to be discussed in the chapter, which if broken down into sub-topics are occupied by the bottom level.

For illustration purposes the flow diagram of chapter 2 is considered, presented in figure 1.5. Chapter 2, Glass balustrade design, can be categorized into three different topics and subtopics as follows:

1. Handrailing and Balustrading Design
 - Deflection
 - Handrail
2. Material Classification
 - Impact test
3. Loading requirements
 - Static load
 - Impact load

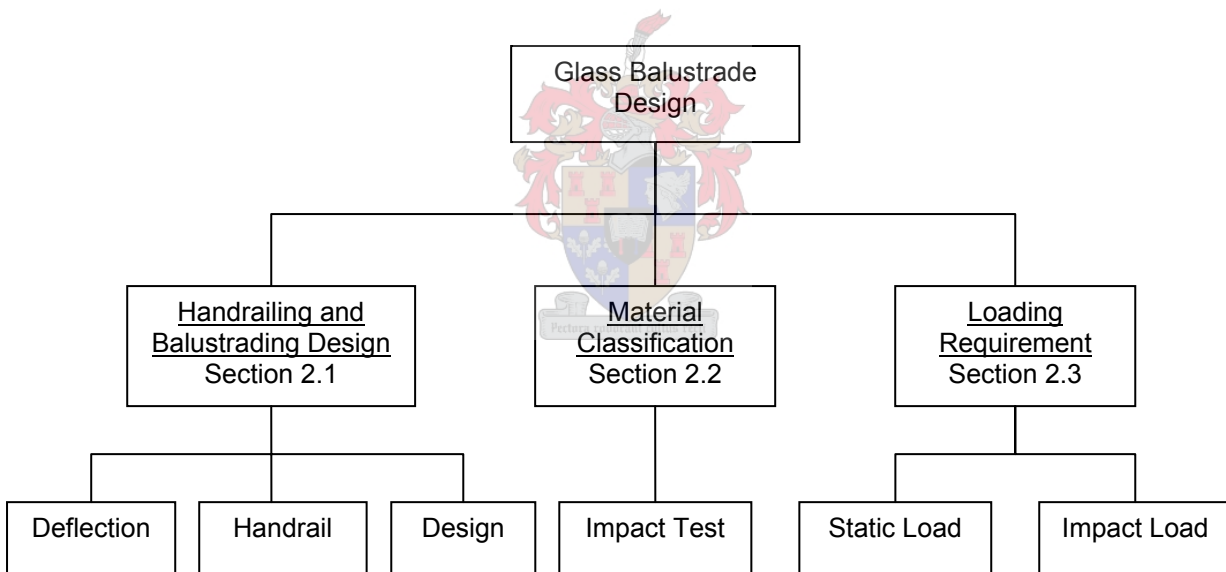


Figure 1.5. Flow diagram of chapter 2

1.8 LITERATURE REVIEW

INTRODUCTION

In 2004 Du Preez [6], performed a number of impact tests on freestanding glass balustrades at the University of Stellenbosch. The balustrade panels were tested and constructed according to guidelines provided by the supplier. It was observed that none of the specimens complied with the guidelines for impact loading stipulated in the SABS [7] loading codes. During the investigation the recommended rigid connection as well as a more flexible connection type was tested. The flexible connection was introduced to act as a medium that undergoes compression in order to absorb a fraction of the applied load. It was concluded that the flexible foundation did not decrease the dynamic impact energy, but did have an effect on the static load the glass panels could sustain.

The overwhelming effect of the impact load on the design criteria of the freestanding glass balustrade nullified the use of a static load requirement. Du Preez suggested the impact guidelines set by the SABS [7] be elaborated to differentiate the magnitude of the impact load requirement accordance to the location and application of the glass balustrade. He encouraged the idea of developing loading scenarios. He further commented on the lack of SABS design guidelines, with respect to glass type, thickness and connection type when dealing with glass balustrades.

CODE DESIGN

The code design section is reviewed in detail in chapter 2.

IMPACTOR

Since the 1960's the pendulum impact test method used to qualify safety glass for use in buildings, have been executed using a lead shot impactor. Since then a number of issues have been raised concerning its conservative nature in simulating human impact. As a result, a test based on a twin tyre impactor (figure 2.7) was developed and implemented in the European codes.

Serruys [8] investigated a number of impactors based on a single tyre, however, this impactor did not give the required performance. The single tyre impactor evolved into a twin tyre impactor concept. This impactor was found to deliver acceptable product performance classification together with breakage. Tests showed that a pressurization of 3.5bar and a weight of 50kg gave the closest representation to that of a human impact.

Oketani [9] investigated the reproducibility, repeatability of the lead shot (figure 2.6) and twin tyre (figure 2.7) impactor. The investigation comprised of five different lead shot - and one twin tyre impactor being tested. The main difference between the impactors was mainly their stiffness. The influence on breakage and fragmentation pattern was also of importance. He recognized the repeatability of the multiple impactors, and found that the reproducibility was found to be determined by the fabrication method. A difference in breakage patterns was found to exist between the lead shot and twin tyre impactor. Impact forces between lead shot and twin tyre impactors could be related with the proper calibration tests.

In another experimental test series, Jacob [10] investigated the impulse generated by the new European twin tyre impactor and compared it to that of the lead shot impactor. A comparison of the horizontal micro-strain measurements versus drop height showed a difference in delivered impact force. He concluded that even though the twin tyre has a larger mass it does not impart as much energy onto the test specimen in comparison to the lead shot impactor.

Foss [11], investigated the ability of lead shot impactor to simulate human impact. The difference between modelled head form and lead shot bag was investigated. Impactor stiffness was determined by a compression loading response experiment and used to calibrate a finite element model. Assuming inelastic collision between human and glass plate, displacement, dynamic force and stress produced was calculated using a finite element model. Four sided linear supported glass plates were investigated. He concluded that the peak glass stress response produced by a head form is higher than that of a lead shot impactor.

BALUSTRADE CONNECTIONS

Communication with designers and suppliers confirmed that connection holes in freestanding balustrades is a common occurrence [47]. An example of typical connections in freestanding balustrades is supplied in a figure in the British code [12], here a designer can choose between a single-, double row or a continuous fixing. Load bearing capacity of continuous and point fixed freestanding balustrades is important.

Daudeville [13], investigated the effect of different hole geometries on the load bearing capacity of glass plates, how the different hole geometries firstly effect the residual stress distribution and secondly the load bearing capacity of the glass plate. The difference in geometry extended to chamfered holes, varying the inner- and outer diameter of hole and chamfer. He found it difficult to accurately measure the residual stresses near edges and around holes, using Photoelastic measurements. However using finite elements [14], he was able to simulate the toughening process and as result compute the resultant residual stresses near holes and edges in glass plates. He introduced the superposition method, where the strength of toughened glass can be expressed as a function of the strength of the glass and the magnitude of residual stress. The loading rate effect was incorporated into the Weibull probabilistic distribution using fracture mechanics parameters, for quasi-static loading rates. He concluded that the Weibull probabilistic distribution could be used to account for the effect of the specimen size, residual stress distribution and the rate of loading.

Schneider [15] investigated the influence of the drilling process on the strength of glass in the area of the holes. Toughened glass panels were destructively tested in coaxial double ring-bending tests. A theoretical model for the prediction of the glass strength using fracture mechanics and measured prestress values was compared with experimental data. It was found that glass strength in the area of drilled holes is dependant on the manufacturing and toughening process. Numerical simulations show that surface stresses at the chamfers of the hole are at least as high as in the infinite part of the plate, whereas the surface stresses are presumably lower in the centre part of the holes.

Siebert [16] investigated the calculation of point bearings for glass as load bearing element. The point bearing itself and the surrounding area was modelled using three-dimensional finite element software. From the investigation, the importance of the mesh size around the hole was noted, and as a result, criteria for adequate modelling by finite elements were formulated.

CONCLUSION

From the previous paragraphs, it can be seen that a considerable amount of both theoretical and experimental work has been performed on the area of structural glass. Despite this, little information exists on the structural capacity of freestanding balustrades subjected to static- or impact loading conditions.

In the next chapter, the design of the glass balustrade is described, with reference to the design codes. The classification together with the loading conditions the balustrade must be able to resist is described.

CHAPTER 2 CODE DESIGN OF FREESTANDING GLASS BALUSTRADES

Introduction

Glass balustrades in and about buildings have evolved over the years into a decorative item, abandoning its primary function and almost losing its definition. Consequently, non-engineers and designers are erecting glass balustrades based on aesthetic beauty rather than functionality. While those who design and construct the balustrade cannot easily be controlled, the standard governing it can. The only solution is to update the relevant design standard to make the effective design and construction of glass balustrades possible.

As technology advances and new material and construction techniques become available, standardized design codes are revised to meet the modern designer's needs. The freestanding balustrade is an example of a modern type of structural system, brought about by the introduction of affordable toughened glass plates onto the construction market. Some countries recognized this, and consequently updated their related design standards to incorporate it...others have yet to do so.

The glass balustrade design process is controlled by three standards, each playing a vital role in the proper design and construction of the freestanding glass balustrade. The three standards are:

- Standard for handrailing and balustrading
- Standard for safety glass classification and the
- Standard for loading requirements

This design process is generic in nature in that the process is the same for all international standards. The individual standards differ, and for this reason are addressed separately in section 2.1, 2.2 and 2.3. In the following paragraphs, each standard playing a role in the design of the freestanding balustrade is discussed. The design process as a whole is illustrated by means of a flow diagram and each standard's role is highlighted.

The Glass balustrade design process

When designing a glass balustrade, where the glass forms part of the structural system, it is the designer's responsibility that the balustrade is designed in accordance with the relevant standards. Glass in balustrades form part of the structural system when it is supported along one, two or three of its edges. When this applies, safety glass is mandatory.

As mentioned before, there are three standards controlling the glass balustrade design. They are:

- Standard for handrailing and balustrading

This standard forms the first step or starting point of the design process and provides the reference to all the other relevant standards. It concerns the overall design of a balustrade, addressing and identifying all aspects, which is relevant to the construction thereof. It provides information and guidance on the positioning, size, handrail, loading and material classification of handrailing and balustrading that are installed to protect people from hazards.

- Standard for safety glass classification

This standard concerns the classification of the material. It provides testing methods for the determination and classification of safety glass.

- Standard for loading requirements

This standard specifies the static and impact loading that the balustrade needs to be able to withstand. Loading condition is dependent on application and location of balustrade.

The overall code design process of a glass balustrade is illustrated by means of a flow diagram in figure 2.1.

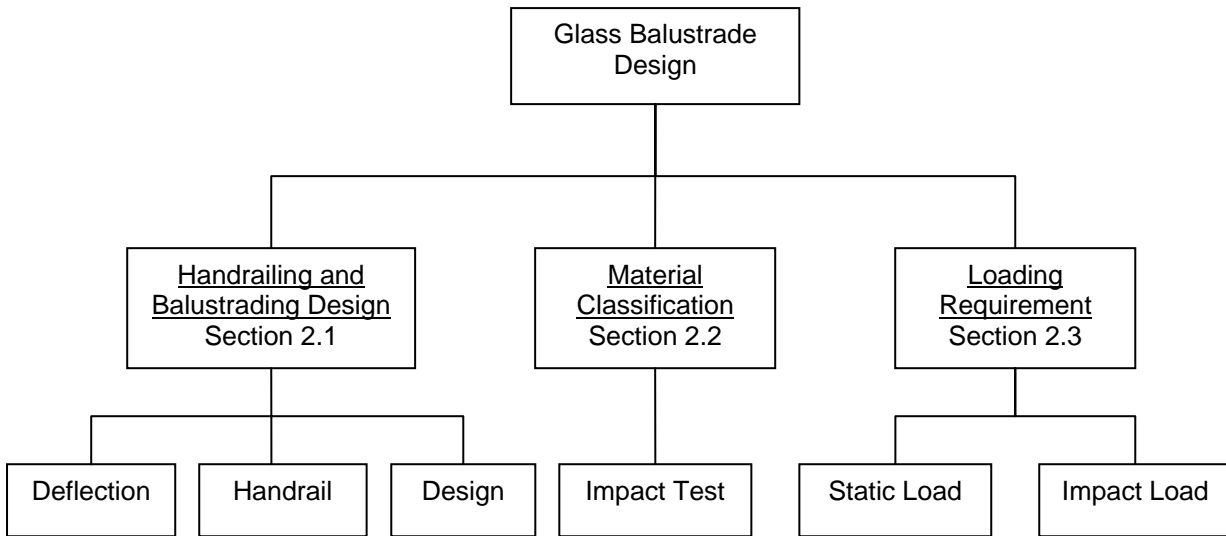


Figure 2.1. Flow diagram to illustrate design process/ requirements of glass balustrade

In the subsequent sections, the three predominant South African standards are reviewed and compared to their international counterparts. Handrailing and balustrading-, loading- and material classification standards from South Africa, Britain and America are compared.

Section 2.1 reviews the handrailing and balustrading design standards under the following topics:

- Design –
- Handrailing –
- Deflection requirements

Section 2.2 reviews the material classification standards under the following topics:

- Procedure
- Impactor
- Drop heights
- Breakage requirements

Finally Section 2.3 reviews the loading requirements of the various standards, under their

- Static loading -
- Impact loading requirements

2.1 HANDRAILING AND BALUSTRADING DESIGN PHASE

Introduction

The handrailing and balustrading standard concerns the overall design of a balustrade, addressing and identifying all aspects, which is relevant to the construction thereof. It provides information and guidance on the positioning, size, handrail, loading and material classification of handrailing and balustrading that are installed to protect people from hazards.

The following section summarizes the South African [17], British [12] and American [18] handrailing and balustrading design standards. Each standard is summarized under the following headings:

- Design-
- Handrail- and
- Deflection requirements

Finally, the differences between these standards are discussed and presented at the end of the section.

The layout of this section is presented by means of a flow diagram in figure 2.2.

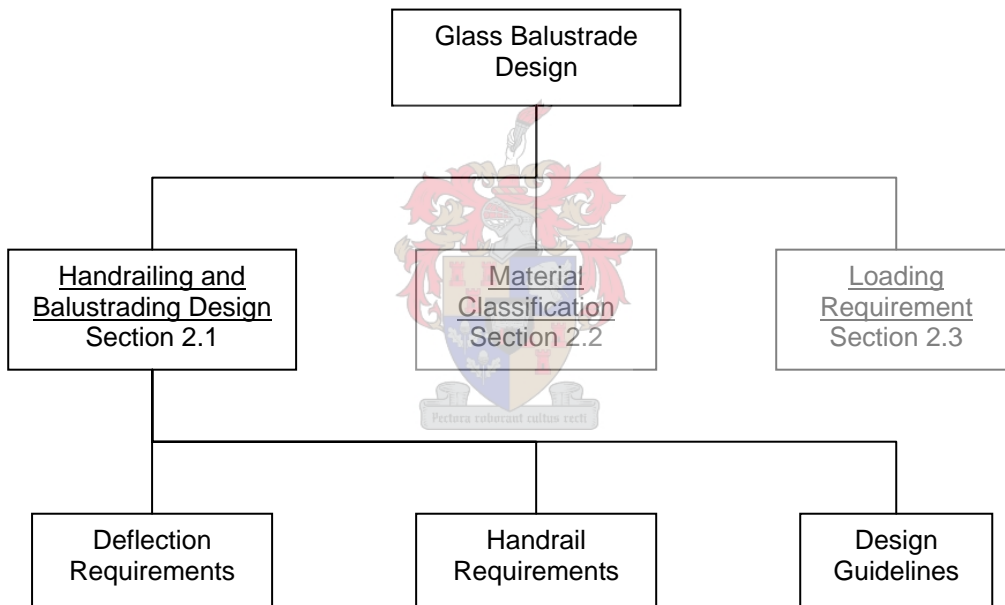


Figure 2.2. Flow diagram illustrating the handrailing and balustrading design phase

2.1.1 South African Handrailing and Balustrading Design Standard (SABS 0104)

The following section summarized the requirements as set out in SABS 0104 [19], with respect to

- Design-
- Handrail- and
- Deflection requirements

2.1.1.1 Design requirements

Balustrade position

Section DD2.2 of SABS 0137 [17] requires that a balustrade to be installed when a change in level is greater than 750 mm.

Connection Type

Nowhere in the SABS 0137 [17] or SABS 0104 [19] are guidelines provided with regard to connection type.

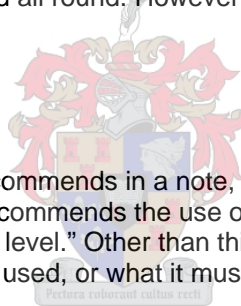
Glass type

The design of glass balustrades fall outside the scope of SABS 0104 [19], further section 5.6 of the standard recommends that the glazing to handrailing be done in accordance with the relevant provisions of SABS 0137 [17].

Section 5.5.5 of SABS 0137 [17], recommend that the glass in balustrades be toughened safety glass, unless rigidly supported all round. However, no guidance to minimum thickness to be used is provided.

2.1.1.2 Handrail Requirements

Section 5.5.5 of SABS 0137 [17] recommends in a note, which reads: "Where glass is used in a balustrade, the glazing industry recommends the use of a handrail. Such handrail should be of at least 1m from the finished floor level." Other than this clause, no other indication is provided when a handrail should be used, or what it must be designed for.



2.1.1.3 Deflection Requirements

The deflection of handrailing, which is provided to reduce the likelihood of people or objects passing over or through the handrailing, is provided in Section 4.6 of SABS 0104 [19], and recommends that handrailing be installed in such a way that the vertical sag of any of its elements does not exceed 50 mm. It also requires that when a load of 1.5A (A = nominal accidental load, as described in SABS 0160 [7]) is applied at any point and in any direction on any element of the handrailing for a period of 1h, the total deflection of that point while under load shall not exceed 100 mm.

2.1.2 British Handrailing and Balustrading Design Standard (BS 6180:1999)

The British design standard BS 6180:1999 [12], Barriers in and about building, are structured in the same way as its South African counterpart, but elaborates to a greater extent. The following section summarizes the requirements as set out in BS 6180 [12] with reference to:

- Design-
- Handrail- and
- Deflection requirements

2.1.2.1 Design requirements

Balustrade position

Section 8.5.2 of BS 6180 [12] requires that a balustrade to be installed when a change in level is greater than 380 mm.

Connection Type

Clamping systems for freestanding barriers are detailed in BS 6180 [12].

Glass type

BS 6180 [12] requires the use a minimum of 12 mm toughened safety glass in freestanding balustrade.

2.1.2.2 Handrailing Requirement

Position

Section 8.5.2 of BS 6180 [12] requires that a handrail be used when a barrier protects a difference in level greater than 600 mm.

Connection

Section 8.5.2 of BS 6180 [12] recommends that a continuous fixing should be used for fixing the handrail to the glass, as individual fixing points may introduce unacceptable stress concentrations. Technical drawings illustrating both point- and continuous connections are provided in figure B.2 of BS 6180 [12] (figure 2.3).

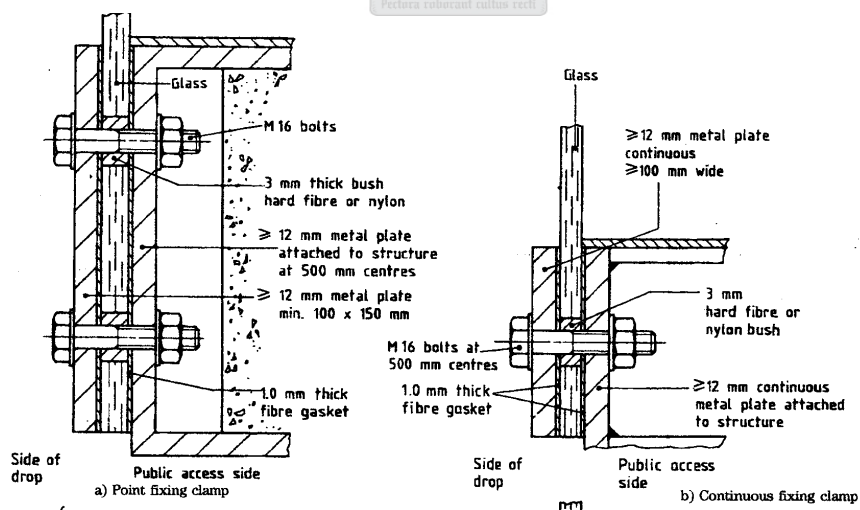


Figure 2.3. Typical balustrade connections illustrated in BS:6180 [12]

Containment

Section 8.5.2 of BS 6180 [12] requires that the handrail be attached to the glass in such a manner that, should a glass panel fail, the handrail:

- Will remain in position
- Will not fail if the design load is applied across the resulting gap

2.1.2.3 Deflection requirement

Section 8.5.1 of BS 6180 [12] requires deflection to be limited to $L/65$ (L =height of balustrade), when subjected to the required static loading conditions as described Table 4 of BS 6399 [20].

2.1.3 American Handrailing and Balustrading Design Standard (CPSC 16 CFR 1201)

The following section summarizes the requirements as set out in CPSC 16 [18] with reference to:

- Design-
- Handrail- and
- Deflection requirements

2.1.3.1 Design requirements

Balustrade position

The CPSC 16 [18] requires that a balustrade to be installed when a change in level is greater than 380 mm.

Connection Type

No guidance provided.

Glass type

Section 2407.1 of CPSC 16 [18] requires glass used as structural balustrade panels to be constructed of either single fully toughened glass or laminated heat-strengthened glass. For all glazing types, the minimum nominal thickness should be 10 mm.

2.1.3.2 Handrailing Requirement

Section 2407.1.2 of CPSC 16 [18] requires that each handrail or guard section be supported by a minimum of three glass balustrades or otherwise constructed to remain in position should one balustrade fail. It clearly states that glass balustrades may not be installed without an attached handrail.

2.1.3.3 Deflection requirement

CPSC 16 [18] requires deflection to be limited to $L/65$ (L =height of balustrade).

2.1.4 Comparison between the international and the South African handrailing and balustrading design standards

Having summarized the South African [19], British [12] and American [18] handrailing and balustrading design standards in the previous section, this section compares each of the standards. Table 2.1, summarizes the different requirements of all the considered standards.

Table 2.1 Comparison between different handrailing and balustrading design standard requirements

International Standard	Design			Handrail			Deflection
	Position	Connection type	Glass type and thickness	Position	Connected panels	Containment Clause	
South African	>750mm	No	No	No	No	No	100mm
British	>380mm	Figure 2.3	toughened >12mm	>600mm	3 or more	Yes	Height/65
American	>380mm	No	toughened >10mm	Always	3 or more	Yes	Height/65

The South African handrailing and balustrading design process was adopted from the American design process; their similarities can be seen through comparison. Both have a central standard (handrailing and balustrading) controlling the design and construction of any balustrade, irrespective of material. The central standard controls all the aspects common to balustrade design and provides reference to the material standard (the installation of glazing in buildings). The material standard provides additional requirements, applicable only to the material under consideration. Effective communication is therefore necessary between the two standards, in order to avoid ambiguous guidelines and classification, a problem seen in the South African standard, which is further discussed in the following paragraph.

Handrailing and balustrading standard

The lack of sufficient guidelines to ensure the safe erection of glass balustrades of the South African design standard can be seen in table 2.1, by comparing the different standards. Considering the design of a balustrade (irrespective of material used), the South African standard fails to provide guidelines to which connection type or height of balustrade to use. Further, most of the provided guidelines are for information purposes only, and as a result are left to the designer's discretion. This is the case for the necessity of handrail. The central standard [Handrailing and balustrading] should be compiled in a manner that addresses all central aspects applicable to the design and construction of a balustrade, irrespective of the material used.

Glazing material standard

The only purpose of the material standard is to provide effective guidance to the safe usage and installation of the specific material. Considering the South African material standard, no guidelines to which connection type or minimum glass thickness to use is provided. The guidelines provided, is for information purposes only.

The British design process differs from that of the South African in that there is only one standard controlling the design of balustrades. This standard [12] accounts for different materials and as a result provides more thorough guidelines, as all aspects are covered in one standard. This can be seen in table 2.1. All aspects necessary for the safe erection and construction of a glass balustrade is covered.

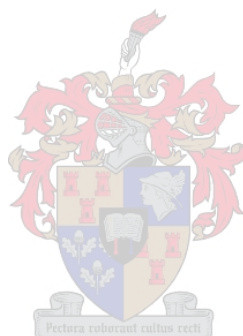
2.1.5 Conclusion

The handrailing and balustrading standard concerns the overall design of a balustrade, which is necessary to ensure the correct installation and construction thereof. Three standards including the South African [19] British [12] and American [18] were summarized and compared under their respective design-, handrail- and deflection requirements.

Comparing the South African handrailing and balustrading standard [19] to its international counterparts, a lack of sufficient guidelines to ensure the safe erection of glass balustrades was established. The following topics, which require attention, were identified:

- Connection type to use with glass balustrade
- Minimum height of balustrade
- Handrail use and details
- Glass type to use
- Minimum glass thickness
- Post failure containment

It was further noted that most of the provided information in the South African standard is for information purposes only, and as a result, the design of a freestanding glass balustrade is left to the designer's discretion.



2.2 MATERIAL CLASSIFICATION IN THE DESIGN PHASE

Introduction

The standard for safety and security glazing materials for buildings concerns the classification of glazing materials under human impact. The purpose of which is to reduce the risk of injuries caused by cutting and piercing in the event of breakage. It provides testing methods for the determination and classification of safety glass.

The classification of safety glass as to its performance under accidental human impact has been undertaken since the development of the standard using a pendulum impact test set-up. A lead shot bag was used as impactor to represent the impulse generated by a human body impact. Since then, a number of problems such as the reproducibility and repeatability have been reported [9]. The following section investigating the applicability of the old lead shot bag and a new proposed twin tyre impactor, before reviewing the relevant material standards.

A number of international standards, including the South African [21], British [22] and American [23], for the material classification of toughened safety glass are reviewed. Each standard is summarized under the following headings:

- Impactor,
- Drop height and,
- Breakage requirements

The layout of the material classification phase is summarized by means of a flow diagram presented in figure 2.4.

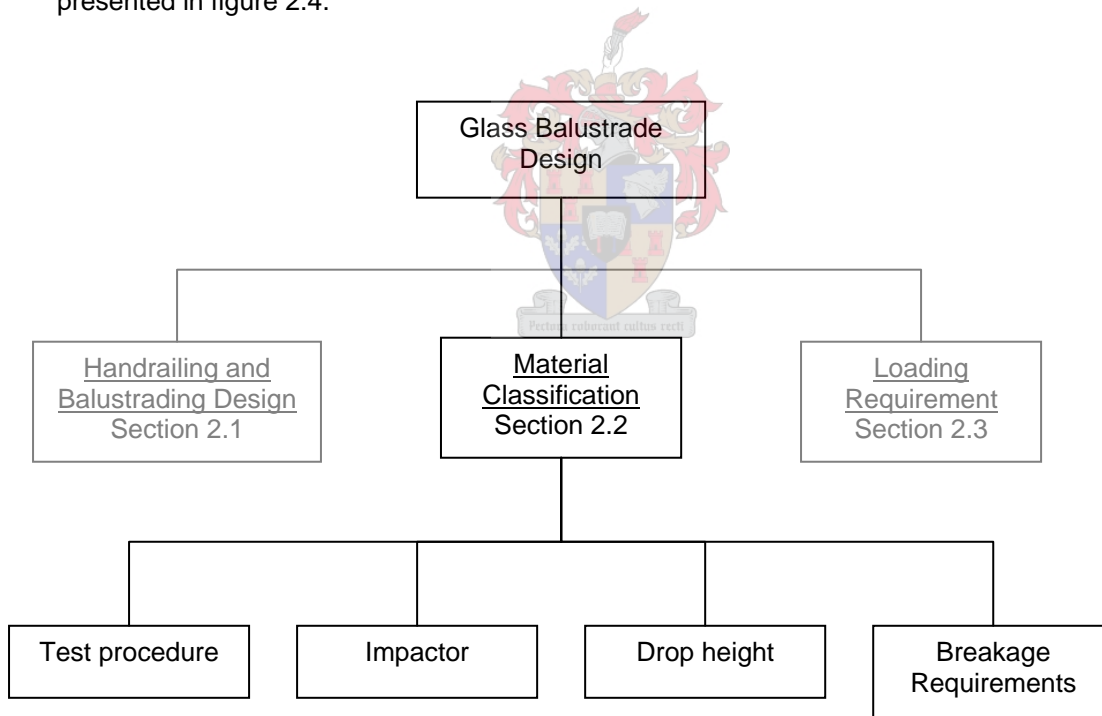


Figure 2.4. Flow diagram illustrating the safety glass material classification phase

2.2.1 Test Procedure (SABS 1263:1986)

The test procedure is generally the same for most of the different international material classification standards [21, 22, 23] and is therefore not compared to one another in this section. The purpose of the test is to determine if the material, upon fracture, will fail in a way that is not harmful to humans.

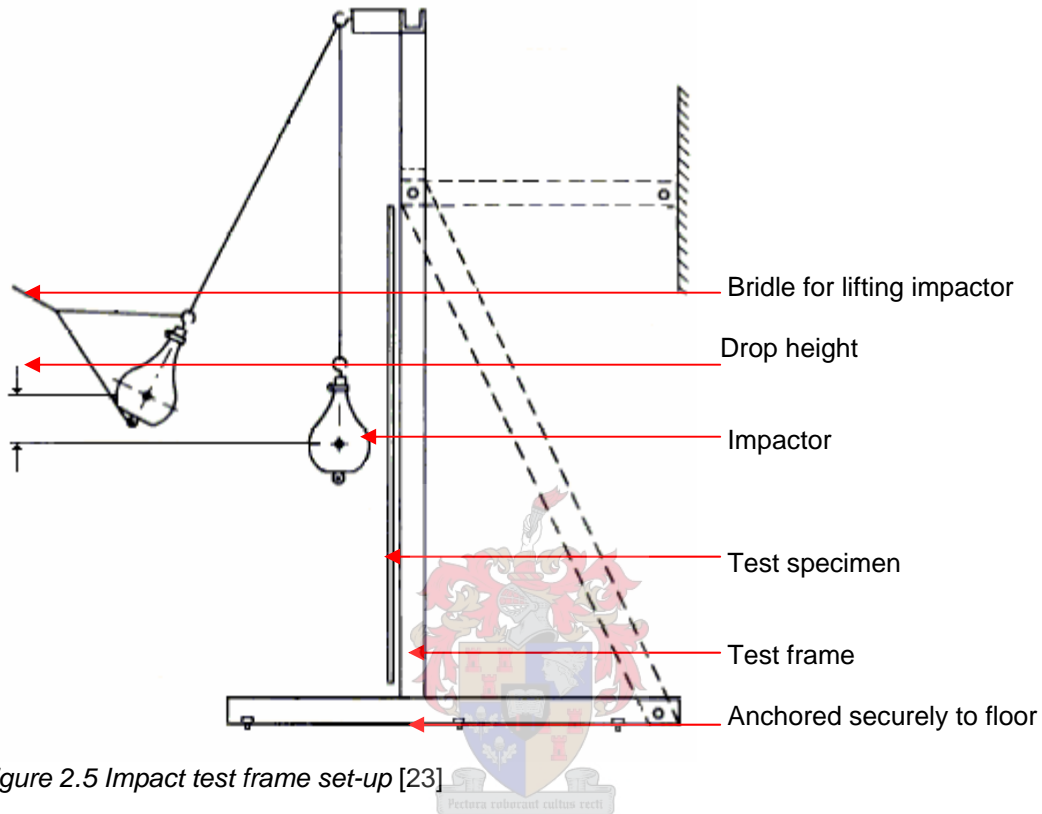


Figure 2.5 Impact test frame set-up [23]

Figure 2.5, illustrates the impact test frame and impactor used to test each specimen. The test procedure consists of three components a test specimen, test frame and impactor.

2.2.1.1 Test specimen

The material classification standard [21] requires that four identical specimens be tested, and that each test specimen is rectangular, 865 mm wide x 1930 mm high. If this size is not available by the supplier, then the maximum size available should be used instead.

2.2.1.2 Test frame

The test frame remains the same for all standards considered in that it is so constructed that the test specimen can be clamped along all four edges. The test frame can be seen in figure 2.5.

2.2.1.3 Impactor

The impact is used to simulate human impact, and differs between the different international design standards. The different impactors are considered in section 2.2.2 of this chapter.

Once the test specimen is placed in position, the impactor is suspended from an overhead support so that the impacting object, when at rest, is no more than 50 mm from the centre of the specimen. Each specimen is then struck only once at the centre with the impacting object swinging at a pendulum arc from an identified drop height above the centre line of the specimen (see figure 2.5 for drop height).

The procedure remains the same for all applications, regardless of the intended use or required performance. For example, a 1 m x 1 m toughened freestanding glass balustrade panel would be tested in the same way as a 2 m x 4 m linear supported sliding door. The only variables in the test procedure are the thickness of the test specimens and drop height, which is determined by the designer.

This section described the procedure of the material classification of brittle materials used in buildings. The next section describes the various impactors that are currently used by the different related standards, and goes on to compare the ability of each to simulate human impact.

2.2.2 Impactors

The classification of safety glass as to its performance under accidental human impact has been undertaken since the development of the material classification standard [23] in the 60's using a lead shot bag [26] (figure 2.6). The lead shot bag was initially designed to represent the impulse generated by human body impact on brittle material. Since then, a number of problems such as the reproducibility and repeatability have been reported [9, 10, 26]. The lead shot bag was also thought of as being conservative, as loads produced by the impactor are much higher than those produced by a human body. As a result, a test based on a twin tyre impactor was developed.

The following section summarizes the difference between the two impactors and compares them on grounds of impulse generated, reproducibility and repeatability.

2.2.2.1 Lead shot impactor

The impactor consists of a leather- or polyvinyl chloride bag consisting of an inner rubber bladder that is filled with No.7 1/2 chilled lead shot till the total mass of the assembly is approximately 45 kg. The exterior of the bag is completely covered with polyester glass fibre-reinforced tape of width 12 mm.

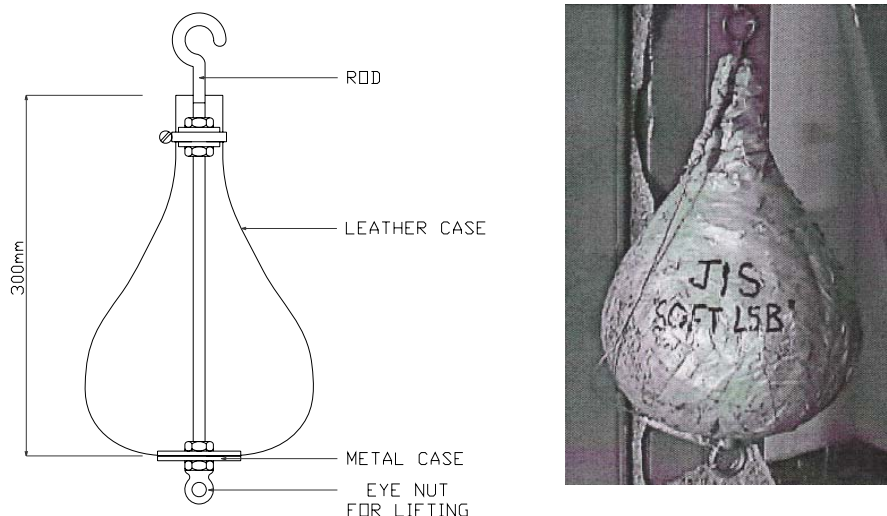


Figure 2.6. Illustration and photo of lead shot impactor [10]

2.2.2.2 Twin tyre impactor

In a previous investigation [8, 9, 10], a number of bodies based on a single tyre impactor were tested; however, this impactor did not give the expected performance. The single tyre impactor eventually evolved into the proposed twin tyre impactor. This impactor was found to deliver acceptable product performance classification together with breakage. Tests showed that a pressurization of 3.5 bar and a weight of 50 kg gave the closest representation to that of a human impact. As a result, the new twin tyre impactor was introduced into the European standard [24] (figure 2.7).

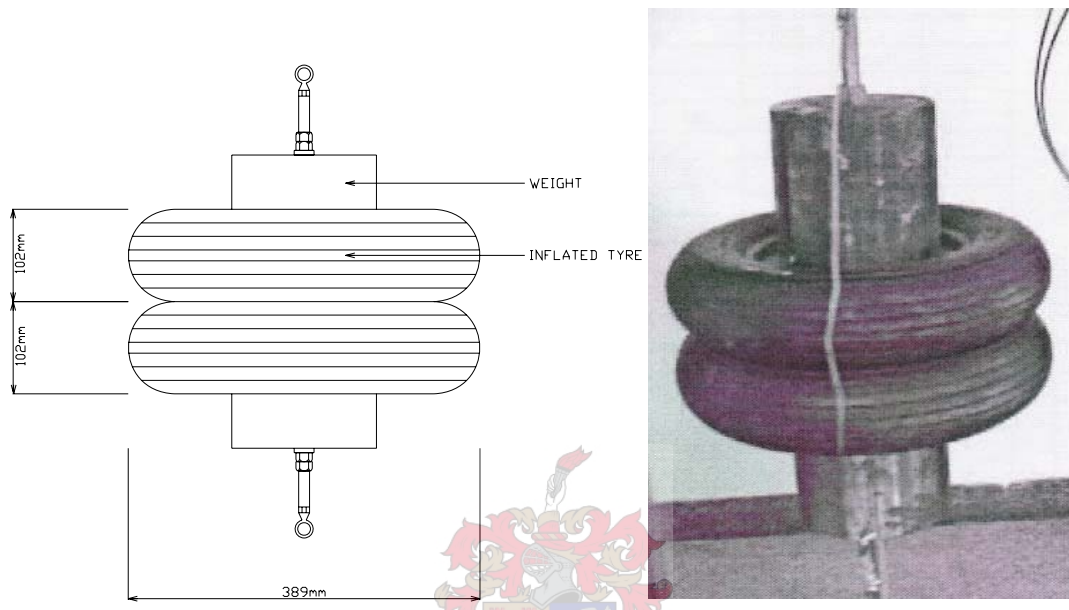


Figure 2.7. Illustration and photo of twin tyre impactor [10]

The following section compares the performance of the lead shot- and twin tyre impactor. Comparisons are made between the two impactors based on:

- Impulse generated,
- Repeatability of the impactor and
- Reproducibility of the impactor, finally conclusions is drawn.

2.2.2.3 Comparison between Lead shot impactor and Twin tyre impactor

2.2.2.3.1 Impulse

Comparative tests [8, 9, 10], were undertaken to establish the difference between the lead shot impactor and twin tyre impactor. The impulse generated by the two impactors were measured and compared to that produced by a human shoulder impact. The force generated as a result of an impact, for a 200 mm drop height, is presented in figure 2.8 for each impactor.

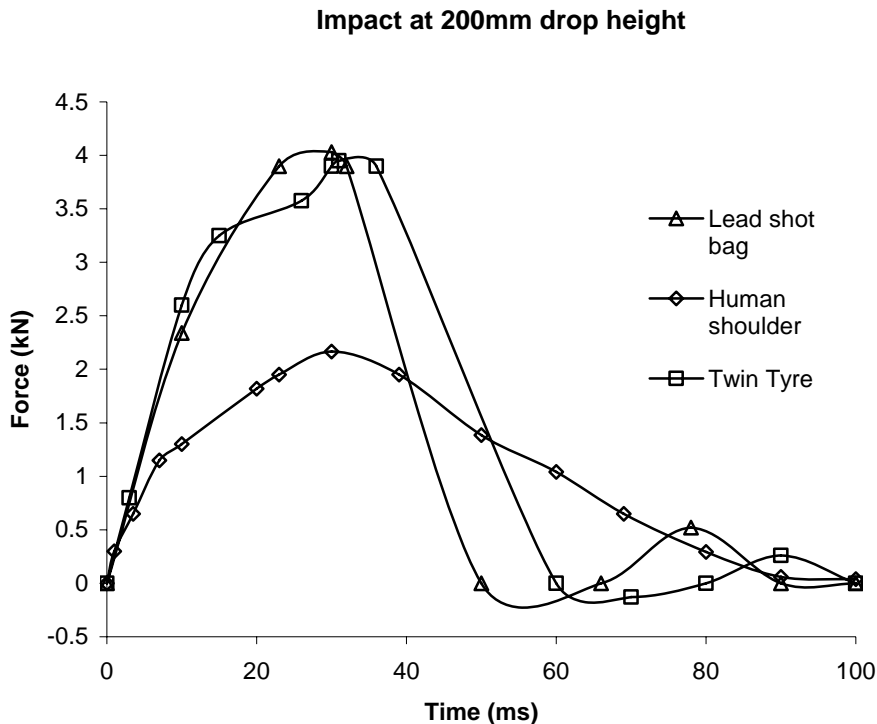


Figure 2.8. Impact force generated by the different impactors [8]

2.2.2.3.2 Repeatability

Oketani [9] measured the impact stresses on the glass surface, during his investigation into the repeatability and reproducibility of the relative impactors. He concluded that all impactors showed good reproducibility. The maximum coefficient of variance for principal stress in all the impactors was 0.01 during the repeatability tests, and as a result, the multiple impact repeatability of the shot bag was accepted.

In another investigation [10] in which glass specimens were tested until failure, it was found that toughened glass with surface compression in excess of 100 MPa, irrespective of glass thickness, was unlikely to be fractured with the twin tyre impactor. Almost all toughened glass test panels with surface compression of 100 MPa or greater were found not to fracture at the maximum drop height of 1200 mm, while the lead impactors almost always eventually fractured the glass specimens, irrespective of level of prestress. This raises the important issue of suitability of using the PrEN 12600 [24] twin tyre impactor for classifying toughened glass as safety product.

2.2.2.3.3 Reproducibility

In the same investigation [10], the reproducibility of the various shot bags was investigated. The reproducibility considers the difference in impact energies delivered by shot bags made by different individuals. For this experiment, three different hard type shot bags made by different companies were used.

It became clear that in the study, strain generated by impact was strongly dependent on the difference of hardness of impactors. As stiffness of shot bag is known to depend on mainly on tapping procedure. It was considered that shot bag reproducibility could be controlled by deciding the fabrication method for the standard shot bag, especially the tapping rule.

Conclusion

From the various investigations, it was determined that the twin tyre impactor does not impart as much energy onto the test sample in comparison with the lead shot impactor. In order to be able to use the twin tyre instead of the lead shot bag, new equivalent drop heights had to be determined first.

It was also evident that the shot bag reproducibility was controlled by deciding the fabrication method, especially the taping rule. Therefore, the inclusion of a taping rule should be investigated. (I.e. all shot bags taped tightly, or all shot bags taped lightly)

From the results, it is recommended that the initial proposed lead shot impactor be left unchanged. Its ease of construction and low cost also plays a part.

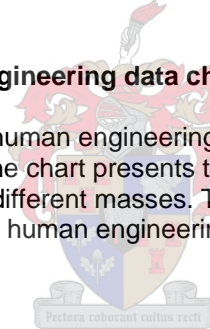
2.2.3 Drop heights

The drop height refers to the vertical height from the horizontal centreline of the impactor when it is released to a similar horizontal centreline when it is at rest vertically (see figure 2.5). The drop height is very important as it ultimately determines the magnitude of the force delivered to the glass specimen.

In the following sections, the origin of the drop height and impact energies is identified and described. Impact energies based on different scenarios are described, and finally drop heights from international standards are compared.

2.2.3.1 Development of human engineering data chart

The drop heights originated from a human engineering chart (Figure 2.9), which was developed by safety experts [23]. The chart presents the impact energies created at different impact velocities by impactors with different masses. Three masses of 45, 68 and 90kg are presented. Figure 2.9, illustrates the human engineering chart.



Human Engineering Data

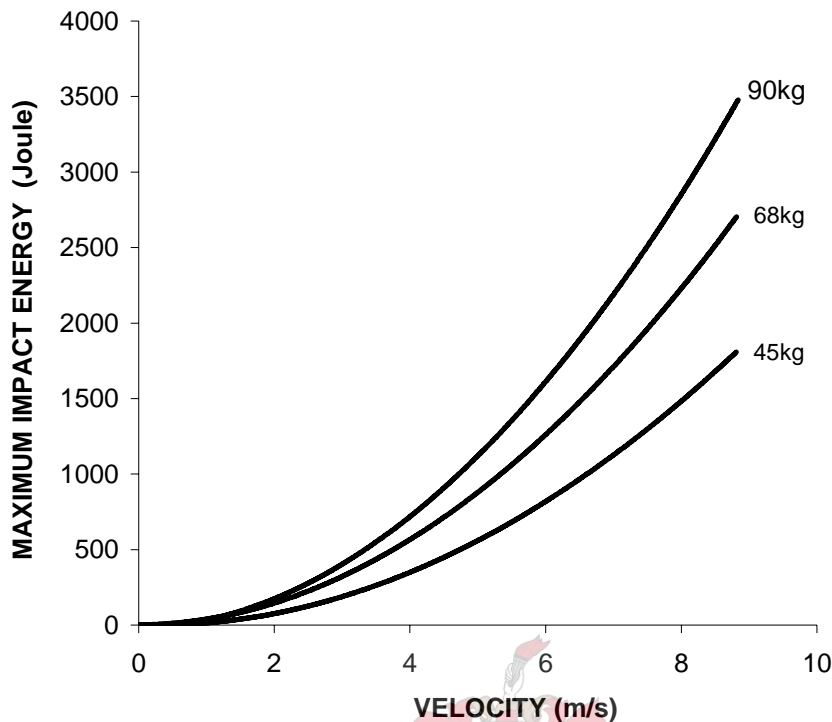


Figure 2.9. Human engineering chart [23]



Equivalent drop heights

Impactor drop heights were chosen based on a few assumptions. Firstly, a 45 kg person was identified to be representative of a typical glass breakage accident victim. Secondly, two situations were identified, and for each situation, a representative velocity was selected. The identified situations were:

- Situations in which limited acceleration path exists
- Situations in which unlimited acceleration path exists

Situations in which limited acceleration path exists

Velocities of 2.5 m/s and 3 m/s were identified as being representative of a typical glass breakage accident victim, for situations where a limited acceleration path exists.

Situations in which unlimited acceleration path exists

A 5 m/s velocity was identified for situations where an unlimited acceleration path exists and a human might develop something approaching his full impact velocity.

Having identified the mass and the velocities of the impactor, the equivalent drop heights were determined. Using energy methods, the kinetic energy of a body could now be calculated as follows:

$$E_k = \frac{1}{2}mv^2 \quad (2.1)$$

Where:

- E_k = kinetic energy (J)
 m = mass of object (kg)
 = 45kg
 v = velocity of object (m/s)
 = 2.5m/s
 = 3m/s
 = 5m/s

Table 2.2 presents each velocity's corresponding kinetic energy.

Table 2.2. Impact energy

Velocity	Kinetic Energy
m/s	J
2.5	135
3	201
5	538

Having identified the kinetic energies the equivalent drop heights could easily be determined using the principals of conservation of energy. The conservation of energy states that the total energy of an isolated system is constant despite internal changes [25]. Therefore, the maximum potential energy (before release) of the impactor is effectively converted into kinetic energy (before impact) when the impactor is at the bottom of the arc, and no energy is lost in the system (equation 2.1 = equation 2.2). The drop height corresponding to each velocity is calculated by making equation 2.1 equal to equation 2.2, and calculating h.

Potential energy is defined as follows:

$$E_p = mgh \quad (2.2)$$

Where:

- E_p = potential energy (J)
 m = mass of object (kg)
 h = drop height (m/s)

Table 2.3 presents each velocity's corresponding drop height.

Table 2.3. Equivalent drop heights

Energy	Drop heights
J	mm
135	305
201	457
538	1219

Therefore, these three different drop heights were adopted by most of the international material classification standards, when this standard was initially developed. These drop heights have changed over the years among standards. The following section reviews the different applicable standards and identifies the different drop heights in used.

2.2.3.2 Comparison between the international and South African drop heights

The American standard [23] was the first standard produced and consequently influenced the other standards, it can be seen in table 2.4 with reference to drop height.

Table 2.4. The different standards with their proposed classification, drop height and impactor used are summarize

Country	Standard	Classification	Drop Height (mm)	Impactor	Energy (Joules)
South Africa	SABS 1263	Safety Glass	410	45kg Lead shot	180
	SABS 0160	Safety Glass	1360	30kg Sand bag	400
USA	ANZI Z97.1	Safety Glass	1219	45kg Lead shot	538
			457	"	201
			305	"	135
UK	BS 6206	Safety Glass	1219	45kg Lead shot	538
			457	"	201
			305	"	135
Australia	AS 2208	Safety Glass	300	45kg Lead shot	300
Europe	PrEN12600	Safety Glass	1200	50kg Twin Tyre	589
			450	"	220
			190	"	93

From table 2.4, it is noted that most of the standards remained the same with reference to drop height. Only the South African and Australian material classification standards have changed from three different drop heights into a single drop height. The South African drop height is based on the average of the three-drop heights while the Australian is the lowest of the initial three-drop heights. Further, the European standards have since introduced a new twin tyre impactor, but have retained the original three-drop heights.

In case of failure of the specimen when impacted at the identified drop height, the fractured specimen has to adhere to certain safe break requirements. The following section describes the different breakage requirements as specified by the different standards.

2.2.4 Breakage requirements

For the material classification of safety glass, the specimen under investigation is not required by specification to be able to fully resist the required impact force produced by the swinging impactor. To be classified as a safety material, the specimen only has to meet the required safe breakage criterion as required by the material classification standards. Breakage requirements are therefore introduced as criterion by which the broken specimen is assessed.

In the following section, breakage requirements from a number of international standards including the South African [21], British [22], and American [23] standards are described. Breakage requirements applicable to each of the standards are then summarized in table 2.5 and presented at the end of this section.

2.2.4.1 Comparison between International and South African classifications

In some countries, fragmentation test procedures in which the glass is broken with a centre punch are used in addition to or in place of the pendulum impact test to classify toughened glass. In most of the standards, there exists a common trend concerning the safety requirements. Listed below are a description of all the requirements as found in the South African [21], British [22], American [23], Australian [27] and European [24] standards. Table 2.5 summarizes the reviewed standards and indicates which of the criteria they require.

- **NO BREAKAGE**

This criterion requires that the test specimen remain unbroken, it need not necessarily have remained within the test frame.

- **BREAKS SAFELY**

This criterion requires that if the test piece breaks, the 10 largest crack free particles remaining 3 minutes after the impact not weigh more than the mass equivalent to 6500 mm² of the original test piece in the test frame.

- **NO OPENING**

This criterion requires that in the case of failure, that no opening be produced through which a sphere of diameter 75 mm can freely pass.

- **NO SPLINES**

This criterion requires that none of the broken glass pieces may have sharp edges that are pointed or dagger like, and that any resulting sharp edge should not be capable of cutting or piercing human flesh.

- **PARTICLE COUNT**

This criterion requires in the case of failure, the test specimen shall have a particle count of 40 particles in a 50 mm x 50 mm².

- **CONTAINMENT**

This criterion requires that in the case of failure, the material remain together.

Table 2.5. Breakage criteria as required by each standard

Breakage Requirements						
Country	No Breakage	Break Safely	No Splines	No Opening	Particle Count	Containment
South Africa	Yes	Yes	Yes	Yes	-	-
USA	Yes	Yes	Yes	Yes	-	-
UK	Yes	Yes	Yes	Yes	Yes	-
Australia	-	-	-	Yes	-	-
Europe	-	Yes	-	Yes	-	Yes

From table 2.5, it is noted that the breakage requirements of South Africa is identical to that of the USA and that of the UK with the exception of the particle count. Upon failure toughened glass fracture into small "harmless" glass cubes. The formation of these glass cubes are brought about by the sudden release of energy, which is introduced into the glass during the toughening process and referred to as the level of prestress (see chapter 1.1). The level of prestress directly influences the strength of the glass specimen and is related to size of the fractured sugar cube. A higher level of prestress will result in a smaller sugar cube. The particle count is therefore an indication of the specimen's strength. The inclusion of the particle count test into the South African code is therefore recommended.

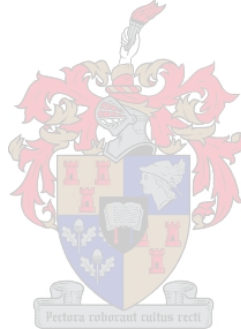
The reason for the difference in breakage requirements of the European standard can be attributed to the type of impactor used.

2.2.5 Conclusion

The classification of safety glass as to its performance under accidental human impact has been undertaken since the development of the standard using a pendulum impact test set-up. A lead shot impactor was used to represent the impulse generated by a human body impact. Since the development of the material classification standards, a new impactor based on a twin tyre set-up has been introduced. From various investigations, it was determined that the twin tyre impactor does not impart as much energy onto the test sample, and it was consequently decided that the lead shot impactor, as used by the South African standard [21], be left unchanged.

Another parameter that influenced the introduced impact energy is the drop height of the impactor. Numerous standards were investigated and consequently, the origin of the drop height and impact energies was identified. It was established that the drop heights originated from a human engineering chart, which was developed by safety experts [23]. Three different drop heights were initially introduced. It was noted that most of the standards retained these drop heights. Only the South African and Australian material classification standards use a single drop height.

In case the specimen fractures upon impact, the material classification standard requires the specimen to adhere to the safe breakage criterion. Breakage criteria from numerous standards was compared to each other. It is established that the breakage requirements of South Africa [21] is identical to that of the American [23] and that of the British [22] with the exception of the particle count. As the particle count is an indication of the strength of the specimen, it was consequently recommended that it be included into the South African material classification standard [21].



2.3 LOADING REQUIREMENT DESIGN PHASE

Introduction

This standard details the minimum design loads to be adopted in the design of freestanding glass balustrades. Loading can be categorized into static- and impact loading requirements. The static- and impact loading is representative of the loading, which can be expected to be imposed on a balustrade throughout its lifetime. It can further be categorized according to application and position.

A number of international standards, including the South African [7], British [20] and American [18] standard, for the loading requirements of balustrades, are reviewed. Each standards are summarized together under the following headings:

- Static loading- and
- Impact loading requirements

The layout of the loading requirement phase is illustrated by means of a flow diagram in figure 2.10.

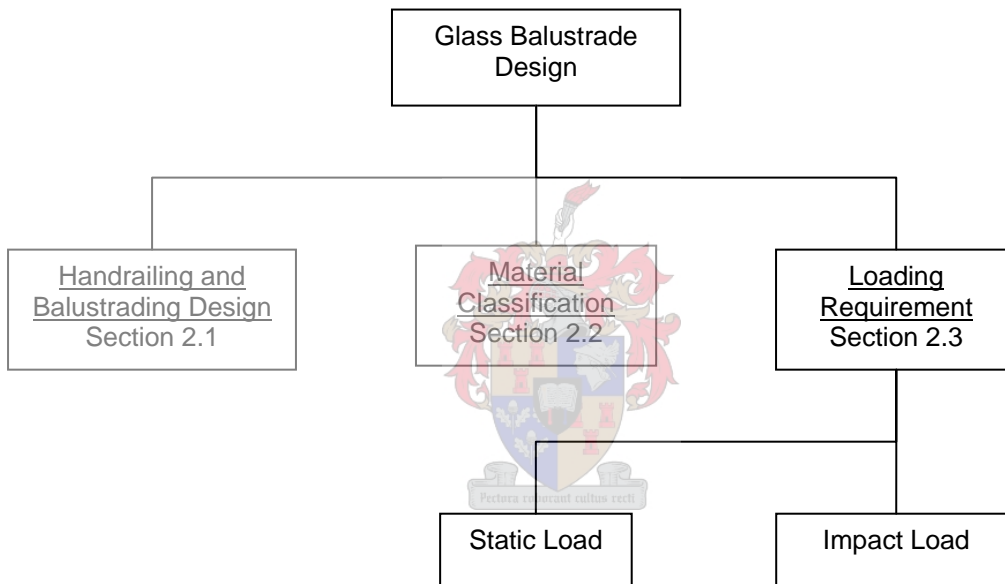


Figure 2.10. Flow diagram illustrating the loading requirement phase

2.3.1 Static loading requirements

Static loads appropriate to the type of occupancy for the building or part of the building or structure are generally categorised according to application and position. Balustrade application and position are categorized into:

- Residential application other than roofs
- Places of public assembly other than grandstands and to roofs to which public has access
- Grandstand

Together with the application of the balustrade, three loading types have to be considered:

- Horizontal Line Load (kN/m)
- Concentrated or Point Load (kN)

Indicative balustrade applications and their associated static loads are presented in table 2.6 for the South African [7] and British [20] loading standards.

Table 2.6. Static loading requirements

Country	Application	Line Load (kN/m)	Concentrated Load (kN)
South African	Residential	0.5	1
	Public	1.5	1
	Grandstand	3	1
British	Domestic	0.36	0.25
	Office	0.74	0.5
	Public	1.5	1.5
	Grandstand	3	1.5

From table 2.6 the similarity in static loading requirements between the South African and British loading standards is seen. Similarities in defined applications and magnitude of required loading are seen. Some small differences do exist between the two standards. A common difference between the two standards can be seen when comparing the different defined balustrade applications; the South African standards define only three applications while the British have four. Another difference is seen in the magnitude of the required concentrated loads associated with each application. While the South African standard requires a concentrated load of 1kN regardless of application, the British requires a different concentrated load for every application.

Balustrades are required to sustain both static- and impact loading conditions. Having compared and presented the required static loading requirements, the following section presents the impact loading requirements.

2.3.2 Impact loading requirements

As for the static loading requirements, impact forces differ according to application and position. Loading standards account for these different applications by introducing multiple classifications. The American standard [18] for example has two classifications, Category 1 and 2, corresponding to 457- and 1219mm drop heights respectively. The different standards with their corresponding impact loading requirements are presented in table 2.7.

Table 2.7. Impact loading requirements

Country	Standard	Classification	Drop Height (mm)	Impactor	Energy (Joules)
South Africa	SABS 1263	Impact load	1360	30kg Sand bag	400
USA	ANZI Z97.1	Category 2	1219	45kg Lead shot	538
		Category 1	457	"	201
UK	BS 6206	Class A	1219	45kg Lead shot	538
		Class B	457	"	201
		Class C	305	"	135
Australia	AS 2208	Grade A	300	45kg Lead shot	300
Europe	PrEN12600	Classification 1	1200	50kg Twin Tyre	589
		Classification 2	450	"	220
		Classification 3	190	"	93

In most of the international standards a similarity exist between the country's material classification- (table 2.4) and impact loading requirements (table 2.7). This can be seen by

comparing table 2.4 to table 2.7. The reason for the similarity in both the use of impactor and drop heights is attributed to the integration of the two standards. Effective communication between the two standards results in the requirement of a single impact test to:

- Classify the material and
- Enforce the impact loading requirements

This is true for the American [18], British [20], Australian [27] and the European [24] design standards. It is only when comparing the South African [21] material classification- and loading requirements that a difference between the two standards is noted. From table 2.7, it is seen that a different impactor and drop height is enforced. No correlation between the two impact tests is seen, and as a result, two individual impact tests have to be performed.

Further, no correlation can be established between the South African- [7] and other international loading standards' [22, 23, 24] impact loading requirements. While most of the other loading standards define two- or three different impact-loading requirements applicable to the application and position of the balustrade, the South African standard defines only one. The single entry, of the South African loading standard, often result in the over design of a glass balustrade.

Conclusion

When designing a glass balustrade the material needs to be classified in accordance with SABS 1263 [21] and the balustrade needs to be able to resist both static- and impact loads as enforced by SABS 0160 [7].

The South African [21] material classification design standards were originally adopted from its American [23] counterpart. The initial purpose of the standard was the classification of brittle materials when impact tested. A human impact was simulated using a pendulum impact test performed by a lead shot bag dropped from an identified height, based on a typical impact scenario (Human engineering data chart, figure 2.9). The material was classified as safety material if:

- 1) the material did not break or
- 2) when broken, adhered to the breakage requirement.

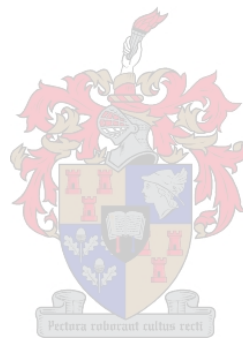
The purpose of the standard later evolved to include impact-loading requirements. Using the same procedure and impactor, different drop heights were introduced. These drop heights were introduced to represent different impact speeds at which a 45 kg teenager could strike a balustrade. Balustrades are therefore classified according to application and position. These classifications are part of the loading requirement and the balustrade need to be designed to resist these loads. Most of the international standards [22, 23, 24] integrated the impact loading- and material classification requirement. Therefore, avoiding separate testing procedures.

The South African [7] standards failed to recognize this, and consequently introduced a brand new impactor. The new impactor consists of a 250 mm diameter bag filled with sand to the weight of 30 kg. This impactor has never been investigated concerning reproducibility, repeatability or the magnitude of impulse generated.

With the introduction of the new impactor, the South African standards [7, 23] now require two separate tests to be performed when designing a glass balustrade. The two tests are:

- Pendulum impact using a lead shot bag for the material classification of the material and a
- Pendulum impact test using the sand bag impactor for the impact loading requirements

Having summarized all of the South African design standards relevant to the design and construction of glass balustrades, and concluding the literature study, the next chapter presents the first phase of the project.



CHAPTER 3 CONNECTION CAPACITY OF FREESTANDING BALUSTRADES

Introduction

In a continuous glass balustrade set-up, the loaded panel can distribute the force to the adjacent panels. A single freestanding balustrade panel however is required to sustain the same loading as a number of connected panels in a continuous balustrade set-up, resulting in a larger and often unacceptable stress concentration at the connections of the panel. As seen in chapter 4, it is at these connections where fracture occurs. Therefore, in a freestanding balustrade the connection type plays a crucial part in the design of the balustrade. Ultimately, the connection set-up controls the structural capacity of a freestanding balustrade.

Typically, freestanding balustrade panels are connected using either numerous point supports or a continuous edge support. The continuous edge support system often consists of a balustrade panel placed in a steel channel that is connected to the adjacent structure. Appendix B of the British standard [12] provides technical drawings of typical connections for freestanding balustrades. In figure 3.1, examples for continuous edge supports can be seen. Silicone or high elasticity modulus sealants are placed between the steel and glass to ensure the continuous support of the glass. This is the most conservative type of support, as no additional stress concentrations are introduced.

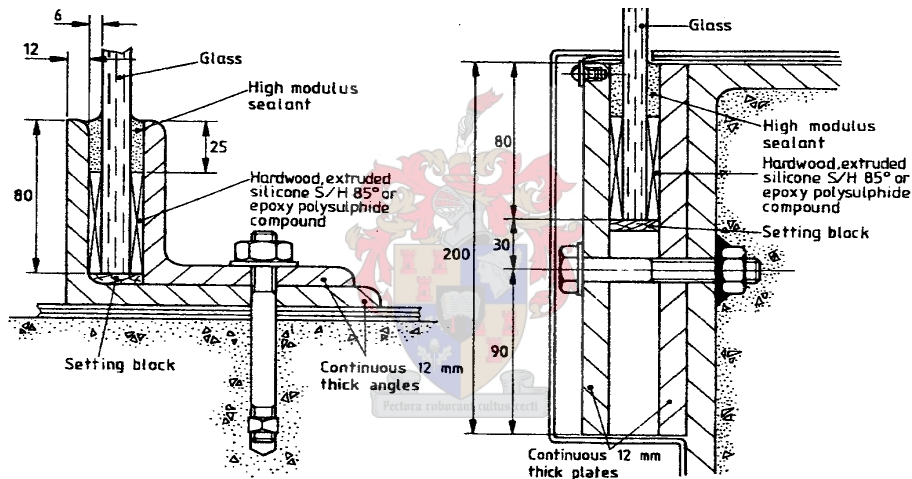


Figure 3.1. Freestanding continuous support system [12]

Alternatively, holed connections through which the glass balustrade is connected to the adjacent structure using bolts are used. These holes, through which the balustrade panel is connected, introduce regions of stress concentrations, therefore reducing the loading capacity of the panel. In figure 3.2, point supported systems can be seen as provided by the British standards [12]. As for the continuous support system, high elasticity modulus sealant is placed in between the glass and steel bolts.

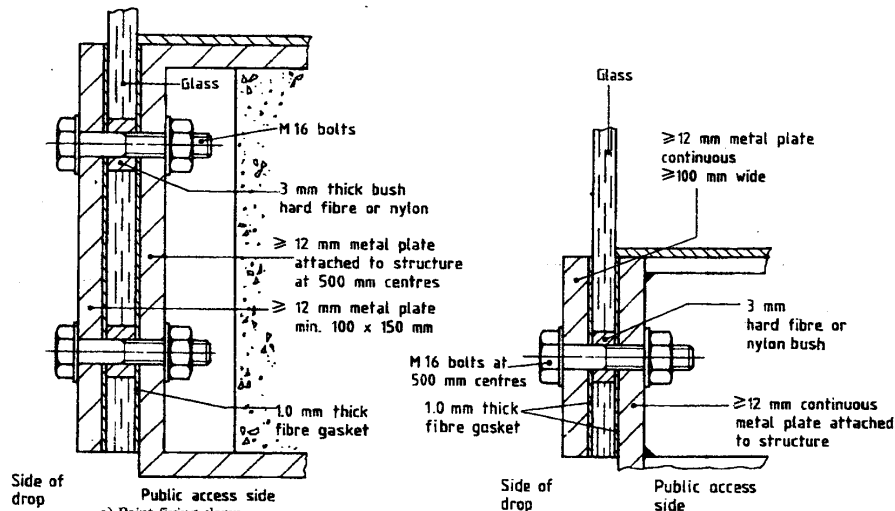


Figure 3.2. Freestanding point support system [12]

Freestanding glass balustrades have to adhere to both static- and impact-loading conditions, as set out in the relevant loading standards [see section 2.3]. Although the static loading requirements are important, it is the impact loading requirements that is the dominant load case [6].

Glass differs from other conventional structural materials in that it exhibits different material properties under varying loading rates. One of these material properties important to structural engineers is that there is an increase in glass strength with an increase-loading rate [28]. Although this is a well-known fact, technical information regarding the mechanical properties of toughened glass extends to the static properties, and provides little information concerning the dynamic properties of the material.

To predict the loading capacity of freestanding glass balustrades, the influence of the connection type and the dynamic material properties of toughened glass have to be known. It was consequently decided that a laboratory test series be undertaken in which:

- The loading capacity and influence of different connections (types and sizes) and,
- The static- and most importantly the dynamic material properties of toughened glass are determined.

This chapter describes the laboratory test series in which 37 scaled down toughened glass panels were tested in bending. These panels were loaded until failure, using three different loading rates.

The layout of the chapter and the manner in which the laboratory test series was undertaken is illustrated by means of a flow diagram in figure 3.3.

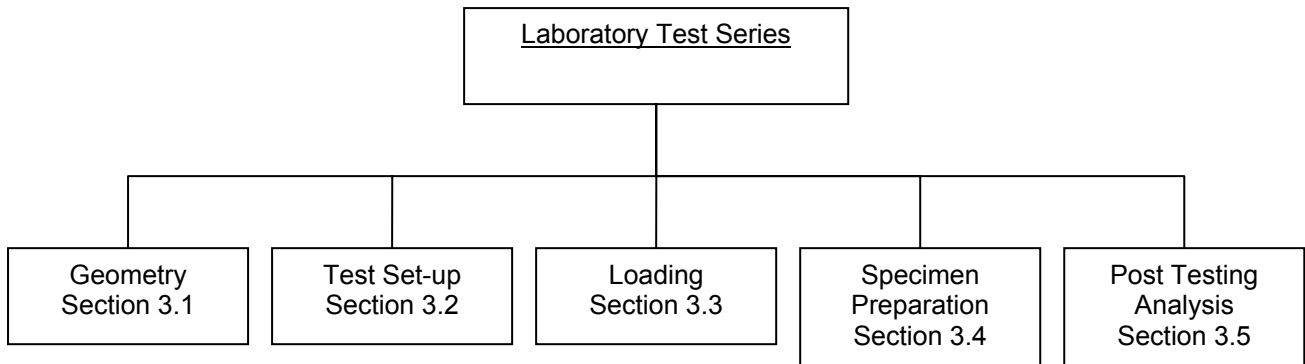


Figure 3.3. Flow diagram illustrating the layout of the laboratory test series

The laboratory test series can be categorized into four steps. In the subsequent sections each of these steps are addressed separately and described in detail, they are:

- **Geometry of the test panels**
Before the commencement of the test series, the test panel geometry had to be determined, which would best represent the real life problem.
- **Design of test set-up**
This section describes the test set-up and test rig in which the glass panels were tested.
- **Loading of test panels**
This section describes the loading rates used for the testing of the glass panels.
- **Test panel preparation**
This section describes the various activities performed on each glass panel prior to the testing. These activities would help with the prediction of panel strength and give insight into the behaviour of glass.
- **Post testing analysis**
Finally, each tested panels is examined. This section describes the various activities performed following the destructive testing of each panel.

3.1 TEST GEOMETRY

Introduction

Typical freestanding glass balustrade panels are usually between 1-2 m wide and are generally 1 m from the finished floor level, as this dimension is controlled by the related handrailing and balustrading design standard [see section 2.1]. Instead of using actual 1x1 m glass panels, it was decided that scaled down panels would be satisfactory in determining the material properties. The scaled glass panels, was chosen based on design standards and supplier specifications.

This section describes the geometry of the scaled down balustrade panels that was destructively tested in the laboratory test series.

The layout of this section is illustrated in the flow diagram in figure 3.4.

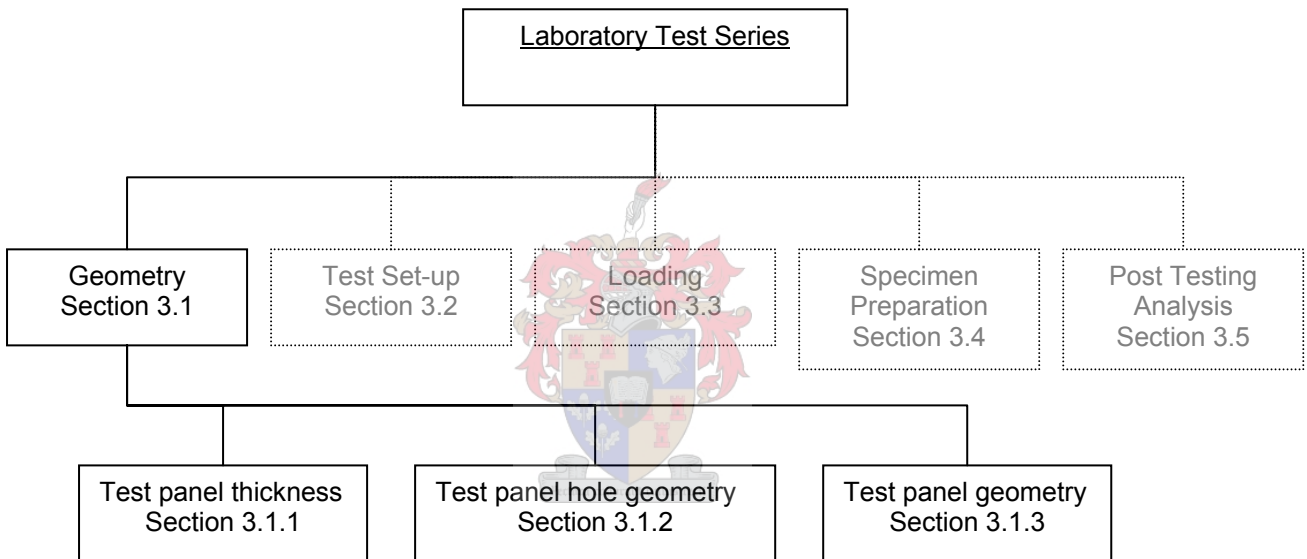


Figure 3.4. Flow diagram illustrating layout of the geometry stage of the laboratory test series.

The following section describes the test panel geometry, and is categorized under the following headings:

- Test panel thickness
- Test panel hole geometry
- Test panel geometry

3.1.1 Test panel thickness

The test panel thickness was chosen based on guidelines supplied in the British Standard [12], which requires the use of a minimum thickness of 12 mm toughened glass in freestanding glass balustrades. Communication with suppliers confirmed that 12 mm thick glass is mostly used in freestanding balustrades with a continuous edge support, and suggested that 15 mm thick glass be used when the glass is not continuously supported (figure 3.5). A third thickness of 10 mm was chosen for extrapolation purposes.

It was consequently decided that 10, 12 and 15 mm thick toughened glass panels be tested.

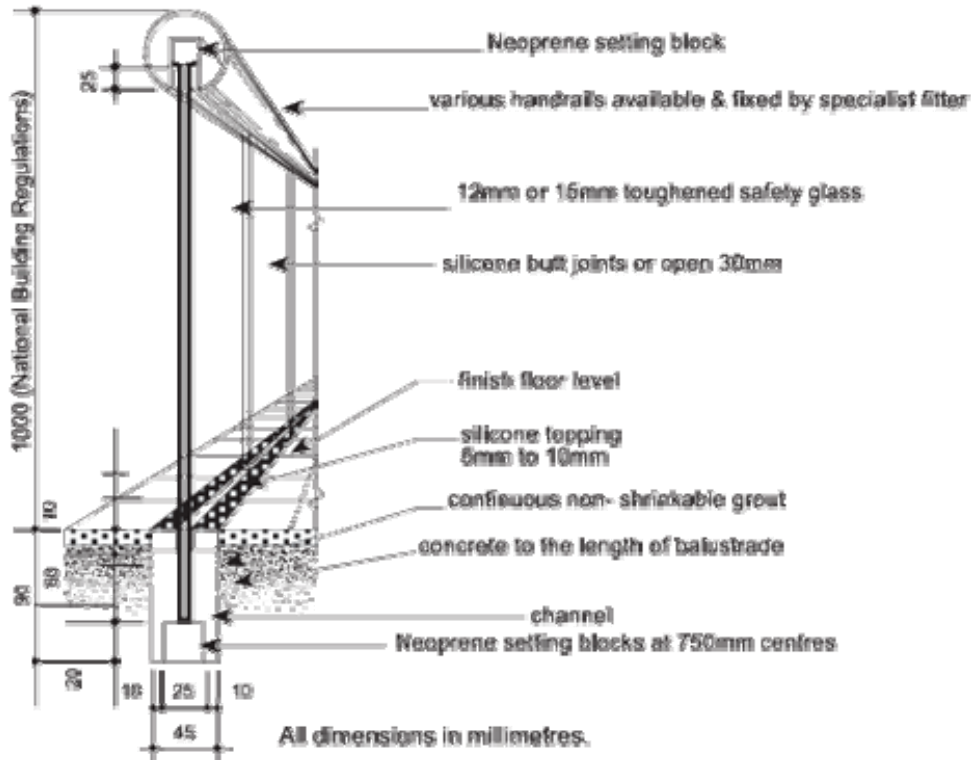


Figure 3.5. Glass balustrade specifications [42]

3.1.2 Test panel hole geometries

Before the test panel geometry could be selected, the placement of holes with regard to distance from edge and distance from each other had to be established. ASTM C 1048 [29] provides guidelines with respect to placement of holes:

Distance between edge and hole

Section 7.8.2.1 of ASTM C 1048 [29] suggests that the minimum distance from any edge of the glass to the nearest point on the rim of a hole must be 6 mm or 1.5 times the thickness of the glass, whichever is greater.

$$X \geq 6 \text{ mm or } 1.5t, \text{ whichever is greater}$$

Distance between two holes

Section 7.8.2.2.1 of ASTM C 1048 [29] suggests that the minimum distance between the centres of adjoining holes in 5 mm or thicker glass must be at least 10 mm or two times the glass thickness times the larger hole diameter, whichever is greater.

$$Y = 10 \text{ mm or } 2tD, \text{ whichever is greater (t = glass thickness)}$$

Hole diameter

Section 7.8.3 of ASTM C 1048 [29] suggests that a minimum diameter holes of 6.4 mm or the thickness of the glass, whichever is greater.

$$D = 6.4 \text{ mm or thickness of glass, whichever is greater}$$

The placement of holes according to ASTM C 1048 [29] is summarized in figure 3.6.

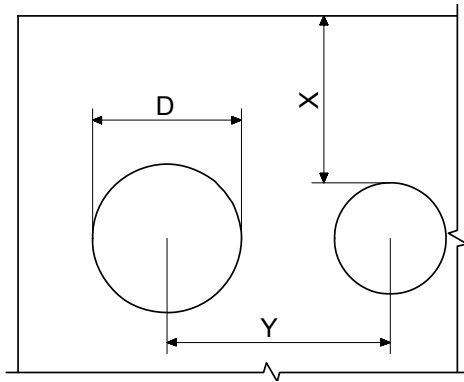


Figure 3.6. Placement of holes as suggested by ASTM C 1048 [29]

With a maximum panel thickness of 15 mm, the minimum diameter of a hole was thus 15 mm. Hole diameters of 15, 20 and 25 mm were consequently chosen. Table 3.1 summarizes the positioning- and placement of the holes which ultimately determined the scaled down panel size.

Table 3.1. Positioning of holes

Thickness	Diameter					
	15mm		20mm		25mm	
	$x \geq$	$y \geq$	$x \geq$	$y \geq$	$x \geq$	$y \geq$
10mm	15	300	15	400	15	500
12mm	18	360	18	480	18	600
15mm	22.5	450	22.5	600	22.5	750

3.1.2.1 Residual stresses near edges and holes

The stress distribution near edges is a result of the interaction of the top- and the bottom surfaces together with the edge cooling rates, as described in chapter 1.2. Therefore, the geometry of the panel had to consider the residual stress distribution near the edges. The geometry of the panels was chosen too prevent any further stress superposition. If the edge and the hole were chosen too close to each other, they could further influence each other's stress distribution. Daudeville [30] determined in an investigation which used a finite element simulation of the thermal tempering of glass that the stress only normalizes at a distance of 10-15 mm from the edge.

If a hole and edge is therefore closer than 30 mm from each other (centre to centre), it will further influence the stress distribution.

3.1.2.2 Cylindrical hole with chamfer (common geometry of hole used in industry)

Holes in glass are drilled from both surfaces towards each other, using a diamond-cutting tool. (see figure 3.7)

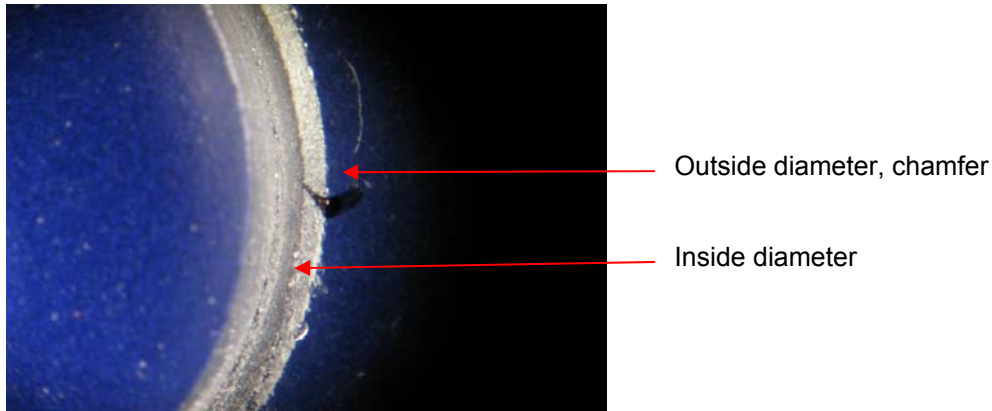


Figure 3.7. Hole with chamfer

This drilling process introduces surface flaws around the hole, which might serve as an additional stress concentration factor and consequently influence the capacity of the glass panel. For this reason, suppliers chamfer the holes to reduce the number of surface defects, caused by the drilling process. The holes are chamfered at 45 degrees, and consequently increase the outside diameter of the hole by 2 mm. It may be noted that the water jet cutting of holes introduce less surface flaws and has consequently become popular in parts of the world. However, this technology is not yet used in South Africa.

3.1.3 Test panel geometry

Typical freestanding glass balustrade panels are usually between 1-2 m wide and are generally 1 m from the finished floor level, as this dimension is controlled by the related handrailing and balustrading design standard [see section 2.1]. Instead of using actual 1x1 m glass panels, it was decided that scaled down 300x300 mm panels would be satisfactory in determining the material properties. Panels with- and without holes were chosen to represent both point- and continuous supported balustrades.

Holes were positioned, taking into account:

- Guidelines with respect to placement of holes provided by ASTM C 1048 [29]
- Residual stresses near edges and holes

The final geometry of the glass panels without holes is illustrated in figure 3.8 and panels with holes in figure 3.9. Figure 3.10, illustrates a section through a hole and indicated the inside- and outside diameter of the hole.

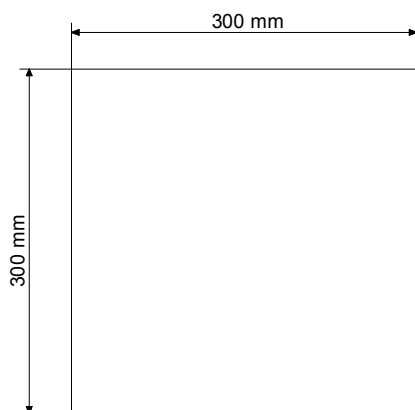


Figure 3.8. Glass panel without hole geometry

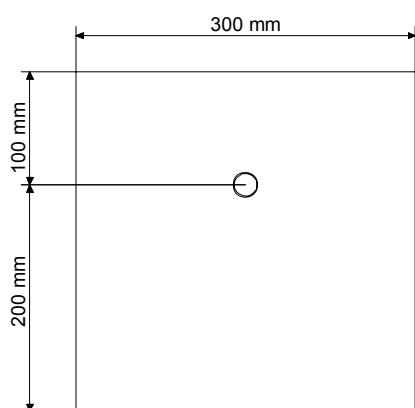


Figure 3.9. Glass panel with hole geometry

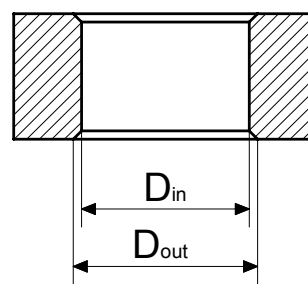


Figure 3.10. Glass hole geometry

Panel thicknesses and corresponding hole diameters are presented in table 3.2.

Table 3.2. Dimensions of chamfered holes

Thickness mm	Diameter inside mm	Diameter outside mm
10	10	12
15	15	17
20	20	22

The variability in the strength of glass, caused by surface defects [31], resulted in the testing of three panels per parameter. Three different thicknesses together with four different connection types were tested under static- and dynamic loading conditions. The number of panels associated with each configuration is given in Table 3.3.

Table 3.3. Number of panels tested

Thickness (mm)	Diameter (mm)				
	10	15	20	no hole	
10	3	3	3	3	12
12	3	3	3	3	12
15	3	3	3	3	12
				Total	36

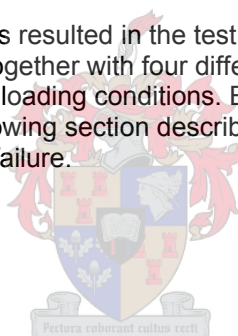
3.1.4 Conclusion

The geometry of the scaled down balustrade glass panels were chosen based on supplier- and manufacturer specifications. Glass panel thicknesses 12- and 15 mm were selected and a third thickness of 10 mm was chosen for extrapolation purposes.

Hole geometry was selected taking into account ASTM [29] guidelines and the residual stress distribution near edges and holes. Consequently, hole diameters of 10-, 15- and 20 mm were selected.

Instead of using actual 1x1 m glass panels, it was decided that scaled down 300x300 mm panels would be satisfactory in determining the material properties, as this panel size adhered to all the minimum requirements.

The variability in the strength of glass resulted in the testing of three panels per parameter. Finally, three different thicknesses together with four different connection types were chosen to be tested under static- and dynamic loading conditions. Before each panel could be tested, a test rig had to be designed. The following section describes the test rig in which each glass panel was loaded out-of-plane until failure.



3.2 DESIGN OF TEST SET-UP

Introduction

The geometry of the test specimens was determined in the previous section. Panels with- and without holes were chosen, representative of different connection types. Therefore, a test set-up had to be designed which was multifunctional, while adhering to various requirements.

This section describes the test set-up, which was designed to determine the out-of-plane bending capacity of the glass panels. The test set-up consisted of a test rig and loading rig, both of which are addressed in detail.

The following section concerns the test set-up, and can be categorized into the following headings:

- The test rig
- The loading rig
- The test measurements

The layout of the test set-up section is illustrated by means of a flow diagram in figure 3.11.

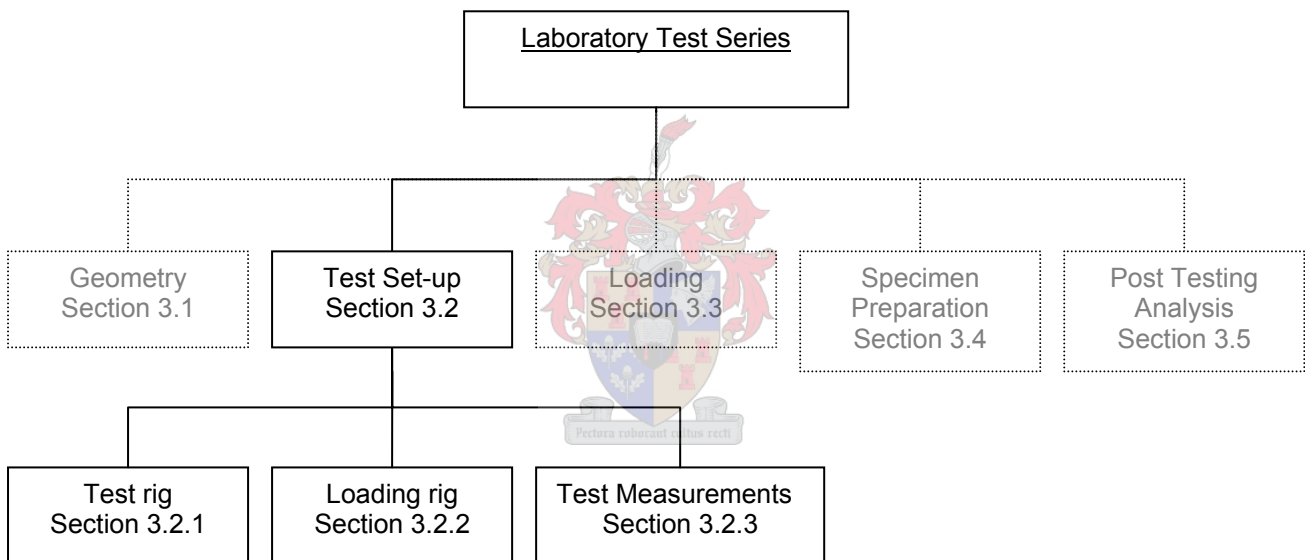


Figure 3.11. Flow diagram illustrating layout of the test set-up stage of the laboratory test series.

3.2.1 Test Rig

The test set-up was designed to determine the out-of-plane bending capacity of glass panels, under various loading rates, and consisted of a test rig and loading rig. The test rig supported the glass panels, while the loading rig was used to distribute the applied load.

In order to minimize the number of variables in the testing procedure, a number of assumptions were made with reference to typical freestanding balustrade connections. [See figures 3.1 and 3.2]

- The Steel channel in the continuous support system and the bolts in the point support system, are rigid in comparison to the rest of the structure.
- There are no further stress concentrations introduced by the support systems. (i.e. The bolt in itself does not introduce any stress concentration)
- The elastic sealant has no effect on the behaviour of the system, and serves the mere purpose of distributing the stress along the channel and around the holes.
- The rubber between the bolt and panel of glass allows enough rotation, ensuring that the glass fractures at the position where the maximum stress concentration occurs around the hole.

With this in mind, the test rig in which the glass panels were tested, was designed. The test rig requirements were considered as follows:

- The test rig had to be multifunctional, in that the out-of-plane bending strength of glass panels for both point- and continuous supported panels could be determined.
- All tests had to be performed using the Zwick 250 kN tension/compression machine. The test rig had to be designed to firstly fit into the Zwick and secondly fit onto the base panel of the machine.
- The test rig had to be rigid in comparison to the glass specimens
- No additional stress concentration were to be created at the supports
- Glass of various thickness had to be tested

With these requirements in mind, a test rig was designed. However, following a number of trial tests, the initial test rig was altered. The altered test rig provided the correct fracture origin while adhering to the initial requirements and was subsequently used for the laboratory test series. The following paragraphs describe and illustrate the initial- and final test rigs.

3.2.1.1 Initial test rig

The initial test rig was based on a cantilever clamping system. The glass panels were to be continuously clamped along one edge while loaded at the opposite edge. Two M16 bolts clamped the glass panel in-between two rectangular hollow sections (Figure 3.12). Both rectangular hollow sections were lined with gasket cork to account for any irregularities and to evenly support the glass panels. The initial test rig is illustrated in figure 3.12 and table 3.4 presents each part with description.

The load was applied to the glass panels using a 30 mm diameter metal rod placed across the surface of the panel, thus evenly distributing the load across the entire surface. Finally, the whole test rig was placed in a Perspex box. With only the necessary holes for the loading rod and measuring devices, the Perspex box was introduced to keep the fractured glass from spraying across the laboratory.

Glass panels without a hole would fracture at the continuous support, as intended. The glass panels with a hole would fracture at the hole, instead of at the support, due to the stress concentration [see chapter 4]. For each panel the ultimate force would be measured, knowing the lever arm, the ultimate out-of-plane bending capacity of each glass panel could be determined.

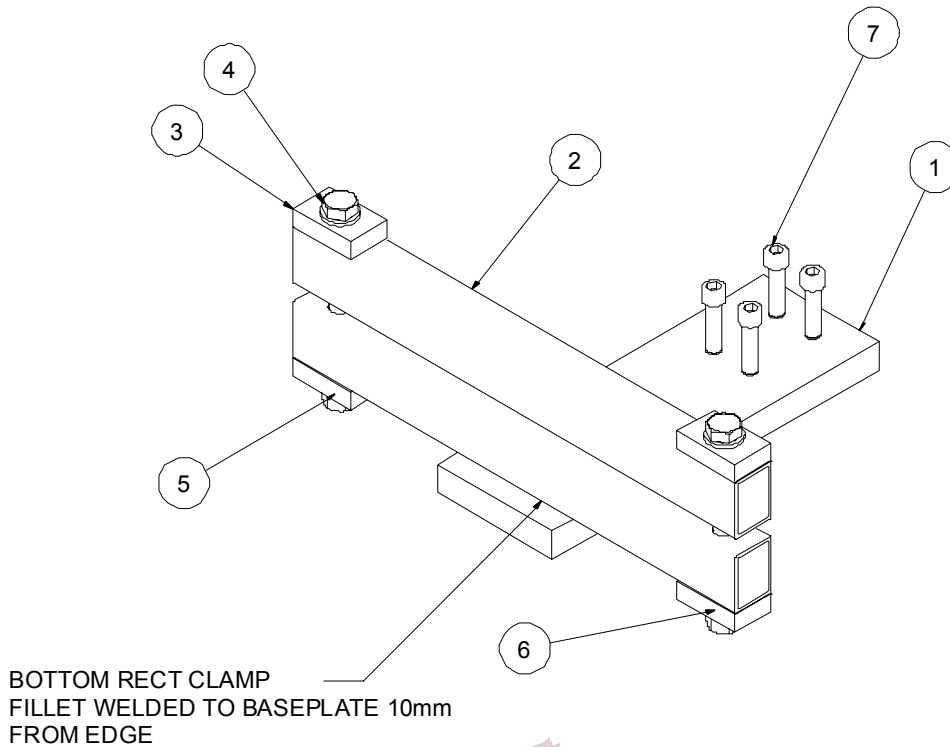


Figure 3.12. Initial test rig

Table 3.4. Initial test rig parts

Item	Qty	Part	Description
1	1	Base plate	300 x 150 x 25mm
2	2	Rectangular hollow section (RHS)	52 x 38 x 3mm
3	4	Spacer	60 x 38 x 16mm
4	2	Bolt M16	
5	4	Washer M16	
6	2	Nut M16	
7	4	Bolt M12	Screw used to bolt test rig to Zwick test machine

After the first trial test, the proposed test rig was altered. Upon loading, the slenderness and flexible torsional resistance of the RHS's permitted the rotation of the glass panel. The test rig was not sufficiently rigid in comparison to the glass panel. The glass panel fractured at one of the clamped corners instead of at the hole where the maximum stress concentration was. The reason for fracture at the corner was attributed to two factors:

- The pressure of the tightened bolts together with the slenderness of the top rectangular hollow section (RHS) caused the RHS to buckle. The buckling of the top RHS resulted in a pressure concentration at the corners greater than that of the hole.
- The metal rod, used to load the panel, did not produce an evenly distributed load across the surface of the glass panel.

Considering these two factors, a new test rig was designed which provided the desired results. The following paragraph describes the design of the final test rig.

3.2.1.2 Final test rig

The final test rig had to address the following issues, as identified from the first trial test.

- Reduce slenderness of the rectangular steel RHS
- Devise a new system for the support of the glass panels to avoid stress concentration
- Alter loading rod to account for the uneven surface of the glass panel

The final test rig can be seen in figure 3.13. The slenderness of the system was addressed with the addition of a 25 mm steel plate (Component 5), which was welded and bolted to the back of the test rig. The top rectangular RHS was bolted to the back steel plate at three positions using three M16 bolts (Component 7). The bolting of the top steel RHS to the back plate eliminated the use of the clamping system. In the final test set-up the glass panels were simply slid in-between the rectangular RHS's to avoid the pressure introduced, as apposed to when the panels were clamped. Three different thicknesses of 10, 12 and 15 mm thick glass panels were tested, therefore the gap between the RHS had to be in excess of 15 mm. Positioning blocks were taped to each panel to account for the various panel thicknesses (Further described in section 3.5.3). To address the issue of excessive rotation, a steel RHS was placed in front of the bottom RHS (Component 2), increasing the lever arm balancing the applied load. The final test rig is illustrated in figure 3.13 and table 3.5 presents each part with description.

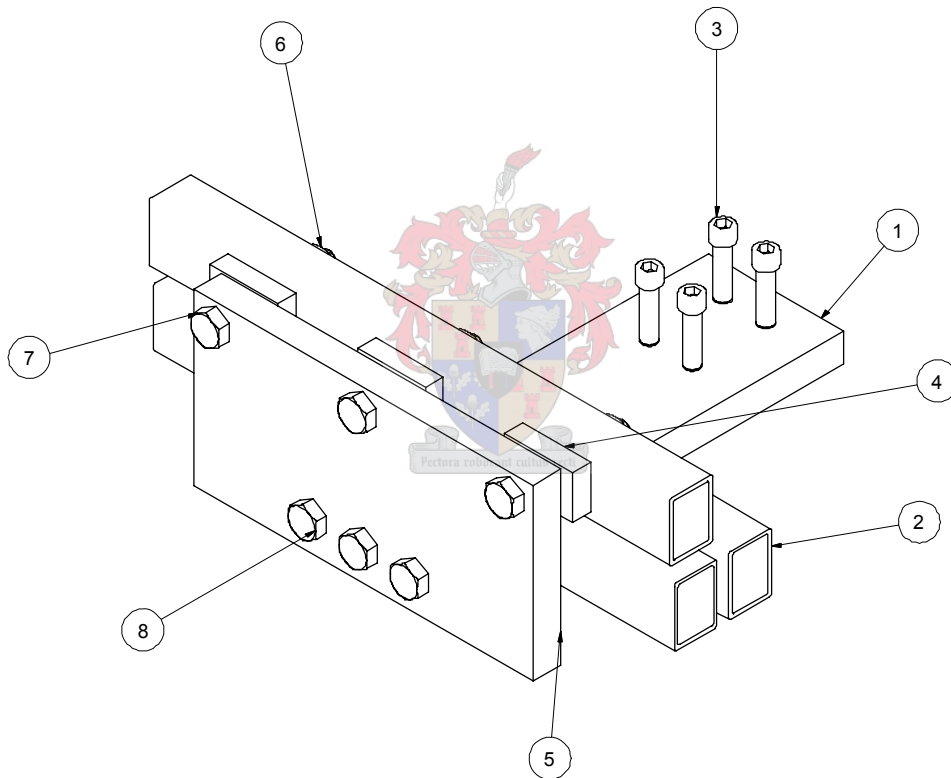


Figure 3.13. Final test rig

Table 3.5. Final test rig parts

Item	Qty	Part	Description
1	1	Base plate	300 x 150 x 25mm
2	3	Rectangular hollow section (RHS)	52 x 38 x 3mm
3	4	Bolt M12	Hexagon socket head cap screw
4	4	Spacer	60 x 38 x 16mm
5	4	Stiffening plate	300 x 150 x 25mm
6	3	Nut M16	
7	3	Bolt M16	90mm
8	3	Bolt M16	38mm

The loading rig was altered based on a ball socket set-up (figure 3.14). Instead of connecting the metal rod to the Zwick, it was rested on top of the glass. The Zwick loading pin would push into a smooth channel to allow the rotation of the rod relative to the glass. This set-up allowed an even distribution of the applied load across the surface of the glass. Figure 3.14 illustrates the initial- and final loading rod.

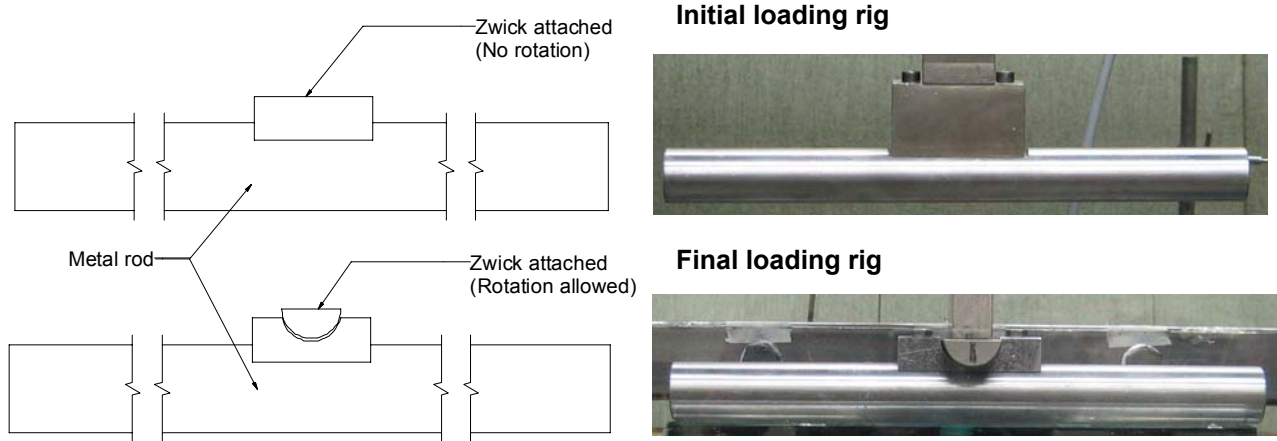


Figure 3.14. Initial- and Final loading rod

The new stiffened test rig together with the improved loading mechanism provided the correct fracture origin (ie. around the hole).

Calibration of test set-up

Before the second trial specimen was tested, the stiffness of the new proposed test rig was established. The stiffness of the new test rig was then compared to that of the initial test rig, to establish whether the new test rig improved the rigidity. A 300 x 300 x 20 mm steel plate was used as a rigid element to determine the stiffness of both test rigs. From the initial test, it was noticed that the measured displacement of the glass panel under the applied load was a combination of the rotation of the panel, displacement of the test rig and the displacement of the glass panel (figure 3.15).

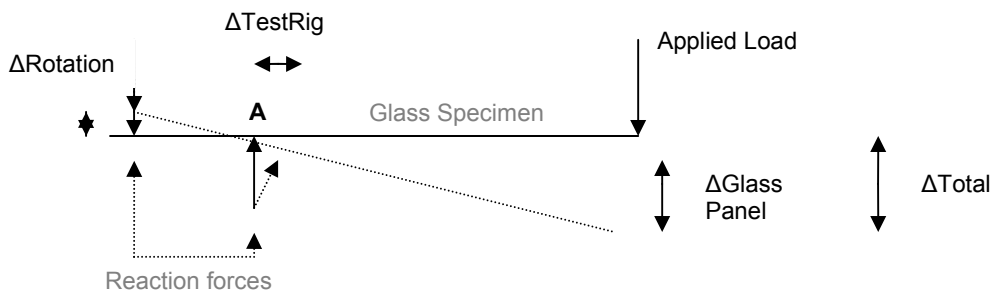


Figure 3.15. Illustration of displacement contribution of each component to total displacement of the system

Where:

- Δ_{Total} = measured displacement
- $\Delta_{Glass\ panel}$ = displacement of panel under applied load
- $\Delta_{Test\ rig}$ = displacement of test rig under applied load
- $\Delta_{Rotation}$ = displacement of glass panel due to rotation about point A

Therefore to determine the displacement of only the glass panel equation 3.1 is used:

$$\Delta_{Glass\ panel} = \Delta_{Total} - \Delta_{TestRig} - \Delta_{Rotation} \tag{3.1}$$

Linear Variable Differential Transformer's (LVDT's) were placed at three different locations, each measuring a different displacement, the LVDT positions can be seen in figure 3.16.

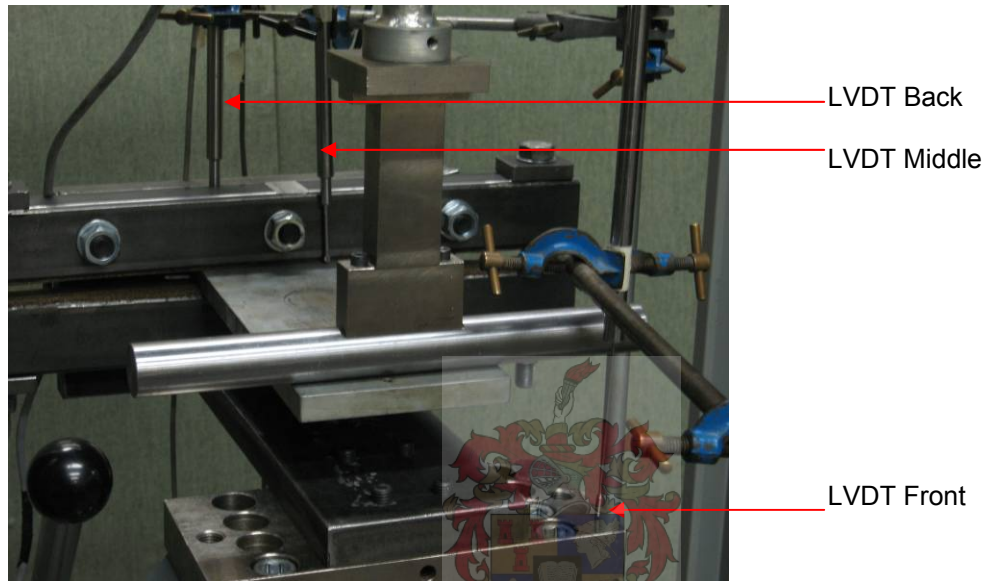


Figure 3.16. LVDT measurement positions

Figure 3.17 illustrates the measured displacement and rotation of both test rigs loaded to 2.3kN.

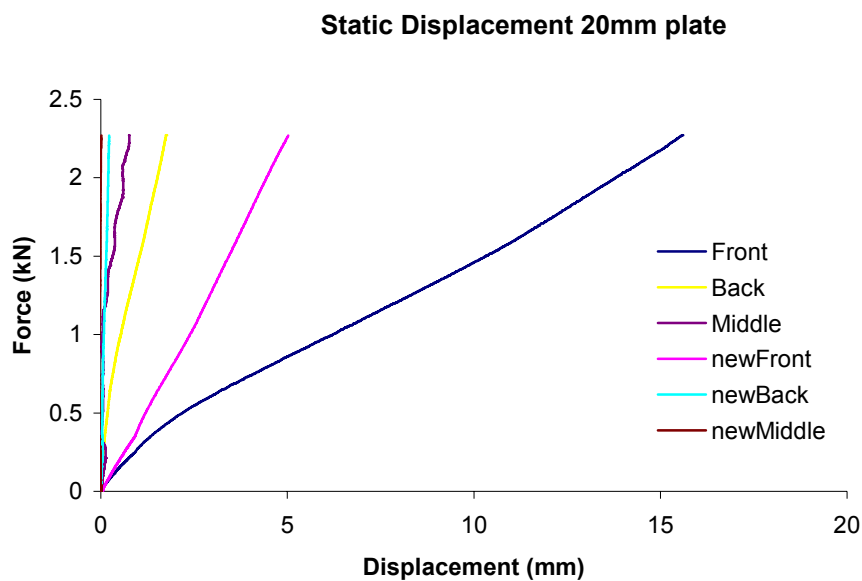


Figure 3.17. Rotation and displacement of old and new test rig

It can be seen that the new test rig provided a better means of support and consequently reduced the rotation of the plate. The displacement of the new test rig was small compared to that of the initial test rig. Under a loading of 2.3 kN, the test rig displaced only 0.017 mm. It was concluded that the test rig is rigid in relation to the glass specimens. For the following tests, it was decided that only the displacement of the system and the rotation of the glass panels had to be measured, as the contribution of the test rig was negligibly small.

3.2.2 Test Measurements

The displacement and the incremental force were measured, in the laboratory test series, to determine the elasticity modulus and ultimate bending capacity of the glass panels.

Displacements were measured using two LVDT's (Linear Variable Differential Transformer) and the ultimate force was measured using a 5 kN load cell. A LVDT is an electromechanical device designed to produce an AC voltage output proportional to the relative displacement of the transformer and armature. The LVDT's were calibrated to interpret a change in voltage as 4 mm. Measurements from the two LVDT's and the load cell were recorded by a digital amplifier (spyder8) and evaluated using the Catman 2.1 software.

The two LVDT's were positioned to measure the rotation of the glass at the back of the two RHS's and the total displacement of the system, respectively. The rotation of the glass at the back of the supporting RHS's is a result of the compression of the gasket cork and rotation of the test rig as the glass panel is loaded.

The glass panels were displacement controlled, in which the bottom half of the Zwick displaced. One LVDT was placed on top of the bottom half of the Zwick, using a tripod. The tripod was placed on top of the Zwick to measure only the displacement of the glass and not the total displacement of the system. This measurement was taken between the back stiffening plate and top RHS, position shown in figure 3.18.

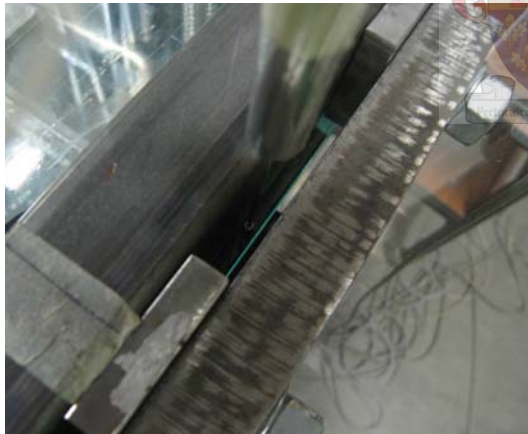


Figure 3.18. Positions of back LVDT

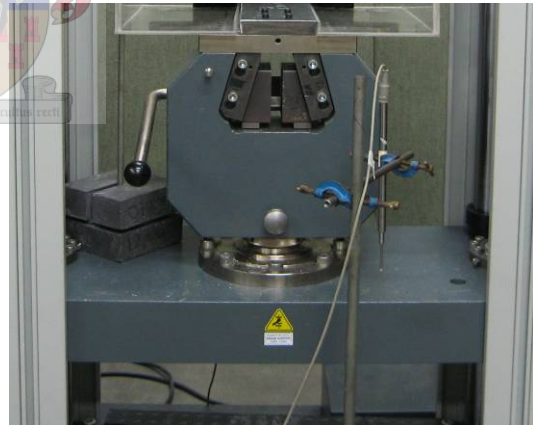


Figure 3.19. Positions of front LVDT

The second LVDT was placed on the ground next to the Zwick and measured the displacement of the Zwick's bottom half, as shown in figure 3.19. This displacement is equal to the total displacement and rotation of the glass panel.

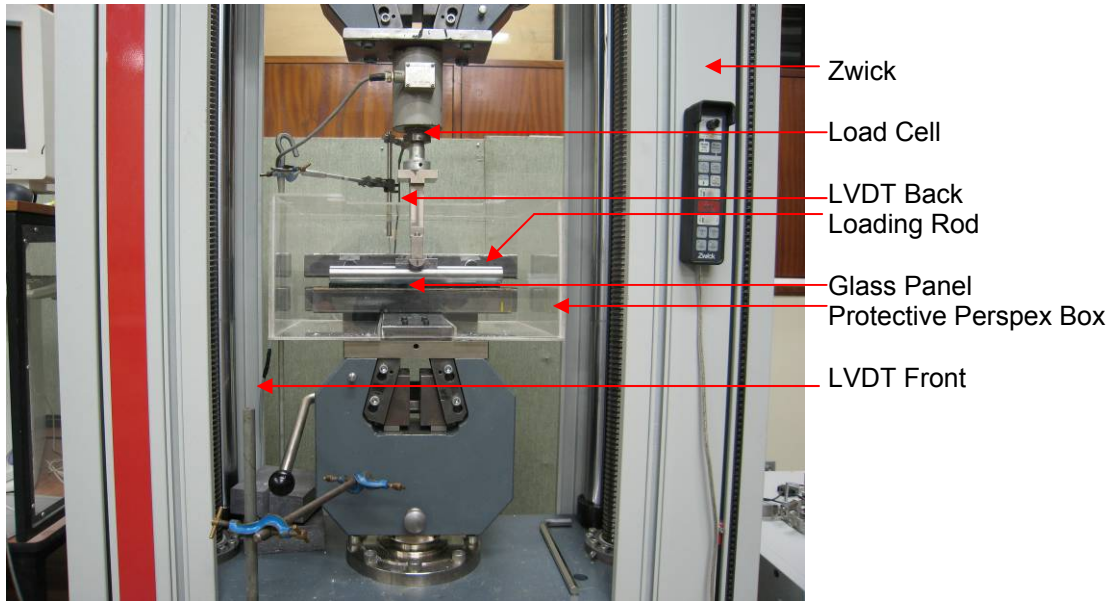


Figure 3.20. Zwick test set-up with test rig

The final test set-up is illustrated in figure 3.20.

3.2.3 Conclusion

From the geometry of the test specimens, determined in the previous section, it was concluded that a test set-up had to be designed which was multifunctional. Consequently, a test set-up was designed to determine the out-of-plane bending capacity of glass panels, and consisted of a test rig and loading rig. The test rig was designed to support the glass panels, while the loading rig was used to distribute the applied load.

The initial test rig was based on a cantilever clamping system, but was altered due to its slenderness. The improved test rig together with the ball and socket-loading rig provided the correct fracture origin.

During the laboratory test series, the displacement and the incremental force were measured to determine the elasticity modulus and ultimate bending capacity of the glass panels. The glass panels were loaded under different loading rates, as it was one of the purposes of the laboratory test series to determine the static- and dynamic material properties of toughened glass. Having described the geometry of the panels and the test set-up, the loading of the glass panels is addressed in the following section.

3.3 TEST LOADING

Introduction

Glass is a material, which exhibit an increase in strength with an increase in loading rate. Since balustrade is required to sustain both static- and dynamic imposed loads, it was consequently decided that the dynamic material properties of glass be determined. Therefore, during the laboratory test series, glass panels would be loaded under various loading rates.

This section describes each loading rate used during the laboratory test series.

The following section concerns the loading of each tested panel, and can be categorized under the following heading:

- Loading rates

The layout of the test set-up section is illustrated by means of a flow diagram in figure 3.21.

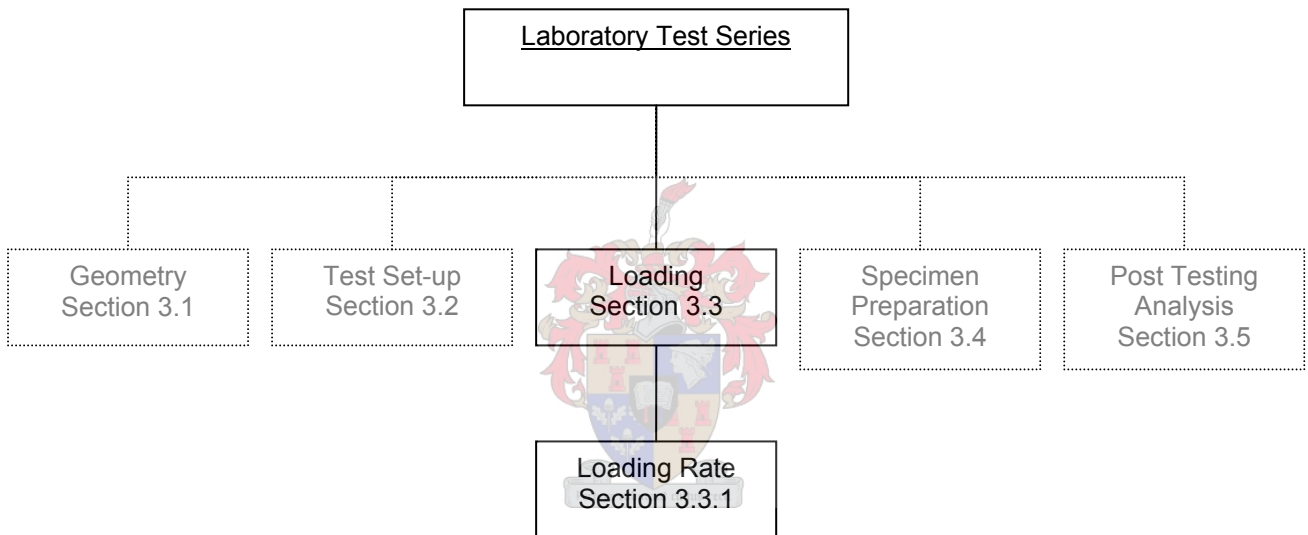


Figure 3.21. Flow diagram illustrating layout of the loading stage of the laboratory test series.

3.3.1 Loading Rate

One of the purposes of the laboratory test series was to determine the static- and dynamic material properties of toughened glass. It was consequently decided that three different loading rates be investigated. They were a:

- Static-
- Quasi Static and
- Dynamic loading rate.

3.3.1.1 Determination of each loading rate

ASTM C 158 [32] provides guidelines on the determination of the modulus of rupture in bending of annealed and toughened glass.

Section 7.1 of ASTM C 158 [32] recommends that prestressed glasses be tested with the increase of maximum stress per minute between 80% and 120% of the modulus of rupture. A static loading rate is therefore the rate of loading which causes the panel to fail in 1 minute.

The modulus of rupture of soda-lime-silica is provided in table 3.6.

Table 3.6. Modulus of rupture for soda-lime-silica glass [Appendix C]

Mean modulus of rupture	
Probability of failure (p.o.f) 50%	165 MPa toughened glass
Typical design modulus of rupture	
Probability of failure (p.o.f) 0.8%	77 MPa toughened glass

The static loading rate was determined for both panels with and without holes. The free body diagram (FBD) of the test set-up is illustrated in figure 3.22.

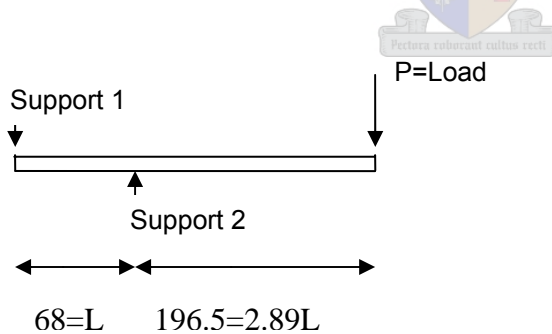


Figure 3.22. Loading and support layout

The equation for the end displacement of the FBD is [33]:

$$\Delta_{end} = P*(2.89L)^2*(L+2.89L)/(3EI) \tag{3.2}$$

Where:

- Δ_{end} = actual displacement
- P = applied load
- L = 68 mm
- E_{glass} = elasticity modulus of glass = 72000 MPa

And $I = (1/12 * b * h^3)$:

$$I = 25000 \text{ mm}^4 \quad (10\text{mm thick panel})$$

$$I = 43200 \text{ mm}^4 \quad (12\text{mm thick panel})$$

$$I = 84375 \text{ mm}^4 \quad (15\text{mm thick panel})$$

3.3.1.1.1 Holed panels

For the panels with holes, the stress concentration around the hole for a unit load was first calculated as follows:

Maximum stress is at hole due to stress concentration, which can be calculated by multiplying the stress at the hole by a stress concentration factor [34].

$$M(x) = -2.89LP$$

$$= -196.5P \text{ N.mm}$$

$$I = 25000 \text{ mm}^4$$

$$y = 10/2$$

$$= 5 \text{ mm}$$

$$\text{Sigma} = My/I$$

$$= -196.5 * 5 / 25000$$

$$= -0.039 \text{ MPa (unit load)}$$

Assume stress concentration at hole is 3

$$\text{Sigma} = 3 * -0.039$$

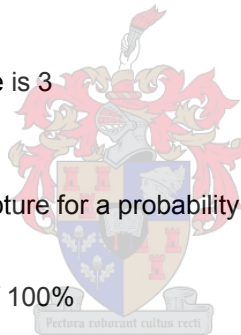
$$= -0.118 \text{ MPa (unit load)}$$

From table 3.6 mean modulus of rupture for a probability of failure of 50%

$$\text{Sigma} = 165 \text{ MPa}$$

Assume for a probability of failure of 100%

$$\text{Sigma} * 2 = 330 \text{ MPa}$$



The loading rate for increase of maximum stress per minute of 100% of the modulus of rupture:

$$\text{Sigma} = 330/60$$

$$= 5.5 \text{ MPa/sec}$$

Since the test series was displacement controlled, the displacement per second was calculated as follows:

Magnitude of force

$$P = 1 * 330 / 0.118$$

$$= 2797 \text{ N}$$

Loading rate (Deflection)

$$V_{\text{end}} = 10.8PL^3/EI$$

$$= 10.8 * 2798 * (68)^3 / (72000 * 25000)$$

$$= 5.279 \text{ mm/min}$$

$$= 0.088 \text{ mm/sec}$$

The loading rates for the panels with holes is summarized in table 3.7.

Table 3.7. Loading rate descriptions WITH HOLE

Designation	Rate (mm/ min)	Stress Rate (MPa/ s)	Duration (s)
Static	5.5	5	60
Quasi Static	50	55	6
Dynamic	500	500	1

The dynamic loading rate was chosen based on the Zwick testing machines upper loading limit, and the Quasi-static- chosen as intermediate loading rate.

3.3.1.1.2 Panel without hole

The same procedure was carried out to determine the loading rate of the panels without holes.

$$M = -2.89LP$$

$$= -196.5P \text{ N.mm}$$

$$I = 25000\text{mm}^4$$

$$y = 10/2$$

$$= 5\text{mm}$$

$$\text{Sigma} = 196.5 * 5/ 25000$$

$$= 0.0393 \text{ MPa}$$

From Table 3.6, Mean modulus of rupture for a probability of failure of 50%
Sigma = 165MPa

Assume for a probability of failure of 100%
Sigma*2 = 330MPa

The loading rate for increase of maximum stress per minute
Sigma = 330/60
= 5.5MPa/sec

$$P = 1 \times 330/ 0.0393$$

$$= 8397\text{N}$$

$$V_{\text{end}} = 10.8PL^3/EI$$

$$= 10.8 * 8397 * (68)^3/(72000 * 25000)$$

$$= 15.84\text{mm/min}$$

$$= 0.26 \text{ mm/sec}$$

The loading rates for the panels without holes is summarized in table 3.8.

Table 3.8. Loading rate descriptions WITHOUT HOLE

Name	Rate (mm/ min)	Stress Rate (MPa/ s)	Duration (s)
Static	15	5.5	60
Quasi Static	150	55	6
Dynamic	500	500	1

The dynamic loading rate was chosen based on the Zwick testing machines upper loading limit, and the Quasi-static- chosen as intermediate loading rate. Table 3.9 presents the loading rate assigned to each group of glass panels.

Table 3.9. Loading rates used for each group of panels

	No hole	Diameter (mm)		
		15	20	25
Thickness (mm)				
10	Dynamic	-	Static	Dynamic
12	Static	Static	Quasi-Static	Dynamic
15	Quasi-Static	Quasi-Static	Dynamic	Dynamic

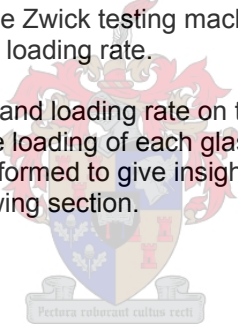
To determine the influence of the panel thickness on the loading capacity of the holed glass, all panels with a 25mm diameter were tested at the dynamic loading rate. Further, to determine the influence of the loading rate on the loading capacity of the glass panel each group of panels that contained no holes were tested at a different loading rate. The rest of the groups were tested with at least one loading rate per glass thickness.

3.3.2 Conclusion

One of the purposes of the laboratory test series was to determine the static- and dynamic material properties of toughened glass. It was consequently decided that a Static-, Quasi Static and Dynamic loading rate be investigated.

The static loading rate was determined as recommended in the ASTM C 158 [32]. The dynamic loading rate was chosen based on the Zwick testing machines upper loading rate and the Quasi-static- chosen as intermediate loading rate.

The influence of the panel thickness and loading rate on the loading capacity of the glass panels were investigated. Prior to the loading of each glass panel, a number of activities were performed. These activities were performed to give insight into the behaviour of toughened glass, and are described in the following section.



3.4 SPECIMEN PREPERATION

Introduction

Prior to the destructive testing of each glass panel, a number of activities were performed. These activities were performed to give insight into the behaviour of toughened glass and ultimately predict the strength of the tested glass panels.

This section describes the significance of each of the activities performed.

The following section concerns the preparation of each tested panel, and can be categorized under the following heading:

- Determination of level of prestress
- Examination of surface flaws surrounding holes
- Taping of compression surface
- Taping of positioning blocks

The layout of the specimen preparation section is illustrated by means of a flow diagram in figure 3.23.

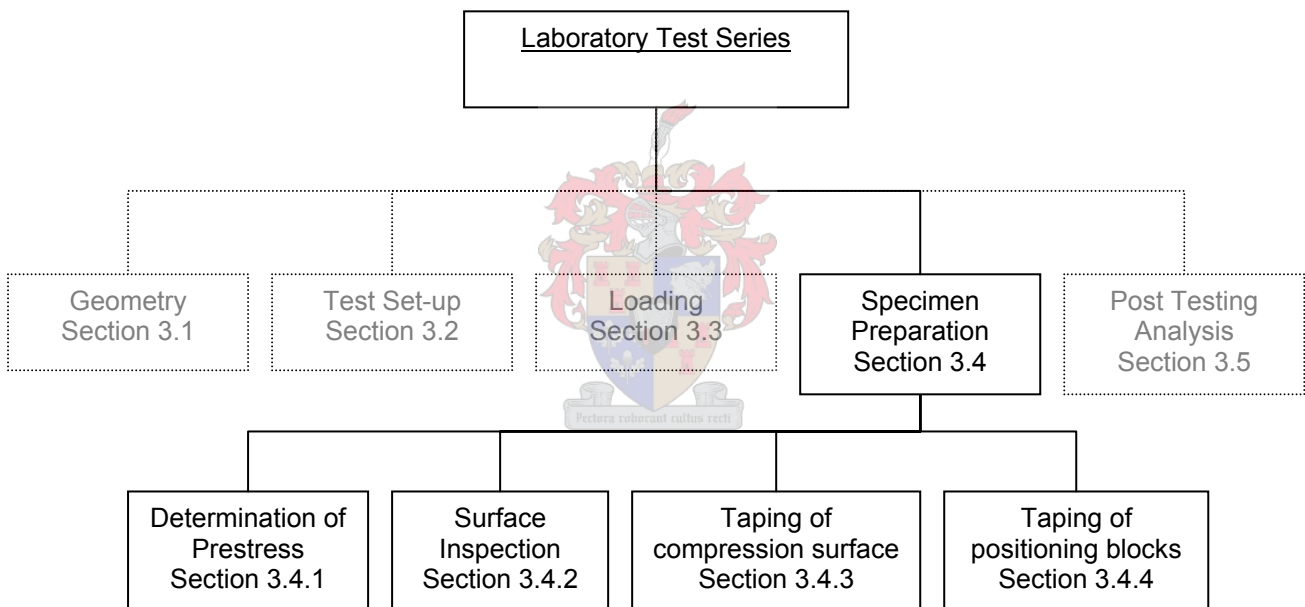


Figure 3.23. Flow diagram illustrating layout of the specimen preparation stage of the laboratory test series.

3.4.1 Determination of level of prestress

The strength and performance of toughened glass are greatly affected by the surface- and edge stress induced during the heat-treating process [13]. It is therefore important to know the level of prestress in order to predict the ultimate strength of a toughened glass panel.

Using Grazing Angle Surface Polarimeter (GASP) technology, the level of prestress of each panel was determined. ASTM C 1279 [35] describes the method for the determination of edge- and surface stresses in annealed, heat-strengthened, and fully tempered flat glass products. This non-destructive test method uses transmitted light and is, therefore, applicable to light-transmitting glasses. Using the procedure described, surface stresses can only be measured on the “tin” side of float glass. Surface-stress measuring instruments are designed for a specific index of refraction, which is different for each measuring device. Each measuring device is calibrated, and has its own conversion table (**see Appendix B**).

As a result of the thermally induced stresses, the material becomes optically anisotropic. When polarized light propagates through anisotropic materials, the differences in the speed of light rays vibrating along the maximum and minimum principal stress introduce a relative retardation between these rays. This relative retardation is proportional to the measured stresses, and can be accurately determined using a polariscope.

3.4.1.1 Procedure

During the float process (see Chapter 1.2), the glass is floated on a bath of molten tin, as a result the tin side of the sheet of glass is flat in comparison with the other side. Therefore, level of prestress is measured from the tin side of the glass specimen. Before the level of prestress was measured, the tin side of the glass panel was identified; this was performed using a spectroscope figure 3.24. Once the tin side was determined, a few drops of index liquid surface were placed on the point of interest, on which the polariscope was placed (figure 3.24) and the reading taken.



Figure 3.24. *Polariscope and Spectroscope*

The angle readings taken from the apparatus were converted into levels of prestress stress using the conversion table applicable to the model (**see Appendix B for standard wedge used in GASP**). The level of prestress was determined at four different locations for each glass panel. These readings were taken at positions where the edge or hole did not have an influence on the level of prestress. The averages of the four readings taken per glass panel, is presented in table 3.10.

Table 3.10. Averages of prestress measurements for panels

Panel#	Thickness (mm)	Hole Diameter (mm)	Centre of panel (MPa)
29, 1, 4, 3	10	NoHole	126.13
22, 13, 37	12	NoHole	121.03
26, 31, 25	15	NoHole	127.04
16, 15, 1	10	10	114.57
27, 30, 33	10	15	106.42
28, 8, 5	10	20	123.39
		Average	114.79
36, 11, 10	12	10	125.72
9, 12, 2	12	15	133.05
20, 19, 18	12	20	124.83
		Average	127.86
7, 34, 6	15	10	122.20
35, 23, 24	15	15	125.99
14, 21, 32	15	20	123.36
		Average	123.85

It is noted that none of the levels of prestress are less than 100 MPa. The highest is 133 MPa and the lowest 106 MPa. Comparing the averages, no common trend in level of prestress was found to exist among the various thicknesses of the glass.

Both the 12- and 15 mm thick panels' measured prestress was higher than that of the 10 mm thick glass panels. Although, the 12 mm average level of prestress (127.86 MPa) was higher than that of the 15 mm (123.85 MPa), an increase in level of prestress with thickness was noticed.

3.4.2 Examination of surface flaws surrounding holes

Fracture is concerned with the initiation and propagation of a crack or cracks in the material until the extent of cracking is such that the applied loading cannot any longer be sustained by the component. All components contain micro cracks or flaws. An engineer, therefore tries to design for non-crack propagation. For this reason, Griffith [31] who tried to explain why the observed strength of a material is considerably less than the theoretical strength, developed linear elastic fracture mechanics (L.E.F.M). He concluded that real materials must contain small cracks or flaws, which reduce their strength. These flaws cause the stress surrounding the flaw to be amplified where the magnification depends upon the orientation and geometry of the flaw. Stress is at a maximum at the crack tip and decreases to the nominal applied stress, with the increasing distance away from the crack. The stress is concentrated around the crack tip or flaw developing the concept of stress concentration. (The topic of stress concentration is further explained in chapter 4)

Therefore, before the laboratory test series, each holed panel was examined using a Lica microscope (magnification 50-times), as illustrated in figure 3.26. Surface flaws in and around the chamfer of each panel (introduced by the drilling of the hole) were photographed. After each hole was photographed, a grid was placed over the photographed image and possible fracture origins were identified, corresponding to a position on the grid. (Figure 3.27) This was only performed on the holed panels, as the hole limited the fracture origin to the edge of the hole. The actual fracture origin would later be compared to the predicted fracture origin to establish to what extent the flaws surrounding the hole influence the bending capacity of the glass panel.

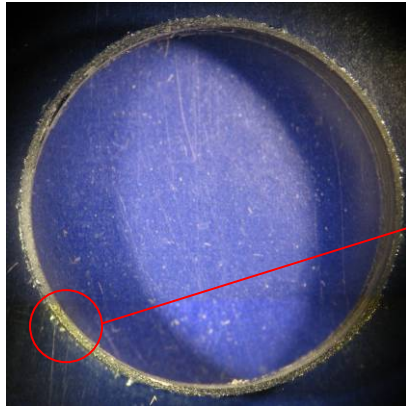


Figure 3.25. Merged hole 21

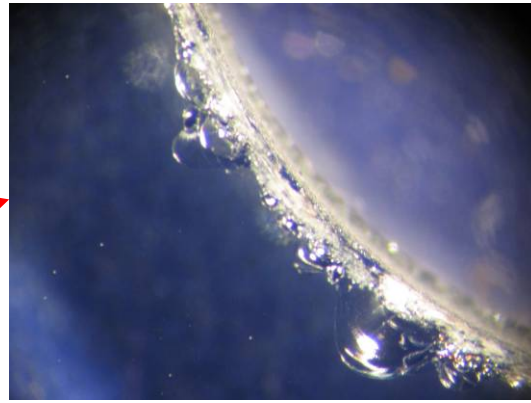


Figure 3.26. Magnification 50x

Table 3.11 presents predicted fracture origins as identified in the examination of the surface flaws, and figure 3.27 illustrates the location on the grid.

Table 3.11. Holed glass panel predicted fracture origin

Glass Panel #	Loading rate	Predicted Fracture Origin
10mm Thickness		
27	Static	32
33	Static	10
28	Dynamic	32
8	Dynamic	28
5	Dynamic	28
12mm Thickness		
36	Static	10
11	Static	10
10	Static	20
9	Quasi-Static	-
12	Quasi-Static	32
2	Quasi-Static	31
20	Dynamic	29
19	Dynamic	27
18	Dynamic	12
15mm Thickness		
7	Quasi-Static	28
34	Quasi-Static	28
6	Quasi-Static	34
35	Dynamic	26
23	Dynamic	12
24	Dynamic	31
14	Dynamic	31
21	Dynamic	24
32	Dynamic	-

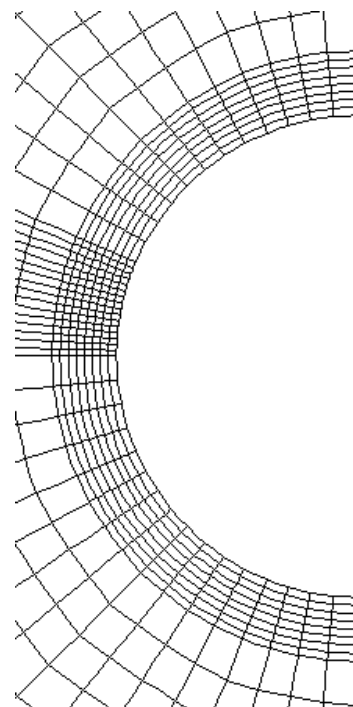


Figure 3.27. Mesh grid placed over hole with grid number

3.4.3 Taping of glass panels

The compression side of each panel was taped with a clear 50 mm wide selotape. The tape kept the fractured particles together at failure and consequently made it possible to establish the origin of fracture. See figure 3.28.

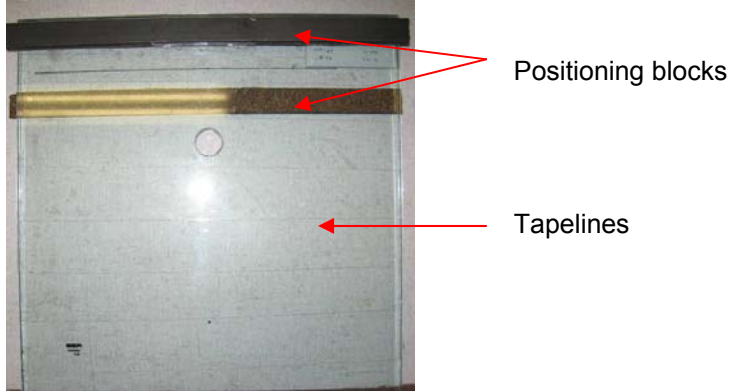


Figure 3.28. Taped glass panel

3.4.4 Positioning blocks

Together with the taping of the panels, positioning blocks were also taped to each panel before it was tested. In the final test set-up the glass panels were simply slid in-between the RHS's to avoid the pressure introduced as apposed to when the panels where clamped. Three different thicknesses of 10-, 12- and 15 mm thick glass panels were tested, therefore the gap between the two RHS's had to be in excess of 15 mm. Positioning blocks were taped to the top and bottom of each panel, according to the panel's thickness as illustrated in figure 3.29.

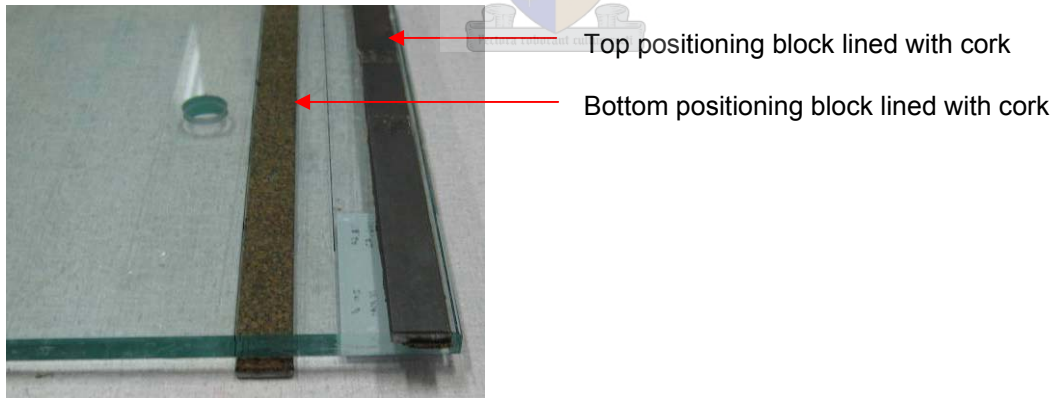
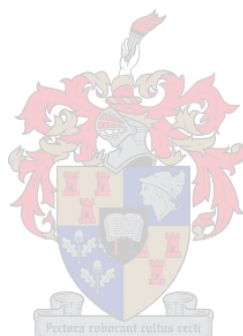


Figure 3.29. Positioning of positioning blocks

3.4.5 Conclusion

Before the testing of the panels, a series of preparations were undertaken which would ultimately help predict and explain the capacity of the glass panels. These activities included the determination of level of prestress, examination of surface flaws surrounding holes, taping of compression surface and taping of positioning blocks.

Having described the geometry of the panel, test set-up, loading and specimen preparation of each tested group of panels, the following chapter discusses the results obtained from the laboratory test series.



3.5 POST TESTING ANALYSIS

Introduction

Following the laboratory test series in which 37 toughened glass panels were tested in bending, a number of activities were performed. This section describes the post failure activities performed, and presents the laboratory test results.

The section can be categorized under the following headings:

- Specimen evaluation
- Test Measurements

The layout of the post failure analysis section is illustrated by means of a flow diagram in figure 3.30.

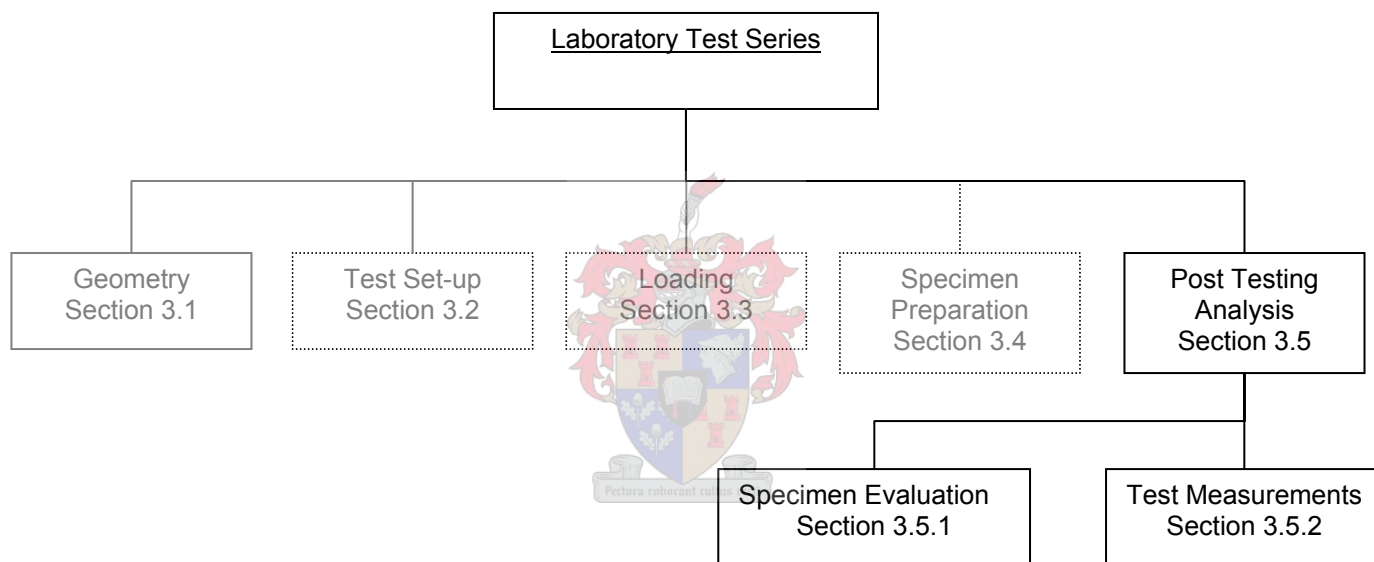


Figure 3.30. Flow diagram illustrating the post failure analysis stage of the laboratory test series

3.5.1 Specimen Evaluation

After the laboratory test series, each panel was closely examined. The tape applied to each panel kept the fractured glass particles together and made the examination of each fractured panel possible. This section describes the fracture pattern of the glass panels and highlights the difference between the different loading rate fracture patterns. Finally, the fracture origin is compared to the predicted fracture origin and the effect of the loading rate on the fracture origin described.

3.5.1.1 Fracture Pattern

After fracture, each panel was carefully removed and the origin of fracture was determined. The taping of the glass panels made the fracture pattern visible, as the tape kept the fractured “sugar cube” pieces together. The fracture origin, illustrated by the circle in figure 3.31 and figure 3.32, was easily identified, for the particle size was the smallest at this point.

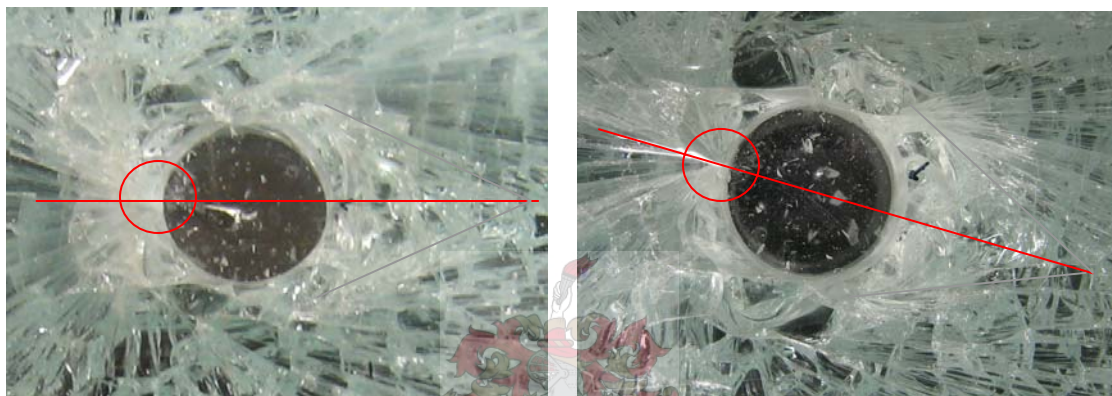


Figure 3.31. Fracture origin and line of symmetry (Panel 19) Figure 3.32. Fracture origin and line of symmetry (Panel 21)

It was noted that the fracture pattern is symmetrical about a line drawn through half of the hole starting at the origin of fracture, as illustrated in figure 3.31, 3.32. This is true regardless of the position of the origin of fracture around the hole. The fracture pattern propagates through the rest of the panel in a shockwave format (radial), as well as in straight lines (linear) in all directions from the point of origin, illustrated in figure 3.33. The particle size therefore increases as the wave moves further from it.

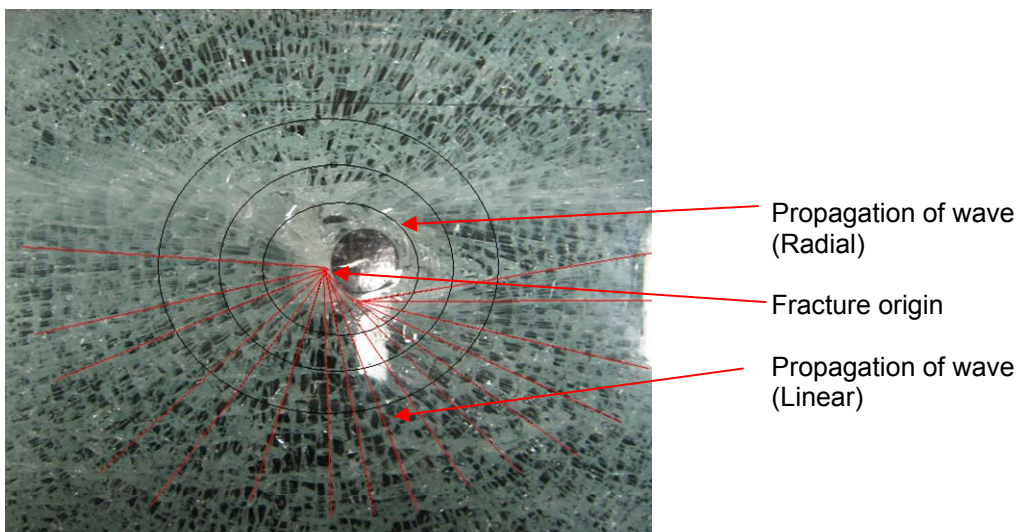


Figure 3.33. Propagation of fracture (Panel 19)

3.5.1.2 Fracture origin

Together with the examination of the fracture pattern, each panel's origin of fracture was determined. This was only performed on the holed panels, as described in section 3.5.2. The taping of the glass panels made the identification of the fracture origin possible. The finite element mesh grid was again placed over the fractured hole to compare the actual fracture origin to that of the predicted origin. The predicted origin was marked with a permanent marker before each panel was tested, as illustrated in figure 3.34, 3.35. Figure 3.34 and 3.35, illustrates the predicted and the actual fracture origin of panel #14 and panel #7. The fracture origins of all the holed panels are presented in table 3.12. Photographs of each hole before- and after failure is presented in **Appendix A**.

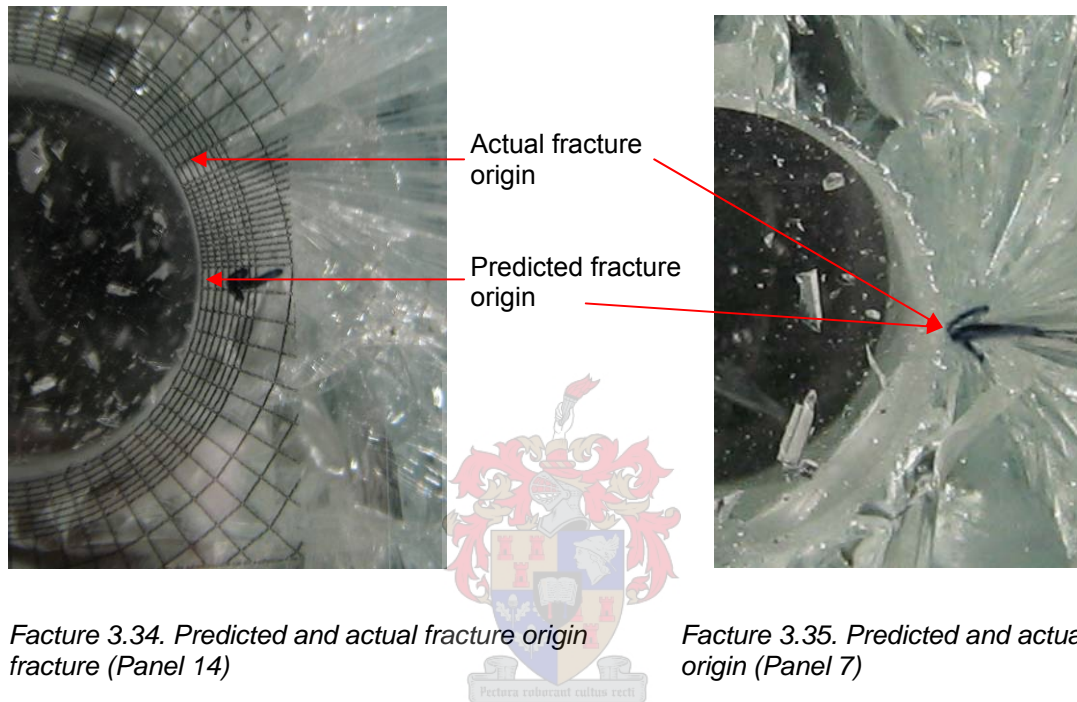


Figure 3.34. Predicted and actual fracture origin fracture (Panel 14)

Figure 3.35. Predicted and actual origin (Panel 7)

Table 3.12. Holed glass panel predicted and actual fracture origin

Glass Panel #	Loading Rate	Predicted Origin on grid	Actual origin on grid
10mm Thickness			
27	Static	32	30
33	Static	10	26
28	Dynamic	32	11
8	Dynamic	28	28
5	Dynamic	28	20
12mm Thickness			
36	Static	10	29
11	Static	10	32
10	Static	20	20
9	Quasi Static	-	28
12	Quasi Static	32	21
2	Quasi Static	31	26
20	Dynamic	29	20
19	Dynamic	27	29
18	Dynamic	12	12
15mm Thickness			
7	Quasi Static	28	28
34	Quasi Static	28	23
6	Quasi Static	34	20
35	Dynamic	26	31
23	Dynamic	12	24
24	Dynamic	31	20
14	Dynamic	31	12
21	Dynamic	24	15
32	Dynamic	-	15

The panels not having any predicted entries did not have any significant macro flaws that could lead to a predicted fracture origin. From table 3.12 it was noted that only 4 of the 23 holed panels fractured at the predicted fracture origin. Further, 2 of the 3 panels, panel #7 and #8, fractured at position #28 on the grid. Position #28 on the grid (figure 3.27), is located in the middle of the hole, the position of maximum stress (chapter 4 finite element analysis). The reason for the fracture at the predicted position can therefore be due to the surface flaw or due to the position of maximum stress.

It was consequently concluded that macro surface flaws surrounding the hole, do not significantly influence the fracture origin and that further research is necessary to draw definite conclusions.

3.5.1.3 Loading rate fracture effect

What appeared to be slower wave propagation (Lagging wave) was noticed to be consistent with the dynamic loading rate. Fracture occurred at a higher position (closer to support) compared to the fracture origins produced by the static loading rate. Figure 3.36, illustrates the lagging wave of panel #21. This lagging wave propagation is verified in table 3.13, where the average quadrant fracture origin of all the holed panels corresponding to the loading rate is compared.

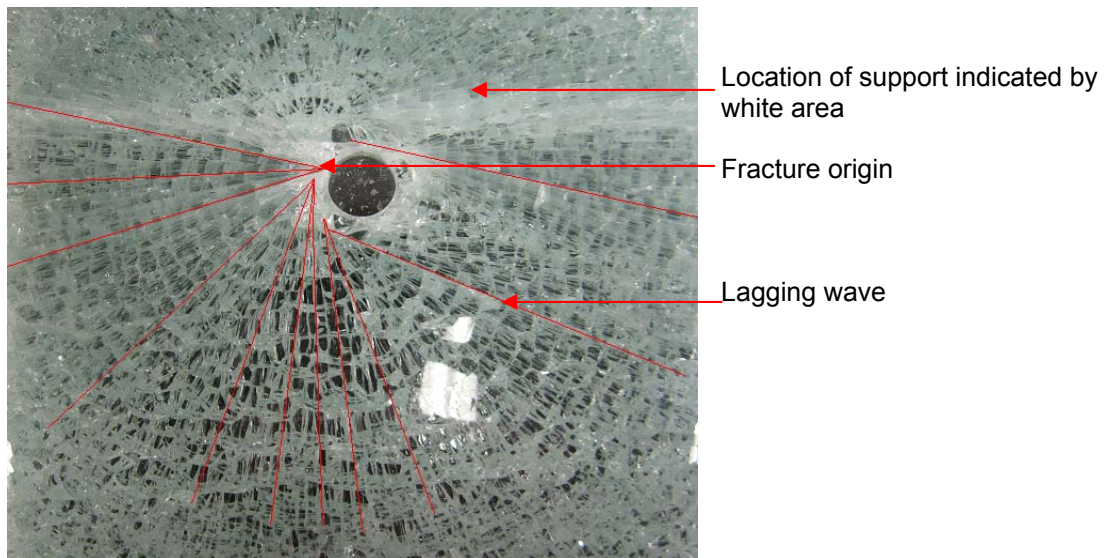


Figure 3.36. Dynamic fracture origin (Panel 21)

Table 3.13. Average quadrant fracture origin corresponding to loading rate

Loading rate	Actual Fracture Origin (identified on grid)
Static	27
Quasi Static	24
Dynamic	21

From table 3.13 it was noted that, as the loading rate increased, the fracture origin moved closer to the support. This can be seen when comparing figure 3.36, with figure 3.33.

During the laboratory test series the force and the displacement of the tested panels were measured and recorded. The next section describes these test measurements.

3.5.2 Test measurements

To determine each panel's bending capacity, the ultimate force of each tested glass panel was measured. Together with the force, the displacement of each panel was measured in order to determine the elasticity modulus of glass under different loading rates.

This section presents the measured ultimate force of each panel, and then compares it to the:

- Level of prestress,
- Fracture origin and,
- Level of prestress and fracture origin.

This is done to determine the effect of each of the above on the loading capacity of the glass panels.

Finally the measured displacement of each panel is presented and the elasticity modulus determined for the:

- Static-,
- Quasi Static and,
- Dynamic loading rate.

3.5.2.1 Ultimate Force

The force was measured using a 5kN load cell. Table 3.14, presents the ultimate force, as measured by the load cell, for each glass panel tested.

Table 3.14. Ultimate force for each panel

Glass Panel #	Hole Diameter	Loading rate	Force measured
	mm		kN
10mm Thickness			
29	-	Dynamic	6.348
17	-	Dynamic	6.822
4	-	Dynamic	6.118
3	-	Dynamic	6.466
27	20	Static	3.075
30	20	Static	Fail
33	20	Static	2.902
28	25	Dynamic	3.47
8	25	Dynamic	3.514
5	25	Dynamic	3.465
12mm Thickness			
22	-	Static	7.984
13	-	Static	7.958
37	-	Static	8.325
36	15	Static	4.626
11	15	Static	5.377
10	15	Static	4.724
9	20	Quasi Static	4.744
12	20	Quasi Static	5.1
2	20	Quasi Static	5.5
20	25	Dynamic	4.605
19	25	Dynamic	5.639
18	25	Dynamic	5.359
15mm Thickness			
26	-	Quasi Static	14.703
31	-	Quasi Static	12.864
25	-	Quasi Static	13.629
7	15	Quasi Static	7.622
34	15	Quasi Static	6.563
6	15	Quasi Static	7.496
35	20	Dynamic	7.758
23	20	Dynamic	8.379
24	20	Dynamic	8.29
14	25	Dynamic	8.835
21	25	Dynamic	7.931
32	25	Dynamic	8.137

3.5.2.2 Level of prestress

The compressive surface stress (prestress), introduced by the toughening process is what distinguishes ordinary float glass from toughened glass, and ultimately what makes toughened glass up to 5x stronger.

The level of prestress of each panel was measured prior to the destructive test series in order to determine the influence of the level of prestress on the ultimate capacity of each panel. Table 3.15 presents the level of prestress of each panel, and compares it to the panel's measured ultimate force.

Table 3.15. Prestress of panels vs ultimate force

Glass Panel #	Prestress at centre of Panel	Hole Diameter	Loading rate	Force measured
	MPa	mm		kN
10mm Thickness				
29	118.64	-	Dynamic	6.348
17	133.61	-	Dynamic	6.822
4	118.64	-	Dynamic	6.118
3	133.61	-	Dynamic	6.466
27	106.42	20	Static	3.075
30	106.42	20	Static	Fail
33	106.42	20	Static	2.902
28	122.23	25	Dynamic	3.47
8	122.23	25	Dynamic	3.514
5	125.72	25	Dynamic	3.465
12mm Thickness				
22	118.64	-	Static	7.984
13	122.23	-	Static	7.958
37	122.23	-	Static	8.325
36	125.72	15	Static	4.626
11	125.72	15	Static	5.377
10	125.72	15	Static	4.724
9	138.04	20	Quasi Static	4.744
12	118.64	20	Quasi Static	5.1
2	142.46	20	Quasi Static	5.5
20	118.64	25	Dynamic	4.605
19	122.23	25	Dynamic	5.639
18	133.61	25	Dynamic	5.359
15mm Thickness				
26	125.72	-	Quasi Static	14.703
31	125.72	-	Quasi Static	12.864
25	125.72	-	Quasi Static	13.629
7	122.23	15	Quasi Static	7.622
34	125.72	15	Quasi Static	6.563
6	118.64	15	Quasi Static	7.496
35	118.64	20	Dynamic	7.758
23	133.61	20	Dynamic	8.379
24	125.72	20	Dynamic	8.29
14	125.72	25	Dynamic	8.835
21	118.64	25	Dynamic	7.931
32	125.72	25	Dynamic	8.137

The variability in strength of glass caused by surface defects [31], resulted in the testing of three identical panels per parameter. Table 3.15 presents the results of the three identical panels together. Since the panels are identical in geometry (thickness and size) and were tested at the same loading rate, they should theoretically have the same ultimate force. However, when comparing each individual panel's ultimate force in table 3.15 to that of the rest of the group, a difference in strength is noticed.

The difference in strength can mainly be attributed to the difference in level of prestress [13] and surface defects. The influence of the level of prestress on the loading capacity of the glass panel is noticed when comparing the highest level of prestress to the highest ultimate force of a group. In 8 out of the 11 groups, the panel with the highest level of prestress fractured at the highest ultimate force. These panels are highlighted in red in table 3.15.

Surprisingly, when comparing table 3.12 (fracture prediction) with table 3.15 (level of prestress), all of the 3 groups, in which the highest level of prestress did not correspond to the highest ultimate force, the predicted origin of fracture corresponded to the actual origin of fracture.

Two of the panels (#7, #8) occupying these groups fractured at position #28 on the grid. Position #28 on the grid (figure 3.27), is located in the middle of the hole, the position of maximum stress (chapter 4 finite element analysis). The reason that the panels fractured at the position of maximum stress can be attributed to the lack of dominant surface flaws.

The other panel (#18) fractured at a position far away from the point of maximum stress, which on the other hand can be attributed to the presence of dominant surface flaws, which ultimately caused premature failure. Table 3.16 presents each panel's level of prestress and fracture origin and compares it to the panel's ultimate force.

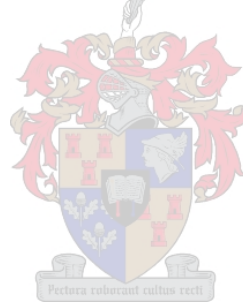


Table 3.16 Ultimate force vs. the origin of fracture vs. level of prestress (failure stress presented in chapter 4)

Glass Panel #	Prestress at centre of Panel	Force measured	Fracture origin	Predicted origin of fracture
	MPa	kN		
27	106.42	3.075	30	32
33	106.42	2.902	26	10
28	122.23	3.47	11	32
8	122.23	3.514	28	28
5	125.72	3.465	20	28
36	125.72	4.626	29	10
11	125.72	5.377	32	10
10	125.72	4.724	20	20
9	138.04	4.744	28	-
12	118.64	5.1	21	32
2	142.46	5.5	26	31
20	118.64	4.605	20	29
19	122.23	5.639	29	27
18	133.61	5.359	12	12
7	122.23	7.622	28	28
34	125.72	6.563	23	28
6	118.64	7.496	20	34
35	118.64	7.758	31	26
23	133.61	8.379	24	12
24	125.72	8.29	20	31
14	125.72	8.835	12	31
21	118.64	7.931	15	24
32	125.72	8.137	15	--

Form table 3.16, it can be concluded that the strength of the glass panels were affected by both the level of prestress and presence of surface flaws.

3.5.2.3 Displacement

During the laboratory testing of the panels the force and displacement were measured to determine the elasticity modulus of the glass. The displacement of the panels was measured at two different locations, since the total displacement of the system is a combination of the rotation and displacement of the panel. One LVDT was employed to measure the displacement at the loaded end of the glass panel, while the other measured the rotation behind the top hollow steel channel. The position of the LVDT's is shown in figure 3.18 and 3.19 in section 3.2.2. Figure 3.37 illustrates the displacement distribution measured by each LVDT.

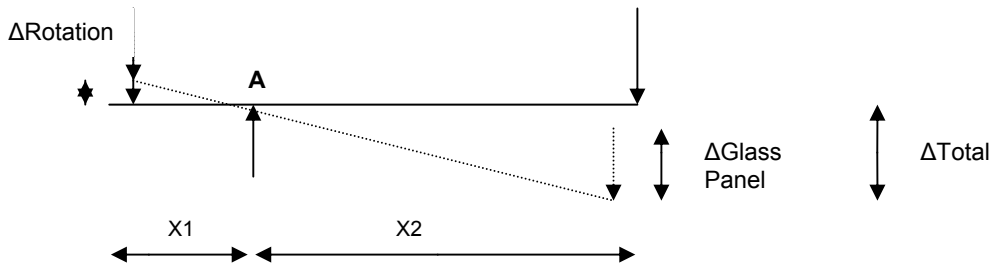


Figure 3.37. Displacement contribution

The rotation, behind the top hollow steel channel, can be defined in terms of the “actual” displacement at the loaded end of the glass panel as:

$$\Delta_{\text{Glass Panel}} = \Delta_{\text{Total}} - (\Delta_{\text{Rotation}}/x_1) \cdot x_2 \tag{3.3}$$

Equation 3.3 was used to calculate the displacement of each glass panel without holes; this was performed for each loading rate. The force displacement graph for the 10 mm thick glass panels without holes is presented in figure 3.38. These plates were tested under dynamic loading conditions. The graph presents the total displacement of the glass panels, together with the actual displacement as calculated using equation 3.3.

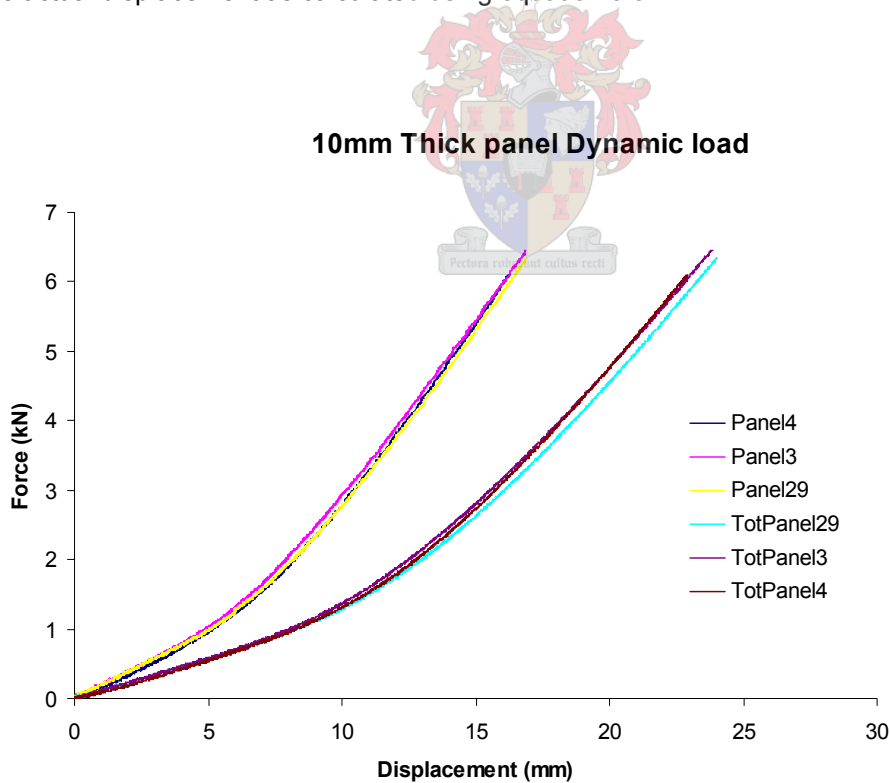


Figure 3.38. Force, displacement graph for 10mm thick, dynamically loaded glass panels

It can be noted that the graph only becomes linear after 2 kN. This can be attributed to the compression of the cork and rotation of the test rig. Although the rotation of the glass kept to a minimum, some rotation was still possible.

3.5.2.4 Elasticity modulus

The measured force together with the actual displacement was used to determine each panel's elasticity modulus. Using equation 3.3, the elasticity modulus can be expressed in terms of the displacement. Figure 3.39 illustrates a simplified beam diagram of the test rig.

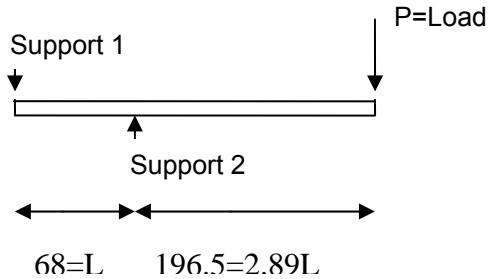


Figure 3.39. Loading and support layout

End deflection at $x = 3.89L$

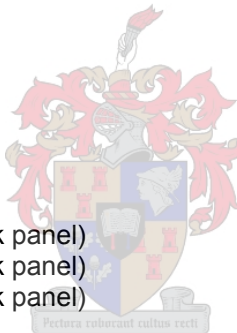
$$\Delta_{end} = P \cdot (2.89L)^2 \cdot (L + 2.89L) / (3EI) \tag{3.4}$$

Where:

- Δ_{end} = actual displacement
- P = applied load
- L = 68 mm
- E_{glass} = elasticity modulus of glass

And $I = (1/12 \cdot b \cdot h^3)$:

- I = 25000 mm⁴ (10mm thick panel)
- I = 43200 mm⁴ (12mm thick panel)
- I = 84375 mm⁴ (15mm thick panel)



Replacing all the variables, equation 3.4 reduces to

- $E_{10} = 136.21 \cdot P / \Delta_{end}$ (10mm thick panel)
- $E_{12} = 78.83 \cdot P / \Delta_{end}$ (12mm thick panel)
- $E_{15} = 40.36 \cdot P / \Delta_{end}$ (15mm thick panel)

The linear gradient of the graph, from 2kN to failure, was used to calculate the elasticity modulus for each of the glass panel's without holes, as the parabolic shape of the graph is indicative of the cork compressing. The elasticity modulus for all the glass panels without holes, as calculated using equation 3.4, is presented in table 3.17.

Table 3.17. Elasticity modulus for all panels without holes

Panel number	Loading rate	P/ Δ (N/mm)	Factor	E _{glass} (N/mm ²)
10mm Thickness				
29	Dynamic	553	136.21	75324
4	Dynamic	576	136.21	78465
3	Dynamic	564	136.21	76822
			Average	76870
12mm Thickness				
22	Static	852	78.83	67163
13	Static	866	78.83	68266
37	Static	833	78.83	65665
			Average	67031
15mm Thickness				
26	Quasi Static	1915	40.36	77289
31	Quasi Static	1861	40.36	75109
25	Quasi Static	1905	40.36	76886
			Average	76427

In order to determine the difference in elasticity modulus, each panel thickness was tested at a different loading rate; Table 3.17 presents the average elasticity modulus for each loading rate.

As can be deduced from the results of the static loading rate in table 3.17, the modulus of elasticity of glass is extremely high (static E_{glass} = 67031 MPa). However, according to manufacturers [Appendix C] the modulus of glass is E_{glass} = 72000 MPa, an underestimation of 6.9%. The discrepancy in the test result can be assigned to the unaccounted rotation of the test rig itself.

From table 3.17, it can also be noted that there is an increase in elasticity modulus with increase loading rate. An increase in elasticity modulus with increase loading rate is common in most materials. An increase of 12.8% between the calculated static- and dynamic modulus was noticed.

3.5.3 Conclusion

Specimen evaluation

After fracture, the fractured panels were examined. The taping of the glass panels made the fracture pattern visible, as the tape kept the fractured pieces together. It was noticed that the fracture pattern propagates through the panel in a shockwave format, as well as in straight lines in all directions from the point of origin.

Furthermore, the fracture origin of the holed panels was determined, which was made possible by the taping of the panel. Post failure fracture origins were compared to predicted fracture origins. However, only 4 out of the 24 predictions coincided. It was consequently concluded that macro surface flaws surrounding the hole did not influence the fracture origin, and that further research is thus necessary to draw definite conclusions. This conclusion should however also be read together with the paragraph which discusses the level of prestress.

Lagging wave propagation was noticed to be consistent with the dynamic loading rate. Fracture occurred closer to the support compared to the fracture origins produced by the static loading rate. This was verified when the average quadrant fracture origin of the different loading rates was compared. The laboratory test series demonstrated that point of fracture origin does not necessarily coincide with the point of maximum tensile stress.

Test measurements

During the laboratory testing of the panels, each panel's force and displacement was measured. The force was measured to determine each panel's bending capacity, while displacement was used to determine the elasticity modulus of the glass.

Prior to the testing of the panels, each panel's level of prestress was determined using GASP technology. The variability in strength of glass caused by surface defects resulted in the testing of three identical panels per parameter. By comparing the highest level of prestress to the highest ultimate force of only the identical panels in a group, the influence of the level of prestress on the capacity of the glass panel, was noticed. In 8 out of the 11 groups, the panel with the highest level of prestress fractured at the highest ultimate force. It was concluded that the strength of the glass panels were predominantly affected by both the level of prestress and presence of surface flaws.

The measured force together with the linear gradient of an actual displacement graph was used to determine each panel's elasticity modulus. The published modulus of elasticity of glass was underestimated by 6.9%. The discrepancy in the test result was assigned to the unaccounted rotation of the test rig itself. Further, an increase of 12.8% between the calculated static- and dynamic modulus was noticed.

As one of the purposes of the laboratory test series was to determine the influence of different connections (types and sizes), three different panel thicknesses together with two different connection types (panels with- and without holes) were investigated. Furthermore, for the panels that contained holes, three different hole diameters were investigated. Stress concentrates around holes much the same way as it does around cracks, and is addressed in detail in chapter 4. This stress concentration is dependent on numerous factors, including the size- and shape of the hole. Since different hole diameters and panel thicknesses were investigated, the stress concentration was different for each hole diameter and panel thickness. The complexity of the hole (hole with chamfer) forced a finite element analysis to be performed to determine each panel's fracture stress. The following chapter describes each panel's finite element model and finally presents the results.

CHAPTER 4 TEST PANEL FINITE ELEMENT MODEL

Introduction

Due to the complex geometry of the glass panels tested (hole with chamfer), the finite element program DIANA [44] was employed to calculate the loading capacity of each glass panel. Having obtained the failure load from the laboratory test series, described in Chapter 3, the finite element program was used to determine each glass panel's related fracture stress. This chapter describes the finite element model used.

This chapter starts by explaining the basic concepts of stress concentration. Stress concentrates around the hole, much the same way as stress concentrates around cracks, developing the concept of stress concentration. Since stress concentrates around the hole, the fracture origin is normally located here (Section 4.1.1).

Using available literature [34, 36, 37, 38] the mesh density of the finite element model is determined to simulate this stress concentration around a hole. This is first determined, in 2D, for a thin panel with a single circular hole under uniaxial tension, and then, in 3D, for the bending of a finite width thin panel with a single circular hole.

The calibrated finite element model is then used to determine the fracture stress of each glass panel. Finally, the Weibull statistical model [39] is used to present the strength of glass under various loading rates.

The layout of the chapter is illustrated by means of a flow diagram in figure 4.1.

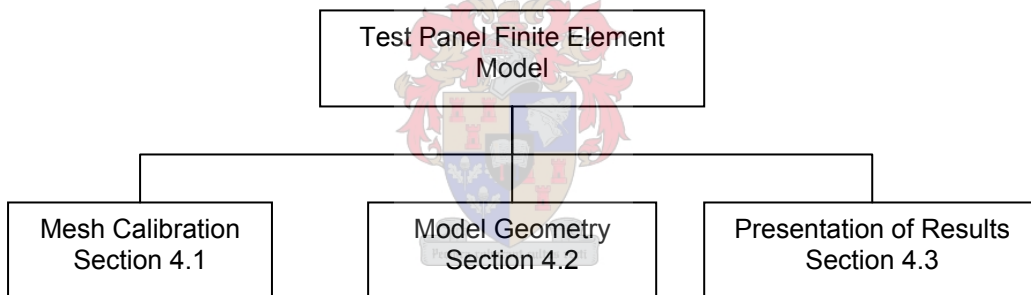


Figure 4.1. Flow diagram illustrating the layout of the finite element model chapter

The finite element model can be categorized into three steps. In the subsequent paragraphs each of these steps are addressed separately and described in detail, they are:

- Mesh calibration

The purpose of the finite element model was to determine the fracture stress corresponding to the applied load of each panel. However, due to a stress concentration around the hole, the density of the mesh of the finite element model plays a vital role in this stress prediction. This section describes the calibration of the mesh used to simulate the stress concentration surrounding the hole.

- Model geometry

This section describes the makeup of the model with reference to the elements used, geometry of the panels, constraints, material properties, loading conditions and mesh size.

- Presentation of results

Finally, the results of the finite element model are presented using the Weibull statistical model [39]. This section describes how the Weibull model was implemented to present the results obtained from the finite element analysis.

4.1 MESH CALIBRATION

Introduction

The elementary stress formula for tension (equation 4.1) and for bending (equation 4.2), used in the design of structural members are based on the members having a constant section. The presence of shoulders, grooves and most importantly, holes result in modifications of the simple stress distributions so that localized high stresses occur.

$$\sigma = \frac{F}{A} \tag{4.1}$$

$$\sigma = \frac{My}{I} \tag{4.2}$$

This idealization of high stress is known as stress concentration, and can be represented by the stress concentration factor K_{tn} . The stress concentration factor K_{tn} can be defined as the ratio of the peak stress in the body (σ_{max}) to a reference stress away from an edge (σ_{nom}) or hole influence (equation 4.3), and is based on the net cross sectional area of the panel.

$$K_{tn} = \frac{\sigma_{max}}{\sigma_{nom}} \tag{4.3}$$

The layout of the mesh calibration stage is illustrated by means of a flow diagram in figure 4.2.

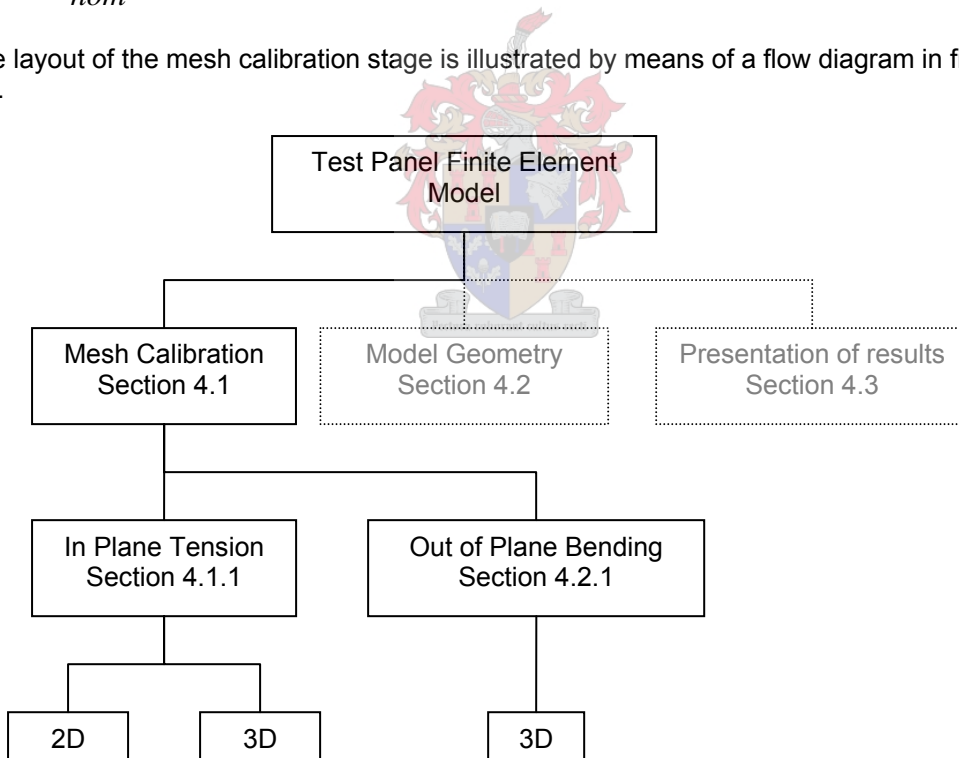


Figure 4.2. Flow diagram illustrating layout of the mesh calibration stage of the finite element model

The following section describes the mesh calibration stage, and is categorized under the following sections:

- In plane tension
- Out of plane bending

4.1.1 In-Plane Tension

Timoshenko (1970) [36] investigated stress distribution around a circular hole in a thin element, subjected to uniaxial in plane tension. Using polar coordinates, equations (equation 4.4, 4.5) were derived to represent the stress at any point in the panel (see figure 4.4).

Where:

- a = radius of the hole,
- r, θ = the polar coordinates of a point in the element.

$$\sigma_r = \frac{1}{2}\sigma\left(1 - \frac{a^2}{r^2}\right) + \frac{1}{2}\sigma\left(1 - \frac{4a^2}{r^2} + \frac{3a^4}{r^4}\right)\cos 2\theta \tag{4.4}$$

$$\sigma_\theta = \frac{1}{2}\sigma\left(1 + \frac{a^2}{r^2}\right) + \frac{1}{2}\sigma\left(1 + \frac{3a^4}{r^4}\right)\cos 2\theta \tag{4.5}$$

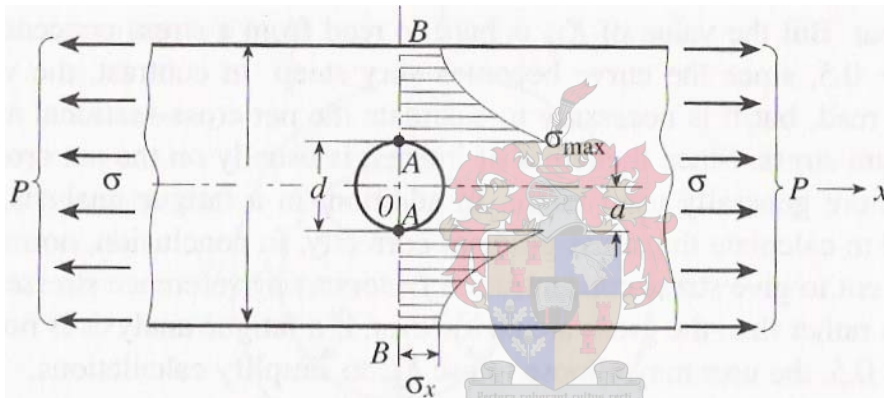


Figure 4.3. Infinite thin element with hole under tensile load [36]

At the edge of the hole, where r = a, equation 4.4, 4.5 reduces to:

$$\sigma_r = 0 \tag{4.6}$$

$$\sigma_\theta = \sigma(1-2\cos 2\theta) \tag{4.7}$$

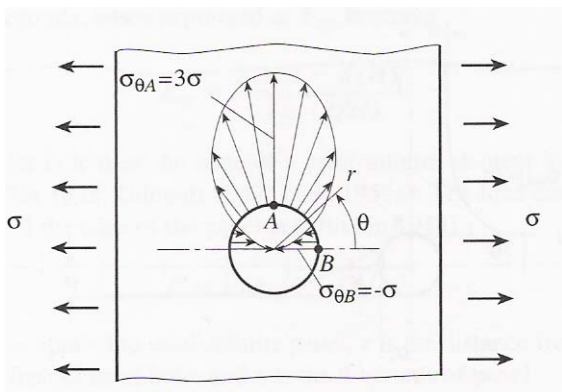


Figure 4.4. Stress distribution on the edge of a circular hole in an infinite thin panel element, at point A, $\theta = \pi/2$ [36]

At point A, $\theta = \pi/2$

$$\sigma_{\theta A} = 3\sigma, \tag{4.8}$$

which is the maximum stress around the hole. Therefore, the maximum stress concentration around the edge of a hole is 3 times the nominal stress.

4.1.1.1 Finite-width panel with a circular hole under in plane tension

The mesh element size was first determined for a finite width panel with circular hole subjected to in plane tension. The purpose of this step of the mesh calibration was to determine the size of elements (width and breadth) which would give the correct extrapolated stress results. Out of plane bending was calculated in a subsequent step, described further in section 4.1.2. The mesh was calibrated by comparing finite element results to that found in literature [37].

Howland (1929-30) [37] developed equation 4.9 for a finite-width thin element with a circular hole under in plane tension.

$$K_m = 2 + 0.284\left(1 - \frac{d}{H}\right) - 0.6\left(1 - \frac{d}{H}\right)^2 + 1.32\left(1 - \frac{d}{H}\right)^3 \tag{4.9}$$

Where:

d = diameter

H = width of the plate

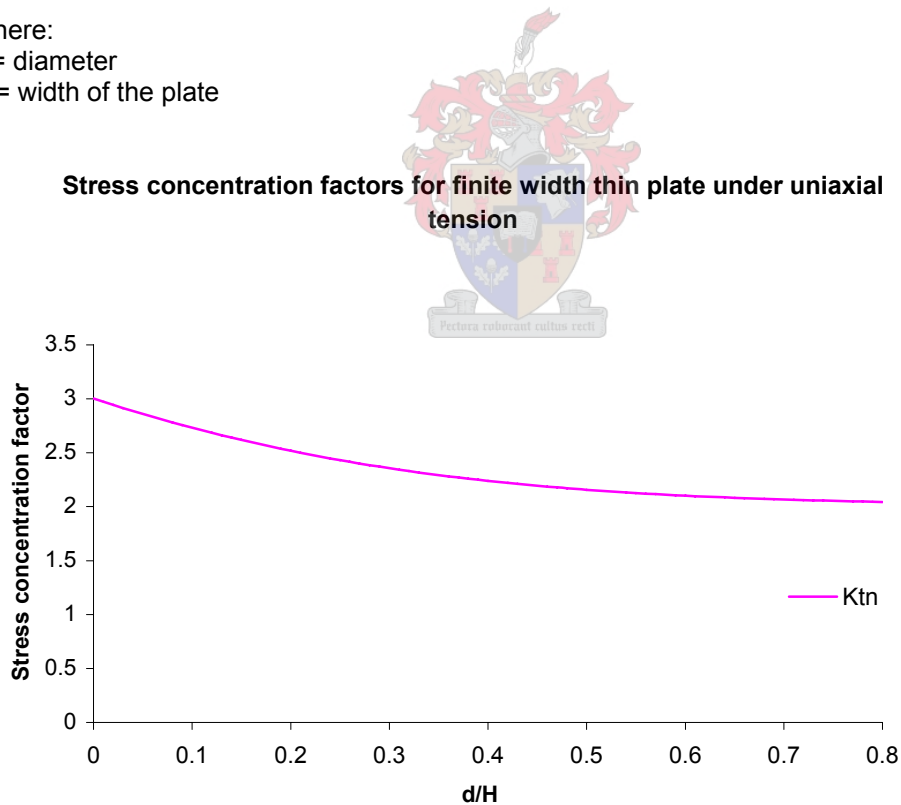


Figure 4.5. Stress concentration factor K_{tn} for the tension of a finite-width thin plate with a circular hole [37]

Equation 4.9 is presented in figure 4.5 for different diameters. From figure 4.5, it is evident that the maximum stress concentration factor (K_{tn}) at a hole in a finite width plate in tension is 3. This maximum stress occurs when the diameter in relation to the width of the plate is extremely small (ie. tends to zero). Therefore, a larger hole leads to a smaller tensile stress concentration.

4.1.1.1.1. 2D Finite element model

Using quadratic flat shell elements (CQ48F) a 300x300x10 panel with 15 mm centre hole was modelled, using the DIANA [44] finite element software.

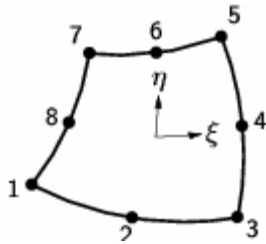


Figure 4.6. Quadratic flat shell element, CQ48F [44]

The CQ48F element is an eight-node quadrilateral isoparametric flat shell element (figure 4.6). The element is based on a quadratic interpolation and numerical integration over the element area.

Quadratic elements were used as apposed to linear elements, due to the sensitivity of the gradient of the stress concentration around the hole. Linear elements would underestimate the stress gradient and ultimately the stress surrounding the hole. Due to symmetry along two axes, only a quarter of the panel was modelled (see figure 4.7). A unit pressure line load was applied to one of the 150 mm quarter edges, and both symmetry edges constrained accordingly.

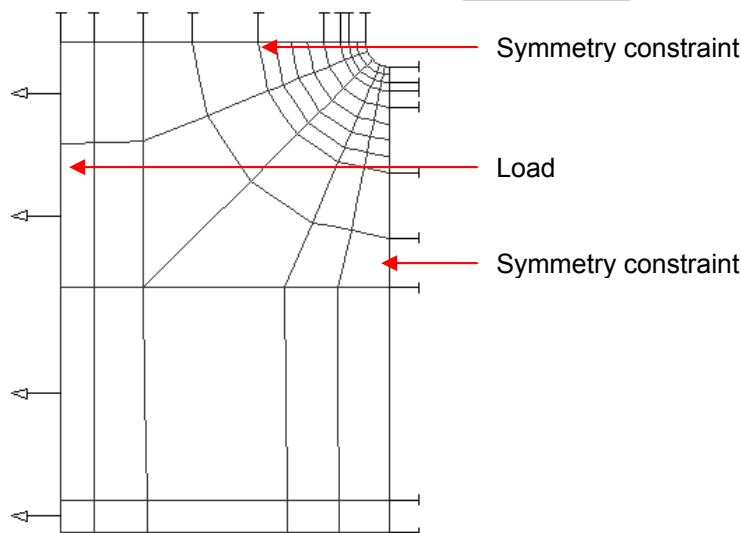


Figure 4.7. Quarter of model constraints and line load

With:

- d = thickness
- = 15 mm
- H = 300 mm

Equation 4.9 yields:

$$K_{tn} = 2.86004$$

$$\begin{aligned} \sigma &= (\text{unit line load} \times \text{length}) / (\text{Area-Area of hole}) \\ &= (1 \times 300) / ((300 - 15) \times 10) \\ &= 0.10526315 \text{ MPa} \end{aligned}$$

The stress concentration at the hole is therefore:

$$\begin{aligned} \sigma_{\max} &= \sigma \times K_{tn} \\ &= 0.10526315 \times 2.86004 \\ &= 0.301 \text{ MPa} \end{aligned}$$

Using equation 4.9, the magnitude of the stress around the hole, as produced by the stress concentration, was calculated. Having calculated the magnitude of the stress, the density of the mesh of the finite element model could now be determined. Table 4.1, presents three different mesh sizes with their corresponding produced principal stress. The dimension corresponding to each mesh density refers to the dimensions of the smallest element in the mesh, situated at the position of highest stress. It is evident that the principal stress becomes more accurate the denser the mesh becomes. A mesh density of 0.74x 0.62 mm quadratic flat shell elements around the hole provided the closest answer of $\sigma_{\max} = 0.300$ MPa.

Table 4.1. Mesh sensitivity of mesh

	Breadth	Width	Calculated Principal Stress
	mm	mm	MPa
Element Size 1	2.96	2.48	0.280
Element Size 2	1.48	1.24	0.287
Element Size 3	0.74	0.62	0.300

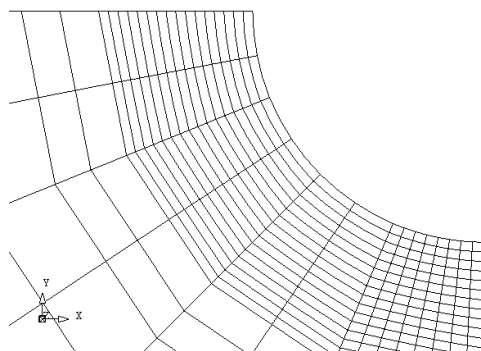


Figure 4.8. Density of mesh around hole

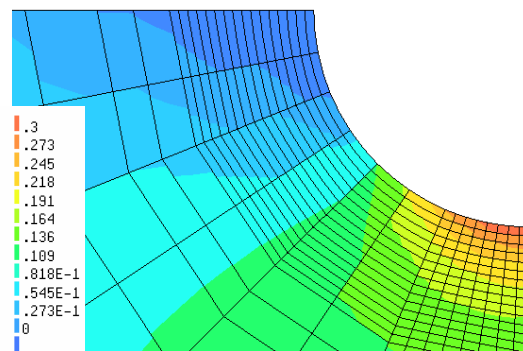


Figure 4.9. Contour levels around hole

The size of the mesh is illustrated in figure 4.8 and the contours as a result of the stress concentration in figure 4.9. It can be seen in figure 4.9 that the maximum stress concentration is found at the edge of the hole parallel to the loaded edge. Having determined the size of the mesh around the hole for the 2D case, the number of elements in the depth had to be determined for volume elements.

4.1.1.1.2 3D Finite element model

As for the previous analysis, the same was performed using volume elements for the 3D case. Using 20 node volume elements (CHX60), a quarter of a 300 x 300 x 10 mm panel with 15 mm hole was modelled. The purpose of this step was to determine the depth of the volume elements. The same width and breadth of the elements determined for the 2D case were used. Using two elements (element size of 0.74x 0.62x 5mm) over the depth provided the same results as for the 2D case.

The following step of the finite element mesh calibration, focused on the out of plane bending of a finite width plate with a circular hole.

4.1.2 Out of plane bending

The final step in the calibration of the finite element mesh was the determination of the mesh element size for a finite width panel with circular hole subjected to simple bending. Having determined the element size for volume elements in tension, this element size could be used as a starting point. The purpose of this step of the mesh calibration was to determine the size of elements (width, breadth and depth) which would give the correct extrapolated stress results. The mesh was calibrated by comparing finite element results to that found in literature [38].

For simple bending (bending around one axis) of a finite width panel with circular hole, Goodier (1963) [38] obtained K_{in} as a function of d/H :

$$K_{in} = C_1 + C_2 \left(\frac{d}{H} \right) + C_3 \left(\frac{d}{H} \right)^2 \quad (4.10)$$

$$C_1 = 1.82 - 0.3901 \left(\frac{h}{d} \right) - 0.01659 \left(\frac{h}{d} \right)^2 \quad (4.11)$$

$$C_2 = -1.9164 - 0.4376 \left(\frac{h}{d} \right) - 0.01968 \left(\frac{h}{d} \right)^2 \quad (4.12)$$

$$C_3 = 2.0828 - 0.643 \left(\frac{h}{d} \right) - 0.03204 \left(\frac{h}{d} \right)^2 \quad (4.13)$$

Where:

$$\sigma_{nom} = \frac{6MH}{(H-d)h^2} \quad (4.14)$$

D = diameter of hole
h = thickness of panel
H = width of panel

Stress concentration factor for bending of finite width plate with circular hole

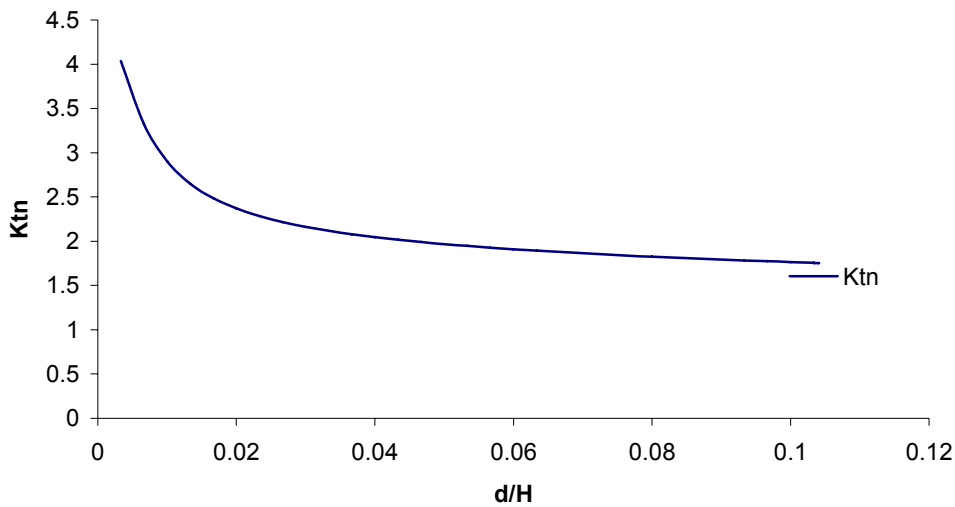
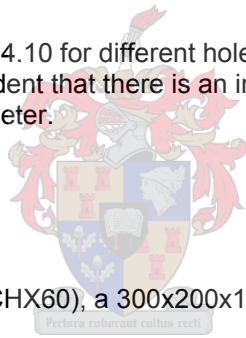


Figure 4.10. Stress concentration factor for bending of finite width panel with circular hole ($h=10$)

Equation 4.10 is presented in figure 4.10 for different hole diameters for a plate thickness of 10mm. From the figure 4.10 it is evident that there is an increase in the stress concentration factor with an decrease in hole diameter.



4.1.2.1 3D Finite element model

Using quadratic volume elements (CHX60), a 300x200x10 mm panel with a 15 mm centre hole was modelled.

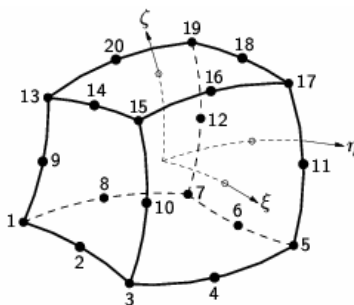


Figure 4.11. Quadratic volume element CHX60 [44]

The CHX60 element is a twenty-node isoparametric solid brick element (figure 4.11). It is based on quadratic interpolation and Gauss integration.

Only a quarter of the panel was modelled (see figure 4.7). A unit pressure line load was applied in the vertical plane to one of the 150 mm quarter edges, and both symmetry edges constrained according to symmetry.

Determination stress concentration around hole

From equation 4.10

$$\begin{aligned} K_{tn} &= 1.92047 \\ C_1 &= 2.07269 \\ C_2 &= -2.21689 \\ C_3 &= 2.49723 \end{aligned}$$

From equation 4.14

$$\begin{aligned} \sigma_{nom} &= (6 \times 1 \times 100 \times 200) / ((200-15) \times 100) \\ &= 6.48864 \text{ MPa} \end{aligned}$$

Therefore:

$$\begin{aligned} \sigma_{max} &= 6.31579 \times 1.92047 \\ &= 12.337 \text{ MPa} \end{aligned}$$

Having calculated the magnitude of the stress concentration around the hole using the information from Goodier [38], the mesh could be calibrated. The element size obtained from the 2D analysis was used as initial element size, and different mesh configurations were investigated. Table 4.2, presents the different mesh configuration together with their corresponding calculated principal tensile stress.

Table 4.2. Mesh density for the bending of finite width panel with a single circular hole

				Gauss 4 x 4 x 4	Gauss 3 x 3 x 3
	Breadth	Width	Depth	Principal Stress	Principal Stress
	mm	mm	mm	MPa	MPa
Element Size 1	0.74	0.62	2	11.2	11
Element Size 2	0.74	0.62	1	11.6	11.4
Element Size 3	0.37	0.62	1	12.2	11.8

The depth of the element affected the calculated stress to a noticeable degree, finally a depth of 1mm was chosen.

Another parameter that influences the stress prediction is the integration scheme. By default, DIANA [44] applies a 3x3x3 Gauss integration scheme. This integration scheme ensured 3 Gauss integration points over the width, breadth and depth of the element. The position of the 3x3x3 integration scheme can be seen in figure 4.12, and it can be noted that the integration points are not situated on the edge of the elements. DIANA [44] extrapolated the stress calculated at the integration points to the nodes situated on the edge of the element. As seen in table 4.2, this integration scheme underestimates the stress concentration, and can be attributed to position of the Gauss points. The Gauss points are situated too far from the edge and simply cannot follow the stress gradient, resulting in the underestimation of the principal tensile stress. Consequently, a 4x4x4 integration scheme (figure 4.13) was implemented for the element surrounding the hole, this scheme provided the best extrapolated results. In this integration scheme, the Gauss points are situated closer to the edge of the hole and can therefore follow the gradient better. Using a larger integration scheme results in an increase in computing time, the integration scheme was therefore only assigned to the elements in the vicinity of the hole.

Finally, a mesh configuration of element size 0.37x 0.31x 1mm volume elements provided the best results.

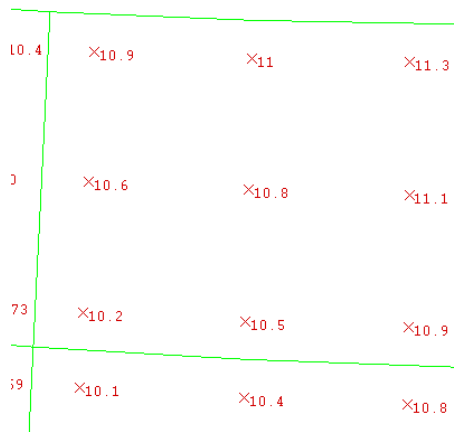


Figure 4.12. 3x3x3 Integration point position

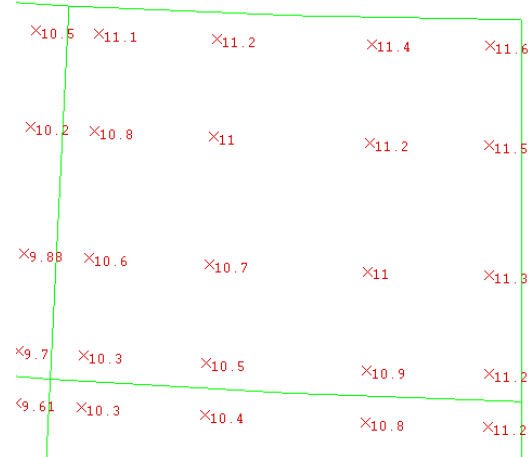


Figure 4.13. 4x4x4 Integration point position

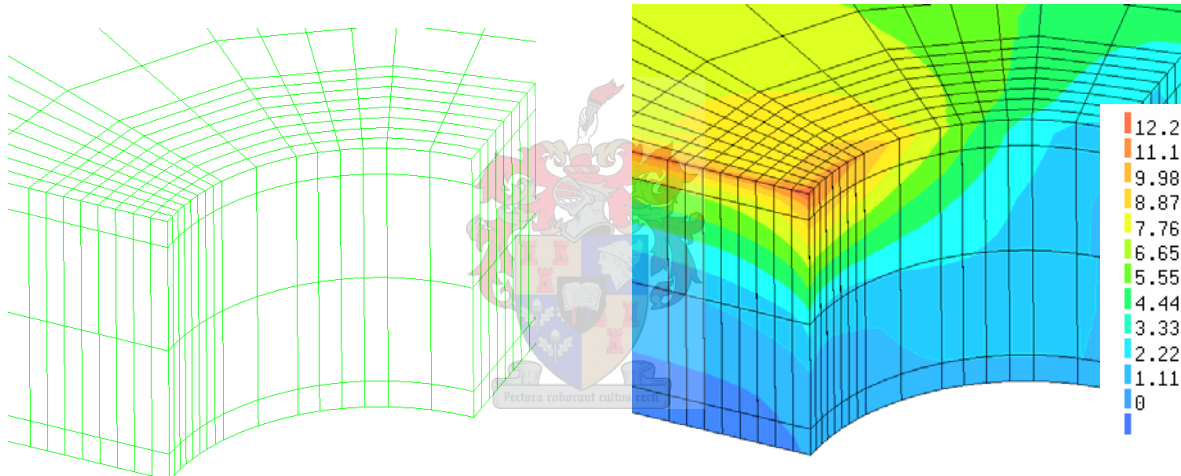


Figure 4.14. Element size around hole

Figure 4.15. Contour levels around hole

4.1.3 Conclusion

Using existing stress concentration data, the size of the elements surrounding the hole was determined, by comparing results obtained from the finite element model to that found in literature [36, 37, 38]. The element size surrounding the hole was refined to 0.37x0.63x1mm elements and could be applied to geometries that are more complex. This mesh configuration, together with a 4x4x4 Gauss integration scheme, provided accurate extrapolated principal stresses. Having calibrated the 3D model the actual geometry of the glass panels could now be modelled. The geometry of the actual models used for the determination of each panels failure stress is addressed in the following section.

4.2 MODEL GEOMETRY

Introduction

The complexity of the chamfered holes of the tested glass panels required a finite elements analysis to be performed to determine the fracture stress of each panel. Available literature [34, 36, 37, 38] covers only symmetrically loaded uniform circular holes, and could not be used for the determination of the failure stress of the chamfered holes.

Having determined the element size and mesh density for the bending of finite width panels with a single circular hole (section 4.1.2), the actual model could now be analysed.

This section defines the finite element models used for the determination of each panel's corresponding failure stress, with reference to the elements used, geometry, constraints, material properties, loading conditions and mesh size.

The layout of the model geometry is illustrated by means of a flow diagram in figure 4.16.

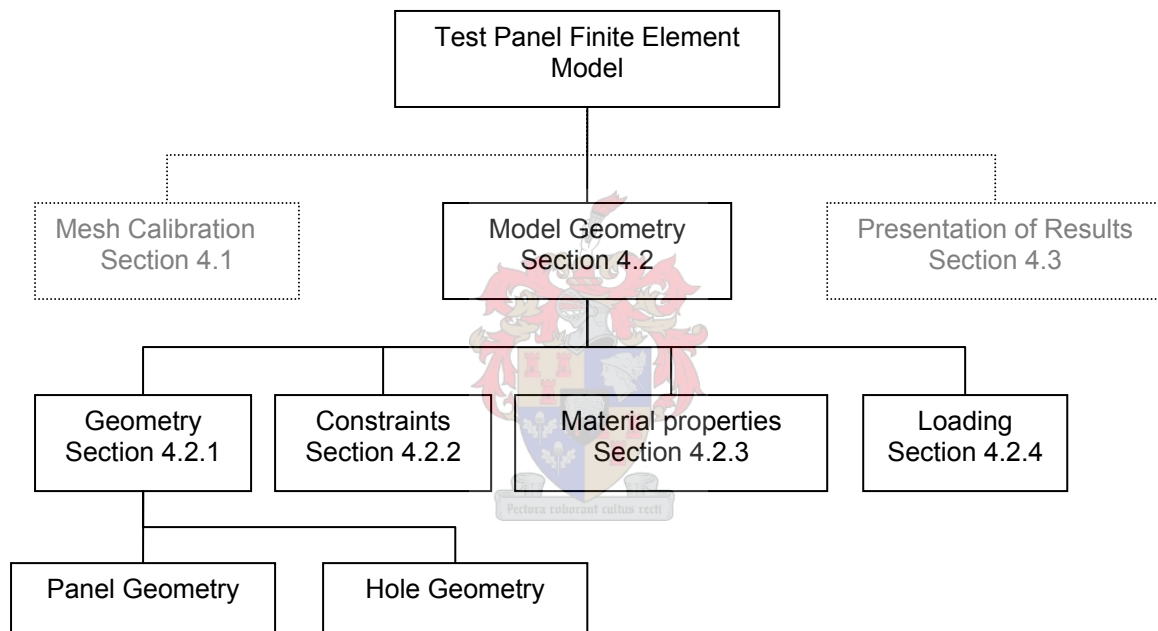


Figure 4.16. Flow diagram illustrating the finite element model geometry

The following section describes the test panel geometry, and is categorized under the following headings:

- Geometry of panels
- Constraints
- Material properties
- Loading

4.2.1 Geometry

4.2.1.1 Hole Geometry

The geometry of the hole of the actual model differed from the previous holes in that it had a 45 degree chamfer at the top and bottom of the hole. The hole was modelled, using the same elements as for the bending of finite width panel with a single circular hole, 20 node brick elements (figure 4.11). The chamfer was modelled using fifteen-node isoparametric solid wedge elements, CTP45, which is based on quadratic interpolation and numerical integration (figure 4.18).

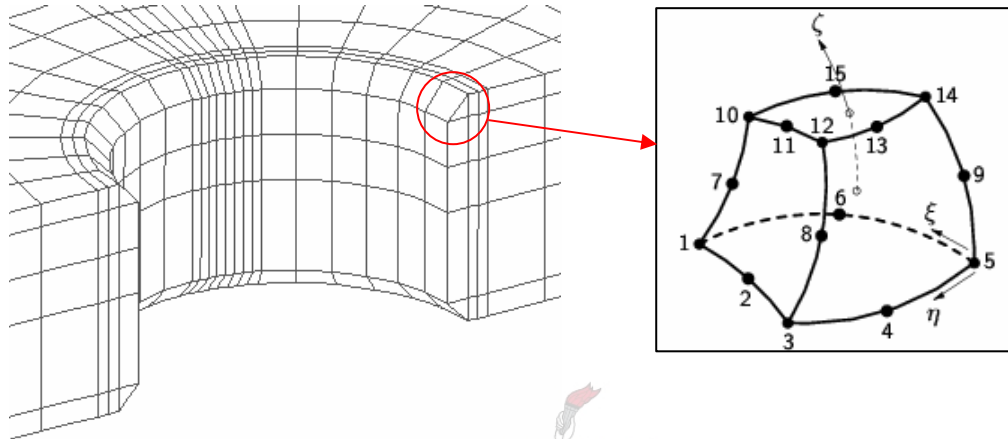


Figure 4.17. Hole with chamfer

Figure 4.18. CTP45 solid wedge element

The makeup of the hole with chamfer is illustrated in figure 4.17.

4.2.1.2 Panel Geometry

Symmetry about one axis permitted that only half of a glass panel had to be modelled, as illustrated in figure 4.19. The glass panels were modelled using 20 node solid brick elements (CHX60). The mesh was refined around the support and hole according to the element size determined in the previous section. The rest of the panel's mesh was relatively coarse in comparison to the mesh around the hole, as the stress gradient standardized away from the hole.

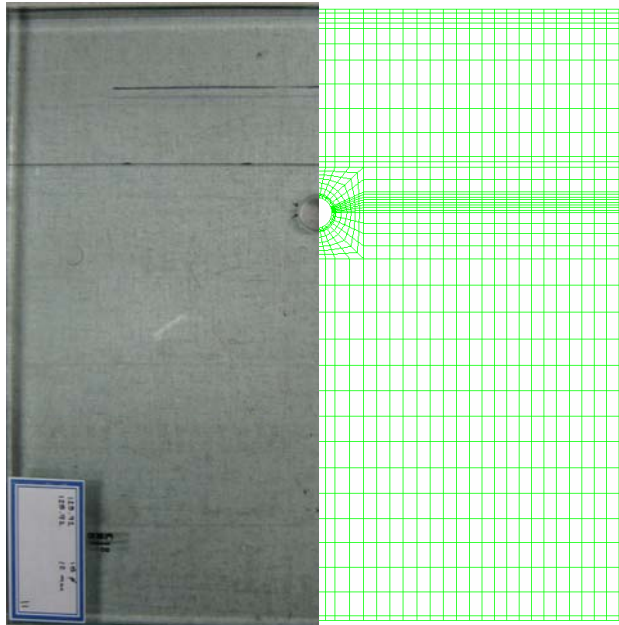


Figure 4.19. Half panel mesh

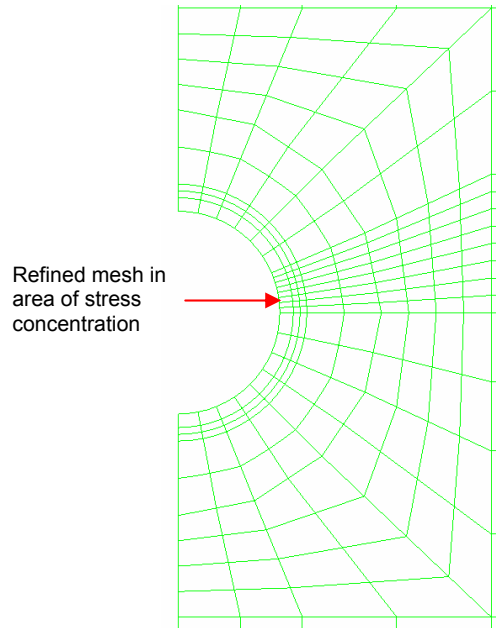


Figure 4.20. Refined mesh around hole

Due to the difference in panel geometry (three different thicknesses and four different hole geometries), twelve finite element models were created (see table 4.3).

Table 4.3. Number of finite element models created

	Diameter (mm)				
Thickness	10	15	20	no hole	
mm					
10	1	1	1	1	4
12	1	1	1	1	4
15	1	1	1	1	4
				Total	12

Figure 4.21, illustrates the three different hole geometries (15, 20, 25mm diameter) for the 10 mm panel thickness.

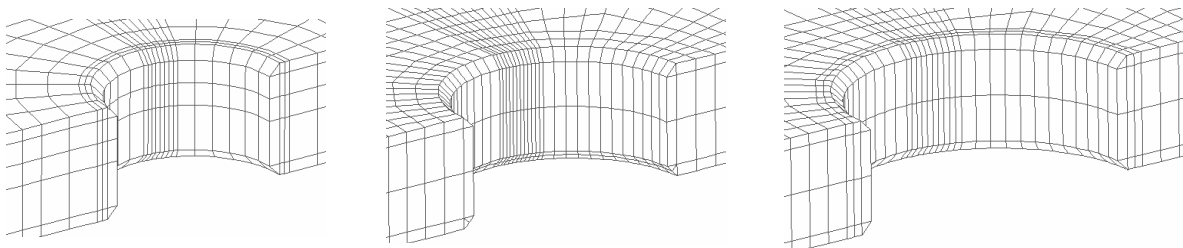


Figure 4.21. Diameter 15, 20, 25mm

4.2.2 Constraints

Solid elements have three degrees of freedom per node, each representing a translational degree of freedom, and consist of no rotational degrees of freedom. Therefore, the panels were only constrained against translation in the vertical direction at the supports and in the horizontal direction on one side, due to symmetry (Figure 4.22).

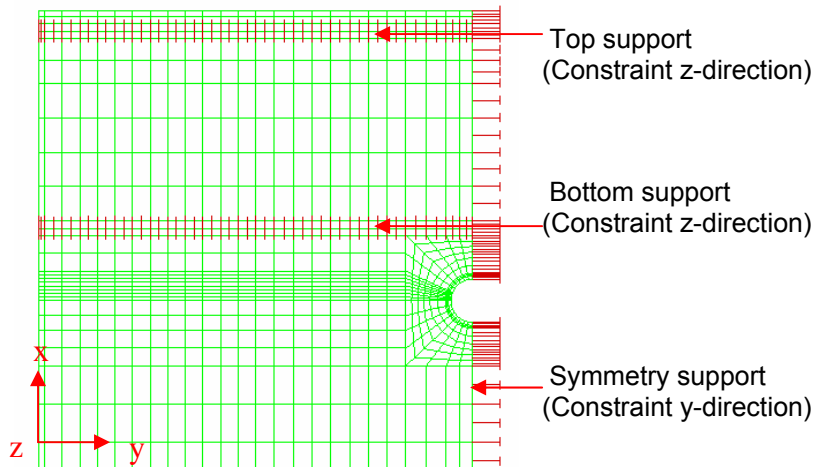


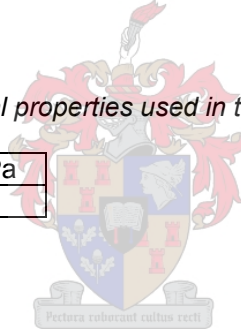
Figure 4.22. Model constraint

4.2.3 Material Properties

The modulus of elasticity and poisson ratio used in the finite element analysis is presented in table 4.4 [Appendix C].

Table 4.4. Toughened glass material properties used in the finite element model

Modulus of Elasticity	72000 MPa
Poisson ratio	0.23



4.2.4 Loading

As only half of each panel was modelled, only half of each panel's ultimate load had to be applied. The load was applied in the form of a distributed load at the position at which the load was applied in the laboratory test series. The magnitude of each panel's applied load is presented in table 4.5.

Table 4.5. Measured force and applied distributed load

Glass Panel #	Diameter	Force measured	Force Applied
	mm	kN	N/mm
10mm Thickness			
29	-	6.348	21.16
17	-	6.822	22.74
4	-	6.118	20.39
3	-	6.466	21.55
27	20	3.075	10.25
33	20	2.902	9.670
28	25	3.470	3.470
8	25	3.514	11.57
5	25	3.465	11.55
12mm Thickness			
22	-	7.984	26.61
13	-	7.958	26.53
37	-	8.325	26.53
36	15	4.626	15.42
11	15	5.377	17.92
10	15	4.724	15.75
9	20	4.744	15.81
12	20	5.100	17.00
2	20	5.500	18.33
20	25	4.605	15.35
19	25	5.639	18.80
18	25	5.359	17.86
15mm Thickness			
26	-	14.70	49.01
31	-	12.86	42.86
25	-	13.63	45.43
7	15	7.622	25.41
34	15	6.563	21.88
6	15	7.496	24.99
35	20	7.758	25.86
23	20	8.379	27.93
24	20	8.290	27.63
14	25	8.835	29.45
21	25	7.931	26.44
32	25	8.137	27.12

Glass is a linear elastic material, as seen in the laboratory test series and shown by [5, 13]. A linear static analysis was performed on all the finite element models. Finally, each panel's fracture stress was determined.

4.2.5 Conclusion

Due to the complex hole geometry (hole with chamfer) of the glass panels tested, a finite element program DIANA [44] was used to calculate the capacity of each glass panel. Having obtained the failure load from the laboratory test series, described in chapter 3.5, the finite element program was used to determine each glass panel's related fracture stress.

Stress concentrates around the hole, much the same way as stress concentrates around cracks [31]. It is at the hole where the fracture originates, and at maximum, this stress concentration is three times larger than the stress away from the hole. In order to calculate this stress concentration around a hole, the mesh has to be dense enough to simulate this concentration. Using available literature [36, 37, 38] the mesh density of the finite element model was determined. The calibrated finite element was used to determine the fracture stress of each glass panel, by applying the failure load from the corresponding laboratory test.

This section defines the finite element model of each glass panel tested. The following section presents the results obtained from the finite element analysis.



4.3 FINITE ELEMENT RESULTS

Introduction

To predict the loading capacity of freestanding glass balustrades the influence of the connection type (point- or continuous support) and the material properties of toughened glass need to be known. A laboratory test series was undertaken in which, 37 scaled down glass panels were tested in bending. The purpose of the laboratory test series was to determine both:

- The loading capacity and influence of different connections (types and sizes) and,
- The static- and dynamic material properties of toughened glass

The complexity of the hole (chamfered hole) forced a finite element analysis of each glass panel to be performed. The finite element analysis was performed to determine the loading capacity and influence of different connections, as well as to determine each tested panel's corresponding fracture stress.

This section focuses on the finite element results. The calculated fracture stress of each panel from the finite element analysis is presented before each connection type's loading capacity is determined, and compared. Finally, the results obtained from of the finite element model, are presented using the Weibull statistical model.

The layout of the model geometry is illustrated by means of a flow diagram in figure 4.23.

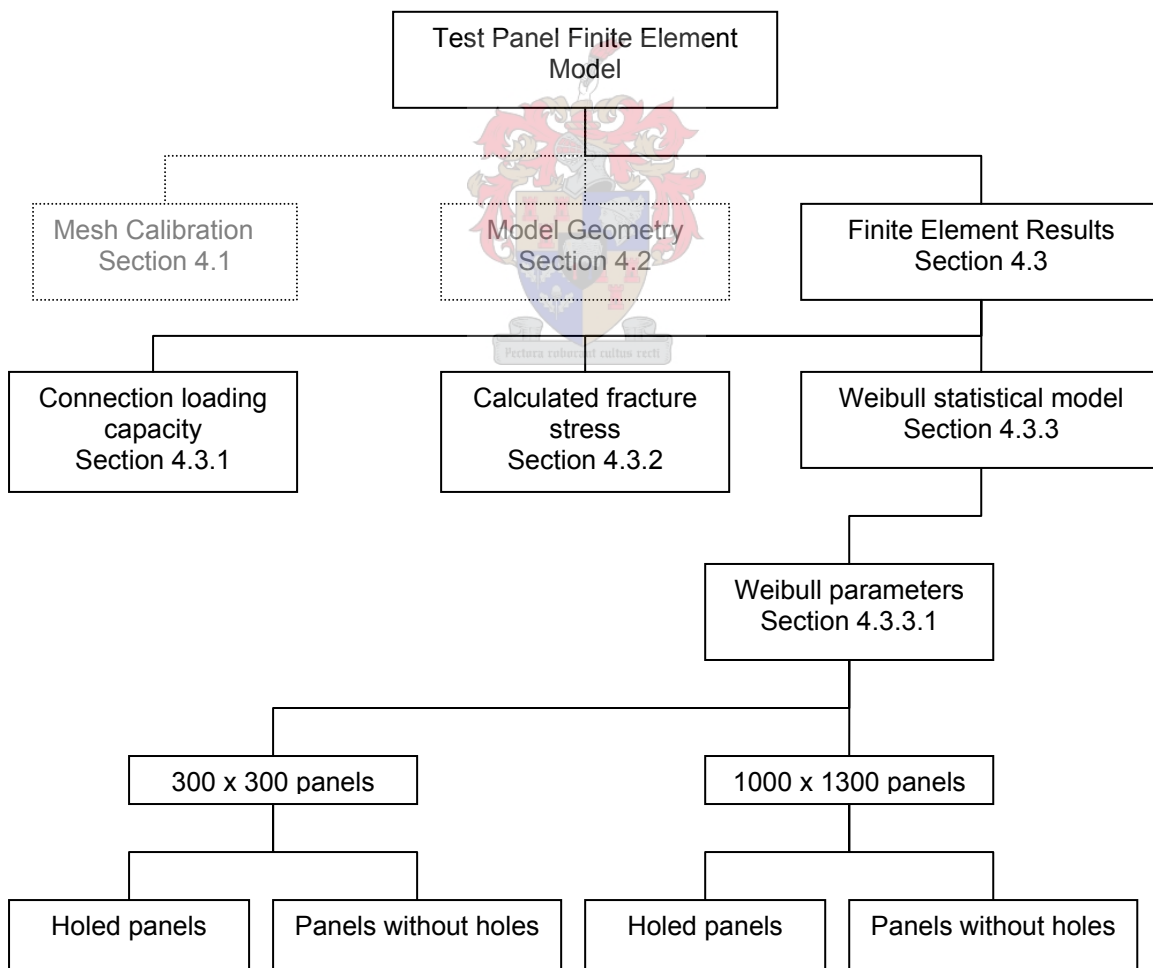


Figure 4.23. Flow diagram illustrating the presentation of results stage of the finite element model

4.3.1 Connection Loading Capacity

Before each panel's fracture stress was determined, a finite element analysis was performed to determine the structural capacity of each connection (type and size). Two different connection types were investigated:

- Point- and
- Continuously supported

4.3.1.1 Point supported

For the point-supported panels, three different hole diameters were tested (figure 4.2.4), together with three different panel thicknesses.

Each connection type was loaded with a unit-distributed line edge load, at the same position as was performed in the laboratory test series. A finite element analysis calculated each connection type's principal tensile stress, and then compared it to predicted stress concentrations [36, 37, 38], the difference being due to the chamfered edge. The area of maximum principal tensile stress is the area of concern. Glass has a high compressive- but low tensile strength, and it is often the point of maximum tensile strength where failure occurs. Figure 4.24, presents the contour representation of the stress concentration around the different hole diameters, for the 10 mm plate thickness. The red contours levels are representative of the principal tensile stresses, while the blue is of the compressive stresses. From figure 4.24, the stress concentration, which develops around a hole, can be seen.

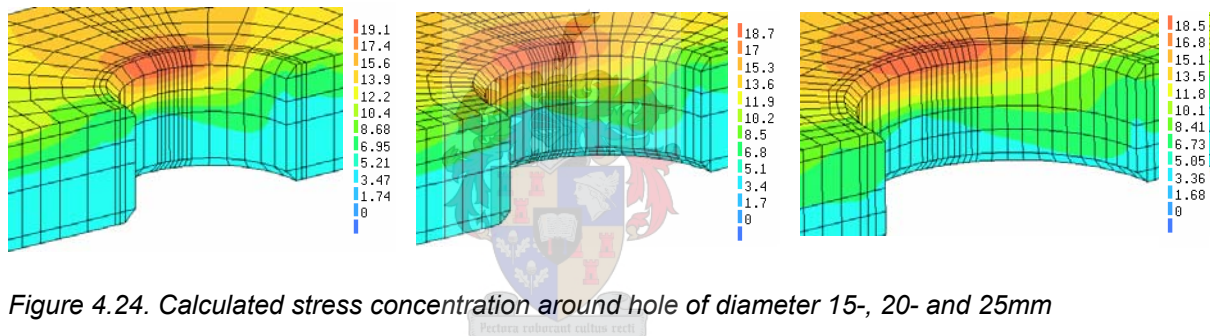


Figure 4.24. Calculated stress concentration around hole of diameter 15-, 20- and 25mm

The stress concentration factor for the chamfered holes was determined using the principal tensile stress calculated from each connection's finite element model. Table 4.6 presents the principal tensile stress for each connection.

Table 4.6. Connection principal tensile stress for a unit-line load

Diameter	Principal Stress
mm	MPa
10mmThickness	
15	19.1
20	18.7
25	18.5
12mmThickness	
15	13.8
20	13.3
25	13
15mmThickness	
15	9.39
20	8.97
25	8.68

Peterson [34] defines the stress concentration factor K_{tn} as the ratio of peak stress to a reference stress far away from an edge or hole influence. Each panel's reference stress was calculated using equation 4.14, as follows:

For a 300x300x10mm plate with 15mm hole,
Load applied 174mm from centre of hole

$$\begin{aligned}\sigma_{nom} &= 6MH/(H-d)h^2 \\ &= 6*300*174/((300-15)*(10^2)) \\ &= 10.989 \text{ MPa}\end{aligned}$$

The finite element stress concentration was calculated by dividing the calculated principal tensile stress for each panel by its unit-nominal stress. The calculated stress concentration factor (K_{tn}) was compared to that obtained by Goodier (1963) [38] for simple bending of a finite width panel with circular hole (un-chamfered), equation 4.10. Table 4.7 compares the calculated and predicted stress concentration factors.

Table 4.7. Calculated and predicted stress concentration factors

Diameter	Nominal Stress	Principal Stress	Calculated SCF	Predicted SCF
mm	MPa	MPa	FEM	Literature
10mm Thickness				
15	10.99	19.1	1.74	1.97
20	11.19	18.7	1.67	1.88
25	11.39	18.5	1.62	1.82
12mm Thickness				
15	7.63	13.8	1.81	2.01
20	7.77	13.3	1.71	1.91
25	7.91	13	1.64	1.84
15mm Thickness				
15	4.88	9.39	1.92	2.08
20	4.97	8.97	1.80	1.96
25	5.06	8.68	1.71	1.88

Considering only the three different hole diameters per panel thickness, it is noticed that there is a decrease in stress concentration with an increase in hole diameter.

Further, it is evident that the predicted stress concentrations are significant less than that of the calculated stress concentration factors. The decrease in the calculated stress concentration factors is representative of an increase in capacity, between the non-chamfered holes and holes with chamfers. The predicted stress concentration factors overestimate the calculated stress concentration factors in some instances by up to 11.67%. Figure 4.25 illustrates the calculated- and predicted stress concentration factors.

These results reinforce the use of the finite element analysis. It is recommended that a finite element analysis should be performed when non-conventional connection types are used.

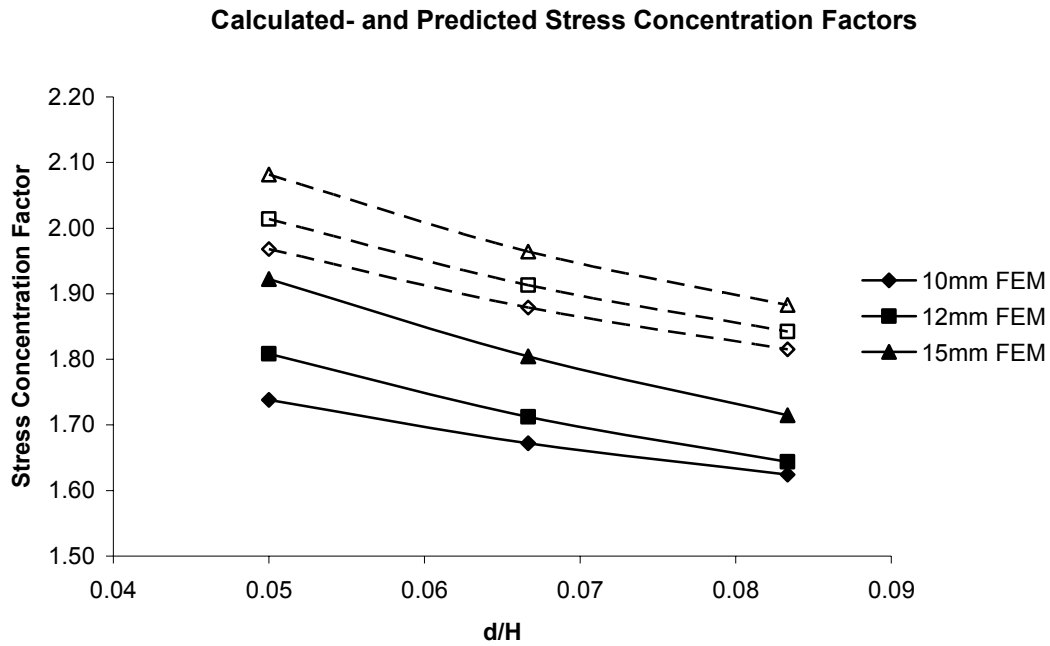


Figure 4.25. Calculated- and predicted stress concentration factors

4.3.1.2 Continuously supported

For the continuously supported panels three different panel thicknesses were tested. Each panel was loaded with a unit-distributed line edge load, at the same position as was performed in the laboratory test series. A finite element analysis calculated each thickness' principal tensile stress, presented in table 2.8. Figure 4.26, illustrates the contour representation of the stress distribution for the 10 mm panel thickness.

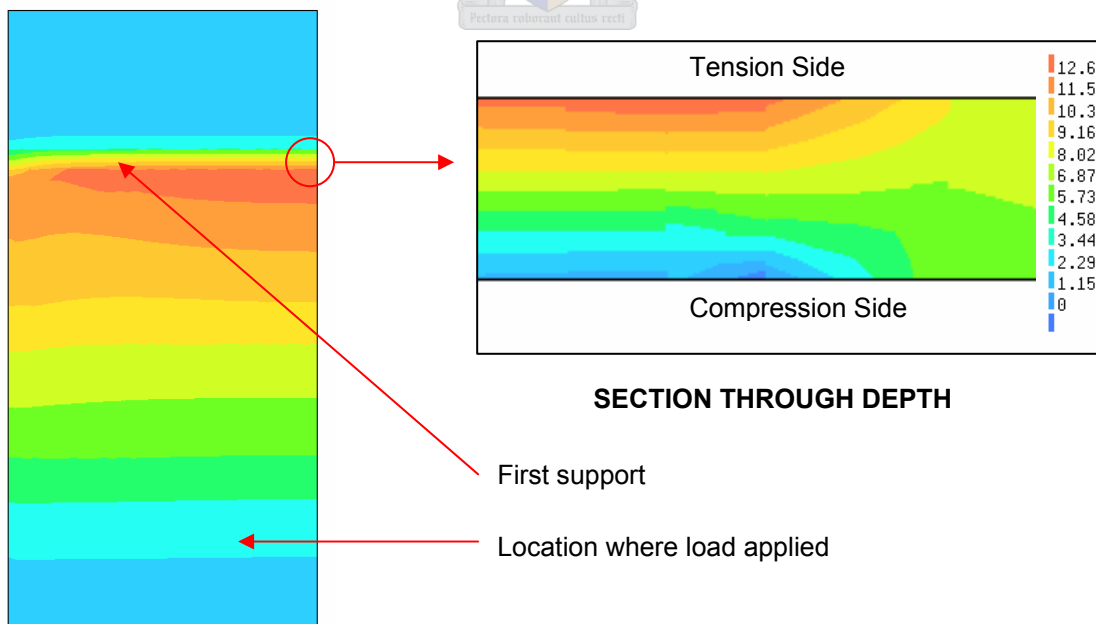


Figure 4.26. Stress distribution for 10mm thick continuously supported panel

Figure 4.27. Stress distribution through depth

From figure 4.26 it can be seen that the maximum principal tensile stress occur in the middle of the panel above the first support. Figure 4.27, illustrates the stress distribution through the depth of the panel. The red contour levels indicate the areas of principal tensile stress, while the blue indicate the areas of principal compressive stress.

The magnitude of principal tensile stress of each panel thickness loaded with a unit-distributed load is presented in table 2.8, and illustrated in figures 4.26 and 4.27.

Table 4.8. Principal tensile stresses for each panel thickness (unit line load)

Thickness mm	Principal Tensile stress MPa
10	12.6
12	8.83
15	5.61

From table 4.8, a decrease in principal tensile stress with increase thickness is noticed. The decrease in principal stress indicates an increase in structural capacity with thickness, which is to be expected.

4.3.1.3 Comparison between point- and continuously supported connections

Each panel, regardless of the connection type was loaded with a unit-distributed line load. The principal tensile stress of both the point- and continuously supported panels is summarized in table 4.9, and illustrated in figure 4.28.

Table 4.9. Principal tensile stresses for each panel thickness (unit line load)

Thickness mm	Principal Tensile stress MPa
No Hole	
10	12.6
12	8.83
15	5.61
15mm Diameter holes	
10	19.1
12	13.80
15	9.39
20mm Diameter holes	
10	18.70
12	13.30
15	8.97
25mm Diameter holes	
10	18.50
12	13.00
15	8.68

Principal Tensile Stress for different connection types and sizes

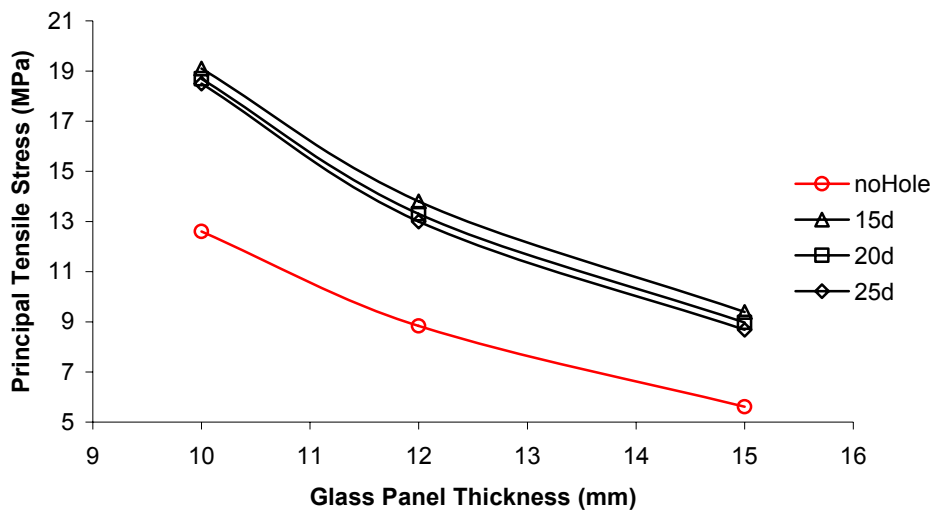


Figure 4.28. Principal tensile stress for different connection types and sizes (unit line load)

The red line in figure 4.28 represents the principal tensile stress for the different thicknesses of the continuously supported panels. The three lines in the top part of the figure represent the holed connections. It can be noted from the figure, that the principal stress lines connecting similar hole diameters, move closer to the continuously supported panels with an increase in hole diameter. As established in section 4.1.2, the stress concentration decreases with an increase in hole diameter.

On average, there is a 34% increase in structural capacity between the continuously- and point-supported panels. The difference in the structural capacity is attributed to the stress concentration, which develops around a hole.

4.3.1.4 Conclusion

Before each panel's fracture stress was determined, a finite element analysis was performed to determine the structural capacity of each connection (type and size). Point- and continuously supported connection types were investigated.

For the point-supported panels, three different hole diameters were tested, together with three different panel thicknesses. Each connection type was loaded with a unit-distributed line load, and the corresponding principal tensile strength determined. Each panel's calculated stress concentration factor (K_{tn}) was compared to similar stress concentration factors found in literature [38]. It was established that the predicted stress concentrations, from literature, were significant less than that of the calculated stress concentration factors. The decrease in the calculated stress concentration factors indicated an increase in capacity, between the non-chamfered holes and holes with chamfers. The predicted stress concentration factors overestimated (no chamfers) the calculated stress concentration factors in some instances by up to 11.7%. The results reinforced the use of the finite element analysis.

For the continuously supported panels three different panel thicknesses were tested. A finite element analysis was used to calculate each panel thickness' principal tensile stress. An increase in structural capacity with thickness was found to exist as expected.

Finally, the principal tensile stress of both the point- and continuously supported panels was compared. An increase in structural capacity of 34% between the continuously- and point-supported panels was noted. The finite element analysis was performed to determine the structural capacity and influence of different connections, as well as to determine each tested panel's corresponding fracture stress.

Having determined the influence and capacity of the different connection types and sizes the next section describes the results of the finite element analysis in which each tested panel's fracture stress was determined.

4.3.2 Calculated Fracture Stress

The complexity of the hole (chamfered hole) forced a finite element analysis of each glass panel to be performed. This section presents the results of the finite element analysis of each tested panel.

Symmetry about one axis enabled the modelling of only half of each tested glass panel. As only half of each panel was modelled, only half of each panel's ultimate load had to be applied. Therefore, each panel was loaded with half of its corresponding ultimate load, and using the finite element program, DIANA [44], the resultant principal tensile stress calculated. Table 4.10 presents each panel's principal tensile stress.

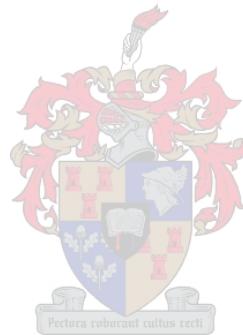


Table 4.10. Calculated principal tensile stress (Fracture stress)

Glass Panel #	Diameter	Loading rate	F measured	Fracture Stress
	mm		kN	MPa
10mm Thickness				
29	-	Dynamic	6.35	267.06
17	-	Dynamic	6.82	287.00
4	-	Dynamic	6.12	257.38
3	-	Dynamic	6.47	272.02
27	20	Static	3.08	192.00
30	20	Static	Fail	-
33	20	Static	2.90	181.20
28	25	Dynamic	3.47	214.28
8	25	Dynamic	3.51	217.00
5	25	Dynamic	3.47	213.97
12mm Thickness				
22	-	Static	7.98	234.96
13	-	Static	7.96	234.20
37	-	Static	8.33	245.00
36	15	Static	4.63	207.34
11	15	Static	5.38	241.00
10	15	Static	4.72	211.73
9	20	Quasi Static	4.74	207.01
12	20	Quasi Static	5.1	222.55
2	20	Quasi Static	5.5	240.00
20	25	Dynamic	4.61	220.51
19	25	Dynamic	5.64	244.00
18	25	Dynamic	5.36	231.88
15mm Thickness				
26	-	Quasi Static	14.70	275.00
31	-	Quasi Static	12.86	240.60
25	-	Quasi Static	13.63	254.91
7	15	Quasi Static	7.62	232.00
34	15	Quasi Static	6.56	199.77
6	15	Quasi Static	7.5	228.16
35	20	Dynamic	7.76	228.69
23	20	Dynamic	8.38	247.00
24	20	Dynamic	8.29	244.38
14	25	Dynamic	8.84	258.40
21	25	Dynamic	7.93	225.32
32	25	Dynamic	8.14	231.17

Glass is a material, which shows an increase in strength with increase loading rate [13, 28]. Since the panels were tested under three different loading rates, the calculated fracture stresses cannot directly be compared. The variability of the results also attributes to this.

Glass has a high variability of strength, which is justified by the existence of surface flaws [31]. The magnitude of the applied stress that will cause fracture depends on the flaw size and geometry, and is therefore a matter of probability. The following section describes the Weibull statistical model that is used to present the loading capacity of the glass panels corresponding to each loading rate.

4.3.3 Weibull statistical model

Introduction

The laboratory test series [chapter 3] demonstrated that the point of fracture does not necessarily coincide with the point or location of maximum principal stress. A different point of fracture can be attributed to the presence due to cracks and flaws in the glass and on the surface.

When a stress is applied to a material containing a crack, the stress concentrates at the crack tip much the same way as stress concentrates around a hole [31]. This stress concentration causes the crack to propagate and finally leads to the failure of the specimen. A high variability in the size-, orientation- and distribution of the surface flaws between specimens in turn, lead to a high variability of strength in glass.

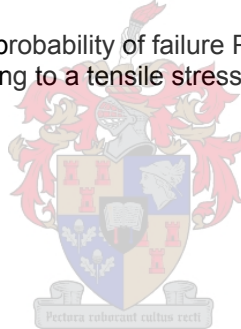
A statistical model is therefore required to give a true prediction of strength of glass. This section describes the Weibull statistical model [39] that was used to represent the failure strength of the tested glass panels and finally, used to predict the capacity of full-scale glass balustrades.

Why was the Weibull statistical model used?

The Euro code, associated with the use of glass in buildings, recommends that the Weibull distribution be used when failure of glass is predicted [40].

Weibull [39] defines the cumulative probability of failure P_f as the percentage of number of specimens that will not survive loading to a tensile stress of σ , by:

$$P_f = 1 - \exp \left[- \left(\frac{\Delta\sigma}{\Delta\sigma_0} \right)^m \right] \quad (4.15)$$



Where;

$P_f = 1 - P_s$ = probability of failure

σ = specimen fracture stress

σ_0 = 37% mean fracture stress

m = Weibull modulus characterizing the width of the fracture stress distribution

The Weibull modulus (**m**) is indicative of the variability in the results, where a low **m** is indicative of a high variability. For modern high quality ceramics, **m** varies in the range of 5-10 and is never significantly greater than 20. For metals, it is typically in the range 50-100 [5]. Accordingly, the Weibull modulus describes the variability or scatter in specimen strength.

Before a specimen's strength can be predicted, according to the data obtained from a test series, the Weibull modulus of the data set needs to be determined first.

The Weibull modulus is calculated by rearranging equation 4.15. The double exponent of equation 4.15 results in:

$$\ln \ln \left[\frac{1}{1 - P_f(V)} \right] = m \ln \left(\frac{\Delta\sigma}{\Delta\sigma_0} \right) \quad (4.16)$$

Equation 4.16 is then in the format of $y = mx+c$, where m (Weibull modulus) is the gradient of a straight line. Where:

$$y = \ln \ln \left[\frac{1}{1 - P_f(V)} \right] \quad (4.17)$$

$$x = \ln \left(\frac{\Delta \sigma}{\Delta \sigma_0} \right) \quad (4.18)$$

By plotting the results of a data set in this format, the Weibull modulus can be determined by simply calculating the gradient of the straight line.

Before the data set can be presented in this format, a number of activities need to be performed. Listed below are the activities:

- Firstly the fracture stress corresponding to the data set is arranged in descending order (Table 4.12, column 1)
- Then, the probability of failure, P_f , for each specimen is estimated as $n/(N+1)$, where n is the ordering number (weakest to strongest) and N is the total number of specimens (Table 4.12, column 3)
- Finally, the x coordinate is calculated with equation 4.18, and the y by equation 4.17. (Table 4.12, column 5 and 6)

Plotting the results, and determining the gradient of the line, yields the Weibull modulus (m) of the data series. σ_0 is representative of 37% of the fracture strength and is calculated by interpolating between the arranged fracture stresses (descending order).

Having determined the Weibull modulus and -mean fracture stress, equation 4.15 can be used to predict each specimen's probability of failure. The following section focuses on the Weibull parameters, and differentiates between the panels with- and without holes.

4.3.3.1 Weibull parameters

Introduction

The Weibull modulus (m) is indicative of the variability in the results for a given data set, and is not affected by the loading rate. Once the modulus is determined for a given material and geometry, it does not have to be calculated for the same material again [13]. Due to the difference in geometry between the holed panels and panels without holes, the same Weibull modulus could not be used. A separate Weibull modulus had to be calculated for the panels without holes. The results are therefore presented for glass panel with holes and glass panels without holes.

Scale panels (300x300mm)

4.3.3.1.1 Weibull modulus for glass panels with holes

Since the largest number of specimens were tested at the dynamic loading rate, the fracture stresses obtained from the finite element analysis for this data set were used to determine the Weibull modulus. All together 12 specimens were tested at a dynamic loading rate; their fracture stresses are summarized in table 4.11.

Table 4.11. Fracture stress for holed panels tested under a dynamic loading rate

Panel ##	Hole Diameter (mm)	Loading rate	Fracture Load (kN)	Fracture Stress (MPa)
10mm Thickness				
28	25	Dynamic	3.47	214.3
8	25	Dynamic	3.51	217.0
5	25	Dynamic	3.47	213.9
12mm Thickness				
20	25	Dynamic	4.61	220.5
19	25	Dynamic	5.64	244.0
18	25	Dynamic	5.36	231.8
15mm Thickness				
35	20	Dynamic	7.76	228.7
23	20	Dynamic	8.38	247.0
24	20	Dynamic	8.29	244.4
14	25	Dynamic	8.84	258.4
21	25	Dynamic	7.93	225.3
32	25	Dynamic	8.14	231.2

Using the fracture stress for holed panels tested under a dynamic loading rate, as calculated by finite element model, the Weibull modulus was determined. The fracture stress corresponding to the data set was arranged in descending order (Table 4.12, column 1), and the probability of failure, P_f , for each specimen was estimated (Table 4.12, column 3). Finally the x and y coordinates were calculated (Table 4.12, column 5 and 6), and plotted in figure 4.29.

Table 4.12. Weibull modulus determination

Fracture Stress (MPa)	n	$P_s = n/(N+1)$	$P_f = 1-P_s$	$\ln(\ln(1/P_s))$	$\ln(FS)$
258.4	1	0.08	0.92	0.94	5.55
247	2	0.15	0.85	0.63	5.50
244.38	3	0.23	0.77	0.38	5.45
244	4	0.31	0.69	0.16	5.44
231.88	5	0.38	0.62	-0.05	5.43
231.17	6	0.46	0.54	-0.26	5.42
228.69	7	0.54	0.46	-0.48	5.42
225.32	8	0.62	0.38	-0.72	5.42
220.51	9	0.69	0.31	-1.00	5.40
217	10	0.77	0.23	-1.34	5.38
214.28	11	0.85	0.15	-1.79	5.37
213.97	12	0.92	0.08	-2.53	5.37

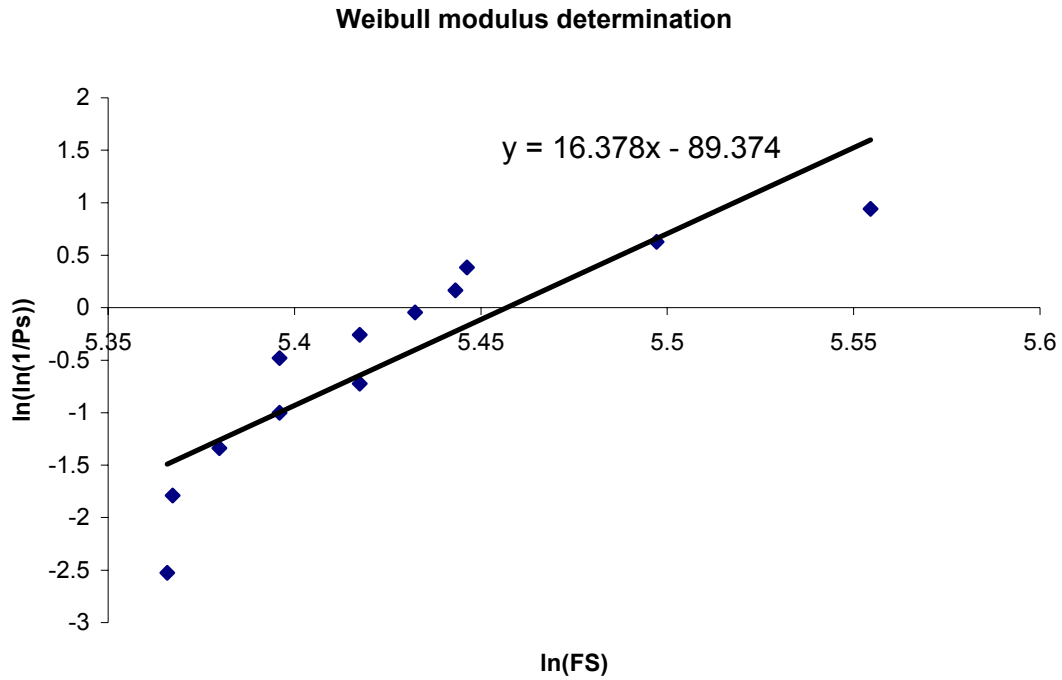


Figure 4.29. Weibull modulus determination

Plotting a linear trend line through the test points, as calculated in table 4.12, reveals the Weibull modulus (m). From the figure 4.29, it can be seen that the Weibull modulus for holed panels tested under a dynamic loading rate was 16.38.

The mean fracture stress (σ_0) was calculated for a probability of survival of 37% (The stress that allows 37% of the specimens to survive). Interpolating between fracture stress of 244 MPa and 232 MPa produced a $\sigma_0 = 234.19$ MPa

Having identified the apparent Weibull parameters (m, σ_0), the probability distribution was plotted (figure 4.30), and each specimen's probability of failure determined (Table 4.13).

Table 4.13. Each specimen's probability of failure

Fracture Stress (MPa)	P_s	P_f
258.4	0.01	0.99
247	0.10	0.91
244.38	0.14	0.86
244	0.15	0.85
231.88	0.43	0.57
231.17	0.44	0.55
228.69	0.51	0.50
225.32	0.58	0.42
220.51	0.68	0.32
217	0.74	0.26
214.28	0.79	0.21
213.97	0.79	0.21

Fracture Stress Predictions with Weibull model for Dynamic loading rate

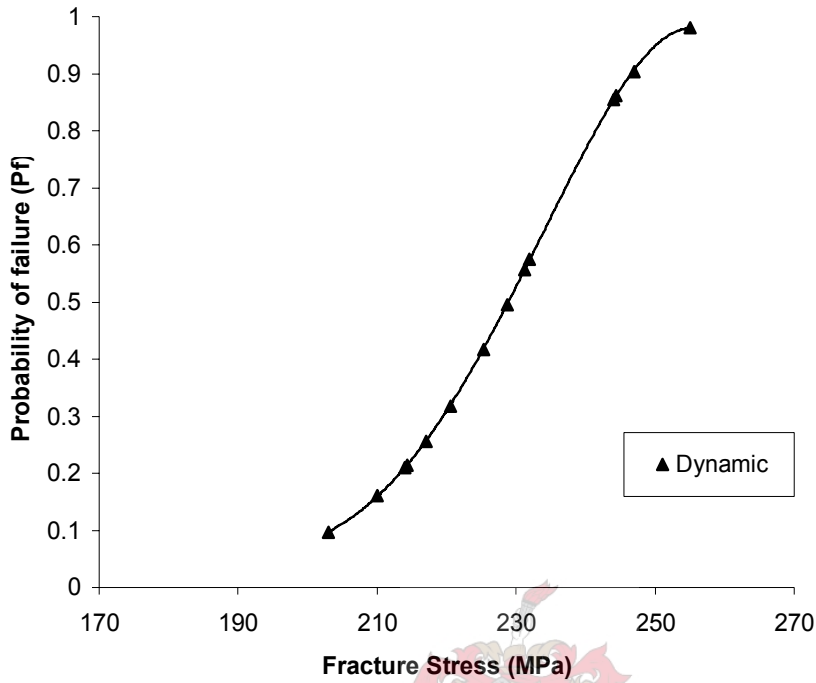


Figure 4.30. Fracture stress predictions for dynamic loading rate

Fracture Stress Predictions with Weibull model

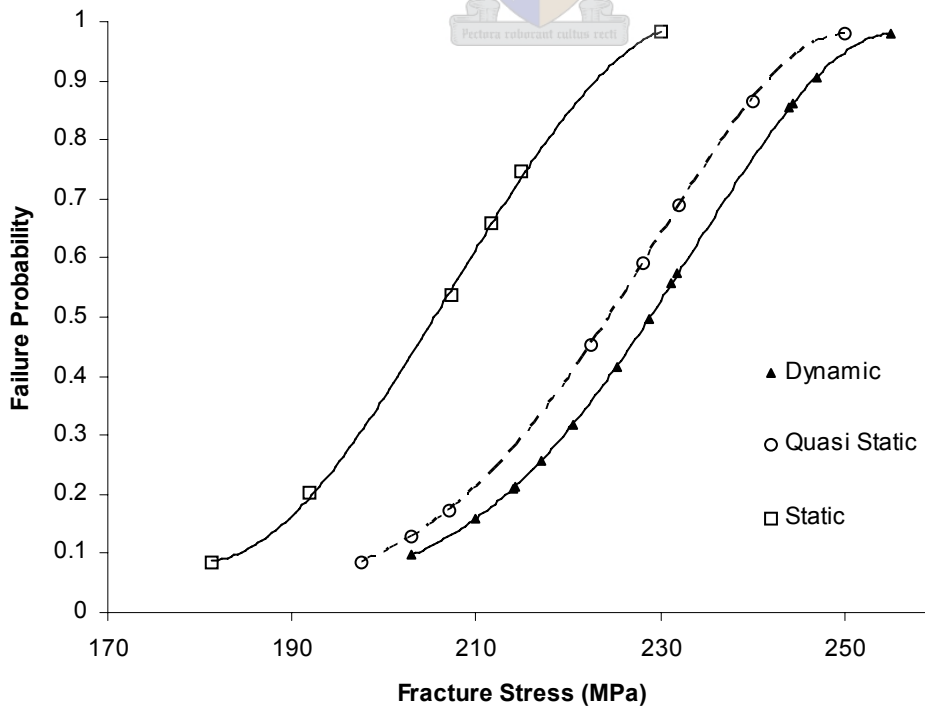


Figure 4.31 Probability distribution of holed panels

In a similar manner, the probability distribution using the Weibull statistical model was determined for both the Static- and Quasi Static loading rates (chapter 3.3.1.1.1 loading rates). Having calculated the Weibull modulus for holed panels under a dynamic loading rate, only the mean fracture stress had to be determined for the different loading rates [13]. The probability distribution for each loading rate is presented in figure 4.31.

Table 4.14. Strength prediction for loading rates for panels with holes

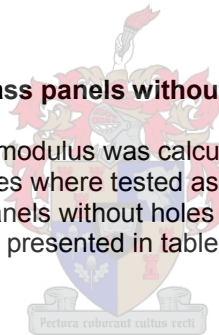
$m=16$

	50% P_f	2% P_f	0.8% P_f
Loading rate			
Static	206	165.5	155.95
Quasi Static	224.55	180.5	169.95
Dynamic	228.89	184	173.23

From the graph in figure 4.31, an increase of 10% in mean strength with increase in loading rate is evident. A parameter that can be seen in table 4.14, is that the mean probability of failure of the Quasi static loading rate prediction is very close to that of the Dynamic loading rate, which might be a possible indication of upper limit or asymptote of the increase in strength of the material. However, due to limited number of tests and range of loading rate, more tests at increase loading rates need to be conducted to provide conclusive results.

4.3.3.1.2 Weibull modulus for glass panels without holes

As for the holed panels, the Weibull modulus was calculated for the panels without holes. However, only 10 panels without holes were tested as apposed to the 27 holed panels that were tested. Fracture stresses for panels without holes that were tested under Static-, Quasi-static and Dynamic loading rates are presented in table 4.15.



Fracture stress predictions using the Weibull model

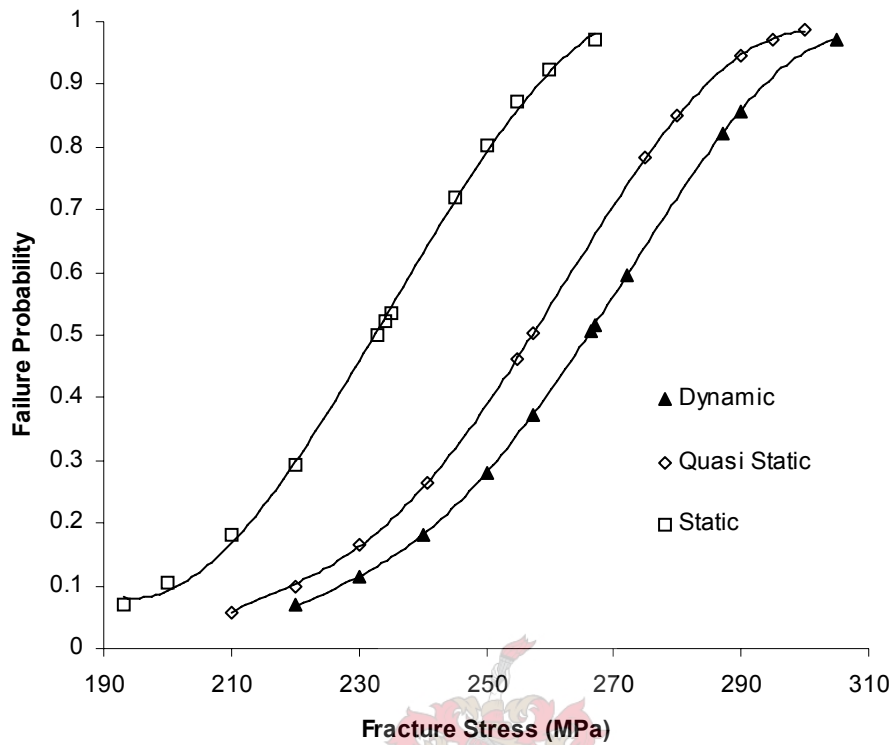


Figure 4.32. Probability distribution of panels without holes

A Weibull modulus of $m=12$ was calculated for the panels without holes. The Weibull modulus is representative of the variability in the results of the data set, and is illustrated in figure 4.32 by the gradients of the graphs.

Table 4.15. Strength prediction for loading rates for panels without holes

$m=12$

	50% P_f	2% P_f	0.8% P_f
Loading rate			
Static	233	174	160.8
Quasi Static	257.5	192	177.6
Dynamic	266.5	198.5	183.5

Although only three panels were tested per loading rate with the exception of four for the dynamic loading rate, a common trend was found to exist between the different loading rates. Comparing the mean probability of failure of the different loading rates, an increase in strength with an increase in loading rate was noticed, reinforcing the idea of static fatigue. From table 4.15, it can also be seen that the mean probability of failure of the Quasi-static loading rate is closer to the mean of the dynamic loading rate, as noticed from in the probability distribution of the holed panels. This might once again be a sign of the strength asymptote of the strength of the material. Results for the static loading rate are verified by available literature [41]. Available literature [41] predicted for tempered glass an $m=11$, and $\sigma(0.8\%) = 185$ MPa, for panels without holes.

4.3.3.1.1.3 Comparison between panels with- and without holes

The difference in panel geometry resulted in a different Weibull modulus being calculated for the panels with- and without holes. A modulus of $m=16$ was calculated for the holed panels and a modulus of $m=12$ for the panels without holes. The decrease in modulus between the holed and panels without holes indicate a greater variability in results. The hole confines the fracture origin to a certain area, resulting in a smaller variability of results. However, a decrease in mean strength is brought about by the drilling of the hole, which is noticed when comparing dynamic mean fracture strength of the holed panels (229 MPa) to that of the panels without holes (267 MPa).

This section described the Weibull statistical model that was used to represent the failure strength of the tested glass panels (300x300). The following section focuses on the Weibull statistical model used to predict the capacity of full-scale glass balustrades (1300x1000).

Full scale panels (1300 x 1000mm)

4.3.3.1.2 Weibull modulus for glass panels with- and without holes

The specimen size effect occurs because the size of the critical defect, on the average, increases with increasing area or volume. The glass panels tested in the laboratory test series were all of the same size, and therefore did not effect the strength predictions.

However, the laboratory test panels (300 x 300) were scaled down from actual glass balustrade panels (1000 x 1300). To account for the difference in strength prediction for the size effect between the test- and actual balustrade panels, the size of the panels have to be included in the Weibull distribution equation 4.15 [39]. This section describes the alteration of equation 4.15, (traditional Weibull equation) to include the difference in volume between the test and actual balustrade panels.

The volume dependence of the material can be included in the Weibull distribution [39] as follows:

$$P_f(V) = 1 - \exp \left[- \frac{V}{V_0} \left(\frac{\Delta\sigma}{\Delta\sigma_0} \right)^m \right] \quad (4.19)$$

The double exponent of both sides of the equation gives:

$$\ln \ln \left[\frac{1}{1 - P_f(V)} \right] = \ln \left(\frac{V}{V_0} \right) + m \ln \left(\frac{\Delta\sigma}{\Delta\sigma_0} \right) \quad (4.20)$$

Equation 4.20 is then of the form $y=mx+c$

Where:

- m = unchanged (Panel with- and without holes)
- V_0 = Test panel fracture area = 300 * 300 (See figure 3.8)
- V = Actual balustrade panel fracture area = 1300 * 1000 (See figure 6.5, 6.6)

Therefore:

$$\begin{aligned} V/V_0 &= (1300*1000) / (300*300) \\ &= 14.4444 \end{aligned}$$

Table 4.16. Strength prediction for loading rates for panels with holes taking into account volume dependence

	50%Pf	0.8%Pf
Loading rate		
Static	174.35	132
Quasi Static	190.05	144
Dynamic	194.35	147

Table 4.17. Strength prediction for loading rates for panels without holes taking into account volume dependence

	50% Pf	0.8% Pf
Loading rate		
Static	187	156.4
Quasi Static	206.8	172.8
Dynamic	213.6	178

The specimen size effect occurs because the size of the critical defect, on the average, increase with increasing area or volume. With the increase in the size of the panels, the probability of failure decreased by 20%.

4.3.3.2 Conclusion

A high variability of strength in glass resulted in the employment of the Weibull statistical model [39] to present the failure strength of the tested glass panels. The difference in panel geometry resulted in different Weibull modules [39] being calculated for the panels with- and without holes.

The increase in strength, with increase in loading rate was noticed in both probability distributions (panels with- and without holes). An increase of 10% in mean strength from the static- to dynamic load rate was noticed for the distribution of the holed panels.

Another parameter common to both distributions (panels with- and without holes) was the grouping of the mean probability of failure of the quasi-static and dynamic loading rates, which could be an indication of the material strength asymptote.

Comparing the two distributions, a decrease in modulus, and mean strength between the panels with- and without holes was noticed. Although the hole confined the fracture origin to a certain area, resulting in a smaller variability of results, the drilling of the hole brought about a decrease in mean strength.

To account for the difference in strength prediction for the size effect between the test- and actual balustrade panels, the size of the panels was included in the Weibull distribution [39]. The specimen size effect occurs because the size of the critical defect, on the average, increase with increasing area or volume. With the increase in the size of the panels, the probability of failure decreased by 20%.

With the loading capacity and influence of different hole geometries together with the material properties of toughened glass determined, the calibrated finite element model will now be employed to analyse full-scale balustrade configurations. The following chapter describes the finite element model in which freestanding- as well as continuous balustrades were analysed.

CHAPTER 5 BALUSTRADA FINITE ELEMENT MODEL

Introduction

In the previous chapter the static- and dynamic material properties of toughened glass were determined, and presented using the Weibull statistical distribution [39]. The Weibull model was modified to include the specimen size difference, and consequently the static- and dynamic material properties for 1x1.3 m glass balustrade panels were determined.

This chapter describes the modelling of actual freestanding balustrades using the determined material properties of toughened glass and the calibrated finite element model from chapter 4. The purpose of which is to determine the loading capacity of freestanding balustrades. Since the design of freestanding balustrades differs, varying geometry, support and loading parameters are investigated and their influence on the loading capacity of the freestanding balustrade panel quantitatively determined.

The balustrade thicknesses investigated is:

- 12 mm and
- 15 mm thick glass panels

The balustrade supports, from supplier guidelines [42] and available literature that is investigated can be categorized into:

- Continuously supported and
- Point supported systems

All freestanding balustrade systems are subjected to the SABS [7] static- and dynamic loading requirements, and can be categorized into:

- Concentrated point load
- Distributed load

A finite element model is used to simulate the SABS [7] required 400 J impact and consequently to determine the dynamic impact force to be used in a static analysis. Finally, a static linear analysis is employed to calculate each balustrade set-up's static- and dynamic loading capacity.

In the second part of the chapter, the influence of the addition of a handrail, used to connect a number of freestanding balustrade panels together, is investigated using the same finite element procedure. The influence of the number of connected panels together with the handrail dimension is quantitatively determined.

Three different numbers of connected panels are investigated, they are:

- 3 panels
- 5 panels
- 7 panels

Three different handrail dimensions are investigated, they are:

- 40x40 mm
- 50x50 mm
- 90x90 mm

The balustrade finite element model can be divided into a freestanding- and a continuous balustrade model, which is illustrated in a flow diagram in figure 5.1.

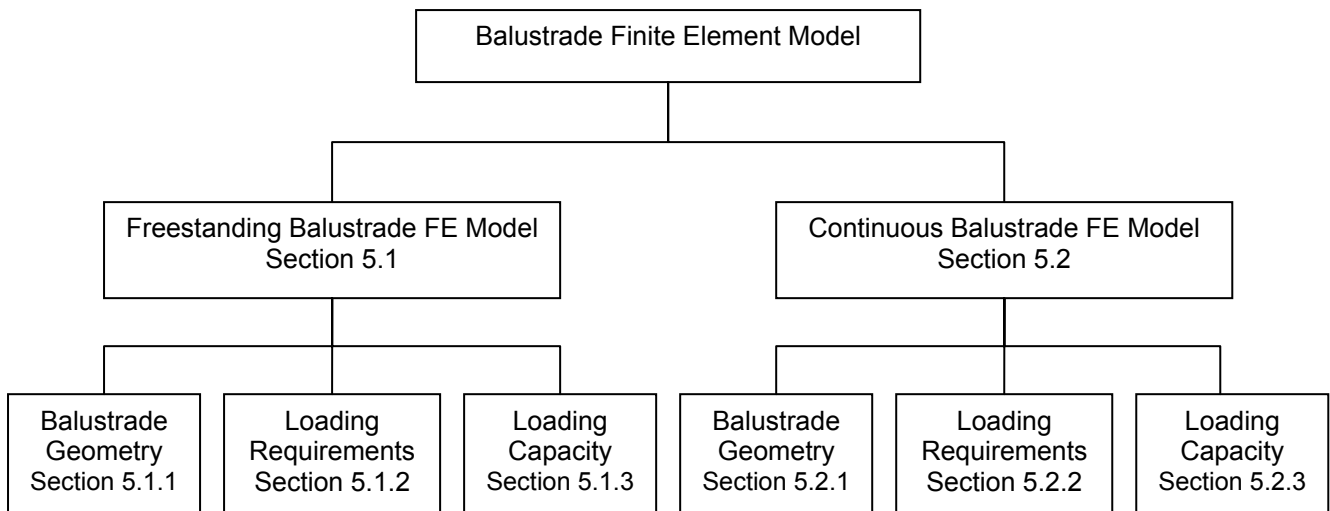


Figure 5.1. Flow diagram illustrating balustrade finite element stage

The geometry of the balustrade finite element model can be categorized into 2 stages:

- Freestanding balustrade finite element model
- Continuous balustrade finite element model

Each of which can further be divided into three steps. In the subsequent sections, each of these steps are addressed separately and described in detail, they are:

- **Geometry of balustrade panels**
This section describes the dimensions and thicknesses of the balustrade panels. The different supports based on continuous- and point-supported balustrades that were investigated together with the finite element model's constraints are also addressed.
- **Loading requirements**
The South African loading requirements can be categorized into static- and dynamic loading requirements. This section describes the different static- and dynamic loading types applied to each balustrade set-up.
- **Loading capacity**
This section presents the static- and dynamic loading capacity for continuous- and point supported freestanding balustrade panels as a result of a linear finite element analysis.

NOTE: There is a distinction between a **continuous support** (i.e. continuously embedded into a support) and a **continuous balustrade**, where individual freestanding panels are interconnected using a handrail.

5.1 FREESTANDING BALUSTRADE FINITE ELEMENT MODEL

Introduction

Since the design of freestanding balustrades differs, different geometry, support and loading parameters were investigated and their influence on the loading capacity of a freestanding balustrade panel was quantitatively determined.

This section describes the geometry of the panels with reference to dimensions of balustrade panels, support conditions and finite element constraints.

1x1.3 m balustrade panels of thicknesses 12- and 15mm thickness were chosen based on supplier specification. Different balustrade supports, commonly seen in practice and found in literature [12] was identified, and their influence on the loading capacity of freestanding balustrade determined. These support systems are categorized into:

- Continuously supported and
- Point supported systems

The geometry of the point-supported panels had to be carefully chosen to avoid any additional stress raisers from edge of neighbouring holes. Since the stress concentrates around a hole (chapter 4), and can be further superimposed if a hole is placed to close to an edge or neighbouring hole, the influence of distance between hole and edge and distance between two holes was investigated prior to the design of the point supported balustrade panels. Finally, the geometry of the holes was chosen based on the identified guidelines.

The layout of this section is illustrated in the flow diagram in figure 5.2.

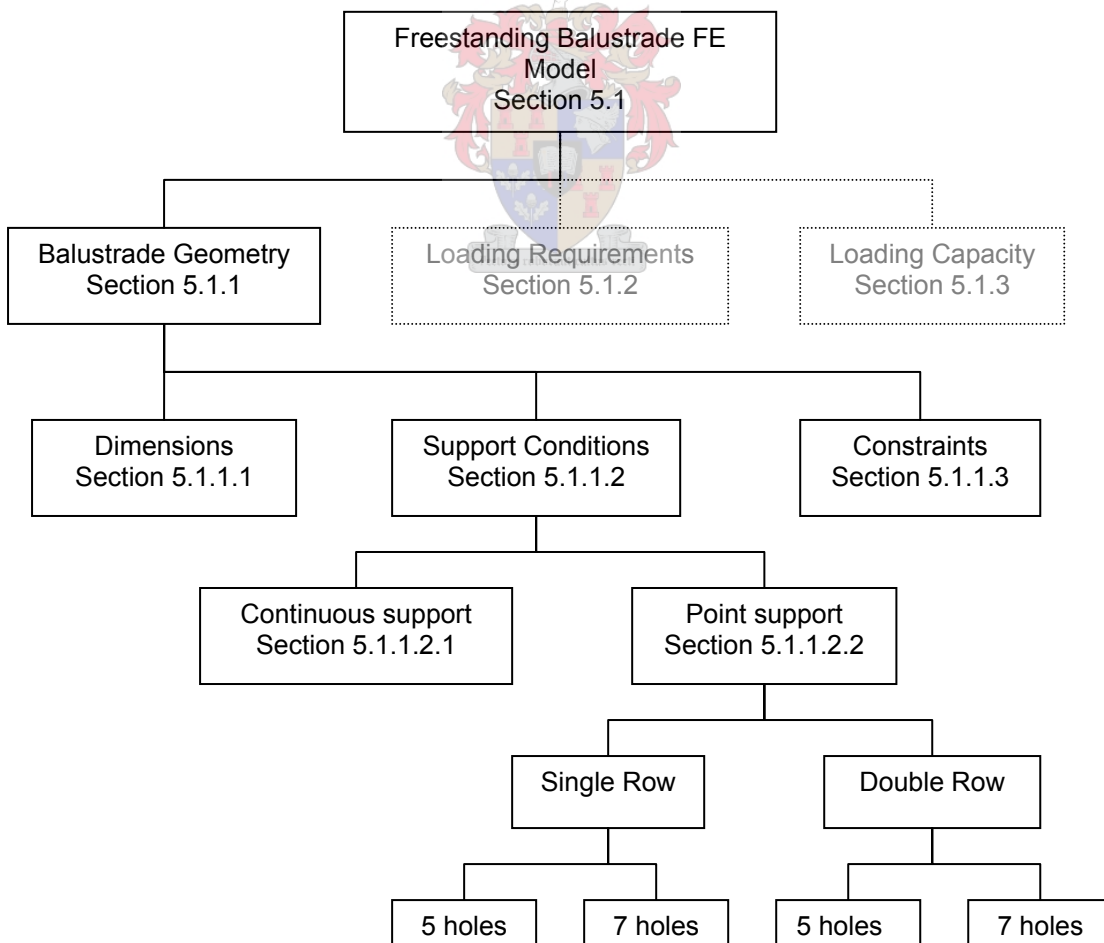


Figure 5.2. Flow diagram illustrating balustrade geometry section of the freestanding balustrade finite element model

5.1.1 BALUSTRADE GEOMETRY

5.1.1.1 Dimensions of freestanding balustrade panels

The dimensions of the balustrade panels were chosen based on suppliers guidelines (figure 5.3) and the relevant SABS [17], where both require that the panel be 1m from the finished floor level. Continuous- or point-supported balustrades are generally attached to the outside of a building, and in many cases attached to the slab (figure 5.7). A slab thickness of 300 mm was assumed and a balustrade length and height of 1m was chosen. Toughened glass with thicknesses of 12- and 15 mm were used throughout the investigation.

Height = 1000 + 300
= 1300 mm

Length = 1000 mm

Thickness
= 12 and 15 mm

The final dimension of the glass panels was 1 x 1.3 m glass panels of thickness 12 and 15 mm.

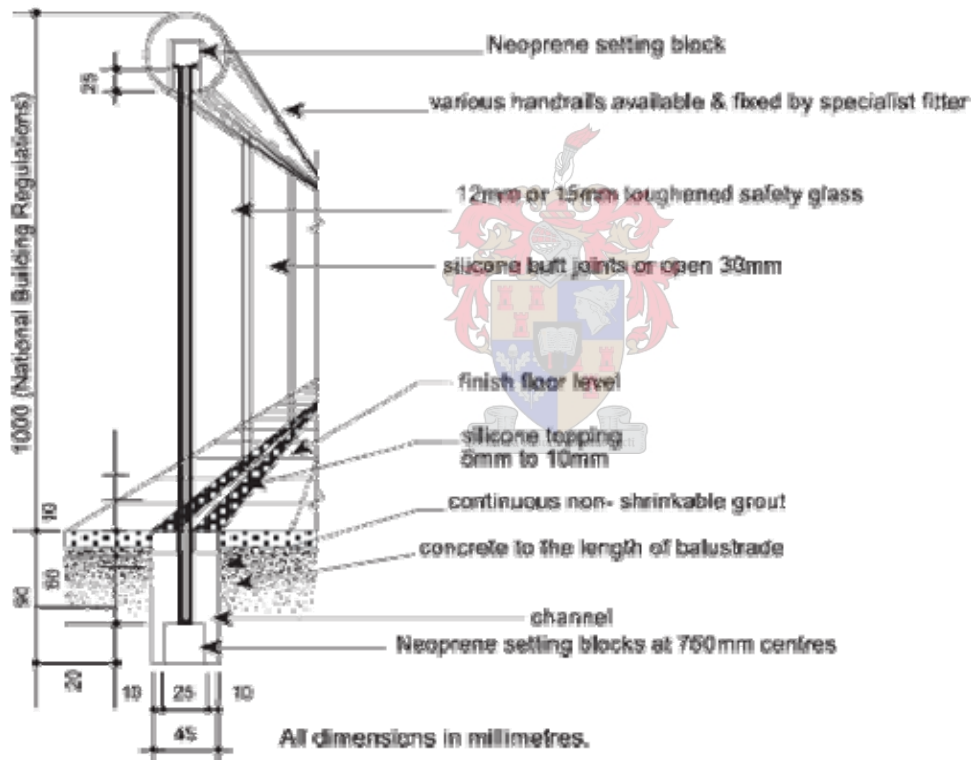


Figure 5.3. Supplier balustrade and handrail specifications [42]

5.1.1.2 Support conditions

Freestanding balustrades are typically connected using either a continuous or numerous point supports, as described in chapter 3. The continuous edge support system often consists of a glass panel placed in a steel channel that is connected to the adjacent structure, while the point supported balustrade is connected using numerous bolts.

Since no stress concentration is introduced in continuous edge connections, it is seen as the best means of support. Freestanding balustrades are however, often designed with point supports, as seen in figure 5.7. Balustrade panels with continuous- and point supports were consequently modelled and their influence on the static- and dynamic capacity of the panels determined.

5.1.1.2.1 Continuous support

An example of a continuously supported freestanding balustrade can be seen in figure 5.4. The continuously supported finite element model is presented in figure 5.5, due to symmetry only half of the balustrade panel had to be modelled.



Figure 5.4. Continuously supported freestanding glass balustrade



Figure 5.5. Geometry of half of FE model

5.1.1.2.2 Point support

The geometry of the holed panels had to be carefully chosen to avoid any additional stress raisers from edge of neighbouring holes. Stress concentration around a hole (chapter 4) can further be superimposed if a hole is placed too close to an edge or neighbouring hole. The influence of distance between hole and edge and distance between two holes was investigated prior to the design of the point supported balustrade panels.

Pectora cuberant cultus recti

5.1.1.2.2.1 The influence of distance between hole and edge

For this investigation, a 3D plate model consisting of two holes of diameter 15 mm and 50 mm apart, were chosen. The distance between the holes was consistent for all the analyses. The plate was loaded out of plane with a unit-distributed load (1N/mm), which was applied to the edge, parallel to the edge joining the holes (figure 5.6). Due to symmetry along two edges, only a quarter of the plate was modelled.

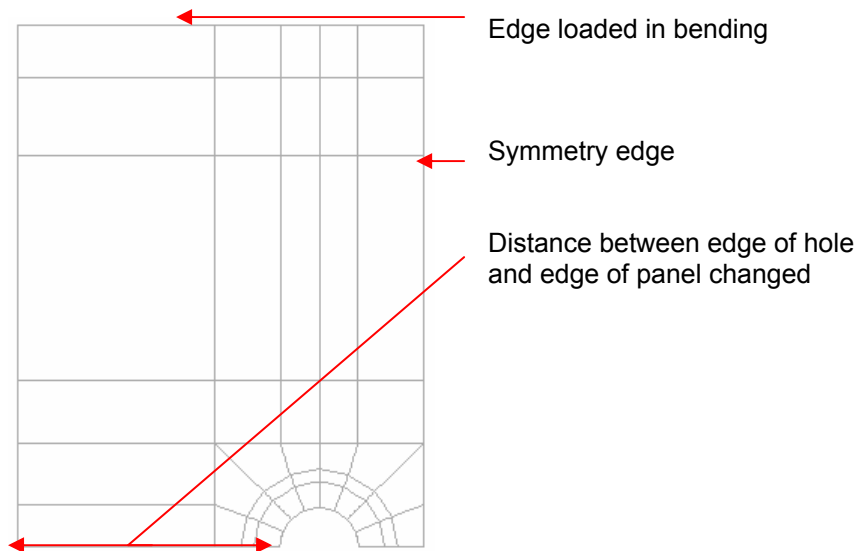


Figure 5.6. The influence of distance between hole and edge

The distance between the holes and the number of holes remained the same throughout the investigation. With each analysis, the distance between the edge and the holes was altered. The purpose of the investigation was to determine the distance at which superposition between the hole and edge does not occur. The 3D calibrated finite element model from chapter 4 was used to determine the maximum principal stress around the holes for five different distances.

Table 5.1. Influence of distance of hole from edge

Distance from edge to edge of hole	Max Principal Stress
mm	MPa
35	135
85	128
125	126
135	125
145	125

From table 5.1, it is determined that superposition between the edge and hole only disappear at a distance greater than 135 mm. It was concluded that, to avoid superposition between edge and hole, holes should not be place closer than 135 mm from the nearest edge (edge to edge) or 9 diameters.

5.1.1.2.2.2 Influence of position of holes relative to each other

The number of bolts, in a point supported balustrade panel, used to connect the panel to the structure is decided by the designer, and ultimately depends on the capacity of the bolts used. Using a weaker bolt would result in the use of more bolts. At some point, the relative distance starts to superimpose the stress increase from one another.

The same procedure that was used to determine the edge influence was applied to determine the influence of the position of holes relative to each other. However, this time the distance between the edge and hole was kept constant while the distance between holes changed with each analysis. For this investigation, a 3D plate model consisting of two holes of diameter 15 mm where chosen at an initial distance 35 mm from each other. The plate was loaded in bending with a unit-distributed load (1N/mm), which was applied to the edge parallel to the edge joining the holes. Due to symmetry along two edges, only a quarter of the plate was

modelled. With each analysis, the distance between the two holes was altered. The purpose of the investigation was to determine the distance at which superposition between the two holes does not occur. The 3D calibrated finite element model from chapter 4 was used to determine the maximum principal stress around the holes for four different distances.

Table 5.2. Influence of position of holes relative to each other

Distance from edge to edge mm	Max Principal Stress MPa
35	120
65	117
85	114
100	113
125	113

From table 5.2, it is determined that superposition between the two holes only disappear at a distance in greater than 100 mm. It was concluded that to avoid superposition between holes, the distance between holes should not be closer than 100 mm (centre to centre) or 7 diameters.

5.1.1.2.2.3 Single and double horizontal rows of holes

The most common type of point support is the double horizontal row system, as seen in figure 5.7, in which the balustrade panel is connected to the structure along two horizontal rows of holes.



Figure 5.7. Glass balustrade with a double row of horizontal holes

Geometry of the double row systems was chosen based on the guidelines determined in the previous section 5.1.1.2.2.

Vertical placement

The diameter of the holes was chosen as 15 mm, as it was assumed that it would allow enough room for the use of M12 bolts. The slab thickness of 300 mm allows the holes to be placed 100 mm apart, however limits the distance between hole and edge to

$$100 - 15/2 = 92.5 \text{ mm,}$$

as apposed to the recommended minimum distance of 135 mm of section 5.1.1.2.2.1.

Horizontal placement

For a 1m wide balustrade, the number of bolts per horizontal row was determined as follows:

Diameter of hole	=	15 mm
Distance between hole centre and edge	=	135 + 15
	=	150 mm
Distance between hole centre	=	100 + 15
	=	115 mm
Determination of number of holes		
Distance from edge	150 x 2	= 300 mm
Distance between bolts	1000-300	= 700 mm
Number of bolts	700/115	= 6 spaces

The maximum number of bolts that can be used in a balustrade of 1m width is therefore 7 bolts. The number of holes per row was chosen as 7- and 5 bolts, both placed at a distance of 150 mm from the edge. In the row containing 7 bolts the holes were placed at a distance of 115 mm apart (figure 5.9), and the row containing 5 bolts (figure 5.8) placed 175 mm apart (centre to centre).

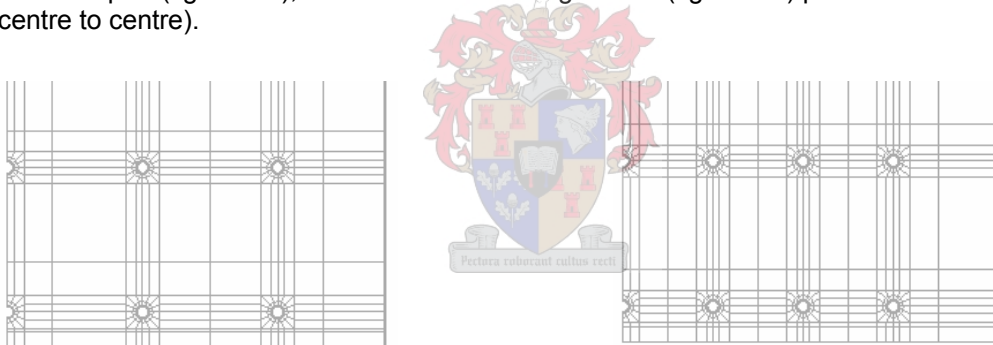


Figure 5.8. Double row of horizontal rows (5) Figure 5.9. Double row of horizontal rows (7)

A new proposed point supported system, based on a single row of horizontal holes was investigated (figure 5.10, 5.11). The proposed system relies on the fact, that when the balustrade is placed on the outside of the structure (figure 5.7) only the top horizontal row of holes supports the balustrade in the case of static- or impact loading. Placement of holes was the same as for the double row of horizontal holes.

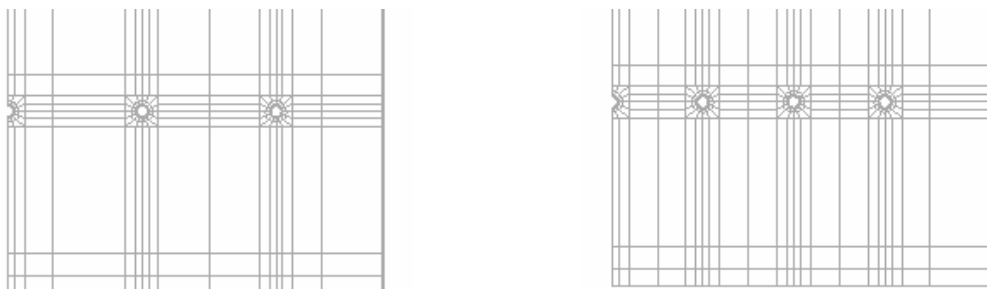


Figure 5.10. Single row of horizontal holes (5) Figure 5.11. Single row of horizontal holes (7)

5.1.1.3 Constraints of Finite element model

Over the years, Pilkington Glass has played a large role in not only the development of the toughened glass but has also had a significant influence in the development of connection types for structural glass systems. One of the major breakthroughs in glass connections, primarily used in façade design, was the spider system [43]. The spider system has formed the basis of various other connection types. An example of such a connection type commonly used in freestanding balustrades is the 444 planar fitting [43] as seen in figure 5.12. This type of connection clamps the glass surface to the adjacent structure, while still allowing some rotation of the glass. The top and bottom end of the connector (button), consists of a ball and socket joint (see figure 5.13), which allows the glass to rotate while the glass is held in position. A rubber lining is usually placed in-between the steel and glass to ensure smooth support conditions.



Figure 5.12. Typical glass point support Figure 5.13. Ball and socket joint (Button)

The finite element modelling of such a connection, which is employed to predict the local behaviour, was performed and is described in the following section. Different materials and contact between numerous components forced the employment of a nonlinear analysis.

Nonlinear analysis

A nonlinear model was conducted to investigate the local connection behaviour (contact between washer and glass surface). A nonlinear analysis is necessary, since contact elements separate the washer from the glass surface.

The purpose of the analysis was to determine the behaviour and identify the point of stress concentration of the bolt connection in bending. A few assumptions were made to avoid the weakening of the hole and make the modelling of the bolted connection possible. They were:

- The bolts do not to weaken the hole due to the induced pressure of the steel button on the glass. (Pressure induced fracture, seen in laboratory test series chapter 3)
- Fracture occurs at position of maximum stress concentration around hole, which is caused by the out of plane bending of the glass and not by the localized stress concentration between steel button and glass. For the fracture origin to be located at the edge of the hole, the connection has to allow for enough rotation of the balustrade panel. Rotation is a combination of rotation of ball and socket joint and compression of the rubber lining.

The 3D finite element model consisted of two 15mm diameter holes placed 100mm apart. Rubber washers of diameter 20mm were placed on top and bottom of the holes to allow the rotation of the glass plate (figure 5.14). Contact surface elements were assigned to the outside of the hole and washer to allow contact and separation between the two surfaces.

The plate was loaded in bending with a distributed unit displacement load at one edge, which was increased incrementally.

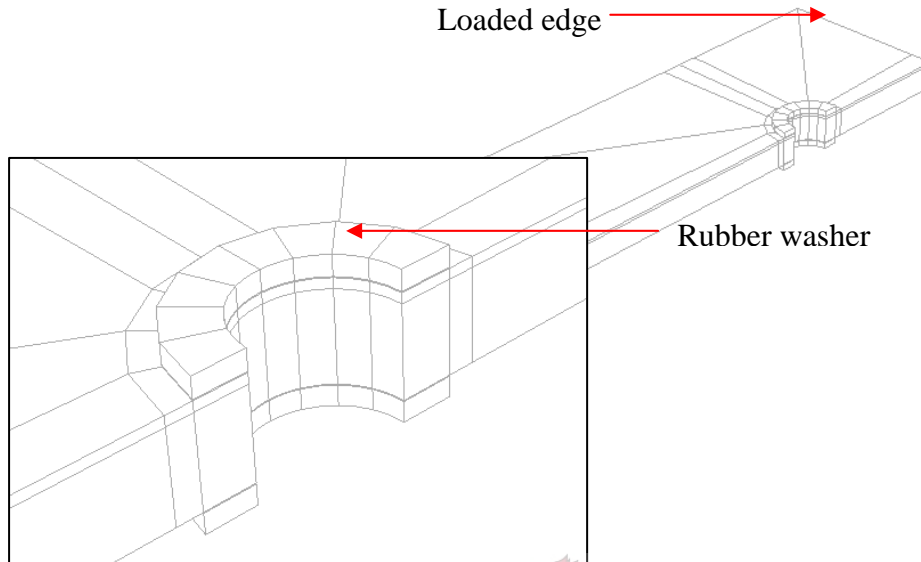


Figure 5.14. Nonlinear contact model

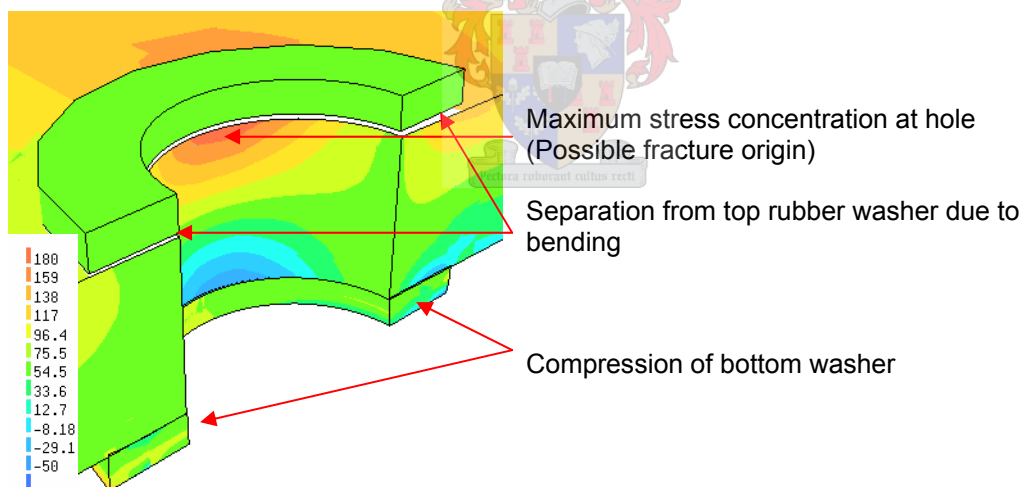


Figure 5.15. Stress concentrations at hole

From figure 5.15, it is evident that the rubber washer alone permits enough rotation of the glass panel to ensure the stress concentration at the hole. The total rotation (ball socket connection + rubber washer) would therefore be sufficient to avoid any additional localized stress concentration arising at the connection.

The nonlinear finite element modelling of such a connection is a time consuming endeavour, and was consequently replaced by a static linear analysis, which is described in the following section.

Linear static analysis

Since it had been determined that the local behaviour of the connection itself was not of concern, a linear static analysis was sufficient to determine the static- and dynamic loading capacity of the balustrade panels. The only criterion of the linear static analysis was that it portrays the behaviour of a point-supported connection of a balustrade panel.

From the nonlinear analysis, it was noted that only the front bottom half of the first support was in contact with the rubber washer. Linear spring elements (SP1TR) were added to the front quarter of the glass panel to represent the compression of the rubber washer and allow the necessary rotation. A rubber thickness of 3.5mm was chosen and the stiffness of the linear springs was calculated as follows:

$$k \cdot \Delta = P$$

where:

$$\begin{aligned} k &= AE/L \text{ (stiffness)} \\ \Delta &= \text{displacement (mm)} \\ P &= \text{force (N)} \\ E_{\text{rubber}} &= 2800 \text{ (N/mm}^2\text{)} \\ L &= \text{thickness (mm)} \end{aligned}$$

To determine the area of an individual spring,

$$\begin{aligned} k_{\text{individual}} &= AE/L/A \\ &= E/L \\ &= 2800/3.5 \\ &= 800 \text{ N/mm} \end{aligned}$$

A spring stiffness of 800N/mm together with this set-up provided the corrected potential fracture origin, and dramatically reduced the computing time as apposed to a nonlinear analysis. The position of the linear springs is illustrated in figure 5.16. This type of support condition was used for all point-supported balustrades and avoided the use of a nonlinear analysis (contact elements).

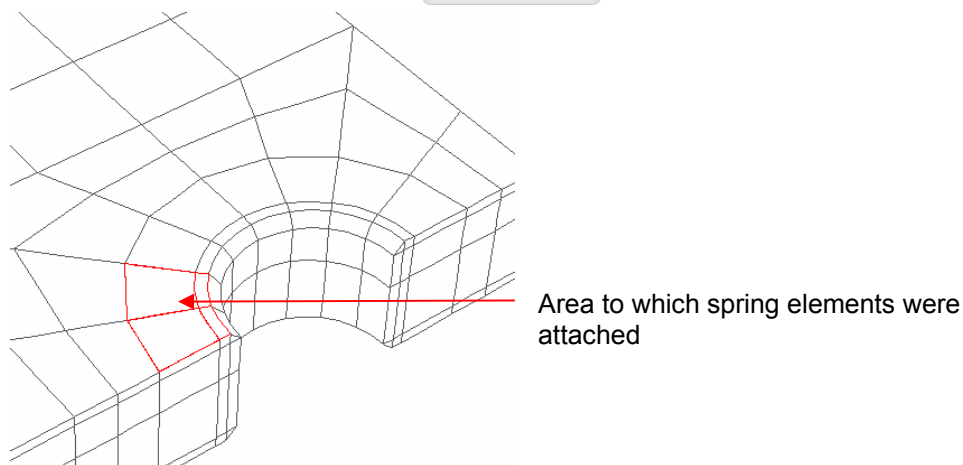


Figure 5.16. Linear spring position at bottom of glass panel

5.1.1.3.1 Single horizontal row of holes

Spring elements were only used at the holed supports, while the continuous support at the back was constraint against vertical translation (figure 5.16). Spring elements were applied to the bottom quarter of the holes closest to the holes, as seen in figures 5.16 and 5.17. This position of the springs provided enough rotation of the glass panel to ensure the fracture of the glass panels at the hole.

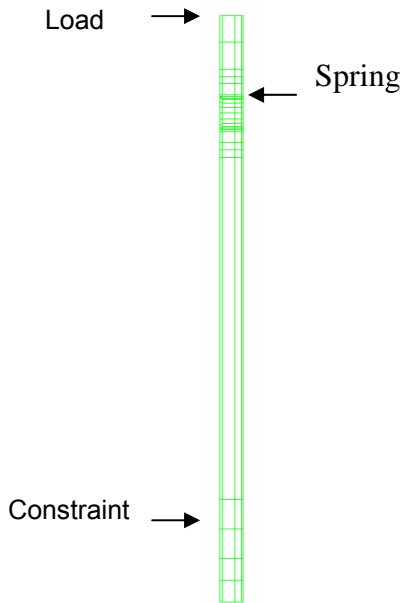


Figure 5.17. Spring position

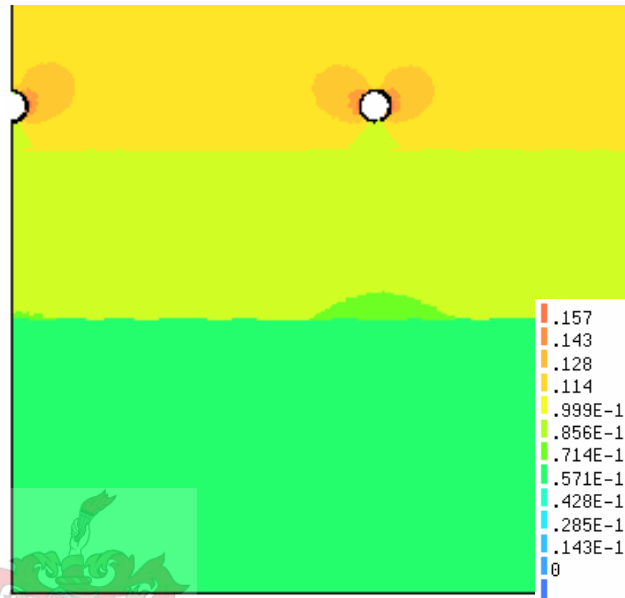


Figure 5.18. Maximum principal stress around hole

5.1.1.3.2 Double horizontal row of holes

Springs were added to the front bottom quarter of the first support and to the top of the back quarter of the second support, for the panels that contained double horizontal holes.

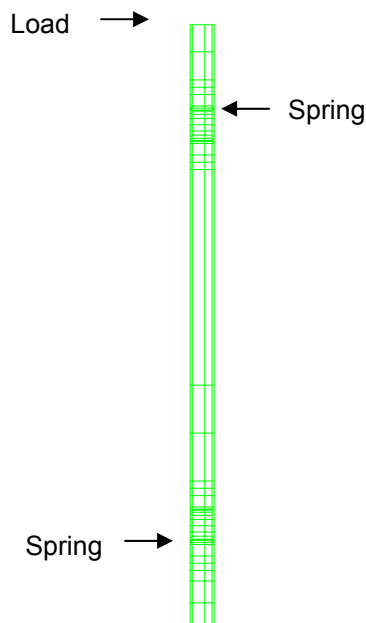


Figure 5.19. Spring position

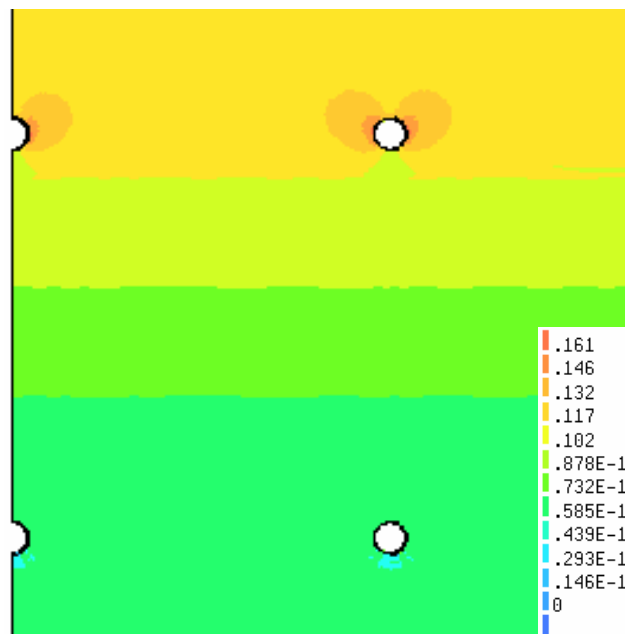


Figure 5.20. Maximum principal stress around hole

5.1.1.4 Conclusion

The conclusions are made and categorized under the geometry and constraint of the finite element model.

Geometry

Based on suppliers guidelines and the relevant SABS standards [19], glass balustrade panels of dimensions 1 x 1.3 m together with two thickness of 12- and 15 mm were chosen as representative of actual freestanding balustrade panels.

Although the continuous support system is the best means of support, the point-supported system is often used. Therefore, balustrade panels with continuous- and point supported systems were chosen to be modelled, as described in the following section. Before the geometry of the point supported panels could be chosen, the placement of the holes as to the influence of distance between hole and edge, and the influence of position of holes relative to each other was investigated. It was concluded that a hole should not be placed closer than 135 mm (9 diameters) from the nearest edge or be placed closer than 100 mm (7 diameters) from another hole.

With the identified guidelines, two different point supported systems were modelled. One of which is commonly used, consisting of a double row of horizontal holes and the other, a new proposed system, consisting of a single row of horizontal holes. Together with the two types of point support systems, a different number of holes per horizontal row was also investigated.

Constraints

A nonlinear model was constructed to investigate the local point supported connection behaviour. The purpose of the analysis was to determine the amount of rotation needed to ensure the fracture at the point of maximum stress concentration due to bending. Since the local behaviour of the bolted connector was found not to be of concern, it was established that a linear static analysis could subsequently be performed to determine the static- and dynamic loading capacity of the balustrade panels (described in section 5.1.3). Linear spring element were used to represent the rubber compression. A spring stiffness of 800 N/mm together with this set-up provided the corrected potential fracture origin, and dramatically reduced the computing time apposed to a nonlinear analysis where surface contact elements were used.

In the following section loading requirements and the static- and dynamic loading of the balustrade panels is described.

5.1.2 LOADING REQUIREMENTS

The South African loading requirements are detailed in chapter 3.3, and can be categorized into static- and dynamic loading requirements. This section describes the different loading types applied to each balustrade set-up.

Due to the variety in application of a balustrade, there is a difference in required static loading capacity of the balustrade. Therefore, static loads appropriate to the type of occupancy for the building or structure are generally categorized according to application and position. Together with the application of the balustrade, two types of load applications were considered:

- Horizontal line load (N/m)
- Point load (N)

The South African [7] loading code also requires that an impact of 400 J be delivered by means of a 30 kg sand bag, where human impact is of concern. An impact based on the SABS guidelines was simulated using a finite element model. In this document it is shown how a static force was used to simulate the dynamic impact force.

The loading requirements phase is summarized in a flow diagram presented in figure 5.21.

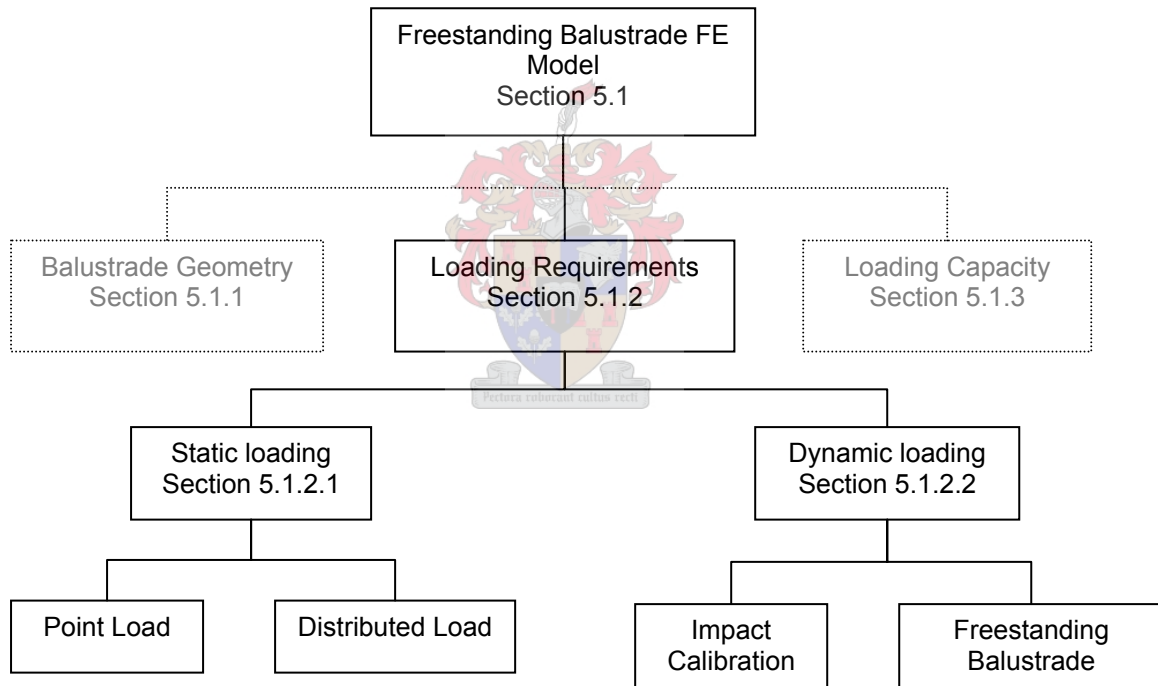


Figure 5.21. Flow diagram illustrating loading requirements of the freestanding balustrade

5.1.2.1 Static Loading

As described in chapter 2, the SABS 0160 [7] requires that balustrades be loaded in accordance to application and position. Together with the application of the balustrade, two types of loading types have to be considered:

- A uniformly distributed line load (N/m), and
- A concentrated or point load (N)

Each balustrade set-up was loaded with both a unit distributed and point load. The following section describes the point and distributed load applied to each balustrade set-up.

Point load

Section 5.2.1 of SABS 0104[19] requires that freestanding balustrades are positioned not to permit the passage of a ball of diameter 100 mm between adjacent panels. Therefore, two connected panels have to be placed closer than 100 mm from each other, and consequently both balustrade panels would absorb an edge load. The dominant load case is therefore the centre point load. The edge point support was not applied.

A unit point load (1N) was applied to the top in the centre of each balustrade set-up. Due to symmetry of the panel and loading conditions, only half of the balustrade panel was modelled.

Distributed load

Similarly, a unit-distributed load (1N/mm) was applied to the top edge of each of the balustrade set-ups. As for the centre point load, only half of the panel had to be modelled.

5.1.2.2 Dynamic loading

Each balustrade set-up was loaded with a **unit** point load applied to the top centre of each panel (Position of impact); using each set-up's corresponding material properties, the dynamic capacity could be determined.

The South African loading code requires that an impact of 400 J be delivered by means of a 30 kg sand bag, where human impact is of concern. An impact based on the SABS [7] guidelines was simulated using the finite element software Abaqus [46]. This was performed by applying an equivalent static load to simulate the dynamic impact load. By applying an equivalent static force unique to each balustrade set-up, the results could be compared to its dynamic loading capacity. This comparison is described in section 5.1.3.2.

This section describes the following two topics:

1. the calibration of the finite element model that was used to determine the equivalent static load which would simulate the dynamic impact force for each balustrade set-up;
2. It also describes the method in which each balustrade set-up's equivalent static impact load was determined.

5.1.2.2.1 Calibration of four side supported model

Before impact tests on freestanding balustrades could be modelled using finite elements, the model had to be calibrated. The experiments by Foss (1999) were used to calibrate the Abaqus [46] model. Foss [11] performed impact tests on 4 side supported glass panels of dimensions 864 x 1930 x 5 mm using the lead shot impactor. The stiffness of the lead shot bag was determined by a quasi-static (50 mm/min) compression loading response experiment, and linear elastic shot bag properties were assumed (Table 5.3).

Table 5.3. Lead shot impactor material properties (Foss [11])

Elasticity modulus	4.9MPa
Poisson	0.3

Foss [11] modelled the lead shot impactor as a 250 mm diameter sphere, which he then verified by means of a dynamic stress response experiment. All impact tests by Foss [11] were performed based on a drop height of 31.87 cm; corresponding test data is given in table 5.4.

Table 5.4. Impact data (Foss [11])

Applied Energy	Impactor mass	Impact velocity
Joule	kg	m/s
140.6	45	2.5

The input data from Foss [11] was used and a similar model was calibrated to be used in this project, using the finite element package Abaqus [46]. Due to symmetry only a quarter of the 864 x 1930 x 5 mm glass panel and impactor was modelled. The panel was continuously supported along two edges, and constrained according to symmetry (see figure 5.22). The material properties of the glass panel and impactor, used in the model, are presented in table 5.5.

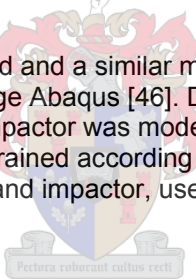


Table 5.5. Material properties (Foss [11])

	Density	Elasticity modulus	Poisson
	Kg/m ³	N/m ²	
Glass panel	2500	7.2e10	0.23
Impactor	3915	4.9e6	0.3

In the Abaqus [46] analysis, the impactor (sphere) was given an initial velocity of 2.5 m/s. Contact surfaces were defined for the glass panel and the impactor, which insured that the impactor made contact with the panel instead of moving through it. A soft elastic collision was assumed between the objects, this allows separation of the two objects after collision. Solid elements were used for both the impactor and the glass panel.

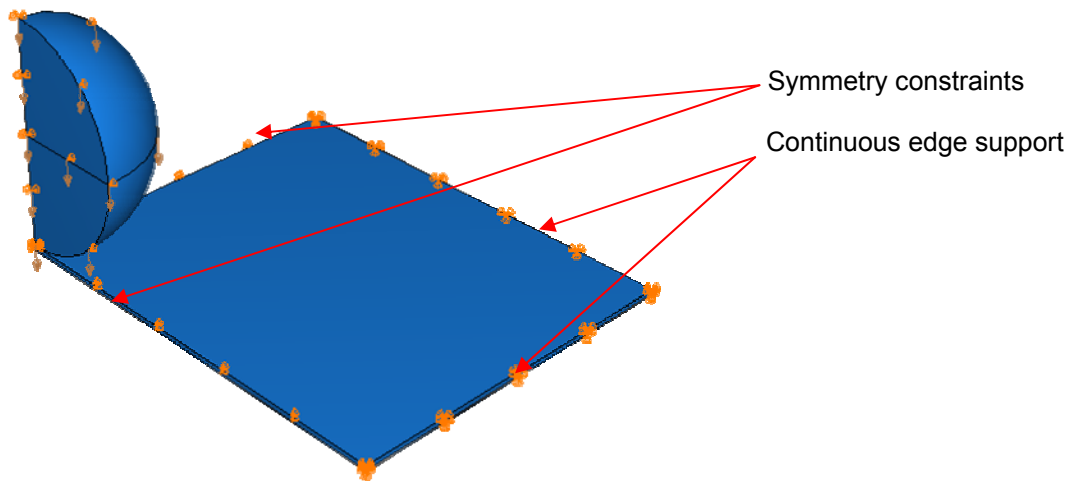


Figure 5.22. Calibration test set-up

The average cycle time and the maximum dynamic impact force (figure 5.23), calculated using Abaqus [46] is compare to that obtained from Foss in table 5.6.

Table 5.6. Comparison between results from literature and Abaqus

	Cycle Time	Dynamic Force
	ms	kN
Foss	44.2	8.010
Abaqus	41.7	8.056

Dynamic Impact force Response

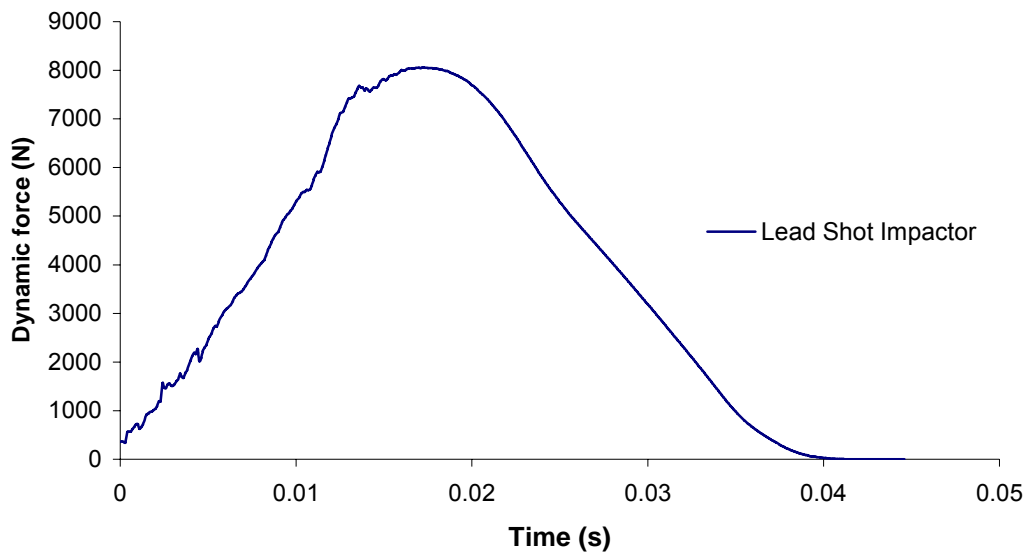


Figure 5.23. Dynamic impact force response calculated using Abaqus

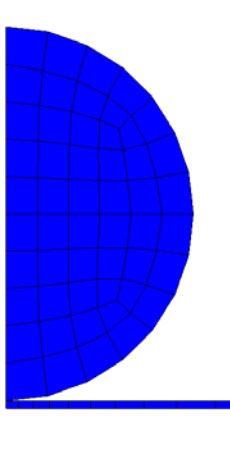


Figure 5.24. Impact at time = 0 sec

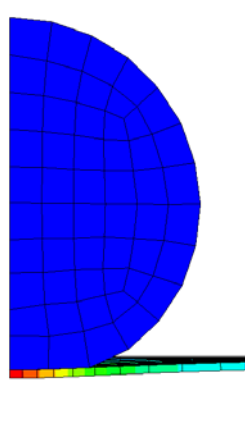


Figure 5.25. Impact at time = 0.0167sec

Good agreement among the results indicated that the model could be used to evaluate different drop heights and balustrade set-ups. The calibrated finite element model could now be used to determine the dynamic impact force produced by the 400 J impact-loading requirement, for each balustrade set-up. The following section describes the freestanding balustrade models used to determine each panel's dynamic impact force.

5.1.2.2.2 Freestanding balustrade Method (equivalent static load)

This section describes the method used to determine the equivalent static impact load for each balustrade set-up. Once the method had been established, the application and results are presented in the following section. Section 5.2.3.4.3.1 describes and presents the results based on the method described here for continuous supported freestanding balustrades, and section 5.2.3.4.3 for the point supported balustrades, all determined using this method.

The purpose of the freestanding balustrade impact model was to determine the dynamic impact force produced by the 400 J impact-loading requirement for each balustrade set-up. Instead of modelling each balustrade's geometry in Abaqus [46] only two continuously supported balustrades were modelled, one for each glass thickness (12, 15 mm). It is described in section 5.1.3.2.1 how the dynamic impact force was determined for each of the different set-ups, which were considered, by altering the stiffness of the models described here. To calculate each set-up's dynamic impact force, the stiffness of the generic models was altered accordingly (section 5.1.3.2.1).

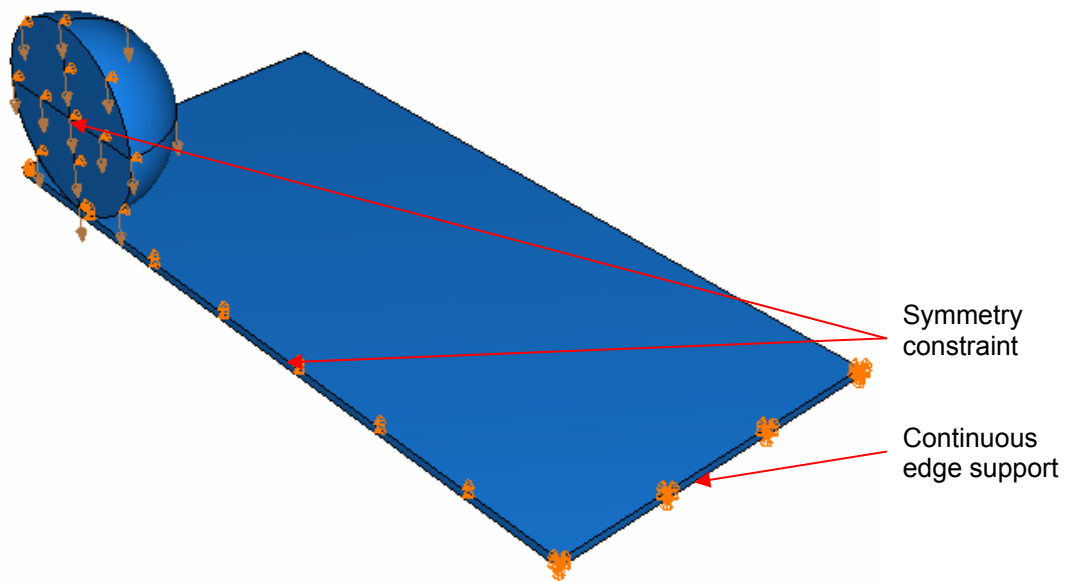


Figure 5.26. Freestanding impact model

For illustration purposes, only the 12 mm model is presented. Due to symmetry, only half of the balustrade and impactor is modelled. The bottom edge was constrained against all translation degrees of freedom, and symmetry conditions accordingly. All the balustrades were tested against the impact loading as required by SABS: 0160 [7]. Knowing the mass of the impactor, the impact velocity was determined as follows:

From chapter 2:

Potential energy at top = Kinetic energy at bottom

$$mgh = \frac{1}{2}mv^2$$

$$400 \text{ J} = \frac{1}{2}mv^2$$

$$m = 30 \text{ kg}$$

$$v = \sqrt{2 \cdot 400 / 30}$$

$$v = 4.216 \text{ m/s}$$



Dynamic Impact Response of a Freestanding Balustrade

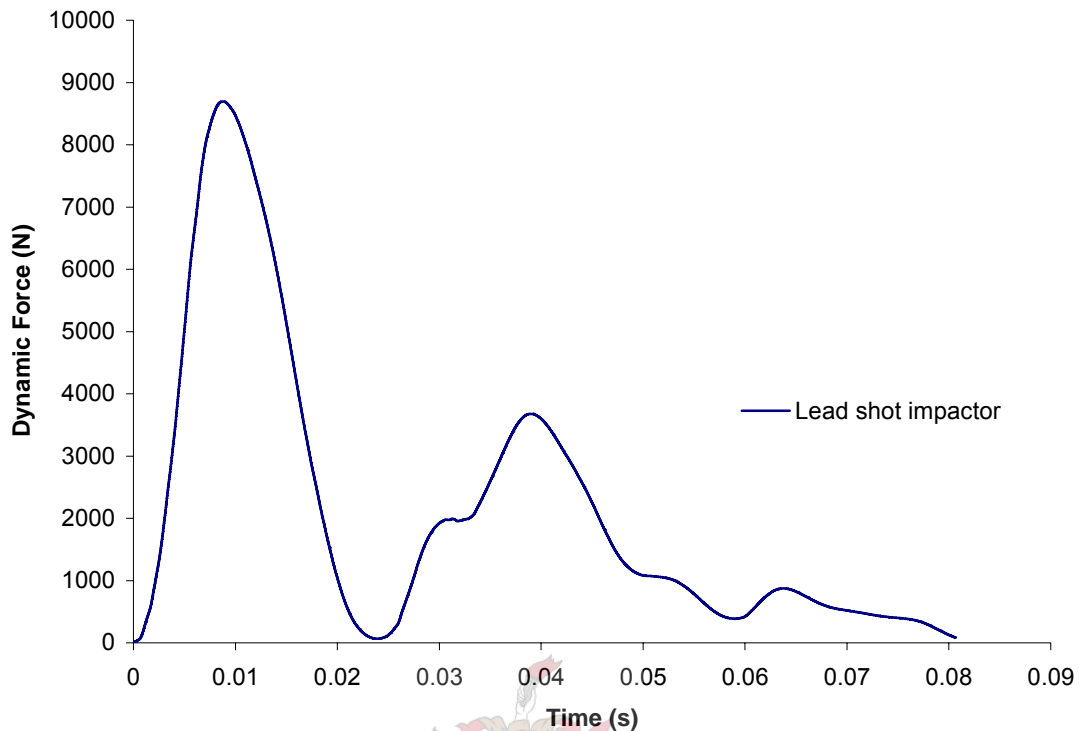


Figure 5.27. Dynamic impact response of freestanding balustrade (velocity 4.216m/s)

From figure 5.27, the total dynamic impact force can be seen. It is noted that the dynamic force produced is almost the same as that of the four side supported glass panels (Foss [11]) even though the initial velocity of the impactor has almost doubled. The reduction in the number of edge supports from 4 to 1, made the panel less stiff and consequently less susceptible to the impact load, resulting in a smaller dynamic impact force.

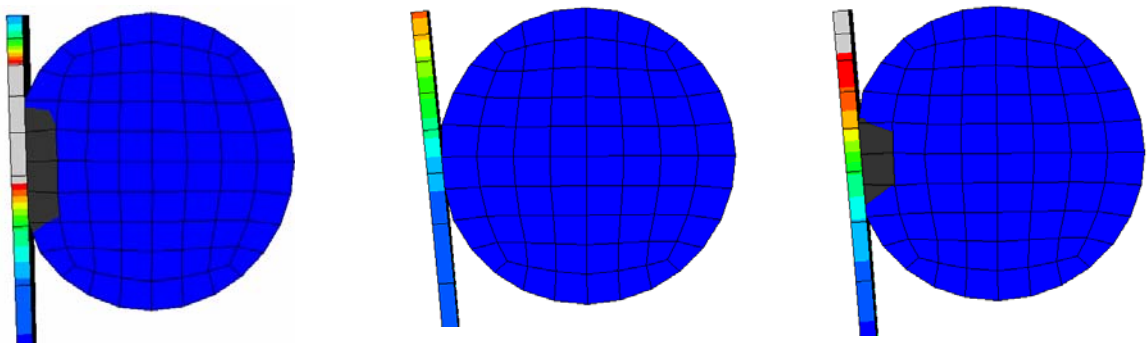


Figure 5.28. Impact at $t=0.00867\text{sec}$, $t=0.024\text{sec}$ and $t=0.038\text{sec}$

Further, a second impact at 0.038 seconds can be noticed (figure 5.28). At the time of the first impact, the impactor transfers all of its own kinetic energy into the panel, almost pushing it away. The second impact is a result of the panel impacting the sphere; the magnitude of this impact is much less than the initial impact, represented by the second peak in figure 5.27.

5.1.2.3 Conclusion

Static loading

Each balustrade set-up was loaded with both a unit distributed and point load. The distributed load was applied in accordance with SABS [7] at the top edge of the balustrade, and the point load at the top centre of each panel.

Dynamic loading

A dynamic impact finite element model was calibrated using literature [11]. As recommended in section 2.3.2, the lead shot impactor was used for the calculation of the equivalent impact force, instead of the sand bag (used by SABS 0160 [7]) which is more variable in results.

Finally, an impact based on the SABS [7] guidelines was simulated on a freestanding balustrade using the calibrated finite element software Abaqus [46]. The equivalent static force was determined to simulate the dynamic impact force. In the next section, the equivalent static force for each balustrade set-up is determined, and compared to its dynamic loading capacity.

The same method is also used to determine the equivalent static force for balustrades with handrails, and is described in detail in section 5.2.



5.1.3 LOADING CAPACITY

Introduction

For the static loading conditions, each balustrade set-up was loaded with a unit point- and -distributed load, as required by the SABS [7]. For the dynamic loading conditions, each balustrade set-up was only loaded with a unit point load, representing the dynamic impact load.

The linear elastic material behaviour that glass exhibits (chapter 3), allowed the execution of a linear analysis. Consequently, a linear static analysis was performed on all loaded balustrade set-ups, and the maximum principal stress and displacement, corresponding to each panel's applied load, were determined.

The following section presents the static- and dynamic loading capacity for continuous- and point supported freestanding balustrade panels, as determined using the finite element software DIANA [44]. The layout of the loading capacity stage of the freestanding balustrade model is presented in the flow diagram in figure 5.29.

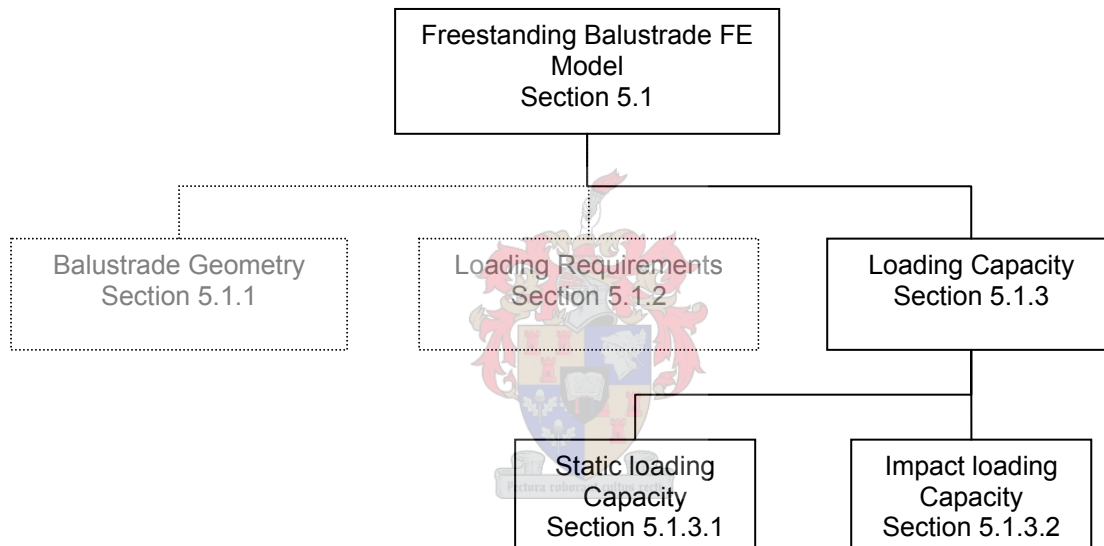


Figure 5.29. Flow diagram illustrating the layout of loading capacity stage

5.1.3.1 Static loading capacity

A linear static analysis was performed and the maximum principal stress corresponding to each panel's applied unit load was determined. Having calculated the maximum principal stress resulting from a unit load, the unit load was extrapolated until the maximum principal stress was equal to that of the material, hence the loading capacity was determined for the particular balustrade set-up. The linear elastic material behaviour of glass allows for the linear extrapolation of the maximum principal stress in order to determine the ultimate loading capacity of each of the panels.

Using the static material properties as determined in chapter 4, the balustrade loading capacity, corresponding to the loading type, was determined for the panels with- and without holes. The static loading capacity was determined for a 0.8% probability of failure, as recommended by Pilkington [Appendix C]. The static material properties used, are presented in table 5.7 for the panels without holes and for the panels with holes.

Table 5.7. Static material properties of glass panels with- and without holes

	50% P_f	0.8% P_f
Without holes	187 MPa	156 MPa
With holes	174 MPa	132 MPa

The following section presents the static loading capacity for continuous- (Table 5.8 and 5.9) and point supported (Table 5.10 and 5.11) freestanding balustrade panels, as determined using the finite element software DIANA [44]. Together with the quantitative loading capacity predictions, the qualitative stress distribution for each balustrade set-up and loading type is illustrated. This is performed to show the areas of maximum principal stress. Glass consists of a high compressive strength and relatively low tensile strength; it is in tension that glass usually fails. The area of maximum tensile stress is therefore of concern.

5.1.3.1.1 Continuous support

Table 5.8 presents the static capacity of the continuously supported balustrades loaded with a point load and table 5.9 presents the static capacity of the continuously supported balustrades loaded with a distributed load. The contours of the maximum principal stress of the point loaded and distributed loaded continuously supported freestanding balustrade panels are presented in figure 5.30, and figure 5.31 respectively.

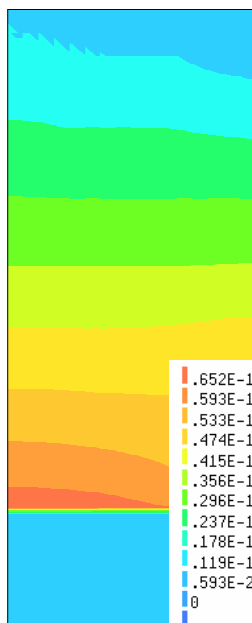


Figure 5.30. Point loaded

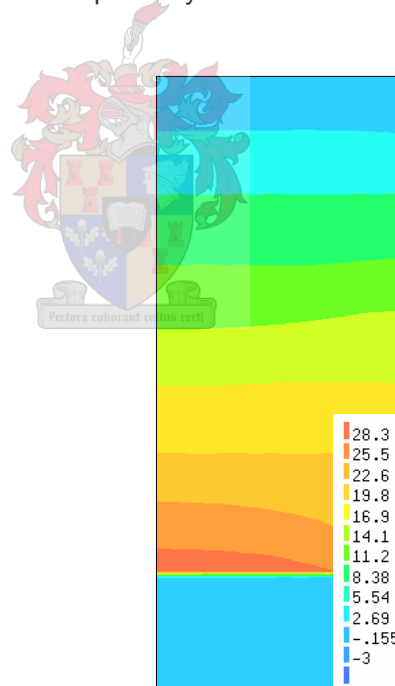


Figure 5.31. Distributed loaded

The minimum stress (blue contour) can be seen in the bottom of the figure, as the bottom 300 mm of the balustrade panels were fixed against translation to simulate a typical continuous steel channel connection.

The stress distribution and point of maximum stress concentration is similar for the point- and distributed loaded panels. The stress distribution at the connection for the distributed loaded panels tends to be more spread out along the connection.

Table 5.8. Static loading capacity of continuously supported freestanding balustrade loaded with a concentrated centre load

Thickness	Displacement	0.8% P_f
mm	mm	kN
12	200	2.6
15	156	4.0

Table 5.9. Static loading capacity of continuously supported freestanding balustrade loaded with a distributed load

Thickness	Displacement	0.8% P_f
mm	mm	kN/m
12	98.72	2.69
15	77.11	4.08

5.1.3.1.2 Point support

Single row

Table 5.10 presents the static capacity of the single row of point-supported balustrades loaded with a point load and table 5.11 presents the static capacity of the single row of point supported balustrades loaded with a distributed load.

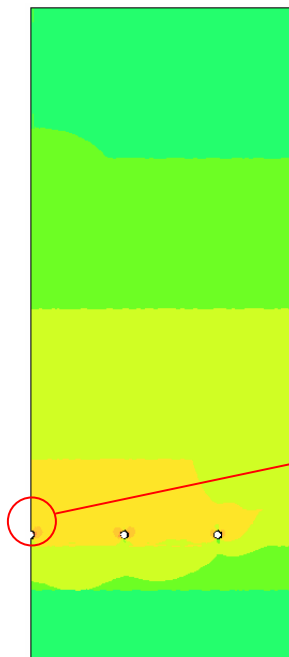


Figure 5.32. Point load

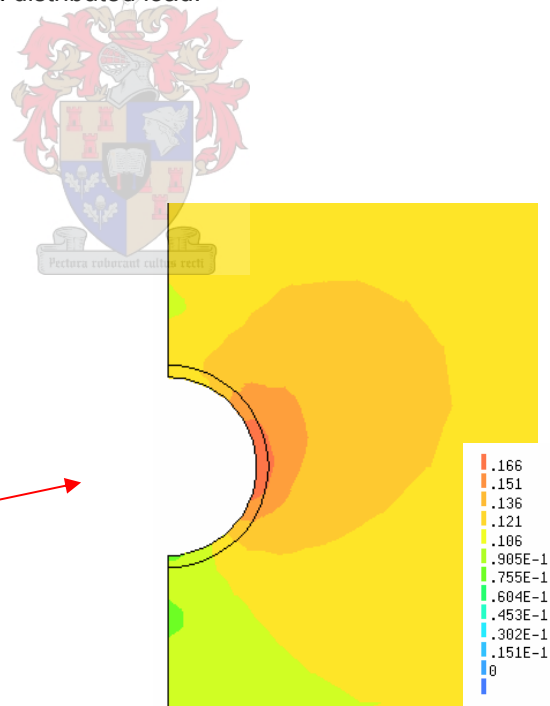


Figure 5.33. Maximum stress concentration at hole

From figure 5.32, it can be seen that the stress concentrates around the holes. The maximum stress concentration is at the hole in the centre of the hole and can be seen in figure 5.33. The stress concentration at the centre of the panel (stiffer vertical sides), is magnified by the introduction of a hole, where further stress concentration takes place.

From figure 5.33, the stress concentration at the edge of the hole can be seen. The point of maximum stress is located on the edge of the chamfer in the centre of the half circle. This particular point indicates that the bending of the panel brought about the maximum stress and that the linear springs correctly simulated the connection behaviour.

Table 5.10. Static loading capacity of point supported freestanding balustrade loaded with a concentrated centre load

Thickness	Holes	Displacement	0.8% P_f
mm		mm	kN
12	5	130	1.59
12	7	142	1.66
15	5	98	2.32
15	7	99	2.4

Table 5.11. Static loading capacity of point supported freestanding balustrade loaded with a distributed load

Thickness	Holes	Displacement	0.8% P_f
mm		mm	kN
12	5	64	1.54
12	7	66	1.61
15	5	48	2.25
15	7	49	2.34

It is evident from tables 5.10 and 5.11 that the balustrade panels containing 7 holes provide a better means of support compared to the panels with only 5. An increase of 4% is noted, which is attributed to the increase in number of supports (holes).

Double row

Table 5.12 presents the static capacity of the double row of point supported balustrades loaded with a point load and table 5.13 presents the static capacity of the double row of point supported balustrades loaded with a distributed load.

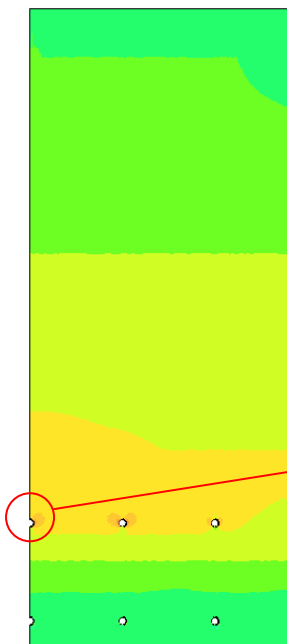


Figure 5.34. Point load

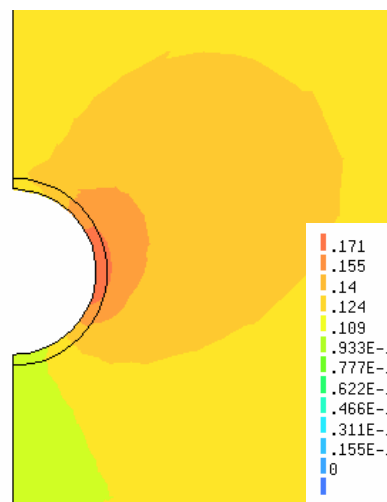


Figure 5.35. Maximum stress concentration at hole

As for the panels containing a single horizontal row of holes, it can be seen (figure 5.34) that the stress concentrates around the holes for the panels with a double row of holes. The maximum stress concentration is in the centre of the hole and can be seen in figure 5.35.

Table 5.12. Static loading capacity of point supported freestanding balustrade loaded with a concentrated centre load

Thickness	Holes	Displacement	0.8% P_f
mm		mm	kN
12	5	127.9	1.54
12	7	135.2	1.64
15	5	96.6	2.26
15	7	101.3	2.38

Table 5.13. Static loading capacity of point supported freestanding balustrade loaded with a distributed load

Thickness	Holes	Displacement	0.8% P_f
mm		mm	kN/m
12	5	63.3	1.50
12	7	66.36	1.58
15	5	47.7	2.19
15	7	49.5	2.29

As mentioned before (single row of horizontal holes), the panels containing 7 holes provide a better means of support compared to the panels with only 5 holes, which can be attributed to the increase in number of supports.

Comparing the loading capacity of the panels containing a single row of horizontal holes to the panels containing only a double row of horizontal holes, a slight decrease in capacity is noticed. The decrease in loading capacity of the panels containing a double row of horizontal rows can be attributed to the influence of the edge, since the slab limited the placement of the holes (see chapter 5.1.1.2.2.1).

5.1.3.1.3 Comparison to SABS 0160 [7] requirements

This section focuses on the interpretation of the finite element results as compared to the South African Structural Design codes [loading, deflection]. The calculated deflection and extrapolated static loading capacity of both the point- and continuously supported balustrades are compared to the corresponding SABS [7] requirements. The results are compared under the:

- SABS static loading requirements and,
- SABS deflection requirements

5.1.3.1.3.1 SABS Static loading requirements

Guidelines for the static load that balustrades must be able to sustain are given in SABS 0160 [7], and chapter 2.3.1. The summation of the guidelines is divided into the:

- Concentrated loading- and,
- Distributed loading requirements

NOTE: SABS 0160 [7] requires a static loading factor of 1.6. All the SABS requirements are presented with- and without the loading factor.

Concentrated loading requirements

Concentration of 1 kN acting horizontally inward or outward over a 100x100 mm area for plate elements at the top of the guard or the most severe position; (factored 1.6 kN)

Distributed loading requirements

Domestic application

Distributed horizontal force of 0.5 kN/m applied at the top of the guard and acting outward; (factored 0.75 kN/m)

Places of public assembly

Distributed horizontal force of 1.5 kN/m applied at the top of the guard and acting outward; (factored 2.25 kN/m)

Grandstands

Distributed horizontal force of 3.0 kN/m applied at the top of the guard and acting outward; (factored 4.5 kN/m)

Table 5.14. Freestanding balustrade concentrated- and distributed loading capacity for a 0.8% P_f

Panel Thick	No of Rows	No of Holes per Row	Concentrated Load Capacity	Distributed Load Capacity	
mm			kN	kN/m	
12mm Thickness					
12	-	-	2.63	2.69	D, P
12	1	5	1.59	1.54	D
12	1	7	1.66	1.61	D
12	2	5	1.54	1.50	D
12	2	7	1.64	1.58	D
15mm Thickness					
15	-	-	4.00	4.08	D, P
15	1	5	2.32	2.25	D, P
15	1	7	2.40	2.34	D, P
15	2	5	2.26	2.19	D
15	2	7	2.38	2.29	D, P

The SABS 0160 [7] requires that all balustrades, irrespective of the location, have to be able to resist a 1.6 kN applied concentrated force. From table 5.14 it is noticed that all the 15 mm thick freestanding balustrade set-ups, regardless of connection type, adhered to the SABS 0160 [7] concentrated loading requirement.

Together with the concentrated loading capacity, table 5.14 also presents each balustrade set-up's distributed loading capacity together with the satisfied SABS requirements. The SABS 0160 [7] distributed loading requirements can be divided into three categories, Domestic (D), Public (P) and Grandstands (G). Next to each balustrade set-up's distributed loading is indicated which SABS 0160 [7] category is satisfied.

Form table 5.14, it can be noticed that none of the freestanding balustrades, adheres to the SABS [7] required distributed loading for grandstands. Predominantly, only the 15 mm thick panels adhere to both the domestic- and public distributed loading requirements.

5.1.3.1.3.2 SABS Deflection requirements

Section 4.6 of SABS 0104 [19] limits the maximum deflection of any (**required loading 1.5A**) loaded balustrade to 100 mm, regardless of location or loading type.

Where:

A = nominal accidental load as described in SABS 0160

Table 5.15 presents the calculated deflection for each balustrade set-up as calculated for the different loading categories.

Table 5.15. Freestanding balustrade calculated deflection for each of the SABS [7] required loading categories

Panel Thickness	No of Rows	No of Holes per Row	Displacement Domestic	Displacement Public	Displacement Grandstands
mm			mm	mm	mm
12mm Thickness					
12	-	-	<u>32.4</u>	<u>97.3</u>	195
12	1	5	<u>58.1</u>	174	348
12	1	7	<u>58.4</u>	175	350
12	2	5	<u>60.6</u>	182	363
12	2	7	<u>56.6</u>	170	340
15mm Thickness					
15	-	-	<u>10.9</u>	<u>32.9</u>	<u>65.4</u>
15	1	5	<u>20.7</u>	<u>62.0</u>	124
15	1	7	<u>19.3</u>	<u>57.8</u>	116
15	2	5	<u>21.3</u>	<u>64.0</u>	128
15	2	7	<u>20.1</u>	<u>60.5</u>	121

Each balustrade panel was loaded with each SABS 0160 [7] required loading category. Table 5.15, presents the calculated displacement for each balustrade set-up. As SABS 0160 [7] limits the displacement to 100 mm, it can be noticed from table 5.15, that only the 15 mm continuously supported balustrade panel adhered to the SABS 160 [7] deflection requirements for the grandstand loading category. The rest of the 15 mm point- and continuously supported panels adhere to the deflection requirements for both the public- and domestic categories. Therefore, if a glass balustrade is to be designed according to the SABS 0160 [7] static loading- and deflection requirements, none of the balustrade set-ups would be able to be used for a grandstand application.

5.1.3.1.4 Conclusion

A unit concentrated- and -distributed load was applied to each balustrade set-up, in accordance with the SABS loading requirements. A linear static analysis was performed and the maximum principal stress corresponding to each panel's applied unit load was determined. Having calculated the maximum principal stress resulting from a unit load, the unit load was extrapolated and the static loading capacity of the particular balustrade set-up was determined.

The static loading capacity and deflection of each balustrade set-up was calculated, using the static material properties corresponding to the balustrade geometry (panels with- and without holes). The static loading capacity was determined for a 0.8% probability of failure, as recommended by Pilkington.

Finally, the calculated static loading capacity and deflection of each balustrade set-up was compared to the SABS [7] loading requirements. It was noticed that all the 15 mm thick freestanding balustrade set-ups, regardless of connection type, adhered to the SABS 0160 [7] concentrated loading requirement. Although all the balustrade panels adhered to the SABS concentrated loading requirements, none of the freestanding balustrades, adhered to the SABS [7] required distributed loading for grandstands. Predominantly, only the 15 mm thick panels adhered to both the domestic- and public distributed loading requirements.

From the SABS deflection requirements, only the 15 mm continuously supported balustrade panel adhered to the SABS 160 [7] deflection requirements for the grandstand-loading category. The rest of the 15 mm point- and continuously supported panels adhered to the deflection requirements for both the public- and domestic categories. It was concluded that, if a glass balustrade was to be designed according to the SABS 0160 [7] static loading- and deflection requirements, none of the balustrade set-ups would be able to be used for a grandstand application.

Having determined the static capacity of each balustrade panel and compared it to the SABS [7] requirements, the next section focuses on the dynamic capacity of each balustrade panel. Finally, the dynamic capacity of each balustrade panel is compared to the SABS [7] impact requirements.

5.1.3.2 Dynamic loading capacity

Each balustrade panel was loaded with a **unit** concentrated load in the top middle of the panel. A linear static analysis was performed and the maximum principal stress corresponding to each balustrade panel's applied unit load was determined. Having calculated the maximum principal stress resulting from a unit load, the unit load was extrapolated and each panel's dynamic loading capacity was determined, using the dynamic material properties as determined in chapter 4. These panel-loading capacities are further compared to the stress generated by the codified loads.

The balustrade dynamic loading capacity was determined for a 0.8% probability of failure for the panels with- and without holes. The dynamic material properties for panels with- and without holes used in the analysis, are presented in table 5.16.

Table 5.16. Dynamic material properties of glass panels with- and without holes

	50% P_f	0.8% P_f
Without holes	213 MPa	178 MPa
With holes	194 MPa	147 MPa

The dynamic loading capacity of each balustrade panel, loaded with a concentrated load in the top middle of the panel, is presented in table 5.17. Both point- and continuously supported balustrade panels are presented together.

Table 5.17. Freestanding balustrades dynamic loading capacity for a 0.8% P_f

Thickness	Rows	Holes	Point loading capacity 0.8% P_f
mm			kN
12mm Thickness			
12	-	-	2.97
12	1	5	1.77
12	1	7	1.85
12	2	5	1.72
12	2	7	1.83
15mm Thickness			
15	-	-	4.52
15	1	5	2.58
15	1	7	2.67
15	2	5	2.51
15	2	7	2.65

In the following section the dynamic capacity of the freestanding balustrade panels are compared to the SABS [7] impact requirements.

5.1.3.2.1 Comparison to SABS [7] requirements

This section focuses on the interpretation of the finite element results when subjected to the South African design standards. The calculated dynamic loading capacity of both the point- and continuously supported balustrades are compared to the corresponding SABS requirements. The results are compared under the:

- SABS dynamic (impact) loading requirements

SABS Dynamic loading requirements

SABS 0160 [7] subsection 5.4.5.5: forces on walls, balustrades and glazing material; requires that:

An impact of 400 J delivered by means of a 250 mm diameter bag filled with dry sand to a mass of 30 kg will represent the most severe condition likely to occur.

Each panel's corresponding impact force was determined, by means of a transient nonlinear analysis using the finite element software Abaqus [46], as described in section 5.1.2.2. The purpose of the nonlinear analysis was to determine the magnitude (equivalent static force) of the 400 J impact on each balustrade panel. The static force magnitude would then be compared to the dynamic capacity of each panel.

Only two continuously supported balustrades were modelled in Abaqus [46], one for each glass thickness (12, 15 mm). These two models would be used as reference models when stiffness is compared to other balustrade set-ups. Using each balustrade panel's stiffness, as obtained in the previous section (5.1.3.1.1), the stiffness of each panel relative to the reference model (12- or 15 mm) could be determined. A stiffness factor was calculated by dividing each balustrade panel's calculated displacement by the displacement of the reference model of the corresponding thickness. Finally, the elasticity modulus of the reference model was multiplied by the equivalent stiffness factor and changed accordingly. Table 5.18 presents each panel's stiffness factor, and elasticity modulus used in the finite element model.

Table 5.18. Equivalent stiffness factors and elasticity modulus

No of Rows	No of Holes per Row	Unit Displacement mm	Equivalent stiffness factor	Elasticity modulus N/mm ²
12mm Thickness				
-	-	0.0758	1.00	72000
1	5	0.0821	0.92	66240
1	7	0.0792	0.95	68400
2	5	0.0829	0.91	65520
2	7	0.0825	0.92	66240
15mm Thickness				
-	-	0.039	1.00	72000
1	5	0.0426	0.92	66240
1	7	0.0411	0.95	68400
2	5	0.0428	0.91	65520
2	7	0.0426	0.92	66240

The displacements of the Abaqus [46] modelled balustrades are highlighted in red, in table 5.18, and the elasticity modulus used for each balustrade panel presented.

The magnitude of the equivalent static impact force of the SABS [7] required 400 J was calculated for each configuration using the procedure in section 5.1.2.2.2. The resulting impact force for each configuration is compared in Table 5.19, to each balustrade panel's dynamic loading capacity for a 0.8% P_f .

Table 5.19. Comparison between freestanding balustrades dynamic loading capacity for a 0.8% P_f and impact load

No of Rows	No of Holes per Row	Loading Capacity 0.8% P_f kN	Static 400J Impact force kN	Result
12mm Thickness				
-	-	2.97	8.8	fail
1	5	1.77	8.1	fail
1	7	1.85	8.4	fail
2	5	1.70	8.0	fail
2	7	1.83	8.1	fail
15mm Thickness				
-	-	4.52	9.2	fail
1	5	2.58	8.5	fail
1	7	2.67	8.7	fail
2	5	2.51	8.4	fail
2	7	2.65	8.5	fail

From table 5.19 it is evident that no single freestanding balustrade can withstand the 400 J impact loading for a 0.8% probability of failure. Even the continuously supported panels cannot withstand the required impact loading. With the increase in capacity between the 12 mm and 15 mm panels, an increase in dynamic impact force can be noticed; this can be attributed to the increase in stiffness, as the increase in stiffness is directly related to dynamic impact force. Figure 5.36 presents the impact force of 400 J vs the equivalent stiffness of each balustrade panel for each panel thickness.

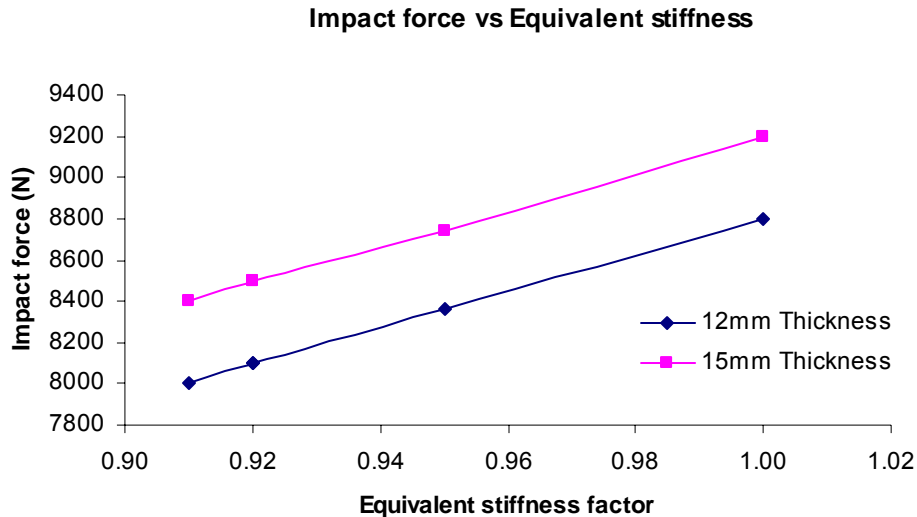


Figure 5.36. Impact force vs Equivalent stiffness of freestanding balustrades

From figure 5.36, a linear increase of impact force with panel stiffness is evident. Using figure 5.36, the impact force resulting from the 400 J impact can be determined for any other type of balustrade panel (ie. 4 or 6 connections), for a panel thickness of 12- or 15 mm.

5.1.3.3 Conclusion

Each balustrade panel was loaded with a unit concentrated load in the top middle of the panel. A linear static analysis was performed and each panel's dynamic loading capacity was determined, using the dynamic material properties. The balustrade dynamic loading capacity was determined for a 0.8% probability of failure for the panels with- and without holes.

Having determined the dynamic capacity of each balustrade pane, the calibrated finite element model was used to simulate the SABS [7] required 400 J impact. Instead of modelling each panel's geometry, two continuously supported balustrades were modelled in Abaqus, one for each glass thickness (12, 15 mm). Each panel's equivalent stiffness was calculated and the elasticity modulus of the modelled panel modified accordingly. Finally, the equivalent dynamic impact force produced by the simulated impact was calculated for each balustrade panel and compared to its dynamic loading capacity.

From the calculated results, it was noticed that no balustrade panel, continuous- or point-supported, was able to resist the SABS [7] 400 J impact-loading requirement. Further, a trend between the stiffness of a panel and the magnitude of the impact force was identified. Consequently, a figure illustrating this relationship was presented.

Since none of the freestanding balustrade panels was able to resist the SABS [7] required impact loading, alterations to the existing set-up was necessary. Consequently, a handrail was suggested to connect a number of panels together to increase the dynamic loading capacity of the system. The next stage investigates the influence of the introduction of a handrail on the dynamic loading capacity of the glass balustrade.

5.2 CONTINUOUS BALUSTRADES

Introduction

In the previous section, different balustrade panel geometries and connection types were investigated and their influence on the loading capacity of the glass balustrade capacity determined. None of the freestanding balustrade panels, point- or continuous supported, was able to resist the impact-loading requirement.

This section investigates the influence of the introduction of a handrail on the dynamic loading capacity of a freestanding glass balustrade. With the introduction of a handrail, the freestanding balustrade is not “freestanding” anymore, and becomes a continuous balustrade.

By connecting a balustrade panel to one or two of its adjacent panels, the handrail increases the global capacity of the glass panel while providing post failure containment. Three different steel handrail dimensions were investigated:

- 40x40 mm
- 50x50 mm
- 90x90 mm

Together with the different handrail dimensions, the influence the number of connected panels has on the loading capacity was also investigated. The number of continuously connected panels investigated, were:

- 3 panels
- 5 panels
- 7 panels

The layout of this section is illustrated in the flow diagram in figure 5.37.

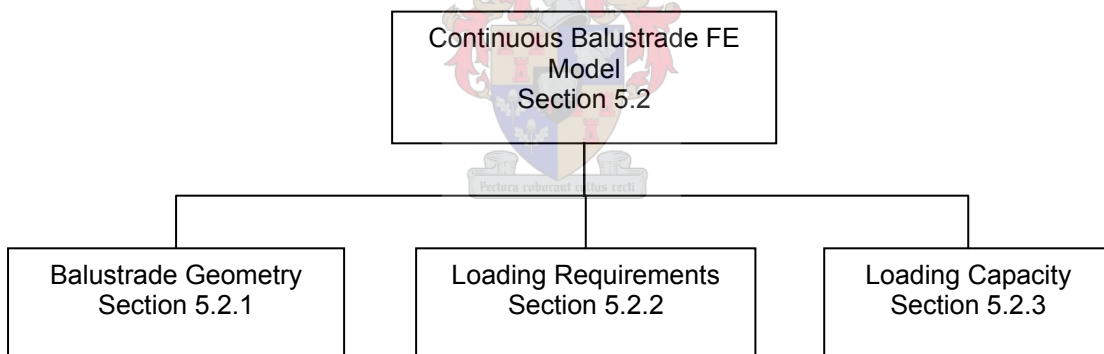


Figure 5.37. Flow diagram illustrating balustrade geometry section of the freestanding balustrade finite element model

NOTE: There is a distinction between a **continuous support** (i.e. continuously embedded into a support) and a **continuous balustrade**, where individual freestanding panels are interconnected using a handrail.

5.2.1 BALUSTRADE GEOMETRY

The geometry of the balustrade panels remained the same as for freestanding balustrades. The only difference is the addition of a handrail.

5.2.1.1 Handrail

A steel handrail was added to increase the dynamic loading capacity of a balustrade set-up. The three different solid steel handrail dimensions investigated were:

- 40x40 mm
- 50x50 mm
- 90x90 mm

Different handrail dimensions were investigated in order to determine the influence of the stiffness of the handrail on the dynamic loading capacity of the balustrade set-up. The stiffness of the handrail is important as it determines the contribution of the connected panels.

Together with the different handrail dimensions, the influence of the number of connected panels on the loading capacity was also investigated. The number of connected panels investigated, were:

- 3 panels
- 5 panels
- 7 panels

The handrail was modelled using quadratic beam elements (L13BE), which was tied to the top of the balustrade panels, illustrated in figures 5.39 and 5.40. The L13BE element (figure 5.38) is a two-node, three-dimensional class-II beam element.

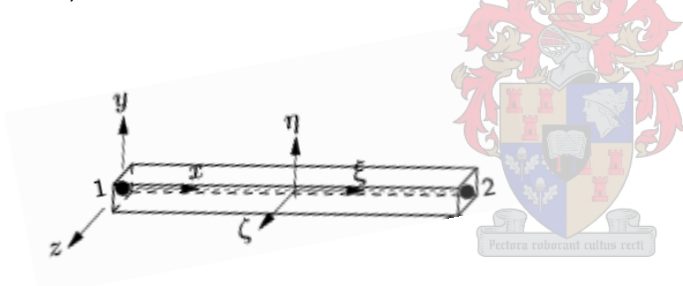


Figure 5.38 Quadratic beam element (L13BE) [44]

Due to symmetry, only half of the continuous balustrade system was modelled. 3 connected balustrade panels are illustrated in figure 5.39, and 5 connected balustrade panels in figure 5.40.

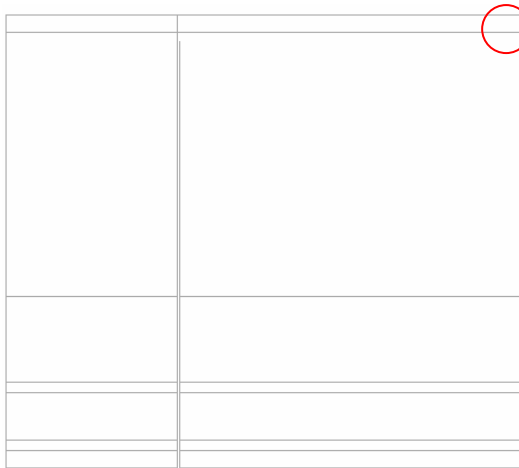


Figure 5.39. Three connected balustrade panels with handrail

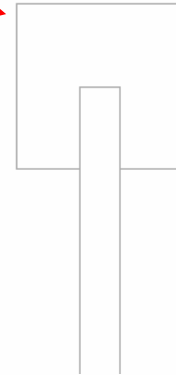


Figure 5.40. Handrail section detail (40 x 40mm)

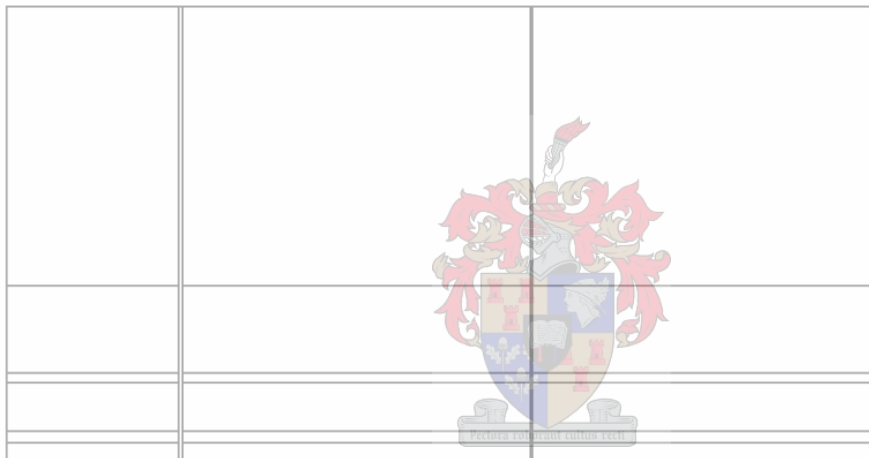


Figure 5.41. Five connected continuously supported balustrade panels

5.2.1.2 Support conditions

The supports of the balustrade systems remained the same, although one of the point support balustrade systems was not included. From the analysis of the freestanding balustrade, it was noted that the single row of horizontal holes had a larger capacity than the double row of horizontal holes. For the continuous balustrades, only the single row of horizontal holes was analysed.

The balustrade supports were reduced to the continuous- and single row of horizontal holes. For the horizontal row of holes, 5 and 7 holes were investigated.

5.2.1.3 Constraints

The centre balustrade panels were constrained against the axis of symmetry, and against translation at the supports as necessary. The holed panels were constrained using linear spring elements, as described in section 5.1.1.3. Due to symmetry, the handrail was constrained against rotation in x- and z direction, and translation in the y direction.

The following section, describes the static- and dynamic loading of the continuous balustrade set-ups.

5.2.2 LOADING REQUIREMENTS

5.2.2.1 Static loading requirements

For the static loading conditions, a unit point load was applied in the top centre of the panel, as described in section 5.1.2.1.

The handrailing and balustrading code [19] requires that the distributed load be applied across the length of the panel or the length of the handrail. As the distributed loading capacity of each panel was determined for each balustrade set-up in the previous section, it was not calculated again.

5.2.2.2 Dynamic loading requirements

Each panel's corresponding impact force was determined, by means of a transient nonlinear analysis using the finite element software Abaqus [46], as described in section 5.1.2.2. The purpose of the nonlinear analysis was to determine the magnitude (equivalent static force) of the 400 J impact on each balustrade panel. The static force magnitude would then be compared to the dynamic capacity of each panel.

Only two continuously supported balustrades were modelled in Abaqus, one for each glass thickness (12, 15 mm). These two models would be used as reference models when stiffness is compared to other balustrade set-ups. Using each balustrade panel's stiffness, the stiffness of each panel relative to the reference model (12- or 15 mm) could be determined. A stiffness factor was calculated by dividing each balustrade panel's calculated displacement by the displacement of the reference model of the corresponding thickness. Finally, the elasticity modulus of the reference model was multiplied by the equivalent stiffness factor and changed accordingly.



5.2.3 LOADING CAPACITY

The dynamic loading capacity of the different balustrade set-ups was determined and compared to the corresponding dynamic impact force. The dynamic impact force was calculated in the same way as for the freestanding balustrades, described in section 5.1.3.2.

The following section presents the dynamic loading capacity for point- and continuous supported continuous balustrade set-ups, as determined using the finite element software DIANA [44]. Before the dynamic loading capacity was determined, the influence of the addition of the handrail was investigated. The different parameters investigated were:

- Handrail stiffness (Table 5.20)
- Number of connected panels (Table 5.20)

5.2.3.1 Handrail influence

Table 5.20 presents the influence of the handrail dimension on the stiffness of the set-up. The panels without holes are used, and the influence is determined by comparing the equivalent stiffness of the continuous balustrade set-up to that of one panel. Consequently, the number of panels contributing to the stiffness of the set-up can be determined. Since, three balustrade panels are connected, the maximum number of panels contributing to the stiffness is three.

Table 5.20. *Handrail dimension influence on dynamic capacity of continuous balustrades*

No. of Panels	Thickness	Handrail	Displacement	Equivalent Stiffness Factor
	mm	mm x mm	mm	
1	15	-	0.039	1
3	15	40x40	0.0144	2.71
3	15	50x50	0.0135	2.89
3	15	90x90	0.0125	3.00

Where:

Equivalent stiffness factor

= displacement single panel/ displacement connected balustrade set-up

= $\Delta_{\text{panels } 1} / \Delta_{\text{panels } 3}$

From table 5.20, the influence of the handrail dimension on the stiffness of the balustrade set-up is evident. An increase of the equivalent stiffness factor with an increase in handrail dimension is noted, which is explained by the increase in stiffness of the handrail. As the continuous balustrade set-up consists of three connected balustrade panels, the maximum equivalent stiffness is therefore 3.0. From table 5.20, it is noted that only the 90x90 mm handrail enforces the contribution of all three-balustrade panels. The 90x90 mm handrail may in practise however be an impractical arrangement.

5.2.3.2 Number of connected panels

Table 5.21 presents the influence of the number of panels on the dynamic loading capacity of the balustrade set-up. A 40x40 mm handrail connects the balustrades and three different balustrade set-ups are investigated.

Table 5.21. *Number of panels' influence on dynamic loading capacity of continuous balustrades*

No. of Panels	Thickness	Handrail	Displacement	Equivalent Stiffness factor	Contribution factor
	mm	mm x mm	mm		
1	15	-	0.039	1	100
3	15	40x40	0.0144	2.71	90.28
5	15	40x40	0.0117	3.33	66.67
7	15	40x40	0.0107	3.65	52.07

The contribution factor represents the percentage of the connected number of panels contributing to the stiffness of the set-up, and is presented in table 5.21. A decrease in contribution with increase number of connected panels is noted. With a 40x40 mm handrail, 90% of the panels contribute to the stiffness of the set-up when three panels are connected. The contribution of the balustrade set-up decline to 52% when 7 panels are connected. The decrease in the contribution of number of connected panels can be attributed to the slenderness of the handrail. Using a larger handrail will lead to a larger contribution of number of connected panels.

Figure 5.42, summarizes table 5.20 and 5.21, and illustrates the number of connected panels vs the number of panels contributing to the stiffness of the set-up, for three different handrail dimensions.

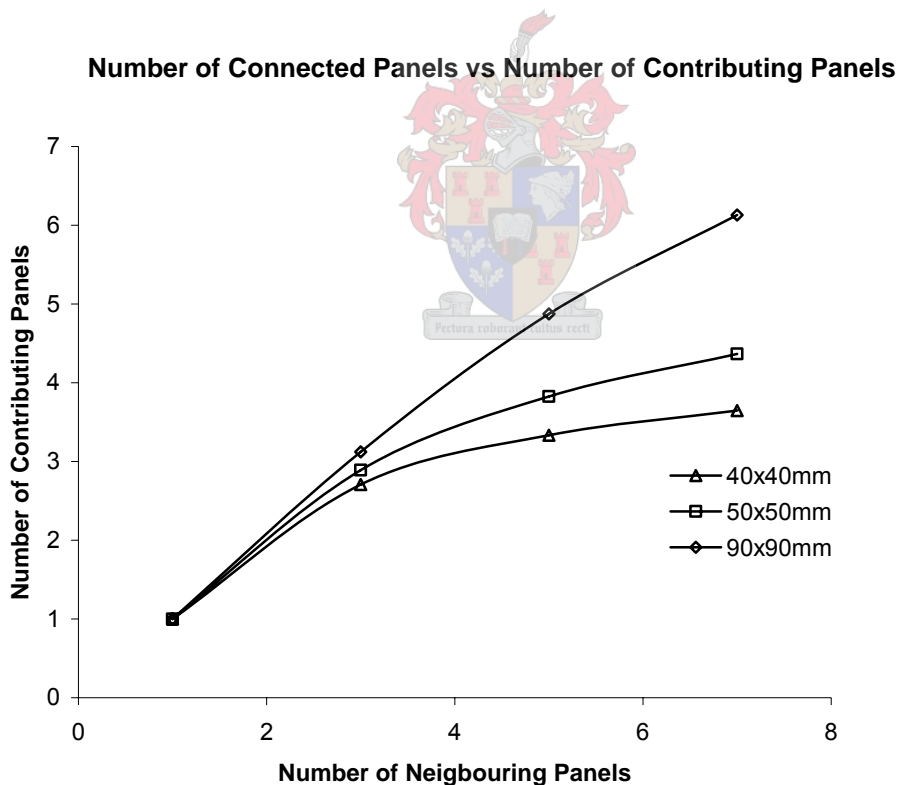


Figure 5.42. *Connected number of panels vs number of contributing panels*

From figure 5.42, the number of connected panels contributing to stiffness of the overall set-up, when using a particular handrail, can be established.

The following section presents the dynamic loading capacity for point- and continuous supported continuous balustrade set-ups, as determined using the finite element software DIANA [44].

5.2.3.3 Static capacity

The static capacity of the various continuous balustrade systems are presented in **Appendix D**.

5.2.3.4 Dynamic capacity

The dynamic capacity was calculated for 3 balustrade systems connected by a handrail. Different handrail systems were investigated and their influence on the loading capacity determined. The results are categorized under:

- Continuous- and
- Point supported balustrade set-ups

Finally, in section 5.2.3.4.3, each balustrade set-up's determined loading capacity is compared to the SABS 0160 [7] loading requirements.

5.2.3.4.1 Continuously supported

The results for the continuously supported balustrades are presented in table 5.22, and are categorized according to handrail dimension. The contours of the maximum principal stress of continuously supported freestanding balustrade panels connected with a 40x40 mm and 90x90 mm handrail are presented in figures 5.43 and 5.44 respectively.

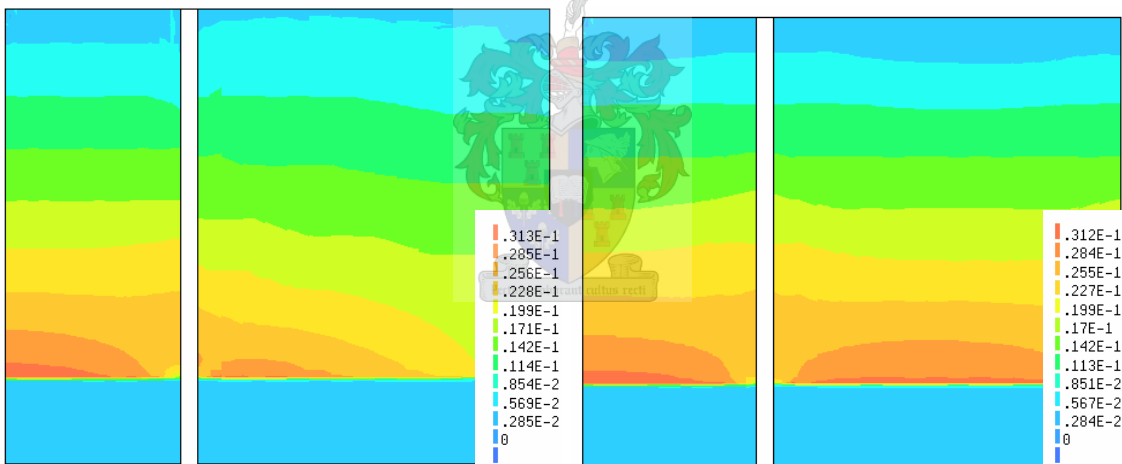


Figure 5.43. 40x40mm Handrail

Figure 5.44. 90x90mm Handrail

From both figure 5.43 and figure 5.44, the difference in stiffness between the two handrails is evident. The red contours indicate the areas of principal tensile stress (ie. Fracture origin). The concentration of the contours in the corner closest to the loaded panel indicates that the slenderness of the 40x40 mm handrail utilizes only a small percentage of the neighbouring panel's stiffness.

From figure 5.44, it can be seen that the increased stiffness of the 90x90 mm handrail evenly distribute the applied point load over the length of the loaded- and neighbouring panels. The increase in stiffness of the 90x90 mm handrail, combine the stiffness of the connected panels and therefore increase the loading capacity of the continuous balustrade system.

Table 5.22 Dynamic loading capacity of continuous supported glass balustrade with handrail

Handrail	Equivalent stiffness factor	Loading capacity 0.8% P_f
mm x mm		kN
12mm Thickness		
40x40	2.84	6.50
50x50	2.98	9.10
90x90	3.15	9.42
15mm Thickness		
40x40	2.71	12.30
50x50	2.89	13.49
90x90	3.12	14.77

5.2.3.4.2 Point supported

The results of the point supported balustrade set-ups are presented in table 5.23 (12- and 15 mm), and are categorized according to the handrail dimension. The contours of the principal tensile stress (red contours) of point supported freestanding balustrade panels connected with a 40x40 mm and 90x90 mm handrail, is presented in figure 5.45, and figure 5.46 respectively.

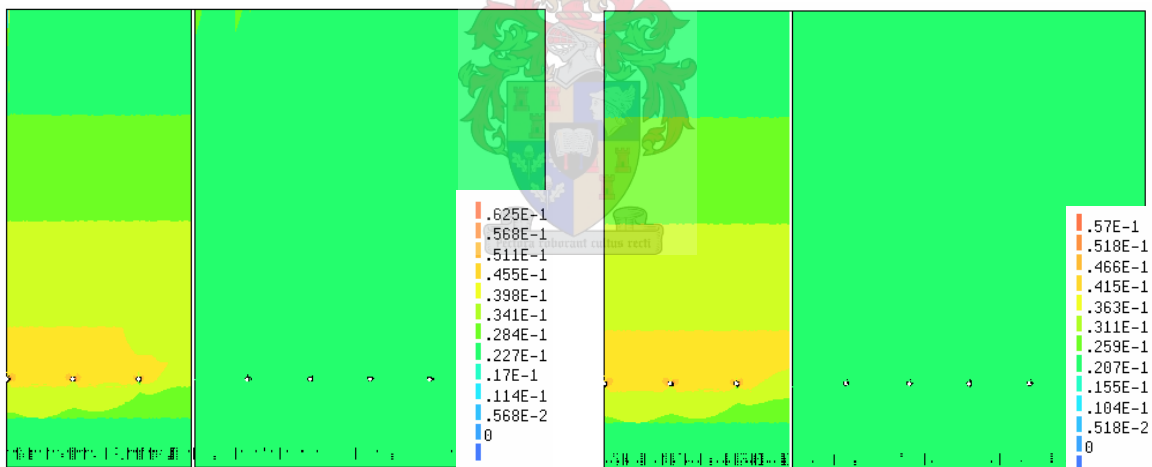


Figure 5.45 40x40mm Handrail

Figure 5.46 90x90mm Handrail

Since the neighbouring panels were only needed to simulate the stiffness of the balustrade panel, they were modelled using quadratic plate elements as apposed to volume elements. As a result, the stress concentration around the holes could not accurately be predicted and are not seen in the figures.

The difference in handrail stiffness can be seen between figure 5.45, and figure 5.46. The stiffer handrail, figure 5.46, distributes the load across the length of the panels as apposed to the slender handrail. The calculated dynamic loading capacity of each continuous balustrade set-up is presented in table 5.23 for the 12 mm thick panels and for the 15 mm thick panels.

Table 5.23 Comparison of dynamic loading capacity of point supported glass balustrade with handrail, with impact load

No. of Holes	Handrail	Equivalent stiffness factor	Loading Capacity 0.8% P _f
	mm x mm		kN
12mm Thickness			
5	40x40	2.47	4.70
5	50x50	2.60	4.92
5	90x90	2.72	5.16
7	40x40	2.47	4.87
7	50x50	2.59	5.09
7	90x90	2.71	5.33
15mm Thickness			
5	40x40	2.35	6.60
5	50x50	2.5	6.98
5	90x90	2.69	7.52
7	40x40	2.34	6.77
7	50x50	2.484	7.17
7	90x90	2.674	7.69

In the following section the dynamic loading capacity of the continuous balustrade set-ups are compared to the SABS [7] impact requirements.

5.2.3.4.3 Results compared to SABS requirements

This section focuses on the interpretation of the finite element results as compared to the South African Design standards [dynamic loading]. The calculated dynamic loading capacity of both the point- and continuously supported continuous balustrade set-ups are compared to the corresponding SABS requirements. The results are compared under the:

- SABS dynamic (impact) loading requirements

SABS Dynamic loading requirements

SABS 0160 [7] subsection 5.4.5.5: forces on walls, balustrades and glazing material; requires that:

An impact of 400 J delivered by means of a 250 mm diameter bag filled with dry sand to a mass of 30 kg will represent the most severe condition likely to occur.

Each set-up's corresponding impact force (static force) was determined, by means of a transient nonlinear analysis using the finite element software Abaqus [46], as described in section 5.1.2.2.

The interpretation of the results of the continuous balustrade set-ups, are categorized under:

- Continuously supported and
- Point supported

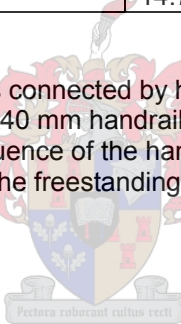
5.2.3.4.3.1 Continuously supported

Table 5.24 presents each continuously supported set-up's calculated impact force (400 J impact force) and compares it to the particular set-up's dynamic loading capacity for a 0.8% probability of failure.

Table 5.24 Comparison of dynamic loading capacity of continuous supported glass balustrade with handrail, with impact load

Handrail dimension	Equivalent Stiffness factor	Loading Capacity 0.8% P_f	Static 400J Impact force	Result
mm x mm		kN	kN	
12mm Thickness				
40x40	2.84	6.50	8.20	fail
50x50	2.98	9.10	8.97	pass
90x90	3.15	9.42	9.20	pass
15mm Thickness				
40x40	2.71	12.30	9.60	pass
50x50	2.89	13.49	10.28	pass
90x90	3.12	14.77	10.50	pass

All continuously supported balustrades connected by handrail, with the exception of the 12 mm thick balustrade connected by 40x40 mm handrail, passed the required impact test for the 0.8% probability of failure. The influence of the handrail on the capacity of the continuous balustrade set-up is clear, as none of the freestanding balustrade panels was able to sustain the required impact loading.



5.2.3.4.3.2 Point supported

Table 5.25 presents each point supported set-up's calculated impact force (impact force) and compares it to the particular set-up's dynamic loading capacity for a 0.8% probability of failure.

Table 5.25 Dynamic loading capacity of point supported glass balustrades with handrail

No. of Holes	Handrail	Equivalent Stiffness factor	Loading capacity 0.8%P _f	Static 400J Impact force	Result
	mm x mm		kN	kN	
12mm Thickness					
5	40x40	2.47	4.70	7.8	fail
5	50x50	2.60	4.92	8.6	fail
5	90x90	2.72	5.16	8.8	fail
7	40x40	2.47	4.87	7.8	fail
7	50x50	2.59	5.09	8.6	fail
7	90x90	2.71	5.33	8.8	fail
15mm Thickness					
5	40x40	2.35	6.59	9.6	fail
5	50x50	2.5	6.98	10.0	fail
5	90x90	2.69	7.52	10.2	fail
7	40x40	2.34	6.77	9.8	fail
7	50x50	2.48	7.17	10.2	fail
7	90x90	2.67	7.70	10.2	fail
Laboratory Test Series 2					
Set-up 1	50x50	2.39	11.16	9.50	pass
Set-up 2	50x50	2.15	10.05	8.6	pass

Comparing the dynamic loading capacity (0.8%P_f) of each balustrade set-up to the SABS [7] required impact loading, it is clear that none of the point supported balustrades could sustain the impact loading, for a 0.8% probability of failure.

Table 5.25 also presents the loading capacity of two identified balustrade set-ups to be tested in a verification laboratory test series (chapter 6). The configuration of the set-ups is described in detail in the following chapter.

5.2.3.5 Conclusion

The dynamic impact analysis on freestanding glass balustrades indicated that none of the balustrade panels could sustain the impact requirements as set out in the South African loading code [7]. It was consequently decided that similar impact tests be performed on continuous balustrades (handrail connected freestanding balustrades).

From the freestanding balustrade impact analysis, it was clear that the dynamic impact-loading requirement was the dominant load case, as a balustrade has only to be designed to sustain the 400 J South African impact-loading requirements [7]. Consequently, all continuous balustrade set-ups were loaded with a unit point load applied to the middle panel in the top centre of the panel. A linear static analysis determined each balustrade set-up's stiffness and dynamic loading capacity.

Before each balustrade set-up's dynamic loading capacity was determined, the influence of the addition of a handrail on continuous balustrades was investigated. Two parameters were investigated which directly influenced the capacity of continuous balustrades. They were:

- Number of connected panels
- Stiffness of handrail

Stiffness of handrail

Three different solid steel handrail dimensions were investigated to determine the influence of the stiffness of the handrail on the dynamic loading capacity of the continuous balustrade set-up. An increase of the equivalent stiffness factor with an increase in handrail dimension was noted, which was attributed to the increase in stiffness of the handrail. Further, it was noted that only the 90x90 mm handrail enforces the total contribution of all three-balustrade panels.

Number of connected panels

Three different numbers of connected panels together with three different handrail dimensions were investigated to determine the influence of the number of connected panels on the dynamic loading capacity of the continuous balustrade set-up. The influence of the number of panels and handrail stiffness was presented by means of a contribution factor. The contribution factor represents the percentage of the connected number of panels contributing to the stiffness of the set-up, and was found to be directly related to the stiffness of the handrail. A decrease in contribution with increase number of connected panels was noted.

Finally, the dynamic loading capacity of the different balustrade set-ups was determined and compared to the corresponding SABS [7] impact loading requirements. The SABS [7] required 400 J impact was simulated using the finite element software Abaqus, and consequently a resultant impact force determined. The dynamic loading capacity was determined for different balustrade set-ups consisting of three connected balustrades for 12- and 15 mm thicknesses.

Comparing the dynamic loading capacity (0.8% P_f) of each balustrade set-up to the SABS required impact loading [7], it was found that only the continuously supported balustrades were able to sustain the required loading. None of the point-supported balustrades could sustain the impact loading, for a 0.8% probability of failure, regardless of handrail stiffness or panel thickness.

Two balustrade set-ups were identified to be tested in a verification laboratory test series (chapter 6), the configuration of which is described in detail in the following chapter.

The next chapter presents the second and final laboratory test series. The purpose of the laboratory test series was to verify the finite element results of this chapter.

CHAPTER 6 VERIFICATION LABORATORY TEST SERIES

Introduction

In the previous chapter the static- and dynamic loading capacity of different balustrade set-ups was determined using the finite element software package DIANA [44]. The static- and dynamic material properties, determined in chapter 4, was used to calculate the loading capacity of each freestanding balustrade. From the finite element analysis, it was concluded that none of the freestanding balustrades, point- or continuous supported, was able to resist the SABS [7] required impact loading. As a result, the influence of an introduction of a handrail, on the capacity of a freestanding balustrade was investigated. In conclusion, different continuous balustrade set-ups which could sustain the required SABS [7] impact loading, were identified (see table 5.25).

This chapter describes the laboratory test series in which 4 full-scale balustrade panels are impact loaded as required by the SABS [7]. Panel geometry, as identified in the finite element analysis of the previous stage, is tested against the impact loading requirements of the SABS [7] loading code. The purpose of the test series is to verify the finite element analysis, and ultimately conclude the investigation into the loading capacity of glass balustrades.

The layout of the chapter and the manner in which the laboratory test series was undertaken is illustrated by means of a flow diagram in figure 6.1.

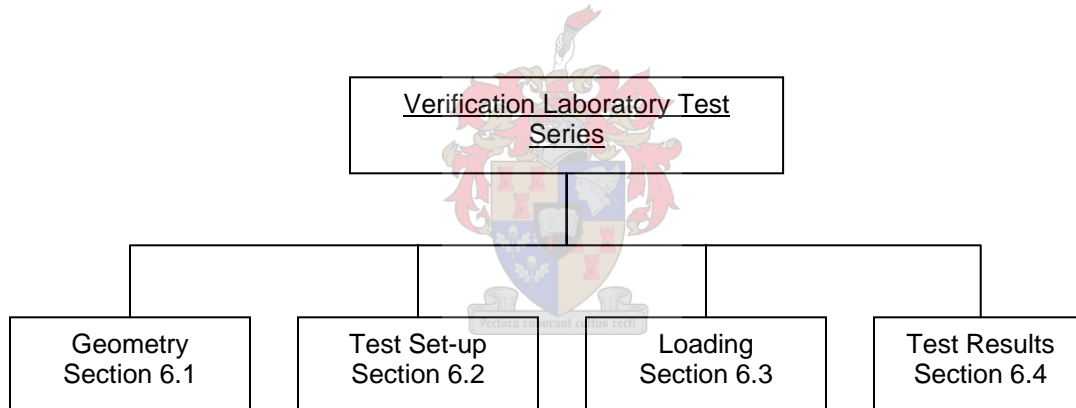


Figure 6.1. Flow diagram illustrating the layout of the laboratory test series

The laboratory test series can be categorized into four steps. In the subsequent paragraphs each of these steps are addressed separately and described in detail, they are:

- Geometry of the balustrade panels
This paragraph describes the geometry of each panel as identified in the finite element analysis.
- Design of test set-up
This paragraph describes the test set-up and test rig in which the full-scale balustrade panels where tested.
- Loading of balustrade panels
This paragraph describes the loading of each glass panel, as identified for each balustrade set-up.

6.1 BALUSTRADE GEOMETRY

Introduction

The geometry of the full-scale balustrade panels were chosen based on the results obtained in the previous chapter 5, balustrade finite element model (see table 5.25). Since none of the freestanding balustrade panels was able to resist the required SABS [7] impact load, the laboratory verification test series only included continuous balustrade set-ups.

The following section describes the test panel geometry, and is categorized under the following headings:

- Test panel thickness
- Test panel supports
- Test panel geometry

The layout of this section is illustrated in the flow diagram in figure 6.2.

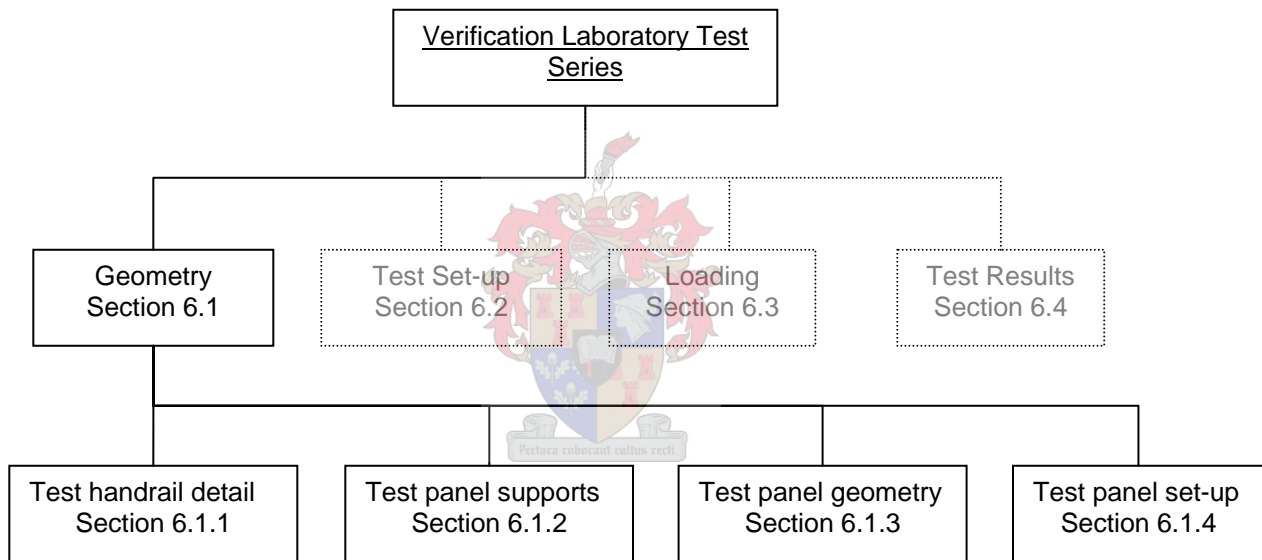


Figure 6.2. Flow diagram illustrating layout of the geometry stage of the laboratory test series.

6.1.1 Test handrail detail

The finite element analysis, of the previous chapter, identified the full-scale balustrade panels which could resist the SABS [7] required impact loading (see table 5.25), based on the glass static- and dynamic material properties determined in chapter 4. From table 5.19, it was concluded that none of the freestanding balustrade panels, point- or continuous supported, could resist the required dynamic loading. As a result, a handrail was added which connected 3 freestanding balustrade panels, thus increasing the loading capacity. For the laboratory test series a handrail of dimension 50x50 mm was chosen. Although the finite element analysis was based on a solid square 50x50 mm handrail, a different handrail section was used in the test series. However, since both handrails had the same stiffness, the influence on the loading capacity remained the same. The dimensions of the new proposed handrail were determined as follow:

Determination of stiffness of original handrail

Description:

Square solid section (figure 6.3)

Dimensions:

50x50 mm

Second moment of inertia:

$$= \frac{1}{12} \cdot (50)^4$$

$$= 520\,833 \text{ mm}^4$$

Stiffness of proposed handrail

Description:

2 x L-section connected back to back (figure 6.4)

Dimensions:

2x 50x50x5 mm L-section

Second moment of inertia of one angle section about mass centre:

$$= 110\,000 \text{ mm}^4$$

Parallel-Axis Theorem

$$I = I + Ad^2$$

$$= 110\,000 + 480(14+7.5)^2$$

$$= 331\,880 \text{ mm}^4$$

2 x Angles

$$= 2 \times 331\,880$$

$$= 663\,760 \text{ mm}^4$$

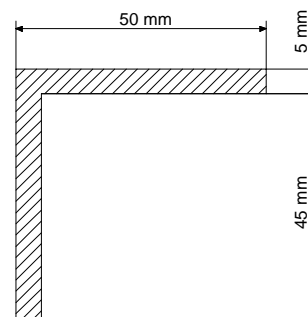
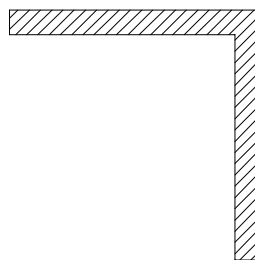
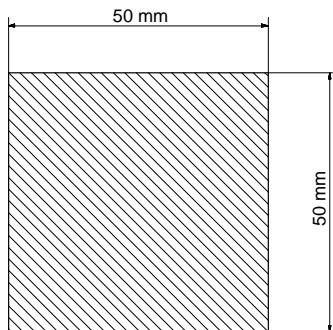


Figure 6.3. 50x50 Square solid handrail

Figure 6.4. Handrail used in laboratory test series

The support conditions of the 12- and 15 mm thick balustrade panels used in the laboratory test series is described in the following section.

6.1.2 Test panel supports

As it was the purpose of the laboratory test series to verify the finite element analysis, and not to determine the dynamic loading capacity of the balustrade set-ups, it was consequently decided that both point supported balustrade panels be tested. Although none of the point supported balustrade set-ups were able to resist the SABS 0160 [7] required impact loading, a set-up (see table 6.3 for set-up description) incorporating both point- and continuous supported panels was introduced to be tested (table 5.25 and 6.1). The point supported balustrade panels consisting of one row of horizontal holes, as determined in the previous chapter, was chosen.

Table 6.1. Dynamic loading capacity of identified glass balustrades with handrail

Laboratory Test Series 2	Handrail	Loading capacity $0.8\%P_f$	Static 400J Impact force	Result
	mm x mm	kN	kN	
Set-up 1	50x50	11.16	9.50	pass
Set-up 2	50x50	10.05	8.6	pass

The panel thickness for each connection type is described in the following section.

6.1.3 Test panel geometry

The size and layout of the full-scale balustrade panels were the same as used in the finite element analysis (1300 x 1000 panels).

For the continuously supported balustrade panels, two 15 mm thick panels- and for the point supported balustrade panels, one 12- and two 15 mm balustrade panel were chosen. All the holes were 20 mm in diameter.

The description of each balustrade panel used in the laboratory test series is presented in table 6.2. The layout of a point supported balustrade panel is illustrated in figure 6.5, and the layout of a continuous supported balustrade panel in figure 6.6.

Table 6.2. Balustrade panel geometry

Designation	Panel Thickness	No of holes	Hole Diameter inside	Hole Diameter outside	Dimension of panel
	mm		mm	mm	mm x mm
Panel 1	12	5	20	22	1300 x 1000
Panel 2,	15	5	20	22	1300 x 1000
Panel 3,4	15	No hole	-	-	1300 x 1000

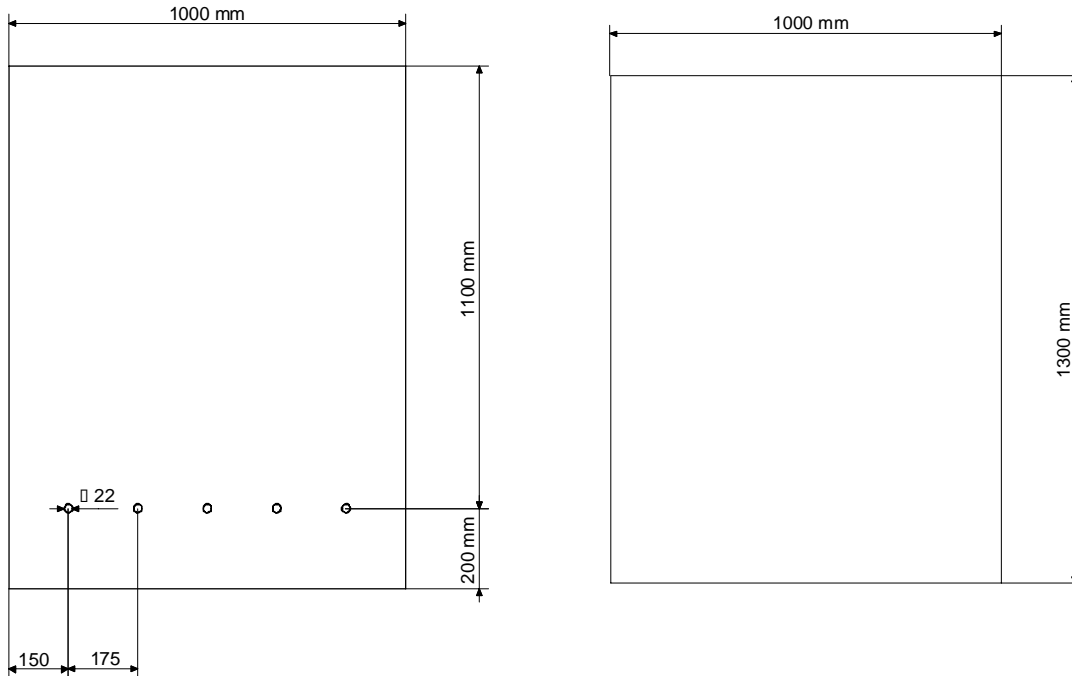


Figure 6.5. Point supported balustrade panel Figure 6.6. Continuous supported balustrade panel

Having described the geometry each of the balustrade panels used in the laboratory test series, the following section presents the make up of the various continuous balustrade set-ups.

6.1.4 Test panel set-up

In the laboratory test series, 2 different continuous balustrade set-ups were tested. However, only 4 panels were used, as only 1 panel was impact loaded at a time. Each continuous balustrade set-up consisted of one point supported balustrade panel, and two continuously supported balustrade panels (table 6.3). In each balustrade set-up the point supported panel, was the panel that was impact loaded, while the two continuously supported panels were always used as the neighboring panels. The increase in loading capacity of the continuously supported panels would ensure the fracture of only the loaded point supported panel, as apposed to all three.

The description of each laboratory tested balustrade set-up is given in table 6.3.

Table 6.3. Balustrade set-ups

Designation	No. of panels	Panels used	No. of loaded panel (See table 6.2)	Equivalent Handrail dimension
				mm
Set-up 1	3	1,3,4	1	50 x 50
Set-up 2	3	2,3,4	2	50 x 50

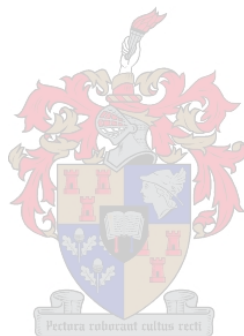
6.1.5 Conclusion

The finite element analysis, of the previous chapter, identified the full-scale balustrade panels which could resist the SABS [7] required impact loading. However, since none of the freestanding balustrade panels was able to resist the required SABS [7] impact load, the laboratory verification test series only included continuous balustrade set-ups.

An equivalent handrail of dimension 50x50 mm was chosen to connect the different balustrade panels. The geometry of the balustrade panels included two 15 mm thick continuously supported balustrade panel and two point supported balustrade panels, one 12- and one 15 mm thick.

Two different continuous balustrade set-ups were identified to be tested. However, only 4 panels would be required, as only 1 panel would be impact loaded at a time.

The next step of the laboratory verification test series, describes the test set-up in which the continuous balustrade panels were impact tested.



6.2 TEST SET-UP

Introduction

The test set-up was designed in accordance with the corresponding SABS 1263 [21] testing procedures and can be divided into the test- and loading rig.

The test rig, which describes the rig in which the continuous balustrade set-ups were tested, had to be multipurpose as to make the testing of both point- and continuous balustrade panels possible.

The loading rig, which describes the impactor which was used to simulate human impact, was designed in accordance with SABS [21] instead of the recommended SABS 0160 [7] impact loading requirements. Consequently, the stiffness of the lead shot impactor was used instead of the recommended sand bag impactor.

The following section concerns the test set-up, and can be categorized under the following headings:

- The test rig
- The loading rig

The layout of the section is presented by means of a flow diagram in figure 6.7.

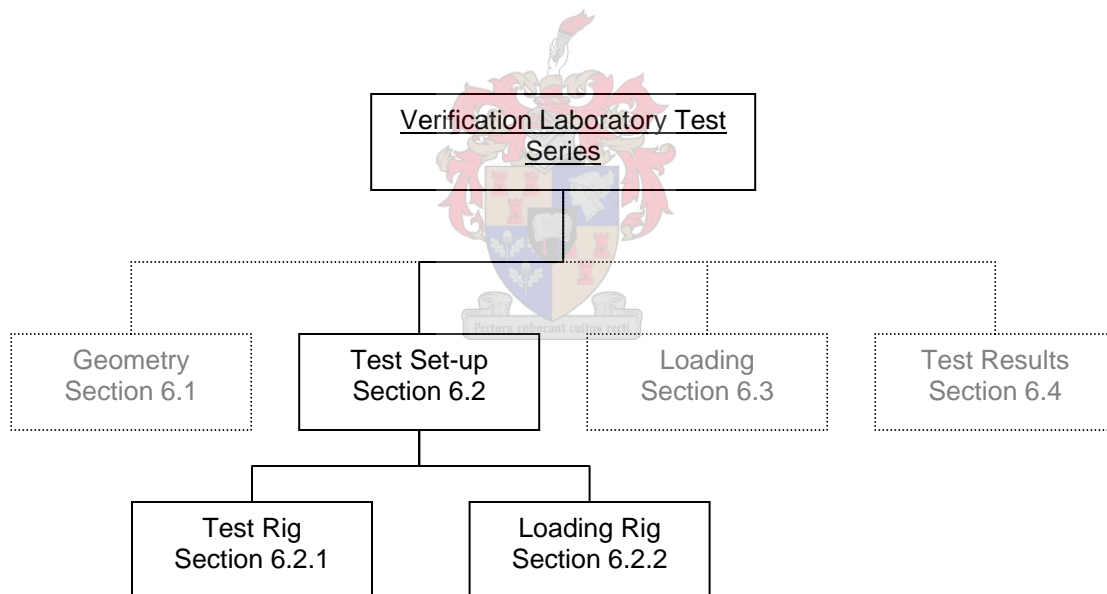


Figure 6.7. Flow diagram illustrating layout of the test set-up stage of the laboratory test series.

6.2.1 Test Rig

Typically, point supported balustrade panels are connected to the adjacent structure using bolts, as illustrated in figures 6.8 and 6.9. Fracture of the balustrade panel occurs in out-of-plane bending, due to a stress concentration at the hole as described in chapter 4. For the simplification of the test set-up, the point-supported balustrade panels were not tied to the supporting structure using bolts, as illustrated in figures 6.10 and 6.11.

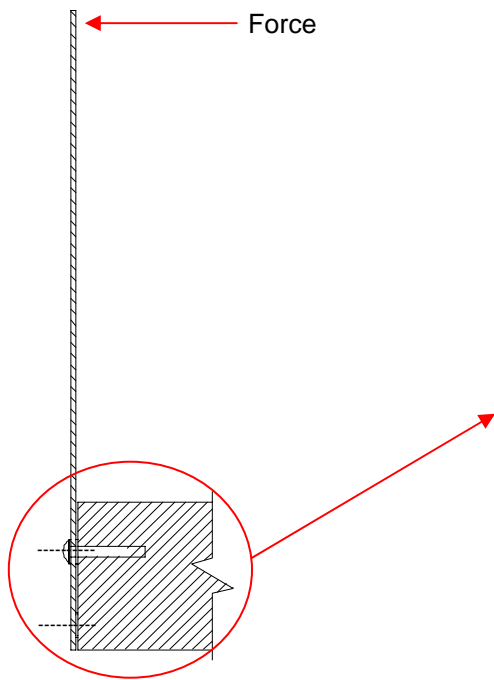


Figure 6.8. Balustrade Slab Connection

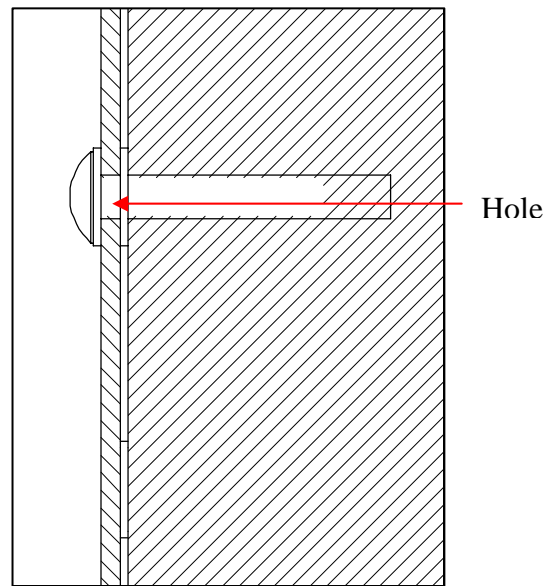


Figure 6.9. Balustrade Connection Detail

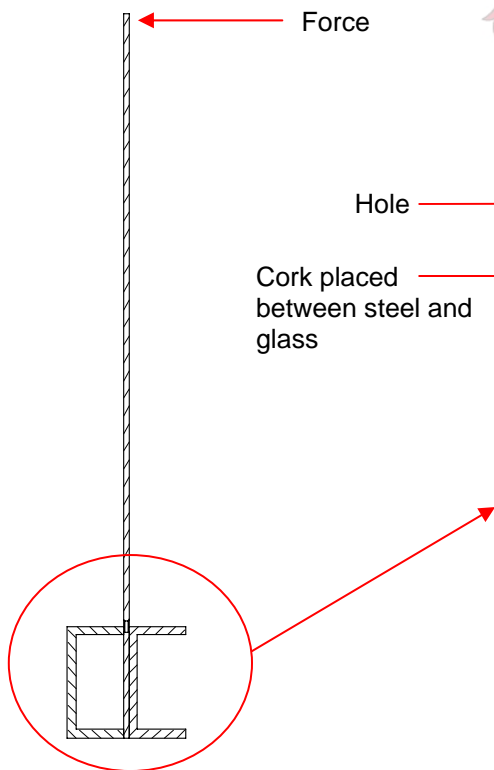


Figure 6.10. Balustrade Test Connection

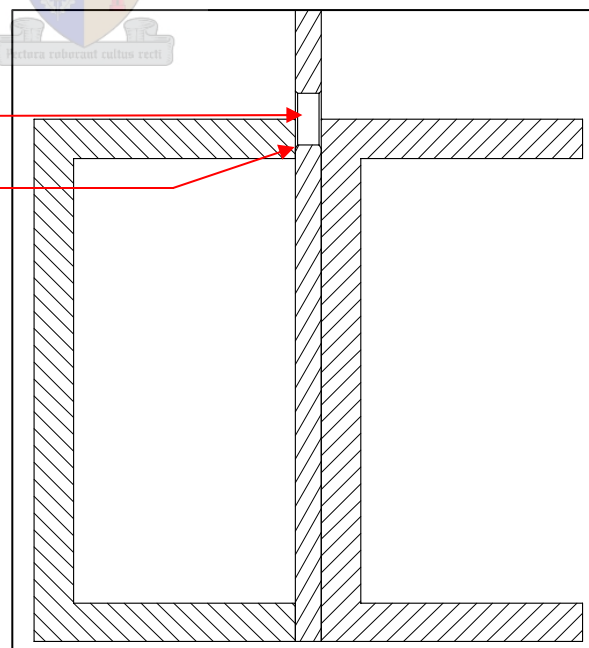
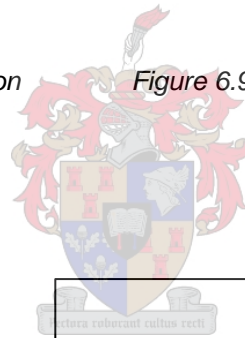


Figure 6.11. Test Set-up Connection Detail

Instead, the balustrade panels were continuously supported along the top bolt location line, as illustrated in figure 6.10. The continuous support allows rotation about the bolt location line as if the panels were fixed using bolts. Consequently, the loading capacity of the point supported balustrade panels is not altered.

This type of test set-up would allow the testing of both point- and continuous supported balustrade panels.

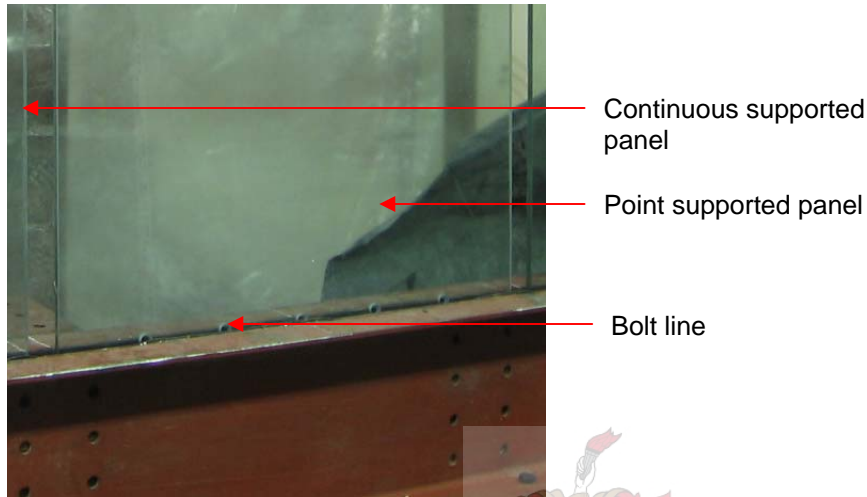


Figure 6.12. Bolt line of point supported balustrade

The physical set-up of the laboratory testing procedure is illustrated in figure 6.13.

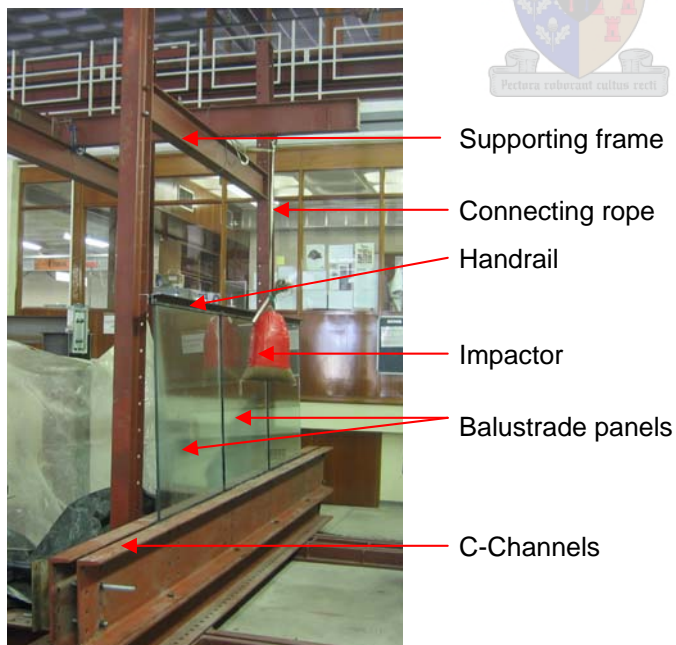


Figure 6.13. Laboratory verification test set-up

The following section, described the loading rig which was used to simulate human impact.

6.2.2 Loading rig

The guidelines for the testing procedure for simulating human impact on glass balustrades are given in SABS [7] paragraph 5.4.5 forces on walls, balustrades and glazing. The standard requires that an impact of 400 J be delivered by means of a 250 mm diameter bag filled with dry sand to a mass of 30 kg.

After consideration of various international loading standards [21, 22, 23] in chapter 2, it was recommended that the sand bag impactor be replaced by the lead shot impactor. The reason for the replacement of the existing sand bag impactor was due to its variability in construction. The vague construction guidelines of the sand bag impactor, results in a variability in stiffness between tests. Whereas, the lead shot impactor provides sufficient guidelines to enable reproducible construction of the impactor. The reproducibility of the lead shot impactor is attributed to the taping of the impactor, which results in the compaction of the material and consequently in a constant stiffness.

Due to the ease in construction, the sand bag impactor was used in the laboratory test series, but with the stiffness of the lead shot impactor as for the finite element analysis of section 5.1.2.2. The sand bag was constructed in accordance with paragraph 5.4.5 of SABS [21], but was tightly taped to the required stiffness of the lead shot impactor. After each round of tape, the test impactor was compressed in the Zwick 250 kN compression machine, illustrated in figure 6.14. The impactor was placed with its long axis parallel to ground.



Figure 6.14. Determination of stiffness of test impactor

The stiffness of the test impactor was compared to that of the available lead shot impactor stiffness determined by Foss [11], and was taped until the required stiffness was reached. Figure 6.15 illustrates the stiffness of the taped and non-taped test impactor, and compares it to the stiffness of the lead shot impactor.

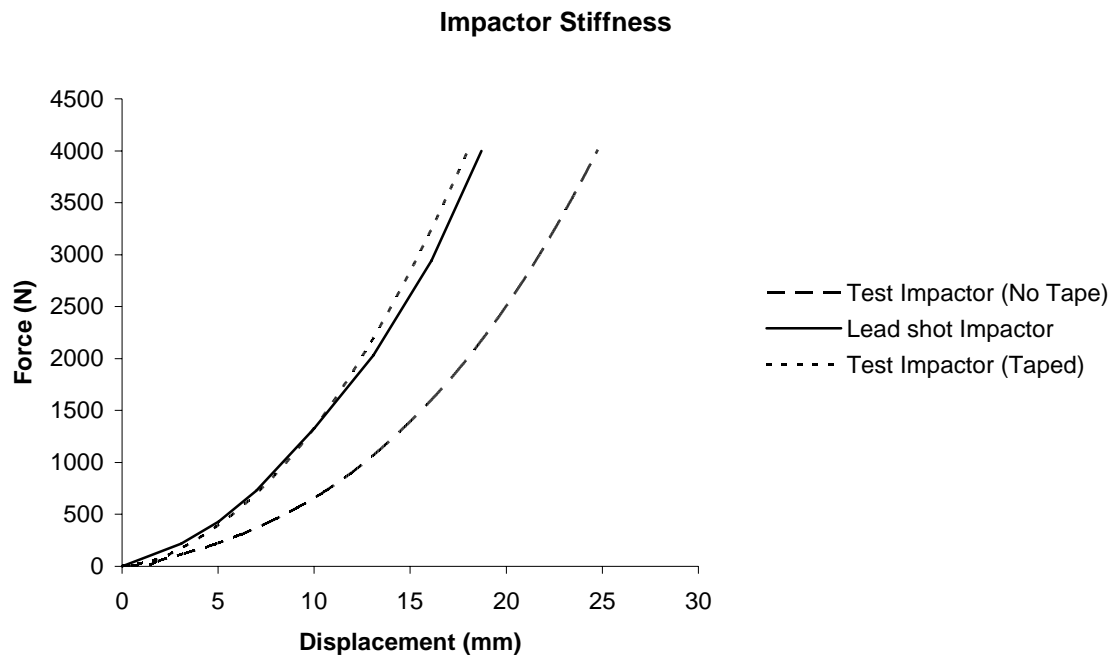


Figure 6.15. Static shot bag response model

The increase in “stiffness” (force/ displacement) with the taping of the test impactor can be seen in figure 6.15. With the taping of the impactor the required stiffness was obtained.

Consequently, the tightly taped sand bag impactor was used to simulate human impact on the glass balustrades during the laboratory verification test series.

6.2.3 Conclusion

The test set-up was designed in accordance with the corresponding SABS 1263 [21] testing procedures.

The test rig, in which the balustrade panels were placed, had to be multipurpose as to make the testing of both point- and continuous balustrade panels possible. For the simplification of the test set-up, the point-supported balustrade panels were not tied to the supporting structure using bolts, instead, they were continuously supported along the top bolt location line. This type of test set-up allowed the testing of both point- and continuous supported balustrade panels.

Due to the ease of construction, the sand bag impactor was used in the laboratory test series, however with the verified stiffness of the lead shot impactor. The sand bag was tightly taped to achieve the required stiffness of the lead shot impactor. After each round of tape, the test impactor was compressed in the Zwick 250 kN compression machine, and the stiffness of the impactor determined. The stiffness of the test impactor was compared to that of the available lead shot impactor stiffness, and was taped until the required stiffness was reached. Consequently, the tightly taped sand bag impactor was used to simulate human impact on the glass balustrades, during the laboratory verification test series.

Having described the loading rig that was used to simulate human impact on glass balustrades, the next section presents the drop heights and impact energy applied to each balustrade set-up.

6.3 TEST LOADING

Introduction

The impact loading of the SABS [7] loading standard requires that an impact of 400 J be performed on glass balustrade. For verification purposes balustrade panel geometry was chosen consisting of both point- and continuous supports. From the finite element analysis of chapter 5, it was concluded that none of the continuous balustrade set-ups consisting only of point supported balustrade panels was able to resist the SABS [7] required impact loading. Consequently two balustrade set-ups consisting of both point- and continuous supported panels were identified to be tested in a verification laboratory test series.

This section describes the loading of each tested balustrade set-up.

The layout of the section is presented by means of a flow diagram in figure 6.16.

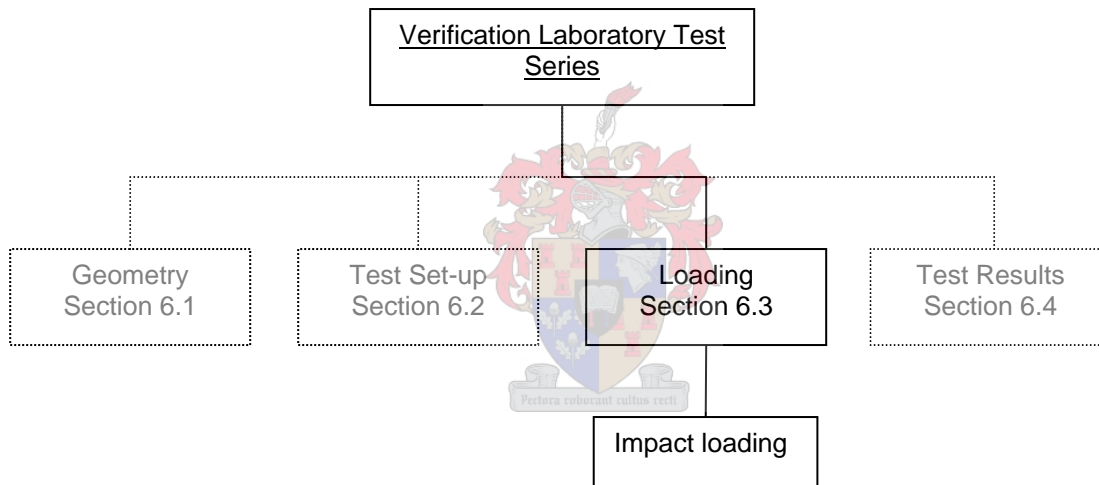


Figure 6.16. Flow diagram illustrating layout of the loading stage of the laboratory verification test series.

6.3.1 Impact loading

The finite element models of the balustrade set-ups, described in the previous chapter, consisted of three identical balustrade panels connected by means of a handrail. A finite element analysis determined each balustrade set-up's dynamic loading capacity and compared to the corresponding SABS [7] impact loading requirements. The required impact loading was simulated using the finite element software Abaqus [46], and consequently the magnitude of the impact force determined. As a result, balustrade set-ups which could sustain the required impact loading were identified.

Two balustrade configurations consisting of both point- and continuous supported balustrade panels were identified to be tested. The finite analysis of chapter 5 determined the loading capacity of the identified balustrade set-ups and compared it to the equivalent static impact force (see Table 5.25). It was concluded that both balustrade set-ups would be able to sustain the 400 J SABS 0160 [7] required impact force.

Having identified the impact energies the equivalent drop height was determined using the principals of conservation of energy. The drop height corresponding to an impact energy of 400 J was determined as follows:

Potential energy is defined as:

$$E_p = mgh \quad (6.1)$$

Where:

m = mass of impactor
g = gravitational acceleration
h = drop height

therefore:

$$400 \text{ J} = 30 \times 9.81 \times h$$

$$h = 1360 \text{ mm}$$

Table 6.4 presents the drop height of each tested balustrade setup

Table 6.4. Balustrade set-up impact force and impactor drop height

Designation	No. of panels	Panels used	Impact energy (Joule)	Impactor drop height (mm)
Set-up 1	3	1,3,4	400	1360
Set-up 2	3	2,3,4	400	1360

No measurements other than the impactor drop height were taken during the impact testing of the balustrade set-ups, as it was the sole purpose of the laboratory test series to verify impact force calculations, of the previous chapter.

6.3.2 Conclusion

The finite element procedure, of the previous chapter, was used to determine the dynamic loading capacity of the balustrade set-ups identified for the verification laboratory test series. Using the dynamic loading capacity of each balustrade set-up a sustainable impact force was determined, and consequently an impactor drop height.

The previous sections of this chapter concerned the geometry of the balustrade set-ups, test rig and the loading applied to each balustrade set-up. The following section presents the findings and test results of the verification laboratory test series.

6.4 TEST RESULTS

Introduction

The previous section determined the dynamic loading capacity of each balustrade set-up, and consequently the corresponding impact force that the set-up can resist. From the impact force an equivalent drop height was determined.

This section describes findings results of the testing of balustrade set-up.

The layout of the section is presented by means of a flow diagram in figure 6.17.

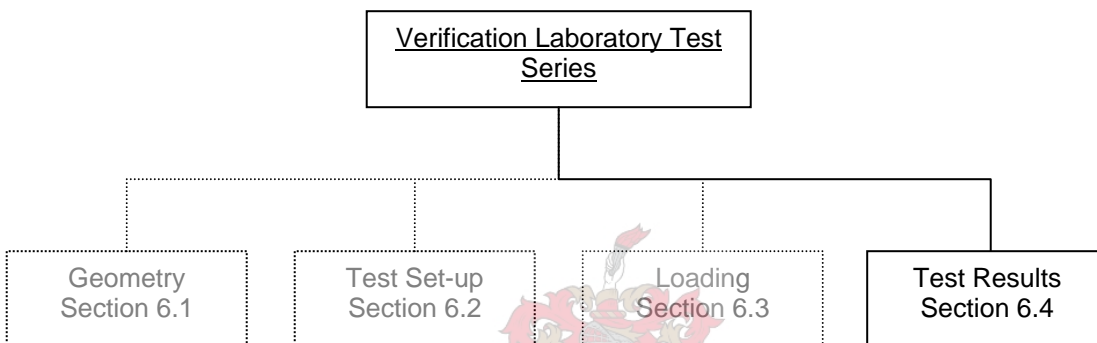


Figure 6.17. Flow diagram illustrating layout of the test results stage of the laboratory verification test series.

6.4.1 Test Results

Each balustrade set-up was loaded with the identified drop height, as described in the previous chapter. The drop height was monitored by means of a surveyor's measuring staff, positioned next to the impactor, as illustrated in figure 6.18.

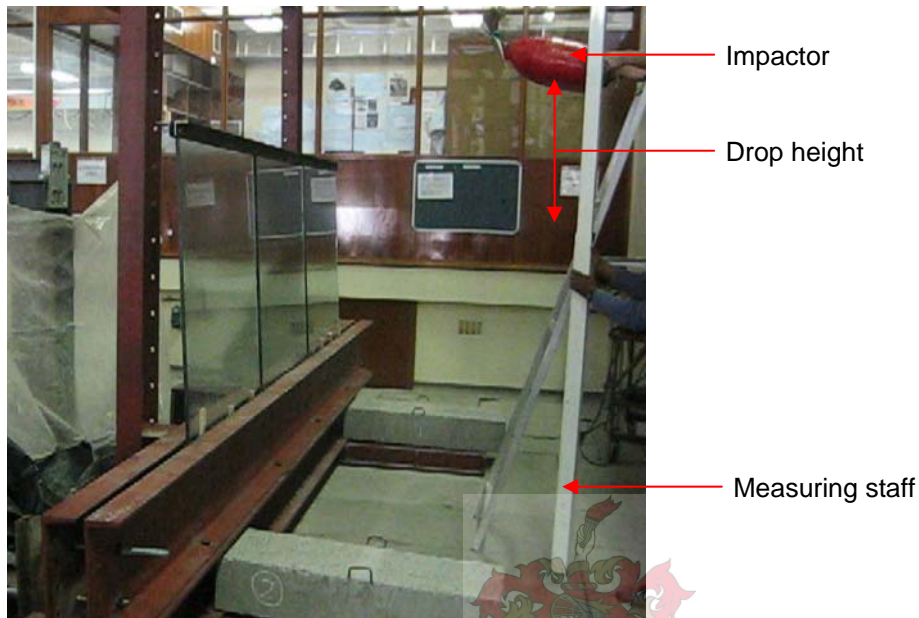


Figure 6.18. Impact of 15 mm balustrade set-up

The first balustrade set-up, presented in table 6.5, was the point supported 15 mm thick panel connected to the two continuous balustrade panels. Although the identified drop height was 1360 mm, the particular balustrade set-up was loaded in increments of 100 mm starting at 1 m. The increment loading was performed to enable the determination of the dynamic loading capacity in case of premature failure. However, since the first tested set-up reached the determined drop height, the rest of the balustrade test set-ups were loaded in one increment.

Following the first balustrade set-up, the second test set-up, which consisted of the point supported 12 mm thick panel connected to the two 15 mm continuous balustrade panels, was performed. The second balustrade set-up was loaded with its identified drop height in one increment.

Table 6.5. Balustrade set-up impact force and impactor drop height

Designation	No. of panels	Panels used	Calculated drop height	Tested drop height
			mm	mm
Set-up 1	3	1,3,4	1360	1360
Set-up 2	3	2,3,4	1360	1360

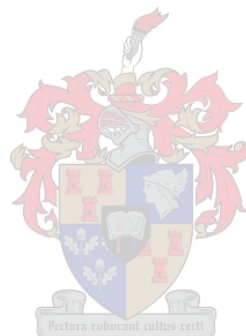
From table 6.5, it can be noted that each balustrade set-up was able to resist the finite element identified drop height. As the first balustrade set-up reached the identified drop height, the second set-up was not tested. Therefore, only two continuous balustrade set-ups were tested in the

laboratory test series, both of which were able to resist the identified drop height. Consequently, the finite element impact force calculations, of the previous chapter, were verified.

6.4.2 Conclusion

Each balustrade set-up was loaded with the identified drop height. The first balustrade set-up was loaded in increments of 100 mm starting at 1 m. The increment loading was performed to enable the determination of the dynamic loading capacity in case of premature failure. As the first tested set-up reached the determined drop height, the rest of the balustrade set-ups were loaded in one increment.

Both of the impact tested balustrade set-ups were able to resist the identified drop height, and consequently, the finite element impact force calculations were verified.



CHAPTER 7 IMPLICATIONS OF EXPERIMENTAL AND NUMERICAL RESULTS

Introduction

The implications of experimental and numerical results are discussed in this section. This section focuses predominantly on the test results obtained from the second laboratory test series, which consisted of both a finite element analysis and verification test series.

7.1 SATISFYING THE SABS REQUIREMENTS

This section discusses the results of both freestanding- and continuous balustrades under the following headings:

- Satisfying the SABS deflection requirements
- Satisfying the SABS static loading requirements
 - Concentrated loading
 - Distributed loading
- Satisfying the SABS dynamic loading requirements

7.1.1 Freestanding balustrades

A freestanding balustrade is a barrier where there are no vertical or horizontal supporting members, or balusters. Each glass panel is fixed to the structure along its bottom edge.

7.1.1.1 Satisfying the SABS Deflection requirements

Section 4.6 of SABS 0104 limits the maximum deflection of any (required loading 1.5A) loaded balustrade to 100 mm, regardless of location or loading type.

Where:

A = nominal accidental load as described in SABS 0160

Pectora robustant culius recti

From the SABS deflection requirements, only the 15 mm continuously supported balustrade panel adhered to the SABS 160 [7] deflection requirements for the grandstand-loading category. The rest of the 15 mm point- and continuously supported panels adhered to the deflection requirements for both the public- and domestic categories

7.1.1.2 Satisfying SABS Static loading requirements

Guidelines for the static load that balustrades must be able to sustain are given in SABS [7], and chapter 2. The summation of the guidelines is divided into the:

- Concentrated loading- and,
- Distributed loading requirements

Concentrated loading requirements

Concentrated force of 1 kN acting horizontally inward or outward over a 100x100 mm area for plate elements at the top of the guard or the most severe position;

Distributed loading requirements

Domestic application

Distributed horizontal force of 0.5 kN/m applied at the top of the guard and acting outward;

Places of public assembly

Distributed horizontal force of 1.5 kN/m applied at the top of the guard and acting outward;

Grandstands

Distributed horizontal force of 3.0 kN/m applied at the top of the guard and acting outward;

It was noticed that all the 15mm thick freestanding balustrade set-ups, regardless of connection type, adhered to the SABS 0160 [7] concentrated loading requirement. Although all the balustrade panels adhered to the SABS concentrated loading requirements, none of the freestanding balustrades, adhered to the SABS [7] required distributed loading for grandstands. Predominantly, only the 15 mm thick panels adhered to both the domestic- and public distributed loading requirements. . It was concluded that, if a glass balustrade was to be designed according to the SABS 0160 [7] static loading- and deflection requirements, none of the balustrade set-ups would be able to be used for a grandstand application.

7.1.1.3 Satisfying SABS Dynamic loading requirements

The guidelines set by the SABS [7] design standard in accordance with the testing procedures for the dynamic impact testing in glass balustrades requires that:

An impact of 400 J delivered by means of a 250 mm diameter bag filled with dry sand to a mass of 30 kg.

From the finite element analysis it was established that no 12- or 15 mm thick freestanding balustrade can withstand the 400 J impact load for a 0.8% probability of failure, regardless of connection type.

Between the South African handrailing and balustrading [19] - and South African loading standards [7], a glass balustrade has to adhere to deflection-, static loading and impact loading requirements. Only when all three of these requirements are satisfactory met, is a glass balustrade “safely” designed.

Comparing the result of the finite element analysis, in which different full scale freestanding balustrades were analysed, to the SABS requirements it was found that no freestanding balustrades was able to meet all the requirements. Although some freestanding balustrades were able to meet both the deflection- and static loading requirement, none of the balustrades was able to meet the SABS [7] impact loading requirement. The impact loading requirement is therefore the dominant load case.

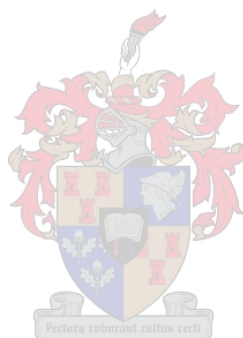
As none of the freestanding balustrades was able to meet the South African loading requirements, a handrail connecting 3 panels was introduced. The purpose of the handrail was to increase the loading capacity of the balustrade setup in order to meet the SABS [7] impact loading requirement.

7.1.2 Continuous balustrade

A continuous balustrade is a balustrade setup in which two or more freestanding balustrades are connected to one another by means of a handrail. From the freestanding balustrade results it was established that the SABS 0160 [7] impact loading requirement is the dominant load case. Therefore only the impact (dynamic) loading requirement is described for continuous balustrades.

7.1.2.1 Satisfying SABS Dynamic loading requirements

The introduction of the handrail, which connected 3 panels, dramatically increased the dynamic loading capacity of the balustrade setup. As a result, balustrade set-ups which could sustain the SABS [7] impact loading requirement were identified. It was concluded that both 12- and 15 mm thick continuously supported freestanding glass balustrades can only sustain the SABS [7] required impact load, when a minimum of three panels are connected by handrail with sufficient rigidity.



CHAPTER 8 CONCLUSIONS

Introduction

The present study was undertaken in order to investigate the behaviour of freestanding glass balustrades. A break down of the study is presented in figure 8.1. The study consisted of two laboratory test series, each playing a vital role. The first laboratory test series comprised of both a destructive test series and finite element analysis, the main purpose of which was to determine the material properties of toughened glass. The second laboratory test series focused on the determination of the loading capacity of various freestanding balustrade set-ups. A test series at the end of the investigation, verified the finite element results.

The objectives of the study were to:

1. Determine the static- and dynamic material properties of toughened glass.
2. Determine the static- and dynamic loading capacity of freestanding glass balustrades, which includes the influence of the following parameters:
 - Connection types and sizes
 - Addition of a handrail
3. To make recommendations to the existing design standards based on the results obtained from the study

The method used to attain these objectives is described in the following paragraphs, in which an overview is presented of each laboratory test series.

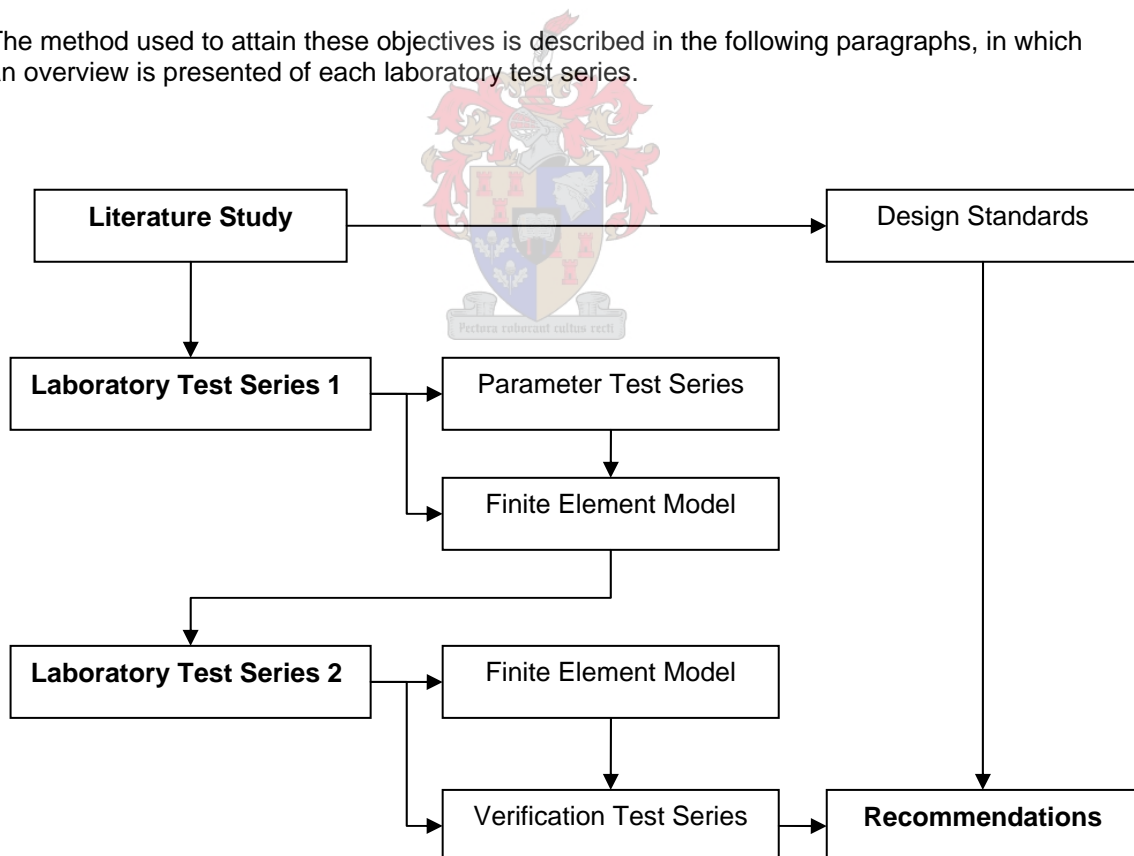


Figure 8.1 Breakdown of study

8.1 LITERATURE STUDY

The literature study identified the three standards vital to proper design and construction of freestanding glass balustrades. The three standards were:

- Standard for handrailing and balustrading
- Standard for safety glass classification and the
- Standard for loading requirements

As part of the literature study, each standard was compared to its British [12, 20, 22] and American [18, 23] counterpart. The conclusions of the literature study are presented under the respective standards.

8.1.1 Handrail and balustrading standard [SABS: 0104]

The handrailing and balustrading standard concerns the overall design of a balustrade, which is necessary to ensure the correct installation and construction thereof. Several standards including the South African [19], British [12] and American [18] were summarized and compared under their respective design-, handrail- and deflection requirements.

Comparing the South African handrailing and balustrading standard to its international counterparts, a lack of sufficient guidelines to ensure the safe design and construction of glass balustrades were established. The following topics, which require attention, were identified:

- Connection type to use with glass balustrade
- Handrail use and details (containment)
- Glass type to use
- Minimum glass thickness

It was further noted that most of the provided information is for informational purposes only, and as a result are left to the designer's discretion.

8.1.2 Material classification standard [SABS: 1263]

The classification of safety glass and its performance under accidental human impact has been undertaken since the development of the standard using a pendulum impact test set-up. A lead shot impactor has been used to represent the impulse generated by a human body impact. Since the development of the material classification standards, a new impactor based on a twin tyre set-up has been introduced internationally. From various investigations [8, 9, 10], it was determined that the twin tyre impactor does not impart as much energy onto the test sample, and it is recommended here that the lead shot impactor, as used by the South African standard [21], be left unchanged.

Another parameter that influenced the introduced impact energy is the drop height of the impactor. Numerous standards were investigated and consequently, the origin of the drop height and impact energies was identified. It was established that the drop heights originated from a human engineering chart, which was developed by safety experts [21]. Three different drop heights were initially introduced. It was noted that most of the standards retained these drop heights. Only the South African [21] and Australian [27] material classification standards use a single drop height.

In case the specimen fractures upon impact, the material classification standard requires the specimen to adhere to the safe breakage criterion. Breakage criterion from several standards was compared. It is established that the breakage requirements of South Africa [21] is identical to that of the American [22] and that of the British [23] with the exception of the particle count. As the particle count is an indication of the specimen's strength, it is consequently recommended that it be included into the South African material classification standard [21].

8.1.3 Loading standard [SABS: 0160]

When designing a glass balustrade the material need to be classified in accordance with SABS 1263 [21] and the balustrade needs to be able to resist both static- and impact loads as required by SABS 0160 [7].

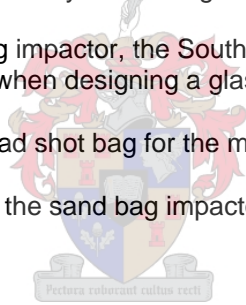
The South African material classification design standards were originally adopted from its American counterpart. The initial purpose of the standard was the classification of brittle materials when impact tested. A human impact was simulated using a pendulum impact test performed by a lead shot bag dropped from an identified height, based on a typical impact scenario. The material was classified as safety material if 1) the material did not break or 2) when broken adhered to the breakage requirement.

The purpose of the standard later evolved to include impact-loading requirements. Using the same procedure and impactor, different drop heights were introduced. These drop heights were introduced to represent different impact speeds at which a 45 kg teenager could strike a balustrade. Balustrades are therefore classified according to application and position. These classifications are part of the loading requirement and the balustrade needs to be designed to resist these loads. Most of the international standards [22, 23, 24] integrated the impact loading- and material classification requirement. Therefore, avoiding separate testing procedures.

The South African [21] standards failed to recognize this, and consequently introduced another impactor. The new impactor consists of a 250 mm diameter bag filled with sand to the weight of 30 kg. No evidence could be found that this impactor has ever been investigated with regards to reproducibility, repeatability or the magnitude of impulse generated.

With the introduction of the sand bag impactor, the South African [21] standards now require two separate tests to be performed when designing a glass balustrade. The two separate tests are:

- Pendulum impact using a lead shot bag for the material classification of the material and a
- Pendulum impact test using the sand bag impactor for the impact loading requirements



8.2 LABORATORY TEST SERIES 1

The first laboratory tests series comprised both a destructive test series, and a finite element analysis. The test series consisted of 37 scaled down toughened glass panels tested in out of plane bending, until failure. Four different connection types and three different panel thicknesses was investigated. Following the destructive test series, a finite element analysis determined each glass panel's fracture stress.

The laboratory test series was undertaken to determine:

- The loading capacity and influence of different connection configurations (hole size and thickness) and,
- The static- and dynamic material properties of toughened glass.

The results of the laboratory test series was used to determine the static- and dynamic loading capacity of full scale balustrade panels tested in laboratory test series 2.

8.2.1 Parameter test series

Specimen evaluation

After fracture, the fractured panels were examined. The taping of the glass panels on the compression side made the fracture pattern visible, as the tape kept the fractured pieces together. It was noticed that the fracture pattern propagates through the panel in a shockwave format, as well as in straight lines in all directions from the point of origin.

Wave propagation

Slower wave (lagging) propagation was noticed to be consistent with the dynamic loading rate. Fracture occurred closer to the support compared to the fracture origins produced by the static loading rate, which was verified when the average quadrant fracture origin of the different loading rates was compared.

Test measurements

During the laboratory testing of the panels, each panel's force and displacement was measured. The force was measured to determine each panel's bending capacity, while displacement was used to determine the elasticity modulus of the glass.

Level of Prestress

Prior to the testing of the panels, the level of prestress of each panel was determined using GASP technology. The variability in strength of glass caused by surface defects resulted in the testing of three identical panels per parameter. By comparing the highest level of prestress to the highest ultimate force of only the identical panels in a group, the impact of the level of prestress has on the capacity of the glass panel was noticed. In 8 out of the 11 groups, the panel with the highest level of prestress fractured at the highest ultimate force. The other group's failure was attributed to the presence of surface flaws. It was concluded that the strength of the glass panels were predominantly affected by both the level of prestress and presence of surface flaws.

Elasticity modulus

The measured force together with the linear gradient of actual displacement graph was used to determine each panel's elasticity modulus. The modulus of elasticity of glass was underestimated by 6.9% when compared to published values. The discrepancy in the test result was assigned to the unaccounted rotation of the test rig itself. Furthermore, an increase of 12.8% between the calculated static- and dynamic modulus was noticed.

8.2.2 Finite element analysis

Connection capacity

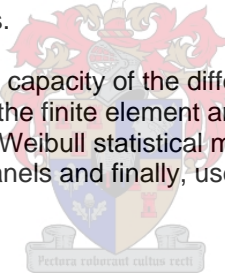
Before each panel's fracture stress was determined, a finite element analysis was performed to determine the structural capacity of each connection (type and size). Point- and continuously supported connection types were investigated.

For the point-supported panels, three different hole diameters were tested, together with three different panel thicknesses. Each connection type was loaded with a unit-distributed load, and the corresponding principal tensile strength determined. Each panel's calculated stress concentration factor (K_{tn}) was compared to similar stress concentration factors found in literature [38]. It was established that the predicted stress concentrations, from literature, were significant less than that of the calculated stress concentration factors. The decrease in the calculated stress concentration factors indicated an increase in capacity, between the non-chamfered- and chamfered holes. The predicted stress concentration factors overestimated the calculated stress concentration factors in some instances by up to 11.7%. The results reinforced the use of the finite element analysis.

For the continuously supported panels three different panel thicknesses were tested. A finite element analysis calculated each thickness' principal tensile stress. An increase in structural capacity with thickness was found to exist.

Finally, the principal tensile stress of both the point- and continuously supported panels was compared. An increase in structural capacity of 34% between the continuously- and point-supported panels was noted. The finite element analysis was performed to determine the structural capacity and influence of different connections, as well as to determine each tested panel's corresponding fracture stress.

Having determined the influence and capacity of the different connection types and sizes the next section describes the results of the finite element analysis in which each tested panel's fracture stress was determined. The Weibull statistical model was used to represent the failure strength of the tested glass panels and finally, used to predict the capacity of full-scale glass balustrades.



Loading rate effect

A high variability of strength in glass resulted in the employment of the Weibull statistical model to present the failure strength of the tested glass panels. The difference in panel geometry resulted in different Weibull modules being calculated for the panels with- and without holes.

The increase in strength, with increase in loading rate was noticed in both probability distributions (panels with- and without holes). An increase of 10% in mean strength from the static- to dynamic load rate was noticed for the distribution of the holed panels.

Another parameter common to both distributions (panels with- and without holes) was the grouping of the mean probability of failure of the quasi-static and dynamic loading rates, which could be an indication of the material strength asymptote.

Comparing the two distributions, a decrease in modulus, and mean strength between the panels with- and without holes was noticed. Although the hole confined the fracture origin to a certain area, resulting in a smaller variability of results, the drilling of the hole brought about a decrease in mean strength.

Volume effect

To account for the difference in strength prediction for the size effect between the test- and actual balustrade panels, the size of the panels was included in the Weibull distribution. The specimen size effect occurs because the size of the critical defect, on average, increases with increasing area or volume. With the increase in the size of the panels, the probability of failure decreased by 20%.

8.3 LABORATORY TEST SERIES 2

The second laboratory tests series comprised of both a finite element analysis, and a verification laboratory test series. The finite element analysis was undertaken to determine and identify the:

- The loading capacity of freestanding- and continuous balustrades and ,
- Balustrade set-ups which could sustain the SABS [7] loading requirements.

Two different panel thicknesses together with three different connection types were investigated, and the influence of each quantified. The outcome of the finite element analysis identified the balustrade set-ups that were tested in a second laboratory test series.

8.3.1 Finite element analysis

Using the static- and dynamic material properties, determined in the first laboratory test series, the loading capacity of freestanding balustrade panel's was determined and compared to the SABS [7] loading requirements. From the dynamic impact analysis, on freestanding glass balustrades, it was noted that none of the balustrade panels could sustain the impact requirements as set out in the South African loading code [7]. It was consequently decided that similar impact tests be performed on continuous balustrades (handrail connected freestanding balustrades).

From the freestanding balustrade impact analysis, it was clear that the dynamic impact-loading requirement was the dominant load case, and that a balustrade set-up has to be designed to sustain the 400 J South African impact loading requirements [7]. Consequently, all continuous balustrade set-ups were loaded with a unit point load applied to the middle panel in the top centre of the panel. A linear static analysis determined each balustrade set-up's stiffness and dynamic loading capacity.

Before the dynamic loading capacity of each balustrade configuration was determined, the influence of the addition of a handrail on continuous balustrades was investigated. Two parameters were investigated which directly influenced the capacity of continuous balustrades. They were:

- Number of connected panels
- Stiffness of handrail

Stiffness of handrail

Three different handrail dimensions were investigated to determine the influence of the stiffness of the handrail on the dynamic loading capacity of the continuous balustrade set-up. An increase of the equivalent stiffness factor with an increase in handrail dimension was noted, which was attributed to the increase in stiffness of the handrail. Furthermore, it was noted that only the 90x90 mm handrail enforces the total contribution of all three balustrade panels (unpractical).

Number of connected panels

Three different numbers of connected panels together with three different handrail dimensions were investigated to determine the influence of the number of connected panels on the dynamic loading capacity of the continuous balustrade set-up. The influence of the number of panels and handrail stiffness was presented by means of a contribution factor. The contribution factor represents the percentage of the connected number of panels contributing to the stiffness of the set-up, and was found to be directly related to the stiffness of the handrail. A decrease in contribution with increase number of connected panels was noted.

Finally, the dynamic loading capacity of the different balustrade set-ups was determined and compared to the corresponding SABS [7] impact loading requirements. The SABS [7] required 400 J impact was simulated using the finite element software Abaqus [46], and consequently a resultant impact force determined. The dynamic loading capacity was determined for different balustrade set-ups consisting of three connected balustrades for 12- and 15 mm thicknesses.

Comparing the dynamic loading capacity ($0.8\%P_f$) of each balustrade set-up to the SABS [7] required impact loading, it was found that only the continuously supported balustrades were able to sustain the required loading. None of the point supported balustrades could sustain the impact loading, for a 0.8% probability of failure, regardless of handrail stiffness or panel thickness. In addition, 2 set-ups consisting of both point- and continuous supported balustrade panels were identified, for verification testing purposes.

8.3.2 Verification test series

The purpose of the second laboratory test series was to verify the finite element analysis, and ultimately conclude the investigation into the loading capacity of glass balustrades.

The finite element analysis, of the previous chapter, identified the full-scale balustrade panels which could resist the SABS [7] required impact loading. However, since none of the freestanding balustrade panels were able to resist the required SABS [7] impact load, the laboratory verification test series only included continuous balustrade set-ups. A handrail of dimension 50x50 mm was chosen to connect the different balustrade panels. The geometry of the balustrade panels included two 15 mm thick continuously supported balustrade panel and two point supported balustrade panels, one 12- and one 15 mm thick. 2 different continuous balustrade set-ups were tested.

Due to the ease of construction, the sand bag impactor was used to simulate the required human impact; however the stiffness was altered to be the same as that of the lead shot impactor.

The finite element procedure, of the previous chapter, was used to determine the dynamic loading capacity of each of the balustrade set-ups. Using the dynamic loading capacity of each balustrade set-up a sustainable impact force was determined, and consequently an impactor drop height.

Each balustrade set-up was loaded with the identified drop height. The first balustrade set-up was loaded in increments of 100 mm starting at 1m. The increment loading was performed to enable the determination of the dynamic loading capacity in case of premature failure.

Both of the impact tested balustrade set-ups were able to resist the dynamic impact load, and consequently, the finite element results were verified.

CHAPTER 9 RECOMMENDATIONS

On the basis of the foregoing conclusions, the following recommendations are made.

9.1 DEVELOPMENT OF SABS GUIDELINES

The literature study of chapter 1 identified the areas of the standards, relevant to the design of freestanding glass balustrades, which required further attention. This section addresses each of these areas.

9.1.1 Standard for handrailing and balustrading

9.1.1.1 Connection type to use with glass balustrade

The South African handrail and balustrading standard fails to provide any guidelines to which connection type to use.

It is therefore recommended that guidelines in the form of a typical technical drawing be provided in the South African handrailing and balustrading standard. The drawings should be as informative as possible and should include both continuous- and point support systems. It is recommended that a finite element analysis should be performed when non-conventional connection types are used. The purpose would be to draw the attention of designers to the importance of connection design.

9.1.1.2 Handrail use and details

The handrail requirement is addressed under the following headings.

- Loading requirement
- Containment requirement



9.1.1.3 Loading requirement

The results of the finite element analysis in which freestanding glass balustrades were analysed indicated that freestanding balustrades are unable to resist the SABS [7] required impact loading. Consequently a handrail which connected 3 freestanding balustrades was added. It was concluded that freestanding glass balustrades can only sustain the SABS required impact load, when a minimum of three panels are connected by a sufficiently rigid handrail.

Therefore, the recommendation of the use of a handrail of Section 5.5.5 of SABS [17] should be altered so that the use of a handrail connecting a minimum of 3 panels is mandatory. The handrail stiffness should be defined as a function of the balustrade stiffness to guarantee load transfer to adjacent panels.

While, at the same time, the required impact loads are considered to be conservative. Relaxing the current impact loading requirements, can result in freestanding balustrades meeting the impact loading strength requirements. However, the inclusion of a handrail into a glass balustrade system can not be only based upon only loading requirements. Therefore the containment of balustrades is recommended.

9.1.1.4 Containment requirement

The primary function of a balustrade is to prevent persons or objects from passing through or over the balustrade onto an adjacent lower level, which indicates that balustrades are usually situated in areas where human safety is of concern. Balustrades should therefore be able to provide containment at all times, before or even after failure. Since toughened glass fractures into small glass cubes, the material in itself provides no containment. A freestanding balustrade made of toughened glass will provide no means of containment once it has fractured. Containment should therefore come from the balustrade system.

A handrail, connecting a minimum of three balustrades, will provide containment even in the case of fracture. It is therefore recommended that a handrail requirement be introduced into the South African handrailing and balustrading design standard. The handrail should connect a minimum of three balustrade panels and should be stiff enough to incorporate the loading capacity of the adjacent panels. The introduction of the handrail will address both:

- Impact loading requirement and
- Post failure containment requirement

9.1.1.5 Glass type and thickness

Toughened glass is inherently five times stronger than ordinary annealed glass. In addition, when toughened glass fails, it fractures into small relatively harmless “sugar cubes”.

For strength and safety reasons, it is recommended that toughened glass be used in glass balustrades. This is to meet the SABS 0160 [7] loading requirements and ensure the safety of the person impacting a glass balustrade.

It is also recommended that glass be laminated when used in a balustrade at a dangerous height. Upon impact, the toughened glass fails and fractures into small pieces; however, it does not stop the falling glass from injuring people below. Laminated glass will ensure that the fractured glass pieces remain together and at the same time provide post failure containment.

9.1.2 Standard for loading requirements and material classification

9.1.2.1 Integration of material classification and loading requirements

The South African material classification design standards were originally adopted from its American counterpart. The initial purpose of the American [18] standard was the classification of brittle materials when impact tested. The purpose of the standard later evolved to include impact-loading requirements. Using the same procedure and impactor, different drop heights were introduced. Balustrades are therefore classified according to application and position. These classifications are part of the loading requirement and the balustrade need to be designed to resist these loads. Most of the international standards [22, 23, 24] integrated the impact loading- and material classification requirement. Therefore, avoiding separate testing procedures.

The South African [21] standards failed to recognize this, and consequently introduced a brand new impactor. The new impactor consists of a 250 mm diameter bag filled with sand to the weight of 30 kg. Although the ease and low cost of construction of the sand bag makes it a user friendly impactor, the reproducibility and repeatability of the impactor is questioned. No two sand bag impactors would deliver the same amount of energy, as the fabrication thereof is too variable of nature. At the same time, two different impact tests are required with two different impactors in different standards.

It is therefore, recommended that the lead shot bag be used for both the material classification and impact loading requirements of glass balustrades. This would eradicate the need for two destructive tests and at the same time integrate these two requirements into a single test.

9.1.2.2 Impact loading requirements

The impact loading requirement is addressed under the following headings.

- Differentiation of balustrade application
- Human engineering chart
- Movement Space

9.1.2.2.1 Differentiation of balustrade application

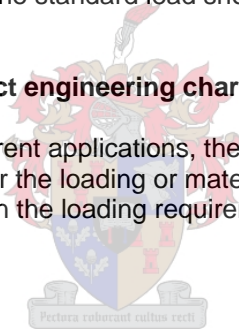
The application of glass balustrades vary over a wide spectrum and the current use of a single specification of 400 J is an over generalization and considered to be conservative. It is recommended that some form of differentiation be made which recognizes different balustrade applications as for the static loading requirements. The specifications for the static load on balustrades are divided into the following applications:

- Domestic-
- Places of public assembly and
- Grandstands

The implication of the project results is that similar criteria should be developed for balustrade designs in terms of dynamic impact on balustrades. Therefore, differentiation of the load conditions can be made for glass balustrades used in the domestic, public places of assembly and grandstands. Each category would be accompanied by an identified drop height and corresponding impact energy using the standard lead shot impactor.

9.1.2.2.2 Inclusion of human impact engineering chart

Together with the generation of different applications, the human engineering data graph (figure 9.1) must be included in either the loading or material classification standard. This would enable a designer to decide on the loading requirement at a specific location.



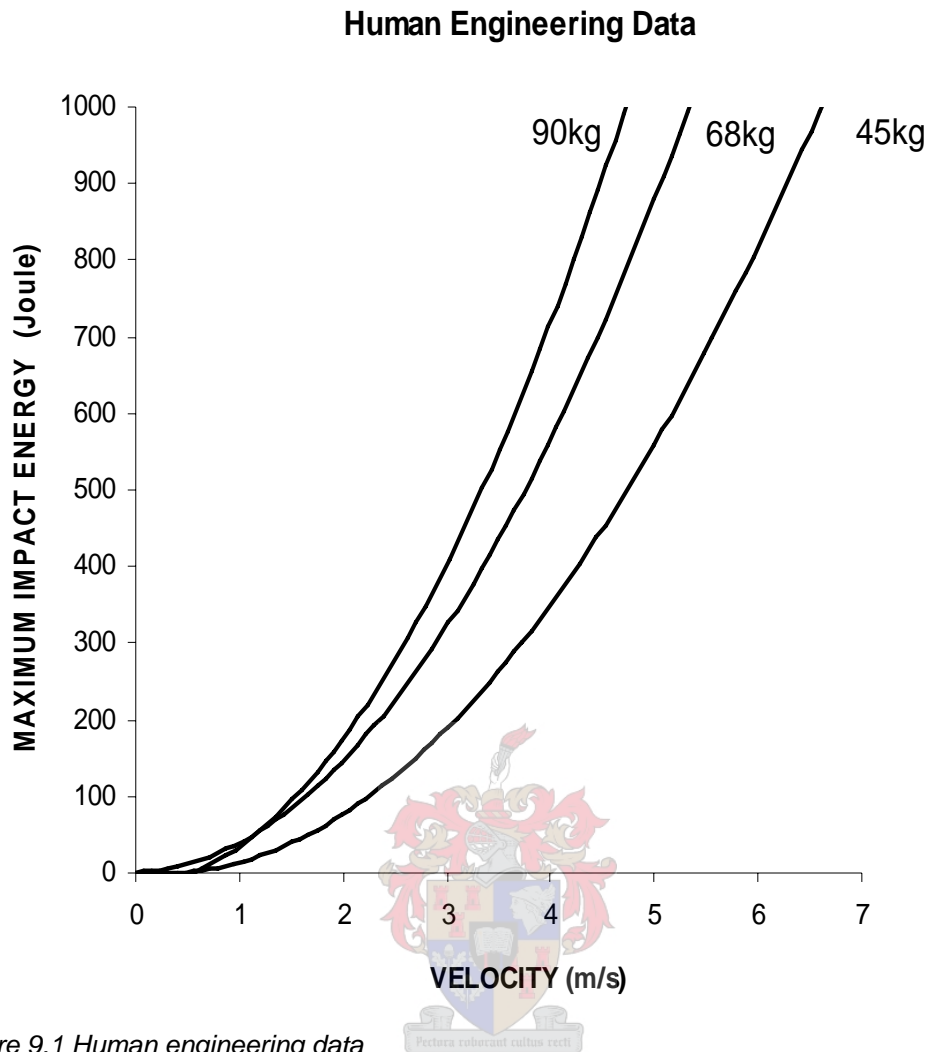


Figure 9.1 Human engineering data

9.1.2.2.3 Movement space

The investigation into quantifying the value of the dynamic human impact that the glass balustrades must be able to sustain in the above mentioned locations must incorporate various external factors.

While some balustrade panels might be at risk to human impact in a certain application, others might not. It is therefore, unnecessary for all panels to be subjected to the same design requirements. For example, a balustrade guarding the side of a 2 m wide passage is unlikely to be impacted throughout its lifetime, as apposed to a balustrade guarding the end of a 10m passage.

Situations should be identified in which:

- Limited acceleration path exists
- Unlimited acceleration path exists

9.2 FURTHER RESEARCH

From the results of the project it was concluded that no 12- or 15 mm thick freestanding glass balustrade is able to resist the SABS 0160 [7] impact loading. A new set-up based on a number of freestanding balustrade panels connected by handrail was investigated, and found to have increased the loading capacity. Since not all possibilities were covered by this study, further work is necessary to:

HANDRAIL

- Investigate the influence of different handrail connection types on the loading capacity of a continuous balustrade set-up
- Investigate the influence of different handrail end connection types (i.e. tied to structure)

LOADING

- Investigate the influence of side balustrade panel impact on the loading capacity of a continuous balustrade set-up
- Investigate the influence of various impact forces on balustrades

CONNECTION

- Investigate intelligent connection types. (i.e. ductile impact absorbing connections)
- Investigate the influence of clamping forces (localized pressure) arising from point fixings on the loading capacity of glass balustrades.

In order to extend the scope, it would be interesting to consider the influence of using laminated glass (annealed and toughened) balustrade panels. The lamination of different thicknesses glass would increase the loading capacity of the balustrade and provide post-failure material containment upon fracture.



REFERENCES

PUBLICATIONS

1. Wigginton, M. (1996), *Glass in Architecture*, Phaidon Press, London
2. Hess, R. (2000), Structural Engineer ETH/SIA/M.ASCE, Glasconsult, 8142 Uitikon, Switzerland
3. Campagno, A. (1995), *Intelligent Glass Facades*, Buxuuser, Basel
4. Dawson, S. (2001), *Glass at the cutting edge*, *The Architectural Review*
5. Callister, W.D., *Material Science and Engineering an Introduction*, Fifth edition
6. Du Preez, P. and Wium, J. (2004), *Human Impact on Glass Balustrades*, University of Stellenbosch
7. SABS:0160 (1989), *The General Procedures and Loadings to be adopted in the design of buildings*, South African Standard
8. Serruys, F. (1999), CEN- Impact Test PrEN:12600, Glass Processing Days Conference
9. Oketani, Y. (2003), *Experimental Study of Shot Bag Impactors for International Standardization*, Glass Processing Days Conference
10. Jacob, L. (2003), *ISO safety glass impact test developments*, Glass Processing Days
11. Foss, R. (1999), *Safety Glass Testing: Human Head Impactor Simulation by Dynamic Transient Analysis*, Glass Processing Days Conference
12. BS 6180 (1999), *Code of Practice for Barriers in and About Buildings*, British Standards Institute
13. Carré, H. and Daudeville, L. (1999), *Load Bearing Capacity of Tempered Structural Glass Plates*, *Journal of Engineering Mechanics*
14. Bernard, F. and Daudeville, L. (2002), *Finite Element Computation of Residual Stresses Near Holes in Toughened Glass Plates*, *Glass Technology vol 43C*
15. Schneider, S. (2001), *Glass Strength of Annealed and Tempered Structural Glass in the Area of Drilled Holes*, Glass Processing Days Conference
16. Siebert, B. (2003), *Calculation of Point Bearings for Glass as Load Bearing Element in Structural Engineering*, Glass Processing Days Conference
17. SABS 0137 (2002), *The Installation of Glazing in Buildings*, South African Standard
18. CPSC 16 CFR 1201 (1977), *Safety Standard for Architectural Glazing Materials*, USA Safety Performance Specifications and Methods of Test, Code of Federal Regulations
19. SABS 0104 (1995), *Handrailing and Balustrading Safety Aspects*, South African Standard
20. BS 6399 (1982), *Code of Practice for Dead and Imposed Loads*, British Standards Institute

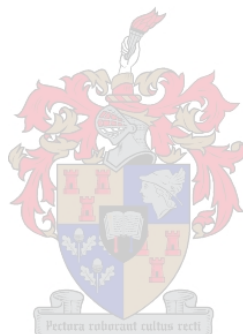
21. SABS 1263 (2002), Safety and security materials for buildings, part 1: safety performance of glazing materials under human impact, South African Standard
22. BS 6206 (1981), British Standard Specification for Impact Performance Requirements for Flat Safety Glass and Safety Plastics for use in Buildings, British Standards Institute
23. ANZI Z97.1 (1994), Safety Performance Specifications and methods of test Safety Glazing Materials used in Buildings, American National Standard
24. prEN 12600 (2000), Glass in Building- Pendulum test- Impact test method and classification for flat glass, European Draft Standard
25. Popov, Engineering Mechanics of Solids, Second Edition, Prentice Hall
26. Jacob, L. (2001), A Critical Review of Impact Testing and Classification of Safety Glass for Use in Buildings, Glass Processing Days Conference
27. AS 2208 (1996), Safety Glazing Materials in Buildings, Australian National Standard
28. Grenet, L. (1899). Thermal tempering of glass, Bull.Soc.Enc.Nat.,Paris, 5(4), 838-848;
29. ASTM C 1048 (1997), Standard Specification for Heat Treated flat glass- Kind HS, Kind FT coated and uncoated glass
30. Carré, H. and Daudeville, L. (1996), Simulation of the Thermal Tempering of a Glass Plates: Inner- and Edge Residual Stresses
31. Griffith, A. (1920), The Phenomena of Rupture and Flow in Solids, philosophical transcript, royal soc., A221, 163-198
32. ASTM C 158 (2002), Strength of Glass by Flexure (Determination of modulus rupture)
33. South African Steel Construction Handbook, Fifth edition, Table 5.19 pg 5.70
34. Pieterse's Stress Concentration Factors, Second edition
35. ASTM C 1279 (2000), Non Destructive Photoelastic Measurements for Non-Destructive Photoelastic Measurements of Edge and Surface Stresses in Annealed, Heat Strengthened, and Fully-Tempered Flat Glass
36. Timoshenko, S.P. and Goodier, J.N. (1951) Theory of elasticity, McGraw-Hill, New York
37. Howland, R.C.J. (1929-30), stresses in the Neighbourhood of a Circular Hole in a Strip under Tension, Phil.Trans.Roy.Soc. London A, Vol.229, p.67
38. Goodier, J.N. and Lee, G.H. (1941), Influence of Circular and Elliptical Holes on Transverse Flexure of Elastic Plates, Structural Eng., Vol.22, p.69
39. Weibull, W.A. (1951), A Statistical Distribution Function of Wide Applicability, Applied Mechanics, 18,293-297
40. prEN 12603 (2002), Glass in Buildings-Determination of the Bending Strength of Glass- Procedures for Goodness of Fit and Confidence Intervals for Weibull Distributed Data
41. Maurizio F. (2004), Probabilistic Assessment of the Bending Strength of Chemically and Thermally Tempered Glass Specimens, University of Piza

INTERNET RESOURCES

42. GSA Armourplate, smart glass specification, Balustrade Specification, www.smartglass.co.za/technical/balustrade
43. Pilkington glass, www.pilkington.com
44. Diana 9, Finite Element Analysis, Release Notes Release 9, www.TNODiana.com
45. Abaqus 6.4 Student Edition, Finite Element Analysis, Documentation, www.Abaqus.com
46. Automobile windshields
www.madehow.com/images/hpm_0000_0001_0_img0021.jpg&imgrefurl=http://www.madehow.com/Volume-1/Automobile-Windshield.html

PERSONAL CORRESPONDENCE

47. Liebenberg, M. (2005), LC Consulting Structural Engineers, Cape Town
48. Wright, N. (2005-2006), Nick Wright Consulting
49. Pote, M. (2005-2006), Glass South Africa



APPENDIX A

This section illustrates each tested panel's hole, fracture origin and magnified fracture origin. Illustrations are arranged according to test.

Test 1, Panel#16



Figure A1.1 Panel#16



Figure A1.2 Hole in panel

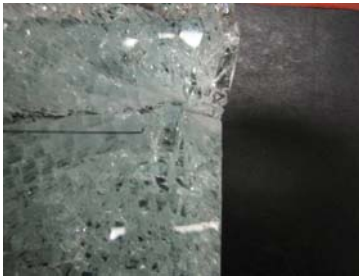


Figure A1.3 Fracture origin



Figure A1.4 Magnified



Test 2, Panel#1



Figure A2.1 Panel#1

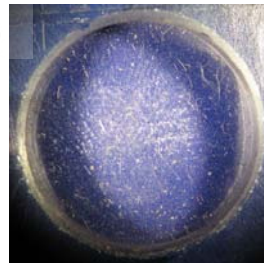


Figure A2.2 Hole in panel



Figure A2.3 Predicted fracture origin



Figure A2.4 Actual fracture origin

Test 3, Panel#15



Figure A3.1 Panel#15

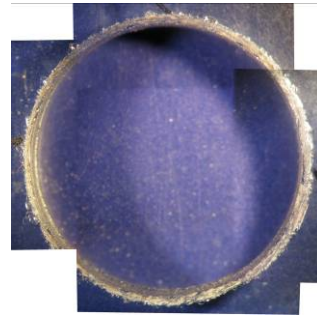


Figure A3.2 Hole in panel

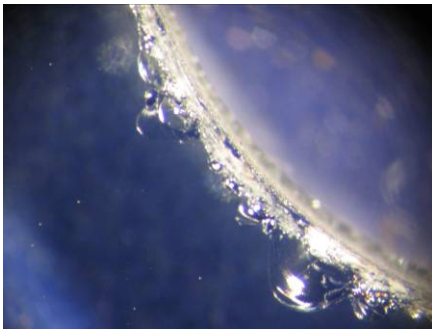


Figure A3.3 Predicted fracture origin



Figure A3.4 Actual fracture origin



Test 4, Panel#30



Figure A4.1 Panel#30

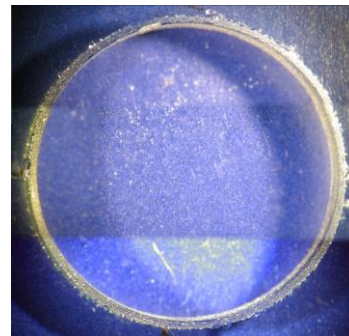


Figure A4.2 Hole in panel

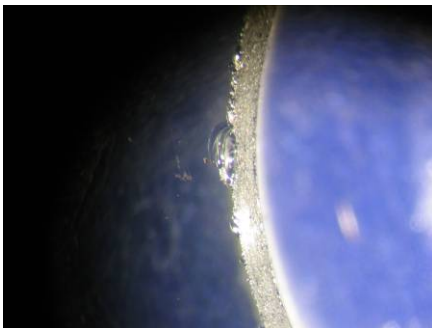


Figure A4.3 Predicted fracture origin



Figure A4.4 Actual fracture origin

Test 5, Panel#33



Figure A5.1 Panel#33

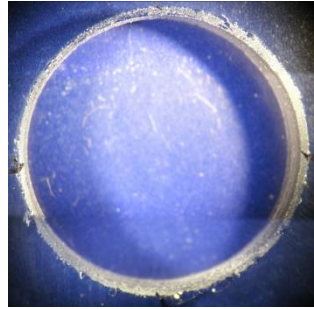


Figure A5.2 Hole in panel

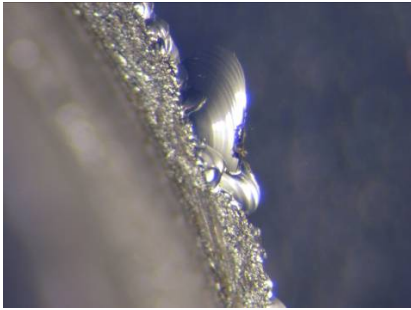


Figure A5.3 Predicted fracture origin



Figure A5.4 Actual fracture origin



Test 6, Panel#27

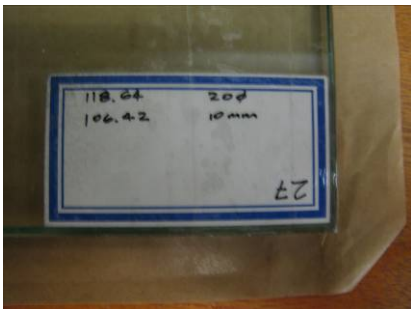


Figure A6.1 Panel#27

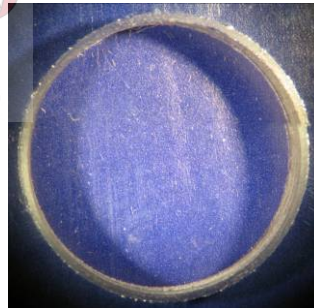


Figure A6.2 Hole in panel

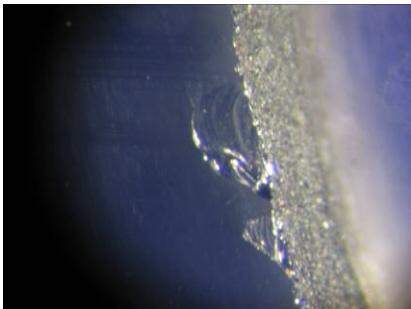


Figure A6.3 Predicted fracture origin



Figure A6.4 Actual fracture origin

Test 7, Panel#5

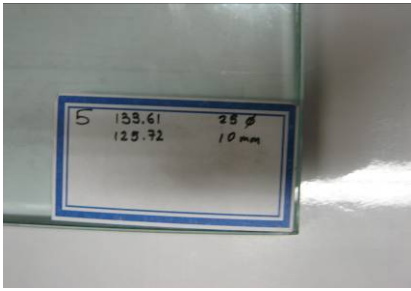


Figure A7.1 Panel#5

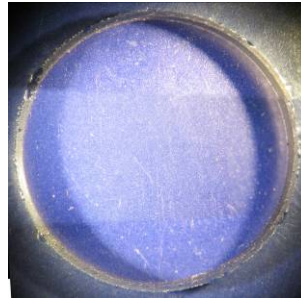


Figure A7.2 Hole in panel

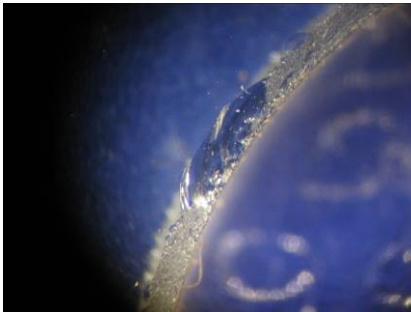


Figure A7.3 Predicted fracture origin



Figure A7.4 Actual fracture origin

Test 8, Panel#8

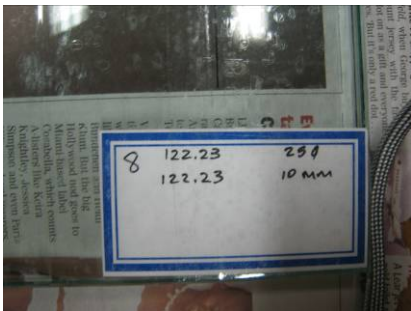


Figure A8.1 Panel#8

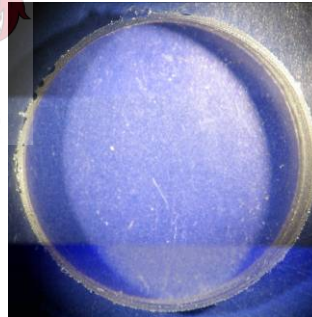


Figure A8.2 Hole in panel

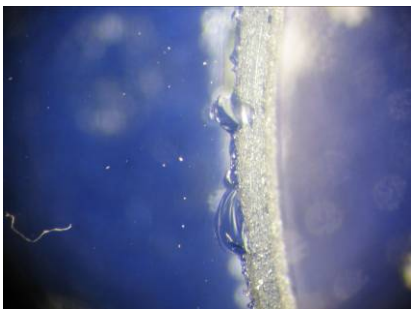


Figure A8.3 Predicted fracture origin



Figure A8.4 Actual fracture origin

Test 9, Panel#28



Figure A9.1 Panel#28

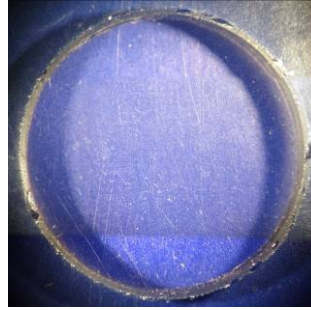


Figure A9.2 Hole in panel

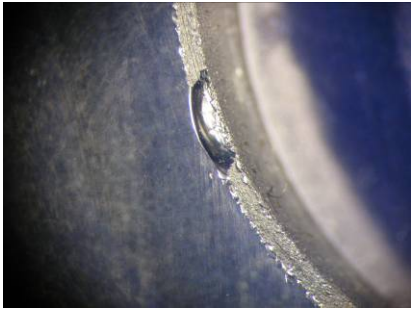


Figure A9.3 Predicted fracture origin



Figure A9.4 Actual fracture origin



Test 10, Panel#10



Figure A10.1 Panel#10

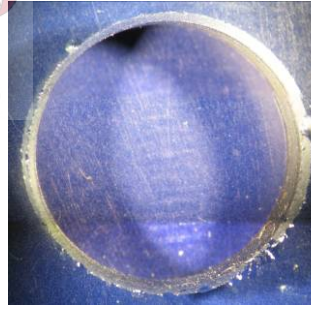


Figure A10.2 Hole in panel

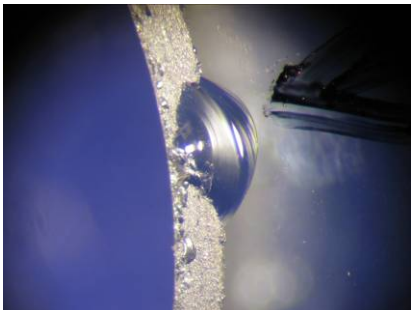


Figure A10.3 Predicted fracture origin



Figure A10.4 Actual fracture origin

Test 11, Panel#11

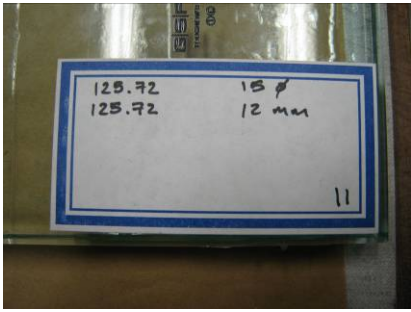


Figure A11.1 Panel#11

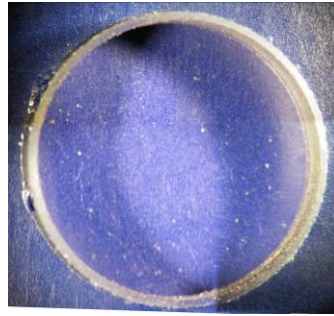


Figure A11.2 Hole in panel

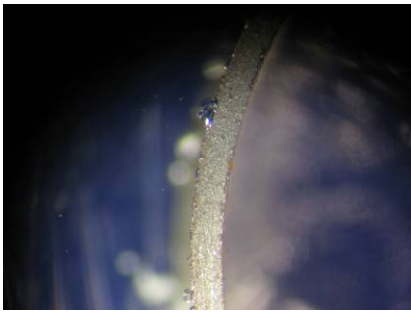


Figure A11.3 Predicted fracture origin



Figure A11.4 Actual fracture origin



Test 12, Panel#36



Figure A12.1 Panel#36

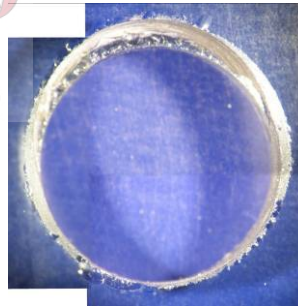


Figure A12.2 Hole in panel



Figure A12.3 Predicted fracture origin



Figure A12.4 Actual fracture origin

Test 13, Panel#18



Figure A13.1 Panel#18

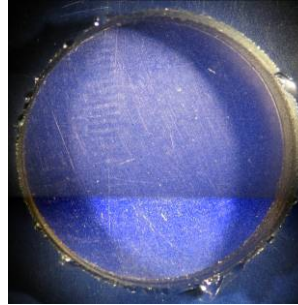


Figure A13.2 Hole in panel

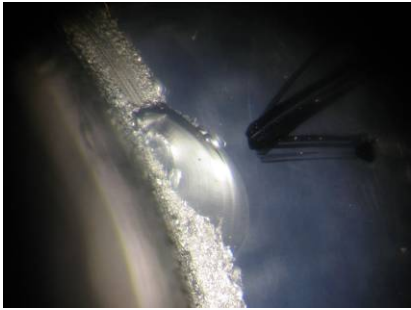


Figure A13.3 Predicted fractured origin



Figure A13.4 Actual fractured origin



Test 14, Panel#19

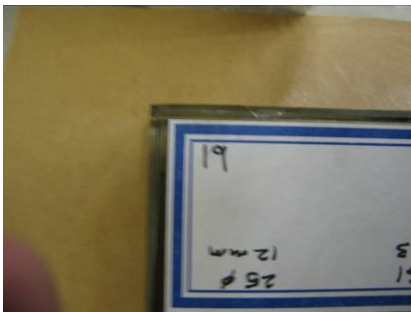


Figure A14.1 Panel#19

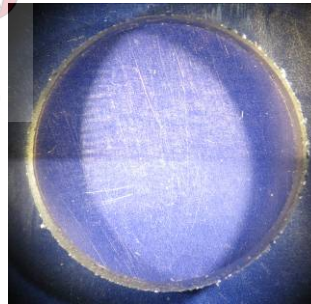


Figure A14.2 Hole in panel

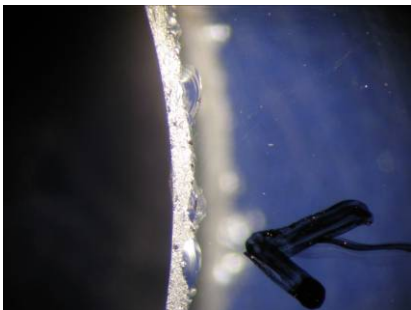


Figure A14.3 Predicted fracture origin



Figure A14.4 Actual fracture origin

Test 15, Panel#20



Figure A15.1 Panel#20

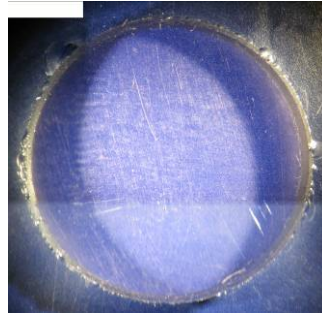


Figure A15.2 Hole in panel

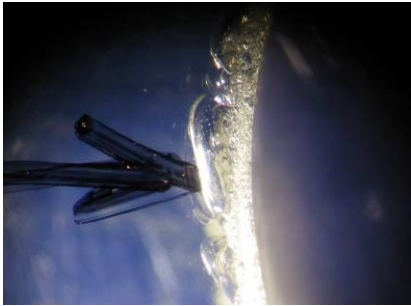


Figure A15.3 Predicted fracture origin



Figure A15.4 Actual fracture origin



Test 16, Panel#2



Figure A16.1 Panel#2

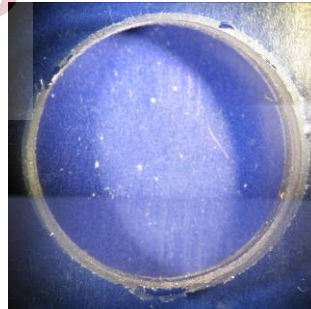


Figure A16.2 Hole in panel

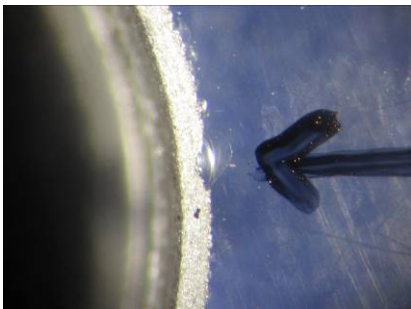


Figure A16.3 Predicted fracture origin



Figure A16.4 Actual fracture origin

Test 17, Panel#12



Figure A17.1 Panel#12

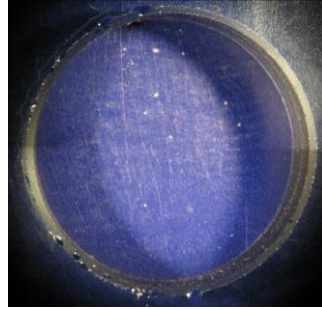


Figure A17.2 Hole in panel



Figure A17.3 Predicted fracture origin

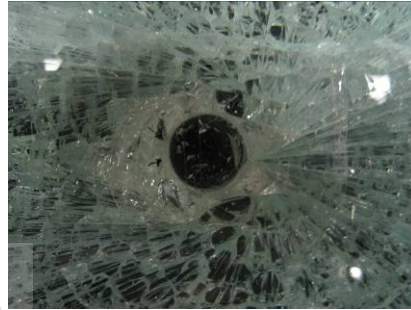


Figure A17.4 Actual fracture origin



Test 18, Panel#9

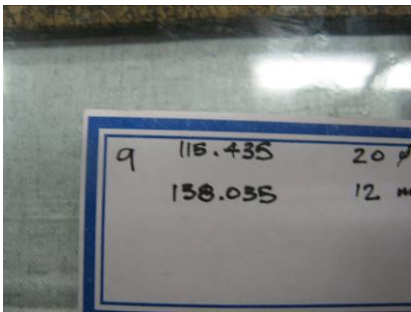


Figure A18.1 Panel#9

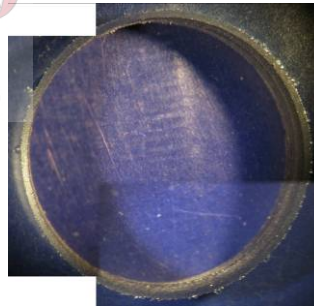


Figure A18.2 Hole in panel

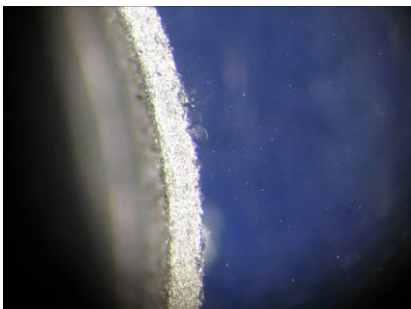


Figure A18.3 Predicted fracture origin



Figure A18.4 Actual fracture origin

Test 19, Panel#34

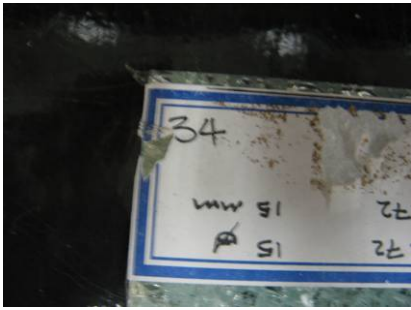


Figure A19.1 Panel#34

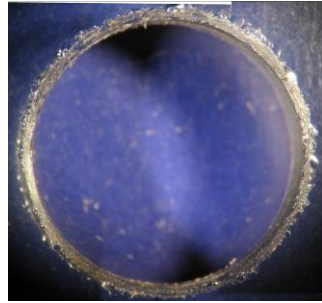


Figure A19.2 Hole in panel

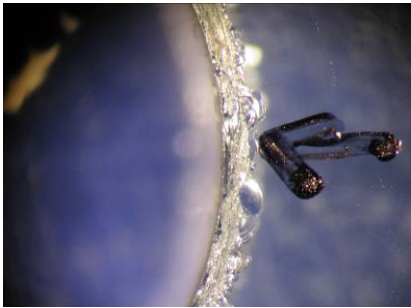


Figure A19.3 Predicted fracture origin



Figure A19.4 Actual fracture origin

Test 20, Panel#6

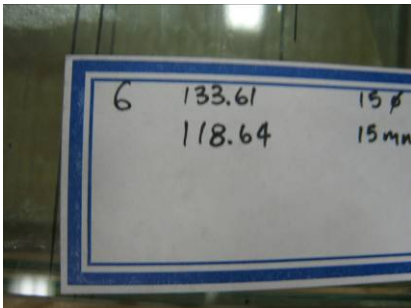


Figure A20.1 Panel#6

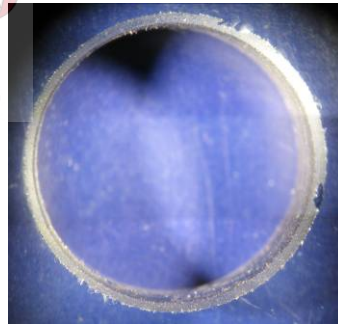


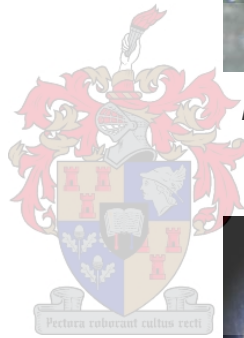
Figure A20.2 Hole in panel



Figure A20.3 Predicted fracture origin



Figure A20.4 Actual fracture origin



Test 21, Panel#7

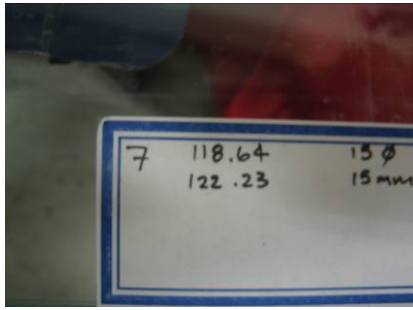


Figure A21.1 Panel#7

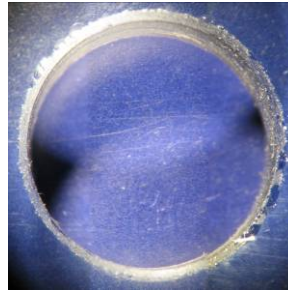


Figure A21.2 Hole in panel

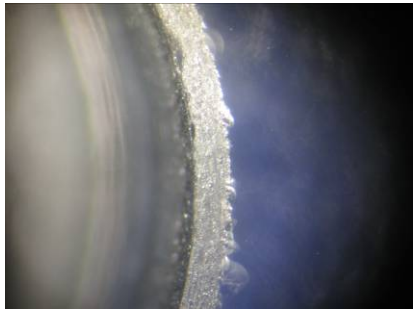


Figure A21.3 Predicted fracture origin



Figure A21.4 Actual fracture origin



Test 22, Panel#24



Figure A22.1 Panel#24

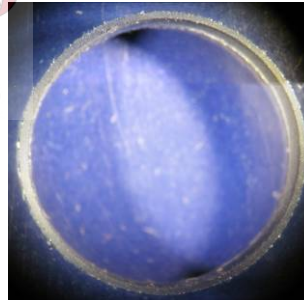


Figure A22.2 Hole in panel

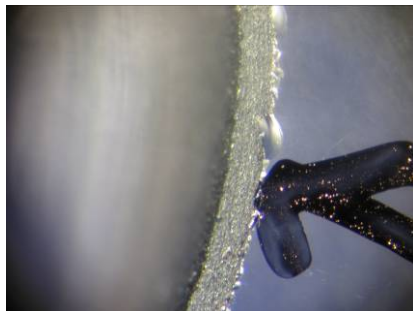


Figure A22.3 Predicted fracture origin



Figure A22.4 Actual fracture origin

Test 23, Panel#23

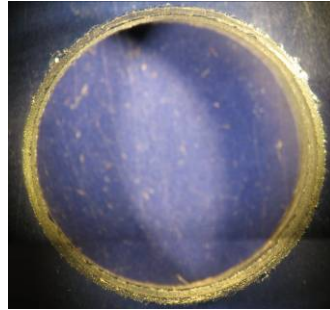
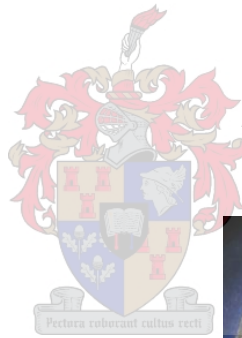


Figure A23.2 Hole in panel

Figure A23.1 Panel#23

Figure A23.3 Predicted fracture origin

Figure A23.4 Actual fracture origin



Test 24, Panel#35



Figure A24.1 Panel#35

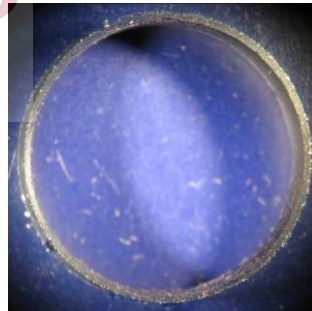


Figure A24.2 Hole in panel

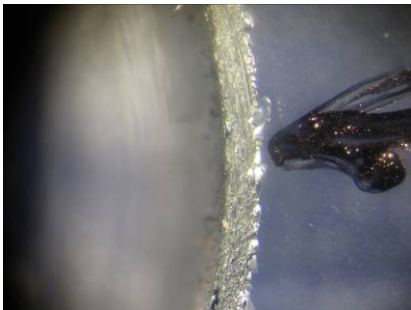


Figure A24.3 Predicted fracture origin



Figure A24.4 Actual fracture origin

Test 25, Panel#21

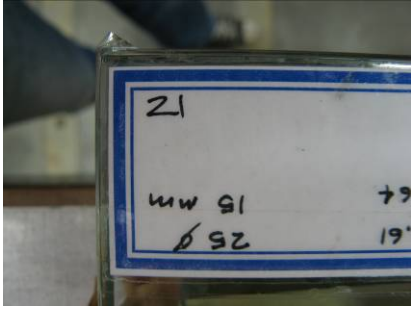


Figure A25.1 Panel#21

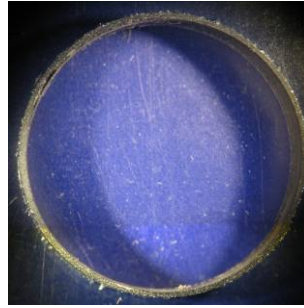


Figure A25.2 Hole in panel

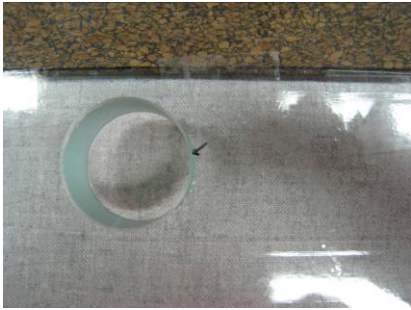


Figure A25.3 Predicted fracture origin



Figure A25.4 Actual fracture origin



Test 26, Panel#14



Figure A26.1 Panel#14

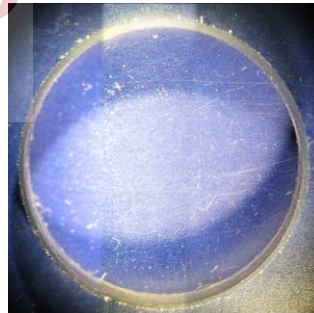


Figure A26.2 Hole in panel

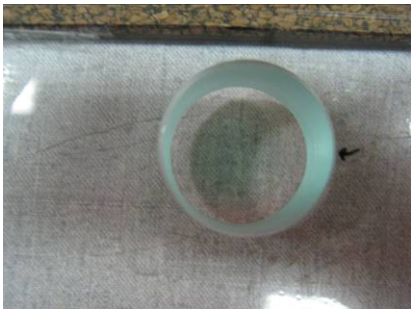


Figure A26.3 Predicted fracture origin



Figure A26.4 Actual fracture origin

Test 27, Panel#32



Figure A27.1 Panel#32

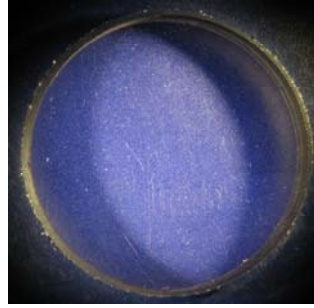


Figure A27.2 Hole in panel

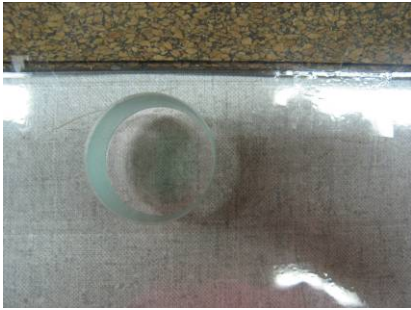


Figure A27.3 Predicted fracture origin

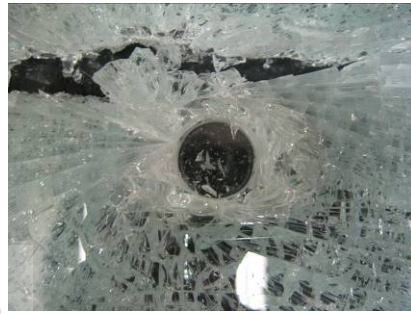


Figure A27.4 Actual fracture origin



Test 28, Panel#37



Figure A28.1 Panel#37



Figure A28.2 Actual fracture origin

Test 29, Panel#22



Figure A29.1 Panel#22



Figure A29.2 Actual fracture origin

Test 30, Panel#13

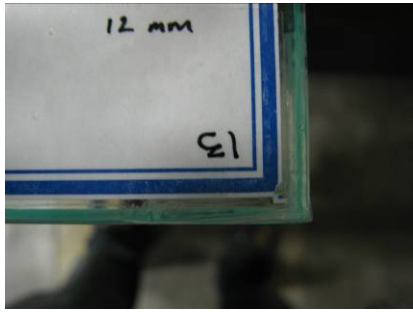


Figure A30.1 Panel#13



Figure A30.2 Actual fracture origin

Test 34, Panel#17



Figure A34.1 Panel#17



Figure A34.2 Actual fracture origin

Test 35, Panel#4



Figure A35.1 Panel#4



Figure A35.2 Actual fracture origin

Test 36, Panel#3



Figure A36.1 Panel#3

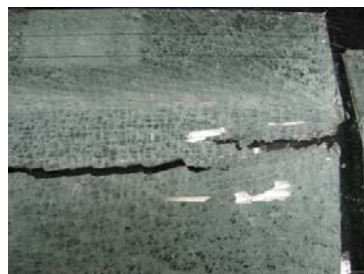


Figure A36.2 Actual fracture origin



Test 37, Panel#29

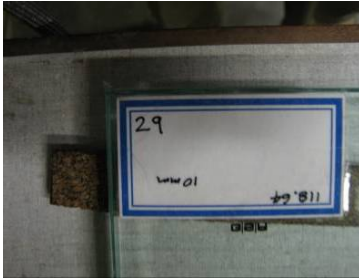


Figure A37.1 Panel#29



Figure A37.2 Actual fracture origin



APPENDIX B

B.1 WEDGE FACTORS

The following table presents the standard wedge used in the GASP measurements

Table B.1. Standard wedge


STANDARD WEDGE USED IN GASP OR LASER GASP							
WEDGE FACTOR = 1.03							
DATE 3/29/01							
Caution: This table is NOT valid if wedge is installed in GASP-CS model.							
angle θ	Stress psi	Stress kgf/cm ²	Stress MPa	angle θ	Stress psi	Stress kgf/cm ²	Stress MPa
1	103	7	0.71	39	4798	338	33.08
2	207	15	1.43	40	4971	350	34.28
3	310	22	2.14	41	5150	363	35.51
4	414	29	2.86	42	5334	376	36.78
5	518	37	3.57	43	5525	389	38.09
6	623	44	4.29	44	5721	403	39.45
7	727	51	5.02	45	5925	417	40.85
8	833	59	5.74	46	6135	432	42.30
9	938	66	6.47	47	6353	447	43.81
10	1045	74	7.20	48	6580	463	45.37
11	1152	81	7.94	49	6815	480	46.99
12	1259	89	8.68	50	7061	497	48.68
13	1368	96	9.43	51	7316	515	50.45
14	1477	104	10.18	52	7583	534	52.29
15	1587	112	10.95	53	7862	554	54.21
16	1699	120	11.71	54	8154	574	56.22
17	1811	128	12.49	55	8461	596	58.34
18	1925	136	13.27	56	8783	619	60.56
19	2040	144	14.07	57	9123	642	62.90
20	2156	152	14.87	58	9481	668	65.37
21	2274	160	15.68	59	9860	694	67.99
22	2394	169	16.50	60	10262	723	70.75
23	2515	177	17.34	61	10688	753	73.69
24	2638	186	18.19	62	11142	785	76.83
25	2763	195	19.05	63	11628	819	80.17
26	2890	203	19.92	64	12147	855	83.75
27	3019	213	20.81	65	12705	895	87.60
28	3150	222	21.72	66	13307	937	91.75
29	3284	231	22.64	67	13957	983	96.24
30	3421	241	23.58	68	14664	1033	101.11
31	3560	251	24.54	69	15434	1087	106.42
32	3702	261	25.53	70	16278	1146	112.23
33	3847	271	26.53	71	17206	1212	118.64
34	3996	281	27.55	72	18234	1284	125.72
35	4148	292	28.60	73	19378	1365	133.61
36	4304	303	29.68	74	20661	1455	142.46
37	4464	314	30.78	75	22111	1557	152.45
38	4629	326	31.92	76	23762	1673	163.84

APPENDIX C

C.2 TOUGHENED GLASS MATERIAL PROPERTIES

The following table presents the static material properties of soda-lime-silica float glass for annealed-, heat strengthened- and tempered glass, as provided by Pilkington.

Table C.2 Toughened glass material properties



PILKINGTON

Technical Information

ATS-129
February 18, 1999

PROPERTIES OF SODA-LIME-SILICA FLOAT GLASS

Modulus of Rupture (M.O.R.) in Flexure for 60-Second Load Duration:		
Mean M.O.R.	6,000 psi (41 MPa)	Annealed
(Probability of breakage 50%)	12,000 psi (82 Mpa)	Heat Strengthened
	24,000 psi (165 Mpa)	Tempered
Typical Design M.O.R.	2,800 psi (19 Mpa)	Annealed
(Probability of breakage 0.8%)	5,600 psi (39 Mpa)	Heat Strengthened
	11,200 psi (77 Mpa)	Tempered
Modulus of Elasticity (Young's)	10.4 x 10 ⁶ psi (7.2 x 10 ¹⁰ Pa)	
Modulus of Rigidity (Shear)	4.3 x 10 ⁶ psi (3.0 x 10 ¹⁰ Pa)	
Bulk Modulus	6.2 x 10 ⁶ psi (4.3 x 10 ¹⁰ Pa)	
Poisson's Ratio	0.23	
Density	158 lb/ft ³ (2.53 g/cm ³)	
Coefficient of Thermal Stress	50 psi/°F (0.62 MPa/°C)	
Thermal Conductivity at 75°F	6.5 Btu·in/hr·°F·ft ² (0.937 W·m/m ² ·°C)	
Specific Heat at 75° F	0.21 Btu/lb _m ·°F (0.88 kJ/kg·°C)	
Coefficient of Linear Expansion (75-575°F)	4.6 x 10 ⁻⁶ in/in·°F (8.3 x 10 ⁻⁶ mm/mm·°C)	
Hardness (Moh's Scale)	5-6	
Softening Point (ASTM C338)	1319°F (715°C)	
Annealing Point (ASTM C336)	1018°F (548°C)	
Strain Point (ASTM C336)	952°F (511°C)	
Index of Refraction:		
(0.5893 μm, Sodium D Line)	1.523	
(1 μm)	1.511	
(2 μm)	1.499	
Emissivity (Hemispherical) at 75°F	0.84	
Stress-Optical Coefficient	Stress (psi) = 2.18 x Retardation (μm) / thickness (in)	

APPENDIX D

D.1 STATIC LOADING CAPACITY OF CONTINUOUS BALUSTRADE SETUPS

The following tables present the static loading capacity of continuous balustrade setups for a probability of failure of 0.8%.

Table D.1 Static loading capacity ($0.8P_f$) for continuous balustrades setups connected by 40x40mm handrail

Designation	No of Panels	No of Holes per Row	Static loading capacity kN
12mm Thickness			
12ttcc	3	-	7.73
HS12t5tcc	3	5	4.19
HS12t7tcc	3	7	4.34
15mm Thickness			
15ttcc	3	-	11.49
HS15t5tcc	3	5	5.87
HS15t7tcc	3	7	6.04

Table D.2 Static loading capacity ($0.8P_f$) for continuous balustrades setups connected by 50x50mm handrail

Designation	No of Panels	No of Holes per Row	Static loading capacity kN
12mm Thickness			
12ttcc	3	-	8.11
HS12t5tcc	3	5	4.39
HS12t7tcc	3	7	4.53
15mm Thickness			
15ttcc	3	-	12.19
HS15t5tcc	3	5	6.22
HS15t7tcc	3	7	6.39

Table D.3 Static loading capacity ($0.8P_f$) for continuous balustrades setups connected by 90x90mm handrail

Designation	No of Panels	No of Holes per Row	Static loading capacity kN
12mm Thickness			
12ttcc	3	-	8.53
HS12t5tcc	3	5	4.60
HS12t7tcc	3	7	4.75
15mm Thickness			
15ttcc	3	-	13.17
HS15t5tcc	3	5	6.7
HS15t7tcc	3	7	6.86